Department of Civil and Structural Engineering

Development of a General-Purpose Component-based Connection Element for Structural Fire Analysis

A thesis submitted in partial fulfilment of the requirements for the degree of Doctor of Philosophy

Gang Dong

Supervised by Professor Ian Burgess & Dr Buick Davison

August 2016

Summary

In fire, elevated temperatures undermine the resistance of structural materials, which leads to steel-framed buildings being subject to very large deformations. Elevated temperatures also cause the affected members to expand, and subsequent cooling induces contraction and recovery of strength. Because of the irreversible nature of plastic straining this causes extremely complex force combinations in connections. Connections which are traditionally idealized as "pinned" or "rigid" in design actually display considerable semi-rigid behaviour, which may contribute to the structure's survival during and after an internal fire.

It will be necessary in future for structural engineers to understand how joints perform in fire, which has been emphasized by a series of case studies, including the official forensic reports on buildings of the New York World Trade complex which collapsed during the "9/11" events in 2001. Eventually, advances in analysis, testing and design codes must allow engineers to design structures which will survive fires without experiencing disproportionate collapse.

This PhD study describes the development of a general component-based connection element, which has been implemented in the *Vulcan* software in order to enable modelling of the robustness and ductility of the connections in fire scenarios. The component-based method which has been adopted is generally accepted as an efficient intermediate way of treating the behaviour of connections in small-deflection ambient-temperature design of semi-rigid frameworks, which is included in Eurocode 3 Part 1.8. This has been developed in the course of several projects at the University of Sheffield towards high-temperature large-deflection representation of connections in a series of stages, including the characterization of individual components, joint testing and component assembly for some conventional connection types. The RFCS-funded project COMPFIRE, of which this work forms a part, extended the data-set to an innovative connection type, the reverse channel, which offers the prospect of greatly enhanced ductility as a way of improving structural robustness in fire. The new data derives from both structural furnace testing and detailed Finite Element analyses. Used in combination with the "static/dynamic" solver in *Vulcan*, the use of the general-purpose component-based connection element has been demonstrated in studies of the performance, including progressive collapse, of planar steel frames in fire scenarios.

The development should allow engineers to identify local failure of joints, and to predict the subsequent failure of the remaining structure, in analytical design. This will enable vulnerable areas to be identified in the structure and their design details to be amended in order to produce a building which is more robust in fire.

Table of Contents

List of figures

List of tables

Chapter 1. Introduction

1.1 Background of fire engineering

Purkiss (2007) defines Fire safety engineering as 'the application of scientific and engineering principles to the effects of fire, in order to reduce the loss of life and damage to property, by quantifying the risks and hazards involved and providing an optimal solution to the application of preventive or protective measures'.

People expect their homes and workplaces to be immune from unwanted fires, which cause many property losses and deaths each year. If fire can be prevented or extinguished in time, fire deaths and property losses can be eliminated. This requires multi-disciplinary efforts, integrating many different fields of science and engineering.

However, some fires will always happen. There are many strategies for preventing fire or reducing its impact. Combustible material can be kept under proper management to reduce the occurrence of ignition. The occupants can be warned instantly by fire detection. Sufficient fire-escapes allow occupants to be evacuated efficiently. Fire damage can also be restricted by containment. Automatically activated sprinklers have shown their capability of controlling or extinguishing fires. The proper selection, design and use of these strategies or combinations of them are vital in fire engineering.

In particular, structural fire engineers are involved in the specification of passive fire protection: thermal effects of fires on structures, designing members capable of resisting thermal effects, and controlling fire spread. All these attempts are intended to ensure that the building maintains its stability for an appropriate period. The following sections will introduce some major events in structural fire engineering.

1.2 Recent major structural fire events

Interest in structural fire engineering has led to much recent development. The following will identify two key events during the last 20 years. Some indications have come from these events that joints are potentially the weakest parts of a structure (Burgess, 2007).

1.2.1 Full scale fire tests at Cardington (1995-96 and 2003)

The purpose of the tests at Cardington was to investigate the behaviour of a real structure under real fire conditions and to collect data that would allow computer programs for the

analysis of structures in fire to be verified. The tested structures included an eight-storey steel-framed composite building (Newman, 2006), a seven-storey reinforced concrete building (Bailey, 2002) and a six-storey timber-framed building (TF, 2000). Newman *et al.* (2006) summarized the observed behaviour in the tests on the steel/concrete frame (shown in Figure 1).

Figure 1: Cardington test building prior to the concreting of the floors

The structure generally performed very well and maintained overall structural stability, although the construction materials weakened with increasing temperature. The results of these tests show the difference between the performance of single unrestrained members in standard fire tests and the performance of the whole building in fire. In a real building structure, its performance is subject to both interactions and changes in load-carrying mechanism. This is considerably beyond what is seen in the simple standard fire test. For example, the Cardington tests demonstrated the ability of a composite floor slab to develop tensile membrane action (Bailey, 2000a and b). This has been adopted by engineers to reduce the cost of fire protection.

The connection fractures observed in the Cardington tests also called attention to the fact that the axial force in a connection is as important as its weakening material properties in fire.

2

There were a series of tests on the steel/concrete frame. In Test 1 a restrained secondary beam was heated by a purpose-built gas-fired furnace. This 9m span beam was heated over its middle 8m region. Its connections were left relatively cool. By visual inspection at the end of this test, the partial-depth end-plate connections at both ends had partly fractured.

In Test 2, the secondary beams on both sides of the primary beams were heated over a length of approximately 1.0m, together with the three primary spans in a complete plane frame. Figure 2 shows that the bolts in a fin-plate secondary beam connection have been sheared.

Newman *et al.* (2006) concluded that all these failures of connections were caused by the contraction of beams during cooling, which generated very high tensile forces. Such connection fractures may cause attached beams to detach from the remainder of the structure, triggering progressive collapse.

Figure 2: Fin-plate connection failure in Cardingotn test

1.2.2 World Trade Centre, 2001

The Twin Towers of The World Trade Centre collapsed on 11 September 2001 following aircraft impacts. In order to understand the mechanisms of collapse and to develop means of preventing disproportionate collapse, several research studies on this fire-induced structural collapse have been conducted. Federal Emergency Management Agency (2002) and National Institute of Standards and Technology (2005, 2008) reported particularly on the major factors in the collapse of the World Trade Centre Buildings 1, 2 and 7.

In particular, Building 7 of the World Trade Centre is deemed to have undergone progressive collapse due to the failure of key connections joining primary beams to columns. Particular attention is drawn to the connection of primary beams to Column 79 on Floors 12-14 as the probable leading factor in the collapse (See Figure 3) these primary beams (44/79) supported several protected secondary beams with long spans, on one side only, with very few secondary beams attached on the opposite side. These secondary beams were heated over a long period to temperatures between 500°C and 600°C during the fire. In order to restrain the secondary beams from expanding by about 100mm the primary beam would have needed connections which were extremely strong in horizontal shear. In the event, large horizontal forces were generated at these connections, which had only been designed against gravity load. The locating bolts at this connection had so little shear resistance that they were easily fractured by the horizontal shear forces produced by restrained expansion of the secondary beams; and the primary beam was separated from Column 79. This separation would have sequentially happened on adjacent lower floors, thus depriving Column 79 of horizontal support from these floors and facilitating its buckling and collapse. In the process of collapse of the floors immediately involved, the falling cumulative mass of these superstructures would generate large dynamic forces, which the lower structure could not resist.
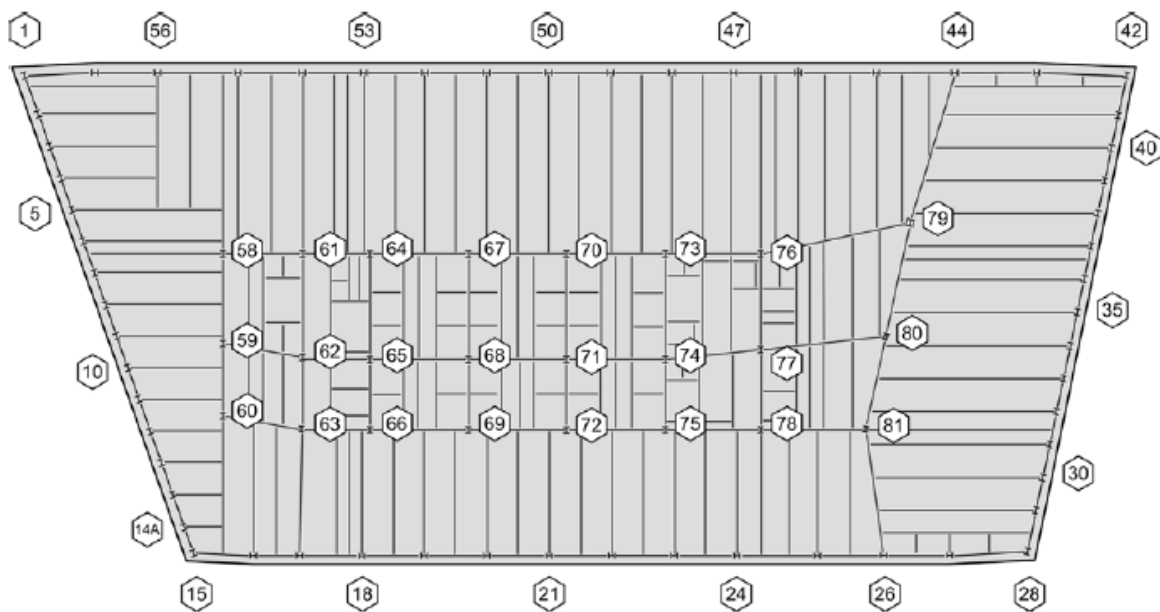
Figure 3: Typical floor plan of WTC building 7 (NIST, 2008)

1.3 Performance-based design

Until recently, most design against fire has been based on the simple 'deemed-to-satisfy' prescriptive building codes. This prescriptive approach is based on experiences accumulated through many years in the light of past fire incidents (Wang, 2013). Since it is simple to put into practice, and has displayed a generally satisfactory level of fire safety, the prescriptive approach has been very extensively used to specify fire strategies. However, design codes based on various aspects of performance have not been extensive enough in scope to be able to cover all cases. Designers also have little or no opportunity to take a rational engineering approach to the conduct of fire safety design. The final alternative is a fully performance-based approach to design, based on the basic principles of fire science, heat transfer and structural mechanics, and aims to provide information on how an integrated building performs under a wide range of ignition scenarios (Custer, 1997).

In 1991, the Building Regulations in England and Wales changed from prescriptive to performance-based requirements. The statutory requirement is that 'the building shall be designed and constructed so that, in the event of fire, its stability will be maintained for a reasonable period'. Practical guidance was also given by Approved Document B, which amplifies the Building Regulations, as 'A fire safety engineering approach that takes into account the total fire safety package can provide an alternative approach to fire safety'.

In performance-based design, any fire strategy can be adopted by fire engineers, when they wish to, and are able to, verify against the agreed fire safety goals. The whole performance of the building under fire is assessed, in the context of both the active fire safety systems and passive fire protection, and the performance of the structure. Variations from the acceptable solutions which offer greater cost savings or other benefits can be assessed. With a correct level of safety plus cost saving, the building's marketing potential is therefore increased, and it will attract a higher income.

In order to allow designers to develop structures which perform well in fires, a trustworthy method is to model the frame using global nonlinear finite element (FE) analysis, which takes account of changing temperatures temperature-dependent material properties and thermal expansion characteristics. With this method, designers are able to develop sufficiently robust connection and structural configurations. This can give more confidence

about the actual structural behaviour in a fire rather than the supposedly conservative protections given by a series of arbitrary rules.

Projects world-wide, such as the China Central Television (CCTV) building in Beijing, have started to use this fire engineering approach to justify the sufficiency of their prescriptive fire protection (Luo, 2005). The application of performance-based design has not only great potential for improving structural safety but also for cutting whole-life cost.

Chapter 2.   Literature review of research on modelling of semi-rigid joints in fire

The importance of joints in fire in general has been highlighted in the previous chapter. To accurately predict the behaviour of steel frames in fire, it is essential to include the effects of connection behaviour, particularly the combined effect of axial force, co-existent large rotation and the reductions of strength and stiffness with elevated temperatures.

One approach to such a problem is to conduct full-scale or isolated fire testing. In 1976, CTICM (Kruppa, 1976) conducted the first experimental fire tests on joints, which showed that the deformation of other elements preceded bolt failure. Since it was intended to investigate the performance of high-strength bolts at elevated temperatures, the performance of the joint as a whole was not presented. Lawson (1990) also conducted a set of moment-rotation joint tests in fire to measure the residual structural continuity afforded by beam-to-column joints at elevated temperatures. The tested joint types included extended endplate, flush end plate and double-sided web cleat. Non-composite, composite and shelf angle floor beams were considered in this study. All the joint rotations reached over 6°. The tests verified the rotational plastic capacity of joints in fire, which could retain up to two-thirds of the ambient design moment capacity at the test temperatures. He also stated that the composite action in fire contributed to the joints' moment capacity, which could be estimated on basis of the combined moment capacities of the bare steel joint and the reinforced concrete slab. A simple rule was also proposed by Lawson to design simply supported beams, taking into account the moment transferred via joints in fire. These early attempts provided some important information for joint modelling during the early stages of the development of performance-based structural fire engineering. However, these tests supplied insufficient data to present the moment-rotation characteristics of the joints, and totally ignored the effects of large axial restraint forces. Since that era, a large number of more focused experimental tests have been conducted to understand various aspects of the behaviour of joints in fire. However, such furnace testing is so expensive that it cannot economically produce a sufficiently large database of results for direct practical design purposes.

The alternative approach is to create numerical models to simulate the joints' behaviour in fire. This chapter will concentrate on previous developments in the modelling of semi-rigid joints at ambient and elevated temperatures.

2.1 Joint material properties at elevated temperature

The material of which a joint is composed will degrade with elevated temperature. EC3 Part 1-2 (CEN 2005c) summarizes the relationships between the Young's modulus of steel and its yield strength at elevated temperatures. These reduction factors are included in Table 1 and Table 2, and also plotted in Figure 4 to Figure 6.

Table 1: Structural steel material reduction factors at elevated temperatures (CEN, 2005b)

Steel temperature (°C)	Yields strength reduction factor	Young's modulus reduction factor
20	1.000	1.000
100	1.000	1.000
200	1.000	0.900
300	1.000	0.800
400	1.000	0.700
500	0.780	0.600
600	0.470	0.310
700	0.230	0.130
800	0.110	0.090
900	0.060	0.068
1000	0.040	0.045
1100	0.020	0.023
1200	0.000	0.000

Table 2: Bolt material strength reduction factors at elevated temperatures (CEN, 2005b)

Temperature (°C)	Strength reduction factor for bolts
20	1.000
100	0.968
150	0.952
200	0.935
300	0.903
400	0.775
500	0.550
600	0.220
700	0.100
800	0.067
900	0.033
1000	0.000
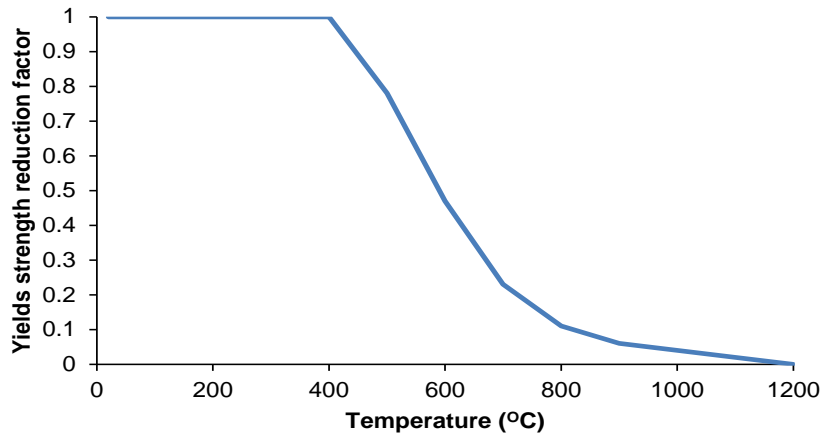
Figure 4: Reduction factors for yiled strength relationship of steel at elevated temperatures (CEN, 2005b)
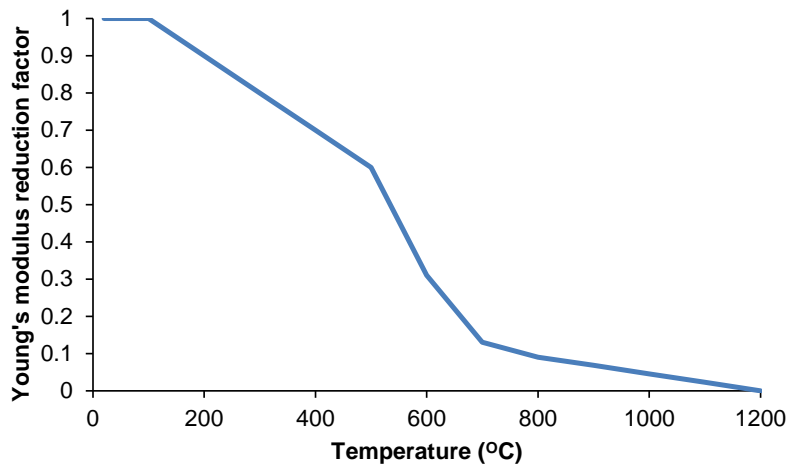
Figure 5: Reduction factors for Young's modulus relationship of steel at elevated temperatures (CEN, 2005b)
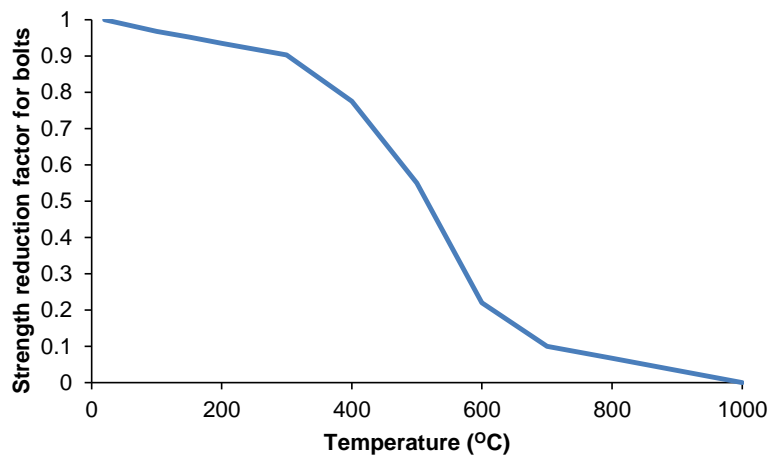
Figure 6: Reduction factors for strength relationship of bolts at elevated temperatures (CEN, 2005b)

2.2 Semi-rigid joint definition

It is generally acknowledged that semi-rigid design of steel frames can result in efficiency, lightness and economical design (Astaneh, 1989). When the connections are designed as semi-rigid, a certain amount of moment is allowed to transfer from the beam-ends to the columns, which reduces the mid-span bending moments in the beams (Anderson, 1987). As a direct result, it is possible to reduce the internal beam cross-sections. Compared to pinned connection, the provision of semi-rigid connection stiffness also helps the columns to resist buckling.

Based on a joint's rotational stiffness, EC3 Part 1-8 (CEN (2005b)) classifies joints as semi-rigid, pinned or rigid (see Table 3).

Table 3: Connection type definitions in EC3 Part 1-8 (CEN, 2005b)

Connection type	Definition
Pinned	Effectively released in terms of rotational constraint. Can transfer internal forces, but will not develop considerable moments.
Rigid	Effectively continuous. Has sufficient rotational stiffness to transfer both forces and moments.
Semi-rigid	Lies between the pinned and rigid connection types. The interaction between members is based on the design moment-rotation characteristics of the joint.

As explained in the previous chapter, the effects of joint behaviour are so influential on the distribution of internal forces and moments within a structure in a fire scenario that they should be taken into account in structural analysis in fire. The deformations at fire temperatures can be several orders of magnitude higher than those used in ambient-temperature semi-rigid design, and so the high-strain properties of connection components become dominant compared with initial stiffnesses.

2.3 Evolution of analysis methods for semi-rigid joints

The early work on semi-rigid joint models has been summarized by Nethercot and Zandonini (1989). This summary will not be repeated here.

The incorporation of semi-rigid behaviour, both axially and rotationally, within global structural analysis for fire cases, is important. In fire, the connections are subjected to high axial forces and large deformations, due to the thermal expansion/contraction of beams and degradation of their material strengths and stiffness.

In general, there are three different ways of modelling semi-rigid joints (Al-Jabri, 2008):

1. Mathematical expressions – curve-fit models;
2. Finite element models;
3. Component-based methods.

2.3.1 Mathematical expressions – curve-fit models

The curve-fit model uses a numerical form (generally polynomial) to represent the moment-rotation relationship of a joint, which is based on experimental test data. Figure 7 illustrates that the joint's behaviour can be represented by different forms of curve-fitting. It can be implemented in analytical models such as finite element models. In order to consider the effects of various parts within the joint, such as bolts, welding and plates, the moment-rotation relationship is generally complicated, and has to be non-linear. Typical mathematical representations include bi-linear, tri-linear and multi-linear curves.
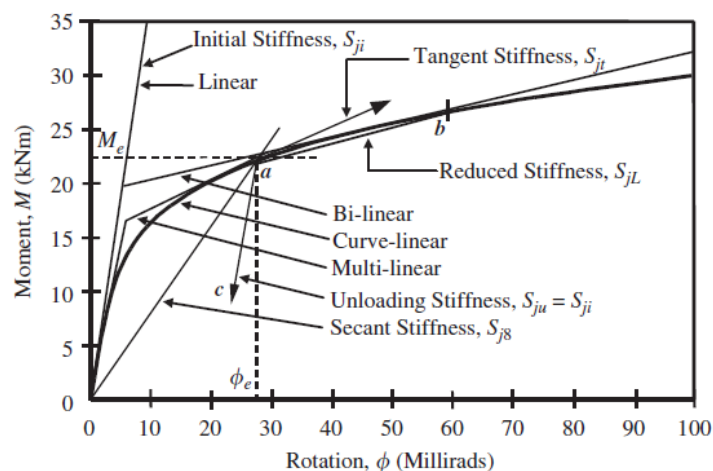
Figure 7: Different forms of curve-fitting representation of joints characteristics (Al-Jabri, 2008)

EI-Rimawi (1997) made an initial attempt to use a curve-fitting method to model joint behaviour in fire. A simple equation with three parameters using a Ramberg-Osgood expression (1943) was proposed in the following form.

$$\phi = \frac{M}{A} + 0.01\left(\frac{M}{B}\right)^{n} \qquad\qquad (2.1)$$

where the relationship between joint rotation (ϕ) and moment (M) are defined by the temperature-dependent parameters *A, B* and *n*. The parameters A and B respectively represent the joint's stiffness and strength, and n defines the sharpness of the "knee" in the curve. This model was extended further by Leston-Jones (1997) and Al-Jabri (1999), to a model which was capable of closely representing a joint's rotational stiffness and strength with increasing temperature. Figure 8 shows that the curve-fit model could even be extended to combine two separate moment-rotation expressions to cope with connections, such as flexible endplate connections, which have two stages of moment-rotation behaviour: before and after contact of the beam flange with column flange.
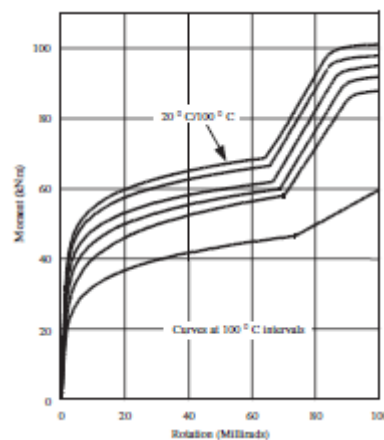
Figure 8: Moment-rotation-temperature curves for a typical flexible end plate joint (Al-Jabri, 2008)

In general, these models predict a joint's rotational behaviour with reasonable accuracy. Since these models are developed on the basis of isolated joints subject only to moment and rotation, they are limited in application to cases where the effect of axial restraint due to thermal expansion/contraction is not critical, and where axial forces superposed on moments are not likely to be serious. However, as discussed in the previous chapter, the axial force due to thermal expansion/contraction can cause connection failure and trigger

progressive collapse. Therefore, global analysis for performance-based design using the curve-fit model cannot represent the structural global behaviour with reasonable accuracy.

2.3.2   Finite element models

The finite element method (FEM) is a powerful tool to investigate joint behaviour in fire. Since Liu (1994, 1996, 1998a and 1998b) made the first attempt to model joint behaviour at elevated temperature, several authors have developed various methods considering geometrical and material nonlinearity.

As Al-Jabri *et al.* (2008) summarized, finite element models can provide good comparisons against tests on joints in fire.   It is a reliable technique, and enables a wider range of parameters to be investigated than is possible in rather complex and expensive tests. However, the cost in terms of time is an obstacle to its practical application in structural fire engineering design.

2.3.3   The 'component method'

EC3 Part 1-8 defines the component method as a design method, in which a joint is modelled as an assembly of basic components, to specify the structural properties of joints in frames of any type. Jaspart (2000) illustrated the component method by analogy with the finite element method, in which each component is equivalent to one finite element in the FE method.   It must be emphasized that all of the above work was done as part of the development of semi-rigid ambient-temperature design methods for steel frames, and is therefore restricted to small rotations, elastic rotational stiffness and plastic capacity.   It completely ignores large deflections, axial force and component fracture; all of these are vital for progressive collapse analysis in fire.

The component method was originated by Zoetemeijer (1974). A simple analytical method for the behaviour of T-stubs, as a common element in conventional steel connections, was developed. This method took into account the plasticity of the flanges and bolts. Two different collapse mechanisms were defined based on the determining factor: bolt facture and flange plate collapse. Accordingly, a number of yield line patterns were specified (examples are shown in Figure 9 and Figure 10). An 'effective length' for a T-stub was calculated on the basis of a number of yield line patterns. This method was validated by a

series of tests. These yield line patterns have been included in so-called 'Green book' (SCI, 1997), and EC3-1.8 (CEN, 2005b).
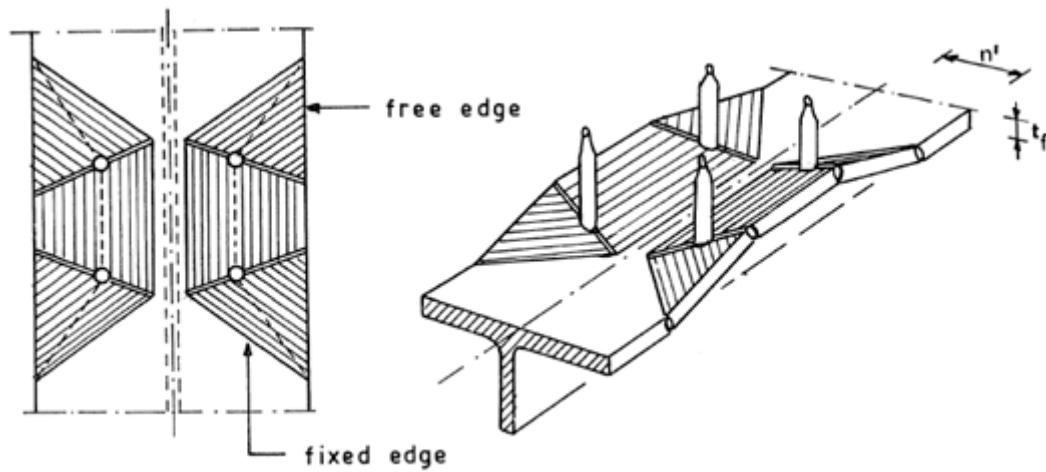
Figure 9: Failure mechanism 1
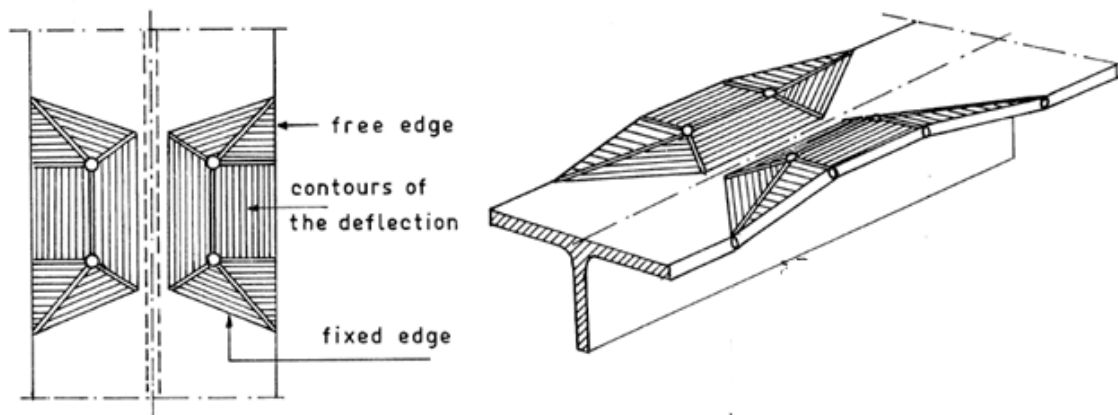
Figure 10: failure mechanism2

After that, Tschemmernegg *et al.* (1987) improved the component method. He investigated the behaviour compression zone in the column web. A series of tests focused on welded and bolted bare-steel endplate joints. The axial column loading was included in some of these tests. He proposed the component-method as a way of determining analytically the nonlinear moment-rotation relationships, in terms of initial stiffness and plastic capacity, for joints (both welded and bolted) in structural steel frames (shown in Figure 11). This development incorporated the most important features of the component method: the joint is composed of several zones, each of which is represented by a non-linear spring.
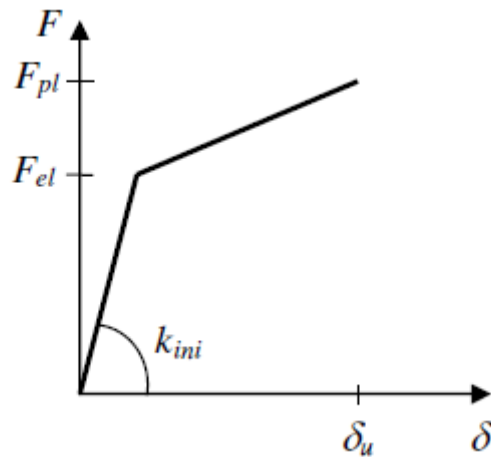
Figure 11: Force-displacement curve after Tschemmernegg *et al* (Block, 2006a)

The component method has subsequently been developed by Jaspart (2000, who summarized the development of component-based models into three steps:

- ➢ Identification of the active components
- ➢ Evaluation of the mechanical characteristics of each individual basic component
- ➢ Assembly of the components

Jaspart listed the relevant components for an extended end-plate connection. Each of the basic components has its own definition of strength and stiffness, in tension, compression or shear. The effects of interaction were also considered within a given component when subject to the coexistence of compression (or tension) and shear. This interaction is likely to reduce the component's strength and stiffness, and to affect its force-displacement curve. Jaspart (2000) also pointed out that the component method could be suitable for the characteristics of joints subjected to extreme loading conditions such as earthquake or fire.

The component-based method has been included in EC3 Part 1-8 as a standard tool to calculate semi-rigid joint behaviour. Compared either with the time consumed in setting-up FE models or in the prohibitive expense of fire tests, the component method is a relatively easy way for structural engineers to predict the joint capacity by hand, and also to offer an intermediate method to model semi-rigid joints within global nonlinear structural analysis software.

Leston-Jones (1997) conducted a programme of moment-rotation-temperature experiments on typical flush end-plate connections, covering a range of temperatures. Both bare-steel and composite arrangements were considered. A spring-stiffness rotational model (shown

in Figure 12) was developed to represent connection degradation at high temperatures. The model was designed for two bolt row flush endplate connection, considering endplate in bending (epb), column flange in bending (cfb), column web in compression (cwc), and bolt in tension (bt). Similar to Eurocode, an equivalent bolt row was adopted to deal with the connection with more than one bolt row. A tri-linear curve was used for each component. Sensitivity studies were then carried out to investigate of the influence of connection response on frame behaviour in fire.
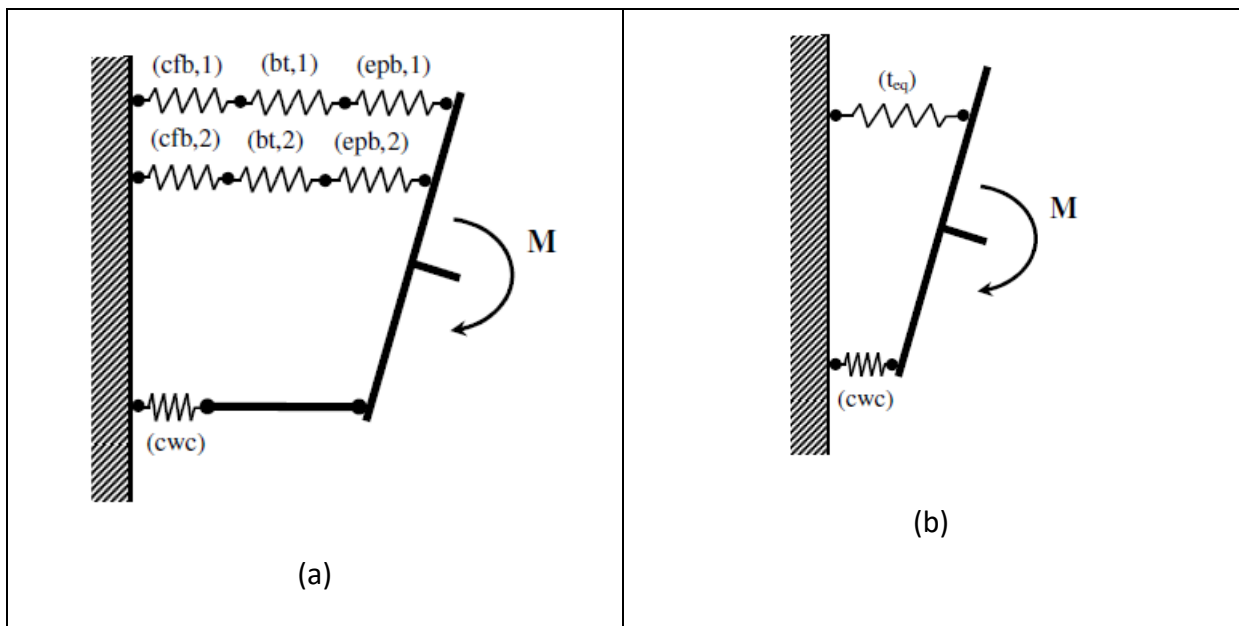
Figure 12: Spring model of a flush endplate connection (a) and equivalent model (b) after Leston-Jones (Block, 2006a)

Al-Jabri (1999) extended Leston-Jones's experimental programme from small section sizes to larger beam and column sections, and concentrated more fully on composite connections. Using the same principles as Leston-Jones, he developed a component-based model to represent his flush endplate connection tests at elevated temperatures. He extended this model for the partial-depth endplate connection, and achieved a good match with the tests. Once again this work was purely rotational.

Simões da Silva *et al.* (2001) proposed a purely rotational component model for bare steel flush end-plate joints (shown in Figure 13). The model was designed to assess the moment resistance and rotational stiffness of a joint at both ambient and elevated temperatures. The components were defined in compliance with EN 1993-1-8. For elevated-temperature cases, the material strength and modulus reduction factors given in EN 1993-1-2 were adopted. In validations against Al-Jabri's tests, a global temperature correction factor (equal

to 0.925 $\theta_{experiment}$) was necessary in order to achieve good agreement between the tests and the model.
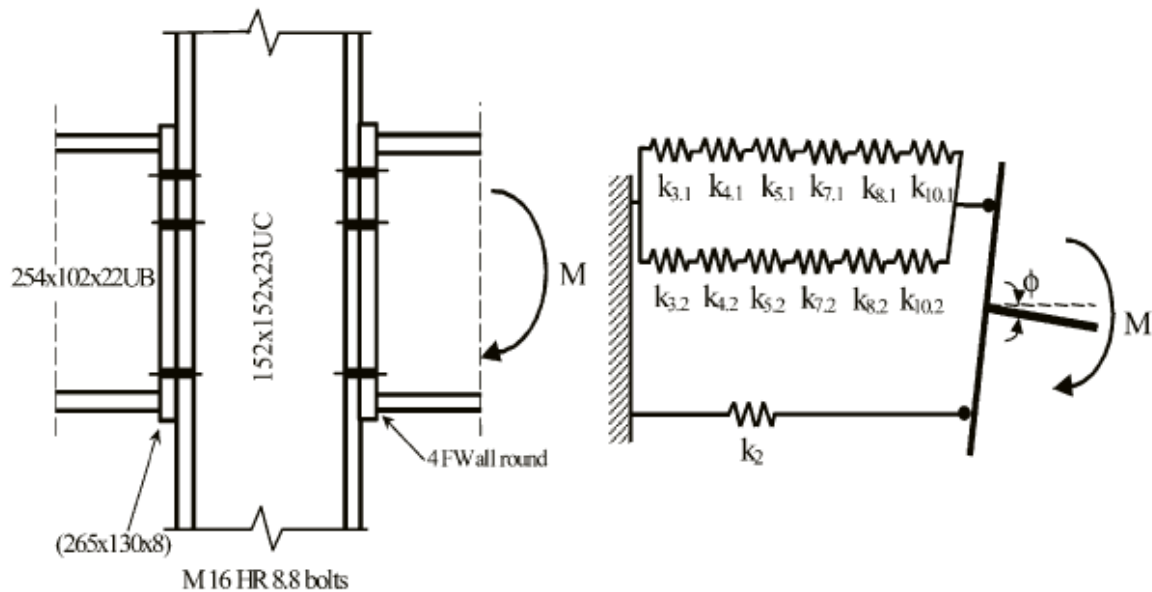
Figure 13: Typical component-based connection assembly (Simões da Silva, 2001)

Spyrou (2002) conducted a series of furnace tests to identify the degradation of the characteristics of T-stubs in tension, and column webs under compression, at elevated temperatures. Detailed finite element studies were also conducted. Based on these tests and finite element models, component models for end-plate/flange T-stubs under tension, and column webs under compression, were developed for modelling of the behaviour of steel-to-steel connections at elevated temperature. The influence of axial forces on joint response and overall frame behaviour was highlighted. Both tensile and compressive axial forces are recognised as reducing the rotational ductility of joints, and therefore limit the ductility of the structural frame. In the fire scenario, the axial force effect will be even more distinct. Hence, in order to provide with acceptable accuracy, it is necessary for the component-based model to include the axial force effect.

Sokol *et al* (2003) developed three nonlinear springs and assembled them to simulate the Cardington fire test No.7, in order to study structural integrity. The three springs respectively represented tension, compression and shear within the connection. This study showed reasonably good agreement during the heating phase of the structure, but experienced some difficulty in representing the cooling phase.

Block (2004a, 2004b, 2005a, 2005b,2006a, 2006b, 2007, 2013a and 2013b) focused on the effect of axial pre-compression in columns, due to superstructure loading, on the behaviour of the column-web compression zone of steel-to-steel end-plate connections. Both furnace tests and finite element modelling were conducted, and simplified component models were developed, from the basis of Spyrou's component model, including the column web under compression. A component-based connection element (Figure 14) was developed and simulated in the *Vulcan* research code, and this was partly validated.
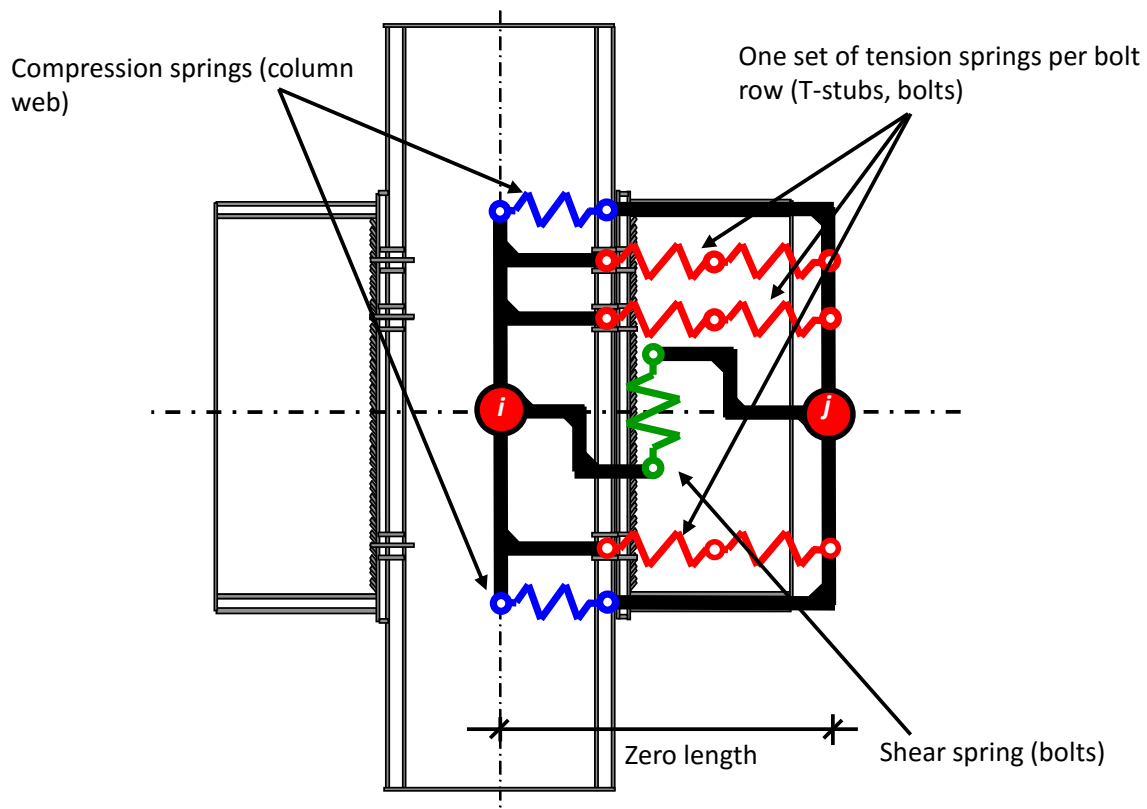
Figure 14: Block's (2006a) component assembly for end-plate connection.

A collaborative EPSRC project (EP/C5109841/1) conducted by the Universities of Sheffield and Manchester investigated the robustness of connections in fire conditions (Yu *et al.*, 2008a, 2008b, 2009a,2009b, 2009c, 2009d and 2011; Hu *et al.*, 2009, Dai *et al*., 2009a, 2009b, 2010a and 2010b). The tested connections encompassed four typical beam-column connections: fin-plate, flush end-plate, flexible end-plate and web-cleat. A selection of connections under inclined forces (Figure 15), as well as structural subframes, was tested to very high deformation, and in some cases to destruction, at temperatures up to 650°C. Yu (2011) also conducted numerical investigations of the tested connections. On the basis of

the yield-line method, Yu (2009) developed a component model for the T-stub, which considers both geometry and material nonlinearity.
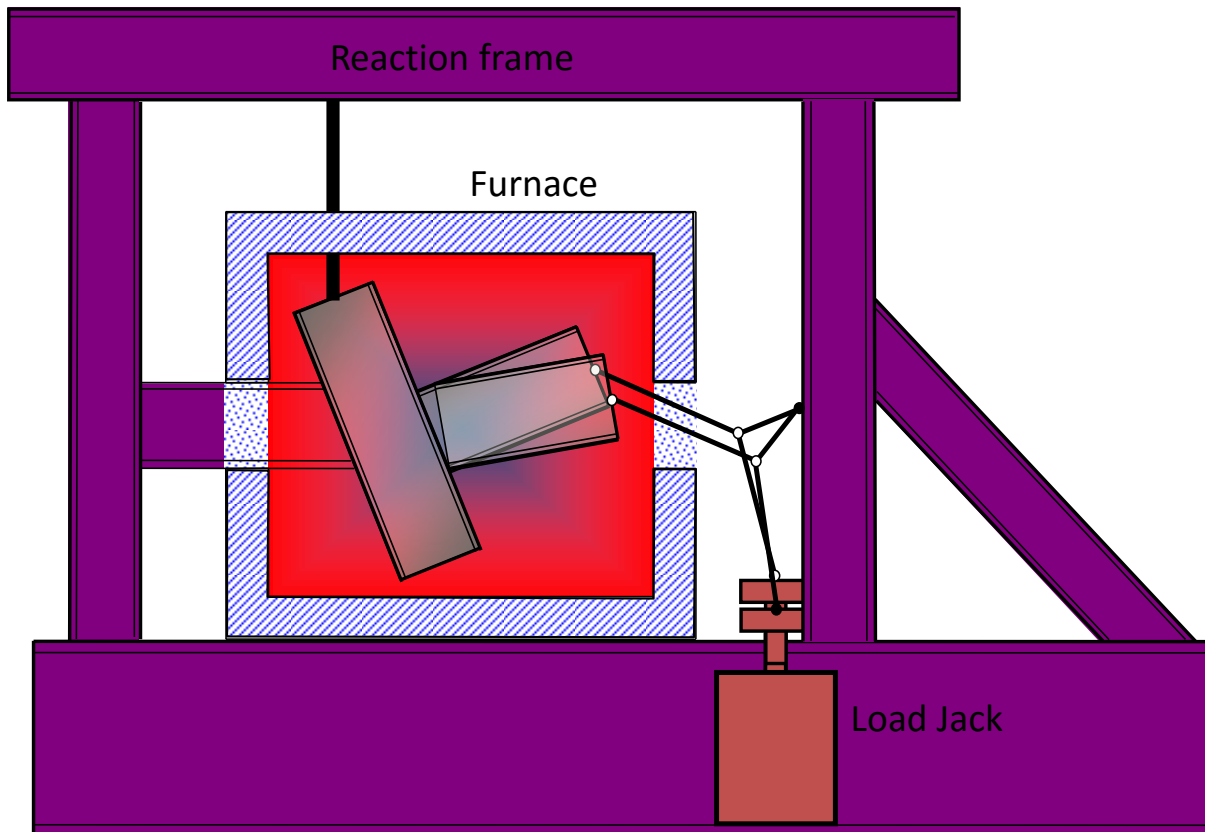
Figure 15: Joint test setup (schematic) by Yu (2011)

Santiago *et al.* (2008a, and 2008b, 2009 and 2010) conducted experimental and numerical studies of six steel subframes under natural fire conditions. The objective was to investigate joint behaviour under combined bending moment and the axial force developed during a natural fire. The study focused on three types of connection: header plate, flush end-plate, and extended end-plate. It was intended to investigate the influence of connection type on the behavior of steel sub-structures in fire. The experimental investigation highlighted the fact that the large tensile forces and reversal of connection moment during the cooling stage can cause failure of bolted joints.

Jones (2008, 2009, 2010a and 2010b), conducted a series of ambient- and elevated-temperature tests on fin-plate connections to tubular columns. These included fin plates under tension (tying) and shear force, and reverse channel legs under shear. After these tests and extensive numerical simulations had been achieved, a component-based method for the tensile behaviour of fin plate connections to concrete-filled rectangular steel tubular columns was developed.

Taib (2012) created an integrated component-based element for fin-plate connections under fire conditions. The development was based on Sarraj's (2007) development of a realistic FE model for fin plate connections in fire. The component-based element considers the influence of both vertical and horizontal forces at bolt rows, as well as incorporating unloading and cooling properties.

2.4   The COMPFIRE project

COMPFIRE was one of the latest joints-in-fire projects, and particularly considered the behaviour and design of joints to composite columns for improved robustness in fire. This project (RFCS, 2009) involved a number of academic research groups and industrial partners, namely

- University of Coimbra
- Czech Technical University
- DESMO
- Luleå Technical University
- University of Sheffield
- University of Manchester
- TATA Steel Tubes (Europe)

This project coincided with the author's PhD studies, and supplied extensive and useful test and numerical data.

The aim of this project was to provide an integrated approach to the practical application of performance-based fire engineering design to composite structures, taking account of joint performance under natural fire conditions, including the cooling phase. The main objective was to develop a comprehensive component-based design methodology for joints to composite columns. The composite joints (Figure 16) under investigation were traditional flush endplate and the novel semi-rigid reverse channel connections. These were applied to connections between steel beams (UB306x165x40 shown in Figure 16) and two types of composite column; concrete-filled tubular (CFT, SHS 224.5x8 in Figure 16b) and partially-encased H-section (PE, 254x254x89 UC in Figure 16a) columns. The reverse-channel connection possesses very high rotational capacity without compromising its ultimate strength under ambient-temperature gravity load.
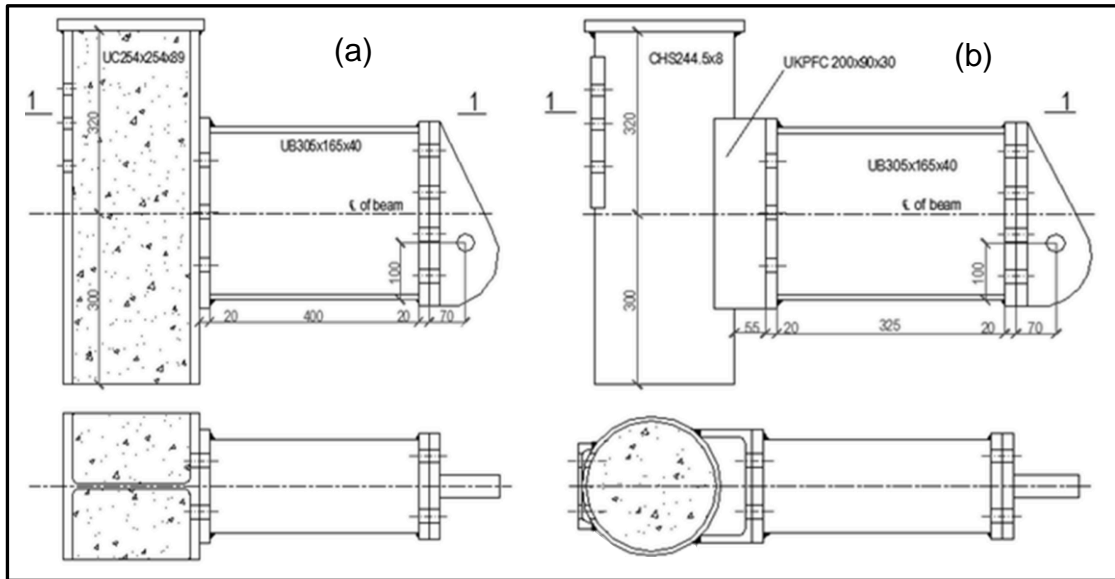
Figure 16: (a) Endplate and (b) reverse-channel connections to composite columns (Huang, 2012)

The project included a number of tests on complete joints, numerical and analytical studies of components, whole connection assemblies and structural subframes. The project included seven work packages:

1. Joint thermal behaviour and modelling: this package was intended to investigate the temperature distributions within the joints in both standard and real fire scenarios.

2. Component behaviour: A comprehensive set of reverse channel component test data was gathered by the Universities of Manchester and Coimbra. The University of Sheffield conducted 20 isolated-joint tests. Based on these data, Luleå Technical University performed simulations using finite element modelling, and expanded the test data. The University of Sheffield developed simplified models to predict the load-deflection curves of reverse channel components at both ambient and elevated temperatures.

3. Component-based joint modelling: The component models developed in Work Package 2 were assembled and validated against the isolated joint tests in Work Package 2.

4. Fire tests on subframes: The Universities of Manchester and Coimbra conducted a total of 11 subframe tests to assess the complicated behaviour between the composite joint and the surrounding structural element under different fire

exposure conditions, including an investigation of how the connections behave during the cooling phase of a fire event.

5. <u>Integrated FE modelling</u>: This work package used both standard finite element analysis, and finite element analysis incorporating a simplified component-based method, to model the subframe tests conducted in Work Package 4.

6. <u>Demonstration fire tests</u>: Two fire tests on a complete composite structure under natural fire conditions were conducted, in order to provide experimental data and to demonstrate impact of joints with improved detailing on structural fire robustness.

7. <u>Development of practical design guides</u>: Based on the previous work package, a practical method was developed to predict composite joint behaviour under fire.

The project data was intended to be used to develop a general component-based connection element, to enable global non-linear structural programs to model the whole structure, including the behaviour of connections. The test data would also be used to validate the component-based connection element.

2.5 Conclusion

The component-based method provides an intermediate approach, using the minimum of computational effort, while retaining the key characteristics of connection behaviour and offering acceptable predictions of frame behaviour.

The above developments by Zoetemeijer, Tchemmernegg and Jaspart were intended for semi-rigid steel connections at ambient temperature against normal design loads. The elastic and yield material properties were considered. The initial elastic rotational stiffness was captured. However, this cannot be used for large deflection, or for material non-linearity at elevated temperature.

The main aim of the research by Leston-Jones, Al-Jabri and Simões da Silva was to develop moment-rotation-temperature characteristics of joints. However, in the wake of observations from both accidental fires and full-scale fire tests at Cardington, the effect of axial force has also risen considerably in importance.

The developments by Spyrou, Sokol, Block , Jones and Taib were limited to one connection type, either flush endplate or fin plate connections.

2.6   Research motivations

Observations from the full-scale fire tests at Cardington and the collapse of buildings of the World Trade Centre in 2001 have raised concerns that joints are potentially the weakest parts of a structure (Burgess, 2007). Due to the combination of thermal and mechanical effects caused by heating, the resultant forces on joints (in addition to vertical shear) are complicated and vary, from pure moment, to moment and compression, and eventually to almost pure tension. Additionally, the connections are subjected to large rotations.

Therefore, engineers must take into account the complexity of actions on the connections, and their response, when designing structures that will perform well in a fire. The incorporation of realistic connection behaviour within global nonlinear finite element programs is important, as it allows designers to be clear about the actual structural behaviour and to ensure the adequacy of the connections in terms of robustness and ductility.

However, incorporation of realistic joint behaviour in the structural analysis is problematic. The test data is limited, and can only reveal how the connections work in fire to a certain extent, as testing is expensive and there is a wide range of joint types. Although general finite element packages can predict the behaviour of connections with a good degree of accuracy, the modelling of connections to obtain this behaviour is prohibitively detailed, and therefore expensive, in practical design situations.

It would be ideal to create a general component-based representation of the 'connection zone' at the column-face of a beam-to-column joint. This requires the minimum of computational effort, while retaining the key characteristics of connection behaviour and offering acceptable predictions of frame behaviour. It enables engineers to predict the behaviour of connections within a structure in fire, to track the progressive collapse sequence, and to design robust structures based on performance-based principles.

2.7   Research aim, objectives and methodologies

2.7.1   Aim of research

This PhD research is intended to develop component-based connection elements for two connection types: flush endplate and reverse channel connections, and to demonstrate their use in case studies.

2.7.2 Detailed objectives

The research activities are:

- Identification of the active components;

- Development of component models;

- Component assembly;

- Tests on connection element.

- Running demonstration cases as examples of application.

2.7.3 Methodologies

Based on the joint test and detailed finite element analysis, both flush endplate and reverse channel connections are divided into several zones, called active component zones, which either contribute to the joint deformation, or limit the joint capacity.

These active components will each be represented by a lateral spring. This spring is termpature-dependent and defined with failure criteria. For flush endplate, Spyrou (2002), Block (2004a, 2004b, 2005a, 2005b, 2006a, 2006b, 2007, 2013a and 2013b), and Yu (2008a, 2008b, 2009a, 2009b, 2009c, 2009d and 2011) have developed the models for some of the key components, including T-stub in tension, and column web under compression. For reverse channel connections, the component models for reverse channel under tension/compression were needed.

In order to enable global (frame analysis) nonlinear structural software to model the structure taking into account the semi-rigid joint behaviour in fire, it is essential to assemble these component models using rigid links. Yu's isolated joint tests and the COMPFIRE project provided comprehensive data to validate this development.

Chapter 3. Development of component models for reverse channel connections

The reverse channel itself is clearly one of the key components of the reverse channel connection. In order to build up the component-based connection element for the reverse channel connection, a force-displacement relationship was developed on the basis of the plastic hinge method. In addition, a bolt pull-out limit derived from a 'cone model' (also called the 'bolt pull-out model') was developed. A series of component tests and whole-joint tests were conducted in the COMPFIRE project, and these provided experimental data which helped to characterise the behaviour of reverse channel connections under tension. Based on these tests, an extensive FEA parametric study was simulated by the COMPFIRE partner at Luleå, which was intended to facilitate the investigation of all the possible behaviour of reverse channels under tension/compression and validation of the component models for the reverse channel under tension and compression.

3.1 Plastic hinge method

The reverse channel supports tensile and compressive loads, primarily through bending action. Therefore, the plastic theory of structures (Horne, 1971) can be used to deal with the behaviour of the reverse channel under tension or compression beyond the elastic limit, with particular emphasis on the failure load. With material properties which degrade either as a result of increasing temperature and/or increasing loading, plastic hinges will gradually form at the most highly stressed points in the reverse channel. Material and geometric nonlinearities are considered, but the effects of shear and axial forces on the plastic hinges are neglected, because their effects on the bending capacity will be small.

Bhatt (1999) explained the effect of shear force on the ultimate bending capacity, and characterised the effect as:

$$M = M_p \left(1 - 0.75(Q/Q_p)^2\right)$$

(3.1)

in which M_p is the section's plastic moment capacity, where the plastic hinge forms; Q_p is the plastic shear capacity; Q is the shear force and M is the moment. In order to assess the effects of shear on the bending capacity, the following is a quick assessment (shown in figure 17), considering 150mm long plastic hinge with 12mm plate thickness. The maximum shear used the maximum tensile resistance based on an 8.8 M20 bolt.

Plate thickness (where the plastic hinge forms) $t_p = 12mm$

Plate length (where the plastic hinge forms) $L_p = 12mm$

Tensile area per M20 bolt: $A_t = 245mm^2$ (Owens, 1989)

Tension strength of per M20 bolt p_t: $p_t = 560\dfrac{N}{mm^2}$ (BSI, 2001)

Tension capacity of M20 bolt: $P_t = \dfrac{p_t A_t}{1000} = 137.2kN$

The maximum shear is limited by the bolt tension capacity. Therefore,

$$Q_{max} = P_t = 137.2kN$$

The plastic shear force is

$$Q_p = \frac{f_y t_p L_p}{\sqrt{3}} = 369kN$$

The plastic moment capacity reduction factor is

$$\phi_r = 0.75\left(\frac{Q\,max}{Qp}\right)^2 = 10.3\%$$

F (based on M12 bolt tensile capacity)

t_p

L_p

Assumed plastic

hinge location
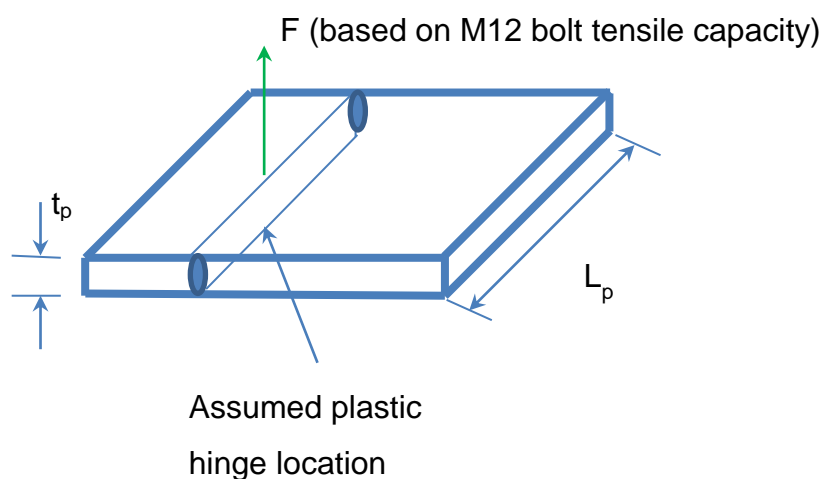
Figure 17: illustration of shear effect on plastic hinge moment capacity

This plastic moment capacity reduction factor can be ignored in the derivation of the component's force-displacement curve, but can be taken into account as a design safety factor in later practice.

According to the energy-balance principle, the external work is equal to the internal work absorbed in plastic deformation of the hinges:

$$F\delta = W_{PH1} + W_{PH2} + W_{PH3}$$

(3.2)

Where $F\delta$ is the external work done by the applied load F in moving through a displacement δ, and W_{PH1}, W_{PH2} and W_{PH3} are the internal plastic work components due to rotations of the plastic hinges PH1, PH2 and PH3.

A three-phase elastic-plastic material property model (Figure 18) is assumed, similar to that used by Yu (2009) for T-stub models. The details of Yu's derivation are documented in 3.2.
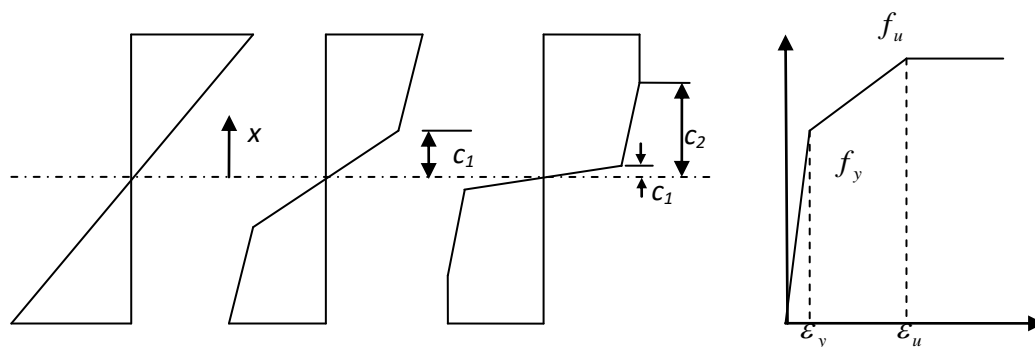
Figure 18: Stress blocks of a plastic hinge (Yu, 2009a)

3.2 Yu's T-stub model (Yu, 2009)

Yu (2009) developed a component model for T-stubs (shown in Figure 19) in fire on the basis of the energy method. The development of the current component model for reverse channel connections under tension and compression uses Yu (2009)'s approach to calculate the strain energy within the plastic hinge. This part will include Yu's derivation in calculating the plastic hinge energy.
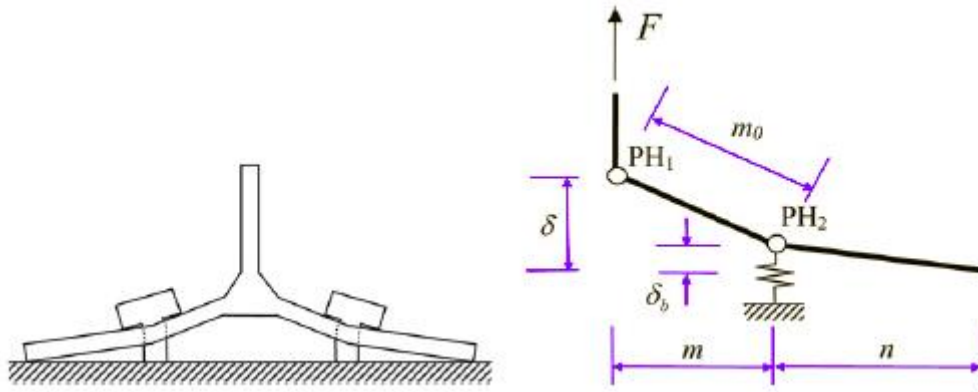
Figure 19: Yu's (2009) mechanism for T-stub

The assumed material model is shown in Figure 18, as a typical elastic-plastic three-phase characteristic. The calculation of strain energy is divided into three possibilities when the strain (ε_m) within the plastic hinge reaches the different stages.

3.2.1   When strain ε_m is lower than yield strain ε_y ($\varepsilon_m \leq \varepsilon_y$, refer to Figure 18)

Stress is

$$\sigma = E \frac{x}{t/2} \varepsilon_m$$

(3.3)

Where E is the Young's modulus, x is the distance to the plate centre line, and t is the plate thickness

The moment at the plastic hinge

$$M = 2Be_{ff} \int_0^{t/2} E \frac{x}{t/2} \varepsilon_m x dx$$

(3.4)

$$M = 2B_{eff} \left(\frac{t}{2}\right)^2 \left\{\frac{1}{3} E \varepsilon_m\right\}$$

(3.5)

Where B_{eff} is the effective width of the plastic hinge.

3.2.2   When strain ε_m is higher than yield strain ε_y but lower than ultimate strain ε_u

($\varepsilon_y < \varepsilon_m \leq \varepsilon_u$, refer to Figure 18))

$$c_1 = \frac{\varepsilon_y}{\varepsilon_m} \left(\frac{t}{2}\right)$$

(3.6)

28

The stress can be written as

$$\sigma = \begin{cases} E \dfrac{x}{t/2} \varepsilon_m & x \le c_1 \\[2mm] f_y + E_t \left[\left(\dfrac{x}{t/2} \right) \varepsilon_m - \varepsilon_y \right] & x > c_1 \end{cases}$$

(3.7)

Where E_t is the tangent Young's modulus. The moment at the plastic hinge is

$$M = 2 B_{beff} \left(\int_0^c E \frac{x}{t/2} \varepsilon_m x \, dx + \int_c^{t/2} \left(f_y + E_t \left[\left(\frac{x}{t/2} \right) \varepsilon_m - \varepsilon_y \right] \right) x \, dx \right)$$

(3.8)

$$M = 2 B_{eff} \left(\frac{t}{2} \right)^2 \left\{ \frac{1}{3} E_t \varepsilon_m + \frac{1}{2} (E - E_t) \varepsilon_y - \frac{1}{6} (E - E_t) \frac{\varepsilon_y^{\,3}}{\varepsilon_m^{\,2}} \right\}$$

(3.9)

3.2.3 When strain ε_m is higher than ultimate strain ε_u ($\varepsilon_m > \varepsilon_u$,refer to Figure 18)

$$c_2 = \frac{\varepsilon_u}{\varepsilon_m} \left(\frac{t}{2} \right)$$

(3.10)

The stress is

$$\sigma = \begin{cases} E \dfrac{x}{t/2} \varepsilon_m & x \le c_1 \\[2mm] f_y + E_t \left[\left(\dfrac{x}{t/2} \right) \varepsilon_m - \varepsilon_y \right] & x \le c_2 \\[2mm] f_u & x > c_2 \end{cases}$$

(3.11)

The moment M is

$$M = 2 B_{eff} \left(\int_0^{c_1} E \frac{x}{t/2} \varepsilon_m x \, dx + \int_{c_1}^{c_2} \left(f_y + E_t \left[\left(\frac{x}{t/2} \right) \varepsilon_m - \varepsilon_y \right] \right) x \, dx + \int_{c_2}^{t/2} f_u x \, dx \right)$$

(3.12)

Therefore,

$$M = 2 B_{eff} \left(\frac{t}{2} \right)^2 \left\{ \frac{1}{2} f_u + \frac{1}{\varepsilon_m^{\,2}} \left[(E - E_t) \left(\frac{1}{2} \varepsilon_y \varepsilon_u^{\,2} - \frac{1}{6} \varepsilon_y^{\,3} \right) + \frac{1}{3} E_t \varepsilon_u^{\,3} - \frac{1}{2} f_u \varepsilon_u^{\,2} \right] \right\}$$

(3.13)

29

3.2.4 Strain energy

The curvature of the cross-section is $\gamma = \dfrac{\varepsilon_m}{t/2}$. This assumes the length of the plastic hinge is t, the rotation of the plastic hinge is

$$\theta = \int_0^t \frac{\varepsilon_m}{t/2} dx = 2\varepsilon_m \tag{3.14}$$

Factor $M_0 = 2B_{eff}\left(\dfrac{t}{2}\right)^2$

$$\tag{3.15}$$

The moment M is simplified into

$$\varepsilon_m \leq \varepsilon_y : M = M_0\left\{\frac{1}{6}E\theta\right\} \tag{3.16}$$

$$\varepsilon_y < \varepsilon_m \leq \varepsilon_u : M = M_0\left\{\frac{1}{6}E_t\theta + \frac{1}{2}(E - E_t)\varepsilon_y - \frac{2}{3}(E - E_t)\frac{\varepsilon_y^3}{\theta^2}\right\} \tag{3.17}$$

$$\varepsilon_m > \varepsilon_u : M = M_0\left\{\frac{1}{2}f_u + \frac{4}{\theta^2}\left[(E - E_t)\left(\frac{1}{2}\varepsilon_y\varepsilon_u^2 - \frac{1}{6}\varepsilon_y^3\right) + \frac{1}{3}E_t\varepsilon_u^3 - \frac{1}{2}f_u\varepsilon_u^2\right]\right\} \tag{3.18}$$

The rotational energy generated at the yield line is calculated by

$$W_{ph} = \int_0^\theta M d\theta \tag{3.19}$$

$\varepsilon_m \leq \varepsilon_y$

$$W_{ph} = \frac{1}{12}E\theta^2 \tag{3.20}$$

$\varepsilon_m \leq \varepsilon_u :$

$$W_{ph} = \int_0^{2\varepsilon_y} \frac{1}{6}E\theta d\theta + \int_{2\varepsilon_y}^\theta \frac{1}{6}E_t\theta + \frac{1}{2}(E - E_t)\varepsilon_y - \frac{2}{3}(E - E_t)\frac{\varepsilon_y^3}{\theta^2} d\theta$$

$$= \frac{1}{12}E_t\theta^2 + (E - E_t)\left[\frac{1}{2}\theta\varepsilon_y + \frac{2}{3}\frac{\varepsilon_y^3}{\theta} - \varepsilon_y^2\right] \tag{3.21}$$

$\varepsilon_m > \varepsilon_u$:

$$W_{ph} = \int_0^{2\varepsilon_y} \frac{1}{6} E\theta d\theta + \int_{2\varepsilon_y}^{2\varepsilon_u} \frac{1}{6} E_t\theta + \frac{1}{2}(E - E_t)\varepsilon_y - \frac{2}{3}(E - E_t)\frac{\varepsilon_y^3}{\theta^2} d\theta$$

$$+ \int_{2\varepsilon_u}^{\theta} \frac{1}{2} f_u + \frac{4}{\theta^2}\left[(E - E_t)\left(\frac{1}{2}\varepsilon_y\varepsilon_u^2 - \frac{1}{6}\varepsilon_y^3\right) + \frac{1}{3}E_t\varepsilon_u^3 - \frac{1}{2}f_u\varepsilon_u^2\right] d\theta$$

$$= E_t\varepsilon_u^2 + (E - E_t)\left[2\varepsilon_u\varepsilon_y - \varepsilon_y^2\right] + f_u\left(\frac{1}{2}\theta - 2\varepsilon_u\right) - \frac{4}{\theta}\left[(E - E_t)\left(\frac{1}{2}\varepsilon_y\varepsilon_u^2 - \frac{1}{6}\varepsilon_y^3\right) + \frac{1}{3}E_t\varepsilon_u^3 - \frac{1}{2}f_u\varepsilon_u^2\right]$$

$$(3.22)$$

3.3 Development of the component model for reverse channel under tension

Following the flush endplate connection, the reverse channel was introduced between the composite column face and endplate. Since the reverse channel is relatively flexible, the connection deformation can be large, which itself may limit the connection's capacity. Hence, it is necessary to implement a component model to represent the reverse channel in the connection element. The following two sections will develop the component model for reverse channels under tension and compression.

The component model developed for the reverse channel under tension adopts the plastic hinge mechanism method to calculate the force/displacement curve. By investigation of the component tests conducted in COMPFIRE (RFCS, 2012a), a reverse channel under tension may form two combined plastic hinge mechanisms:

- A 'cone' with a circular plastic hinge around the bolt head (Figure 20a).
- Straight line plastic hinges (Figure 20b)

Both of the plastic hinge mechanisms are identified in the component test in Figure 21 Figure 22. In the straight-line plastic hinge mechanism, 6 plastic hinges form. The tops of the two legs are moved slightly towards each other by the bending deformation in the web.

The 'circular' plastic hinge is due to the bolt head being pulled-out from the bolt hole in the reverse channel web. The conical wall is under circumferential tension, and a circular plastic hinge forms at the bottom of the cone due to the rotation of the cone wall.

a) Circular yield line

b) Straight yield line
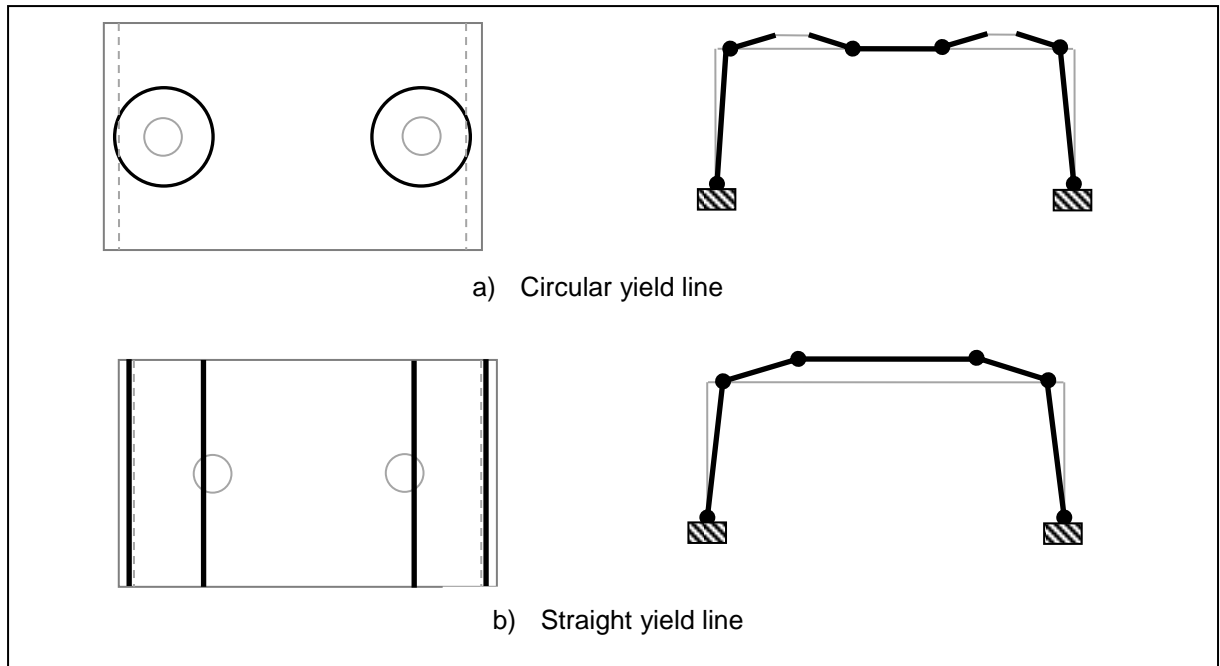
Figure 20: Plastic hinge mechanisms

Figure 21: Straight yield line plastic hinge mechanism (RCT 8) (RFCS, 2012a).

Figure 22: Circular yield line pattern and plastic hinge mechanism (RCT3) (RFCS, 2012a).

3.3.1 Straight-line plastic hinge mechanism

For the straight-line plastic hinge mechanism, the reverse channel works similarly to a single-span portal frame. From the bending moment diagram (shown in Figure 23), three plastic hinges (PH1, PH2 and PH3) gradually form. Figure 24 shows straight-line plastic hinge locations for two types of reverse channel: a parallel-flange rolled channel (PFC) and a channel cut from a structural hollow-section rectangular tube. PH1 is assumed to be at the edge of the bolt head. PH2 and PH3 are respectively on the legs near the root of the tube-cut and on the web of the PFC near to the root. This is because the maximum moment happens at the intersection of web and leg, but the PFC and tube-cut sections have different local wall thicknesses; the PFC has a thicker leg, and a gradually-changing thickness in the root area. PH3 is at the bottom of the reverse channel leg. In order to allow sufficient space to install the bolts on-site, it is considered that the minimum clear distance between the reverse channel leg and bolt head should be 1.5 times the bolt diameter.
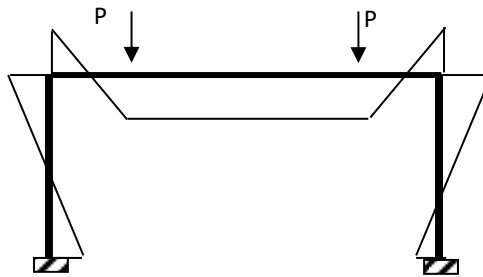
Figure 23: Bending moment diagram for single-span frame.

Based on the plastic hinge method (Figure 25), the rotations of the plastic hinges for a PFC are calculated as:

$$\theta_1 = \arcsin\left(\frac{\delta + h - \sqrt{h^2 + m_0^2}\cos(\theta_0 + \theta_3)}{m - m_0} \right)$$

(3.23)

$$\theta_2 = \theta_1 + \theta_3$$

(3.24)

$$\theta_3 = \arcsin\left(\frac{m - (m - m_0)\cos\theta_1}{\sqrt{h^2 + m_0^2}} \right) - \theta_0$$

(3.25)
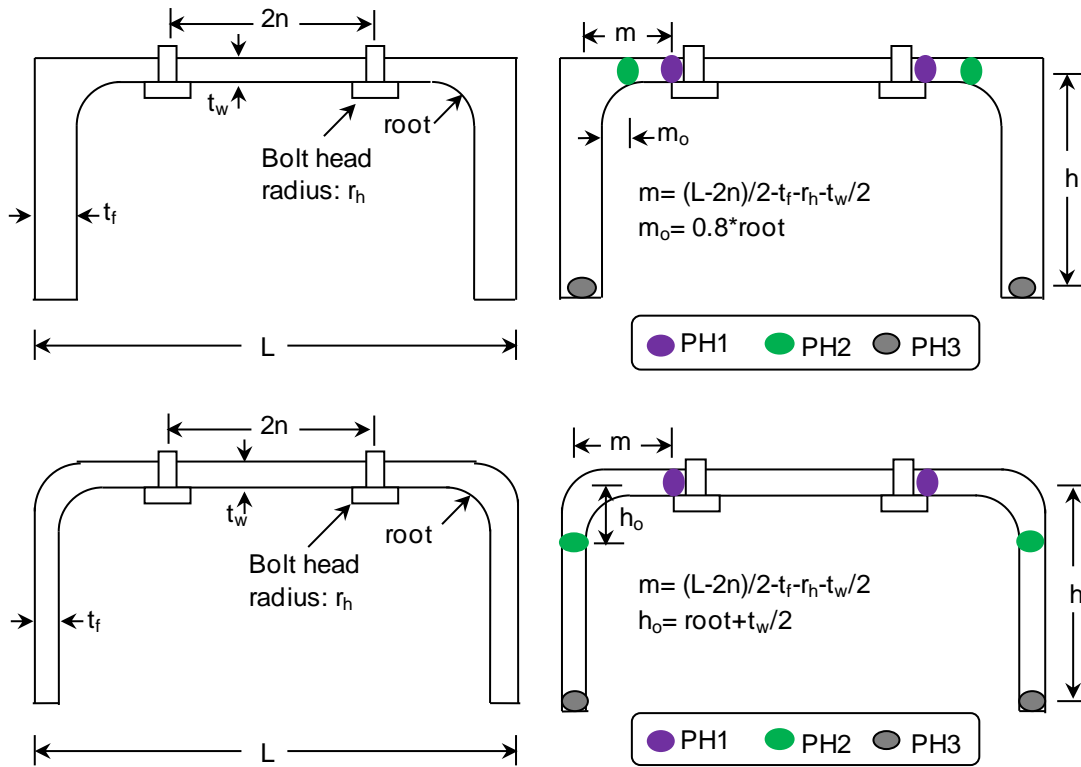
Figure 24: Reverse channel under tension: plastic hinge locations.

a) Cut tube

b) PFC
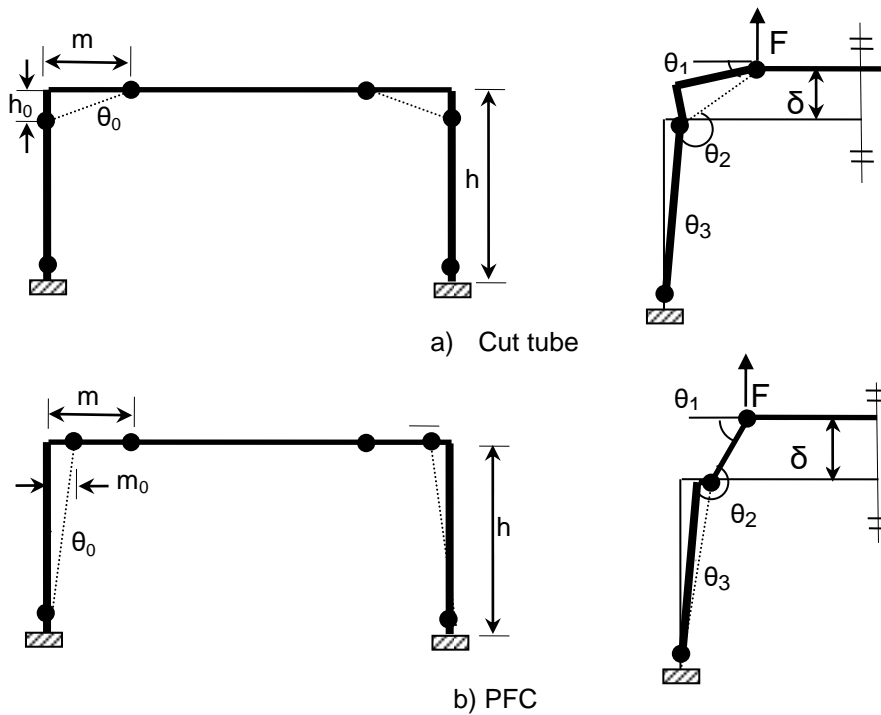
Figure 25: Plastic hinge rotations

For the channel cut from tube, the plastic hinge rotations are calculated as:

$$\theta_1 + \theta_0 = \arcsin\left(\frac{\Delta + (h - h_0)(1 - \cos\theta_3) + h_0}{\sqrt{h_0^2 + m^2}}\right)$$

(3.26)

$$\theta_2 = \theta_1 + \theta_3$$

(3.27)

$$\theta_3 = \arcsin\left(\frac{m - \sqrt{h_0^2 + m^2}\cos(\theta_0 + \theta_1)}{h - h_0}\right)$$

(3.28)

3.3.2   Bolt pull-out 'cone' model mechanism

The bolt pull-out 'cone' model (Figure 26) is a simplified model used to calculate the local deformation of the reverse channel web around a bolt hole before the bolt is pulled out. The work done by the bolt tension force is assumed to be absorbed only by deformation of the reverse channel web; the effect of stress concentrations, cracking around the bolt hole and the non-uniform contact between the reverse channel and the bolt head are beyond the scope of this analysis. Equating the internal absorbed work (W_{total}) to the external work done:

$$W_{total} = F\delta$$

(3.29)

The internal work (W_{total}) in the 'cone model' includes the absorbed energy in the circular plastic hinge ($W_{circular}$), and the strain energy due to the circumferential stretching of the cone wall (W_{strip}).

$$W_{total} = W_{circular} + W_{strip}$$

(3.30)
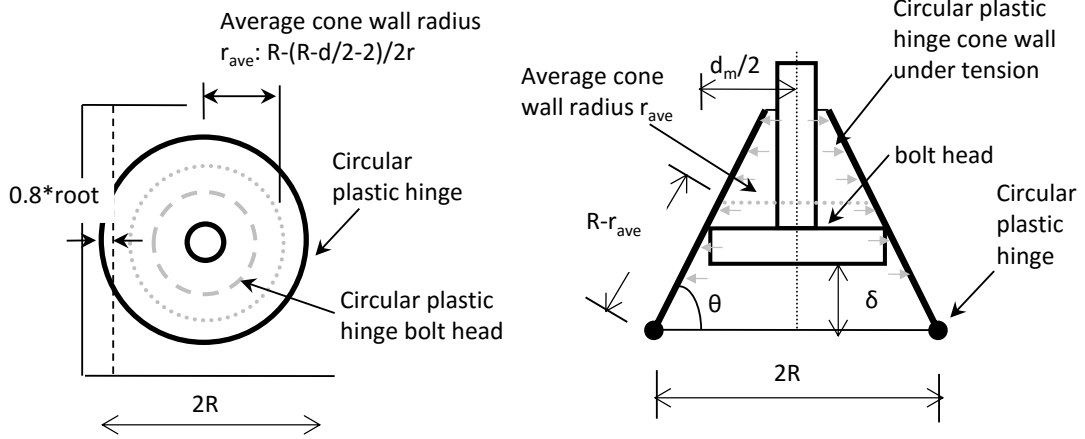
Figure 26: Circular plastic hinge strain energy calculation

For the cone wall under tension, the average width of this area (r_{ave}) is

$$r_{ave} = \left(R - \frac{d}{2} - 2mm \right) / 2$$

(3.31)

In this equation, the d is the bolt shank diameter, and 2mm is the clearance between the bolt hole and the bolt shank.

The average section area is:

$$A = \left(R - \frac{d}{2} - 2 \right) \times t_w$$

(3.32)

Where t_w is the reverse channel web thickness.

The average cone wall radius is:

$$r_{ave} = R - \left(R - \left(\frac{d}{2} + 2 \right) \right) \Big/ 2$$

(3.33)

The average length of the cone wall is:

$$L_{strip} = 2\pi r_{ave}$$

(3.34)

The rotation of the circular plastic hinge is:

$$\theta = \arctan\left(\frac{\delta}{R - d_m / 2} \right)$$

(3.35)

Where d_m is the mean of the dimensions of the bolt head across the points and across the flats.

The average elongation of the cone wall is:

$$\Delta L_{strip} = 2\pi\left(R - \left(R - r_{ave}\right)\cos\theta\right) - L_{strip}$$

(3.36)

The initial axial stiffness is:

$$k = \frac{EA}{L_{strip}}$$

(3.37)

The tangent stiffness is:

$$k_T = \frac{E_T A}{L_{strip}}$$

(3.38)

The Yield resistance is:

$$F_y = f_y A$$

(3.39)

The ultimate resistance is:

$$F_u = f_u A$$

(3.40)

The axial deformation along the bolt pull-out direction at the yield load is:

$$\Delta L_y = F_y / k$$

(3.41)

The axial deformation at the ultimate load is:

$$\Delta L_u = \Delta L_y + \left(F_u - F_y\right) / k_T$$

(3.42)

The work absorbed at a given bolt head movement (δ) is:

$$W_{strip} = \begin{cases} \dfrac{1}{2}k\Delta L_{strip}^2 & \Delta L_{strip} \leq \Delta L_y \\[2mm] \dfrac{F_y^2}{2k} + \dfrac{1}{2}\left(2F_y + k_T\left(\Delta L_{strip} - \Delta L_y\right)\right)\left(\Delta L_{strip} - \Delta L_y\right) & \Delta L_y < \Delta L_{strip} \leq \Delta L_u \\[2mm] \dfrac{F_y^2}{2k} + \dfrac{1}{2}\left(F_y + F_U\right)\left(\Delta L_u - \Delta L_y\right) + F_U\left(\Delta L_{strip} - \Delta L_u\right) & L_{strip} > \Delta L_u \end{cases}$$

(3.43)

Figure 26 shows the principles of the rotation calculation for $W_{circular}$, where

$$W_{circular} = M_p \times 2\pi R \times \theta = \left(\frac{f_y \times t_p^2}{4}\right)\theta \tag{3.44}$$

When the bolt is pulled out (Figure 28), the cone wall rotation (θ at unit of radians) reaches its maximum (θ_{max}):

$$\theta_{max} = \arccos\left(\frac{R - \dfrac{d_m}{2}}{R - \dfrac{d}{2} - 2}\right) \tag{3.45}$$

The bolt head maximum movement (δ_{max}) is:

$$\delta_{max} = \left(R - \frac{d}{2} - 2\right)\sin\theta_{max} \tag{3.46}$$

Therefore, the Force (F) is:

$$F_{max} = \frac{W_{total}}{\delta} \tag{3.47}$$

Accordingly, the bolt pull-out limit (F_{max}) is:

$$F_{max} = \frac{W_{total,max}}{\delta_{max}} \tag{3.48}$$
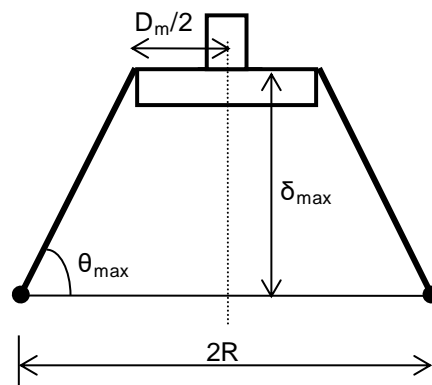
Figure 27: Cone model for bolt pull-out limit.

3.4   Validation of the plastic hinge model for reverse channel under tension

A wide-ranging validation was performed using a series of tests and FEA simulations on reverse channels of various geometries for ambient and elevated temperatures. In COMPFIRE (RFCS, 2012a), a set of component tests on reverse channels under tension were

performed by the Universities of Manchester and Coimbra with the aim of providing experimental data to characterize the behaviour of the reverse channel under tension. Following the test setup, the preliminary finite element model was simulated by the author using ABAQUS, to investigate the reverse channel under tension behaviour. Based on the tests in COMPFIRE, a further intensive FEA parametric study was conducted by Luleå Technical University to investigate all possible modes of behaviour (RFCS, 2012a).

All the test and analysis results are represented as force/displacement curves (using the measurements shown in Figure 28). The force is the total reaction force at the base of the reverse channel, and the displacement is the movement measured at the bolt. In order to investigate the 'cone model' contribution (the displacement due to the bolt being pulled through the bolt hole), a force/displacement curve is also plotted for some of the tests, for which the deformation is the local displacement of the bolt.
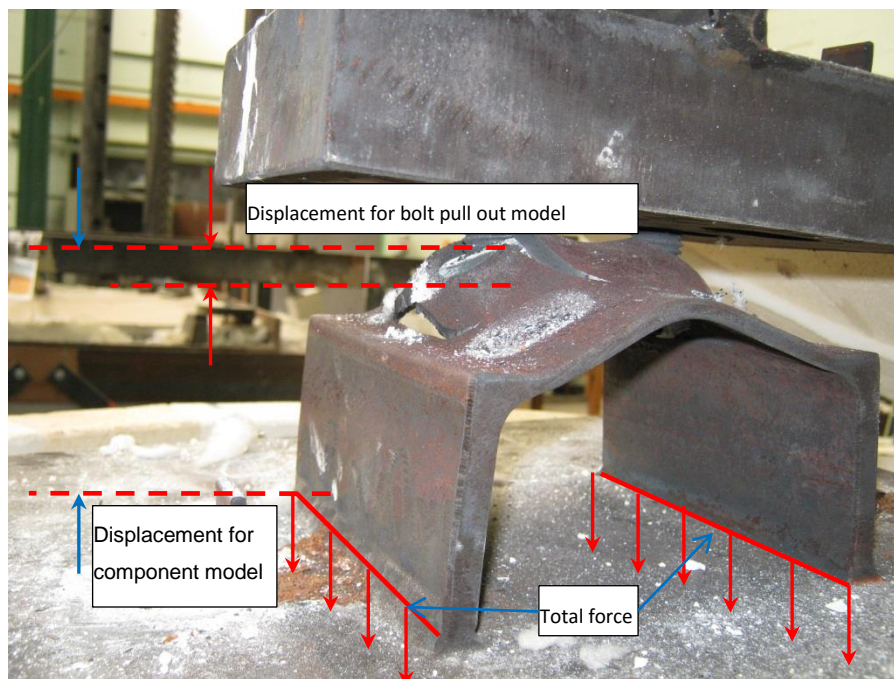
Figure 28: Displacement measurements for the component model validation.

3.4.1 Preliminary finite element simulation

While the University of Manchester was conducting the reverse channel component test (shown in Figure 29), a preliminary finite element model was created to investigate the behaviour of the reverse channel under tension. This preliminary finite element model was general in nature, but was particularly focused on Test 7 (RCT 7).

Figure 29: Manchester componest test setup (RFCS, 2012a)
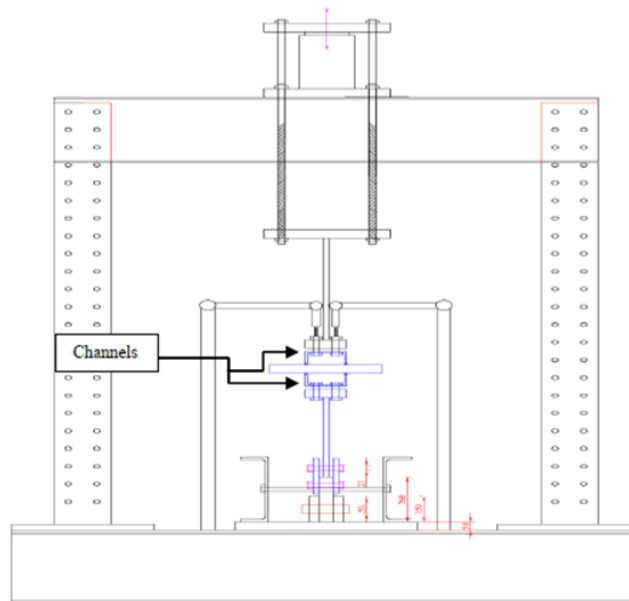
Figure 30: Manchester componest test rig arrangement (RFCS, 2012a)

To conduct the component tests, the University of Manchester designed the test rig which is shown in Figure 30. This consisted of two side columns providing reaction forces for two opposed channels (shown in Figure 31). The tensile force on the channels was applied via hydraulic jack, supported by the top cross-beam.
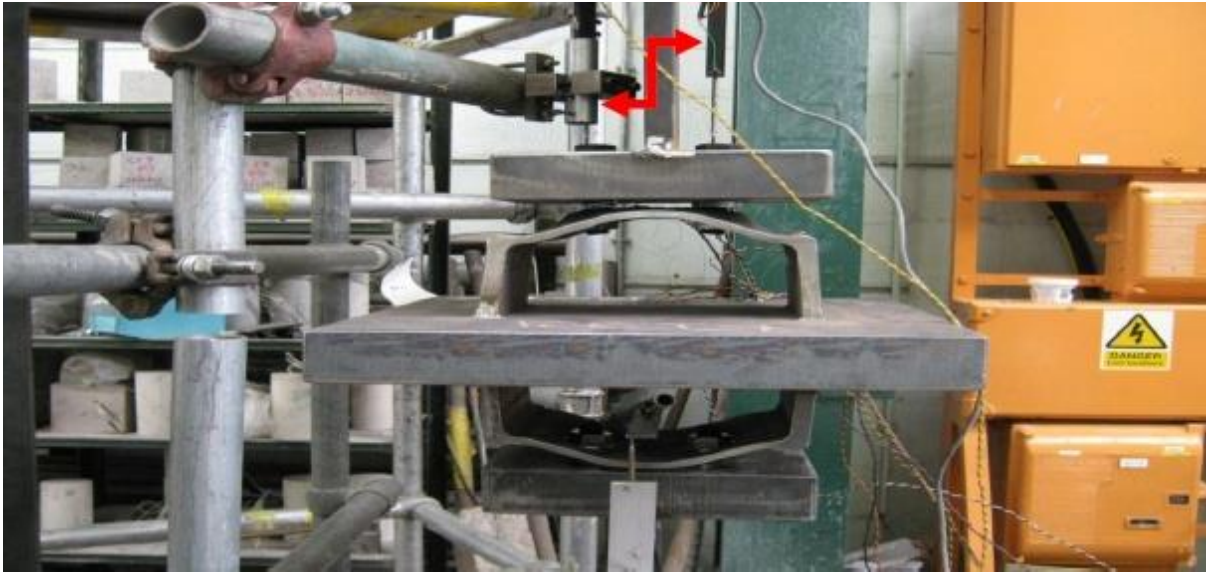
Figure 31: detailed view of tested channels in a Manchester component test (RFCS, 2012a)

Figure 32 shows the FE model setup, which was created using ABAQUS Dynamic/Explicit. It adopted the methodology and material properties in Yu (2008b). All the elements used the element type C3D8R, which are 8-noded solid (brick) elements. Figure 33 shows a sectional view of the FE model. In order to save computation time, boundary conditions representing an axis of symmetry were applied. A fixed boundary was applied at the reverse channel leg, and vertical movement was applied at the top of the bolt. In order to simulate the contact between bolt head and the channel web, a 1mm gap was initially assumed.
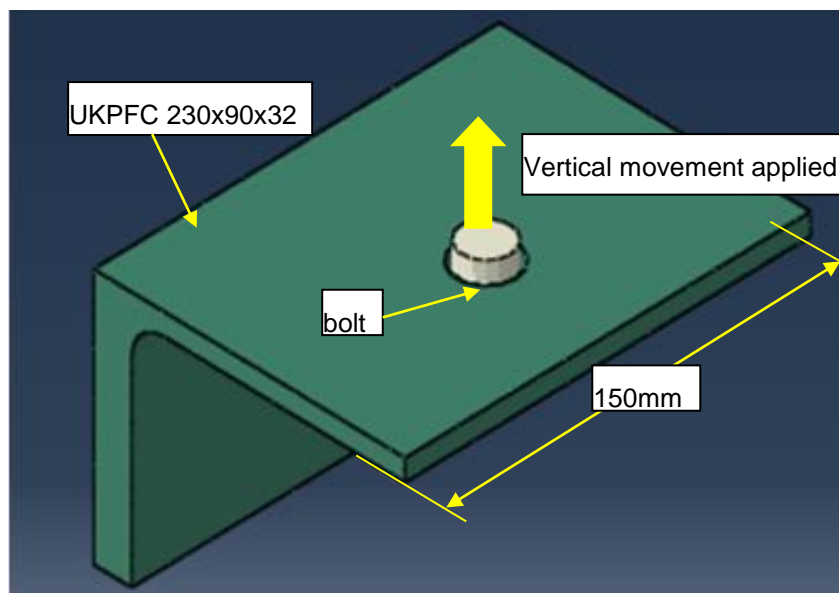
Figure 32: FE model of Manchester RCT-7 test 9 (3D view)
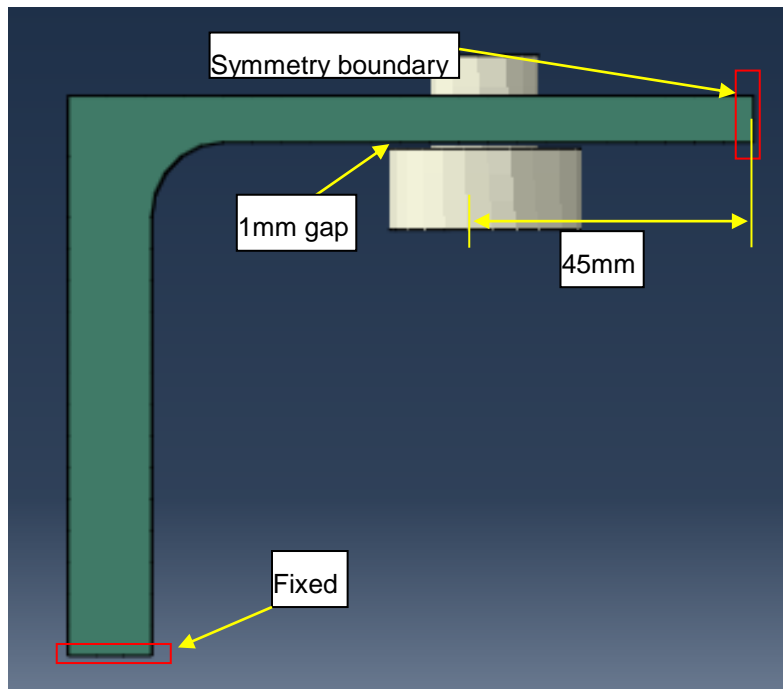
Figure 33: FE model of Manchester RCT-7 test 9 (side view)

Figure 34 shows the deformed channel at a relatively early stage of the analysis. The dashed line shows the straight-line idealisation of the plastic hinge mechanism. The channel leg is rotating inwards, and has one plastic hinge near to its bottom. One of the plastic hinges is located at the inner side of the bolt head; another plastic hinge is located near to the root radius on the channel flange. The bolt shank comes into contact with the bolt hole inner side, and is slightly bent, which is also shown in the 3D view (Figure 35).
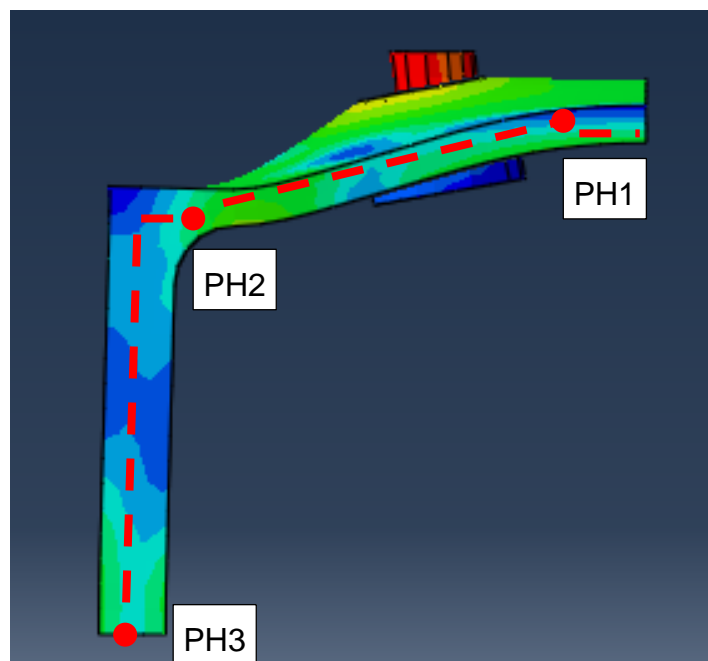
Figure 34: Mancheser RCT-7 test preliminary model deformed shape 1
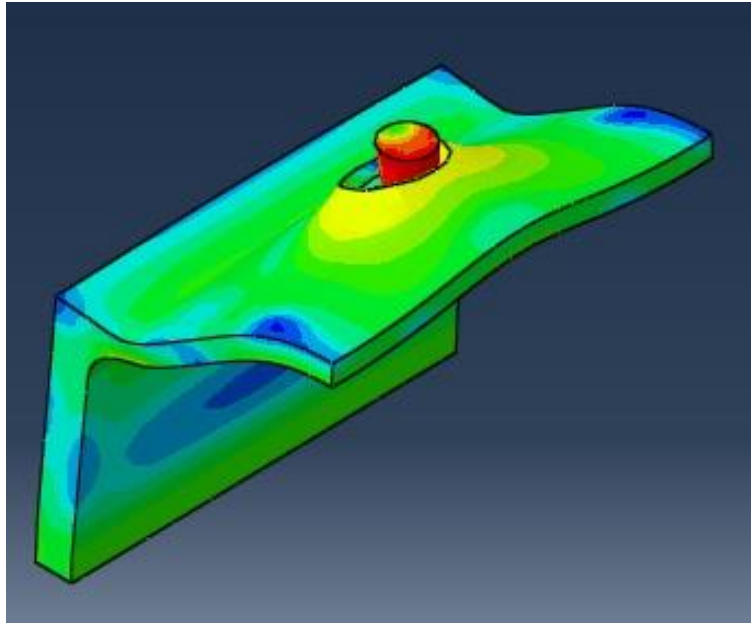
Figure 35: Mancheser RCT-7 test preliminary model deformed shape 2

Figure 36 shows the deformations at the end of the simulation, after the bolt has completely pulled out. The bolt hole is then conical, which is also highlighted in Figure 37.
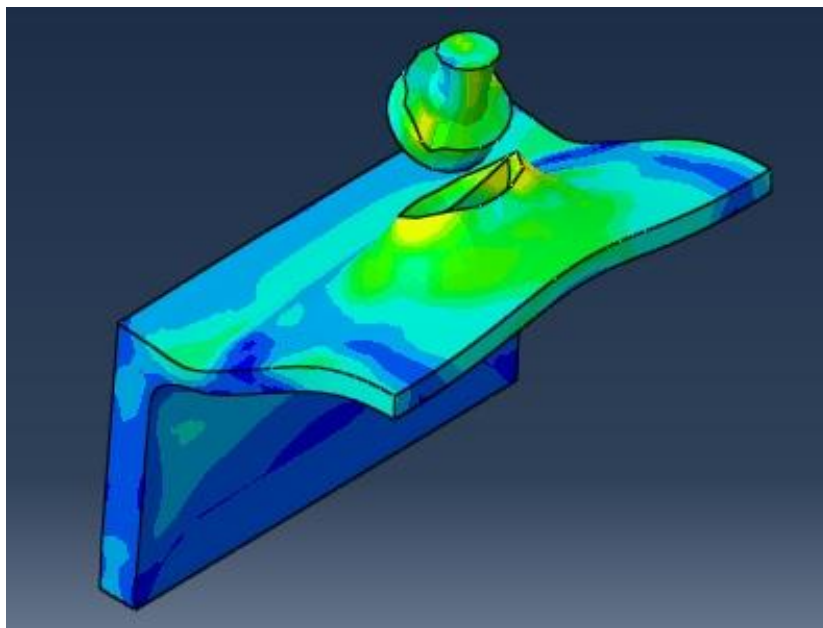
Figure 36: Mancheser RCT-7 test preliminary model deformed shape 3

Figure 38 shows a comparison of the force/displacement predictions against the test results. The force plotted is the total reaction at the reverse channel leg base, and the displacement is the upward movement of the bolt head.
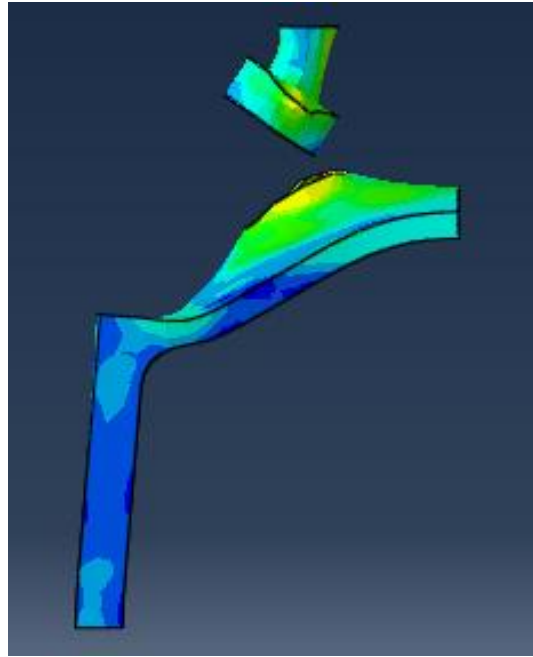
Figure 37: Mancheser RCT-7 test preliminary model deformed shape 4

The Force/Displacement (F/D) curve from the Finite element model starts from 1mm, at which the assigned gap between the bolt head and channel web is fully closed and contact force is transmitted. The F/D curve from the FE model is nearly of the same shape as that given by the test. The peak reaction force occurs when the bolt has very nearly been pulled out. The predicted bolt pull-out limit from the ABAQUS model is also very close to that experienced in the test. This comparison at least partly validates the FE model. The detailed information given by the FE model shows the process of bolt pull-out, and the gradual combination of deformation from the "straight-line" plastic hinge mechanism and the local "cone" model representing bolt pull-out.

It can be summarized from Figure 38 that, if the initial gap imposed in the FE model is closed-up, the experimental and modelling curves very nearly coincide, although the peak load in the test produces a very sudden drop-off in force, probably because the test setup is not sufficiently stiff to allow a gradual negative-stiffness path to be stable.

3.4.2 *Selected tests conducted by the University of Manchester*

One test result (RCT7) from Manchester, which measured the reverse channel deformation, can be used directly for component model validation. The key parameters are shown in Table 4.

Table 4: Material properties in Manchester component test RCT7

Test No.	Element	Coupon position	Thickness (mm)	E (N/mm^2)	E$_t$ (N/mm^2)	f$_y$ (N/mm^2)	f$_u$ (N/mm^2)
RCT-7	UKPFC 230x90x32	Web	7.5	190190.4	6035	442.11	669.48
		Flange	14	186669.9	6008	416.21	643.142

The force-displacement relationship for the reverse channel (RCT7) given by the component model is compared with the test data in Figure 39.

The bolt pull-out model's contribution to the deflection is shown in green, and the total component model deflection is shown in blue. The component model clearly successfully captures the stage at which the first plastic hinge forms. After the formation of the first plastic hinge, the component's stiffness is reduced considerably. This is because, beyond this stage, the reverse channel web contributes most to the overall component model deformation.
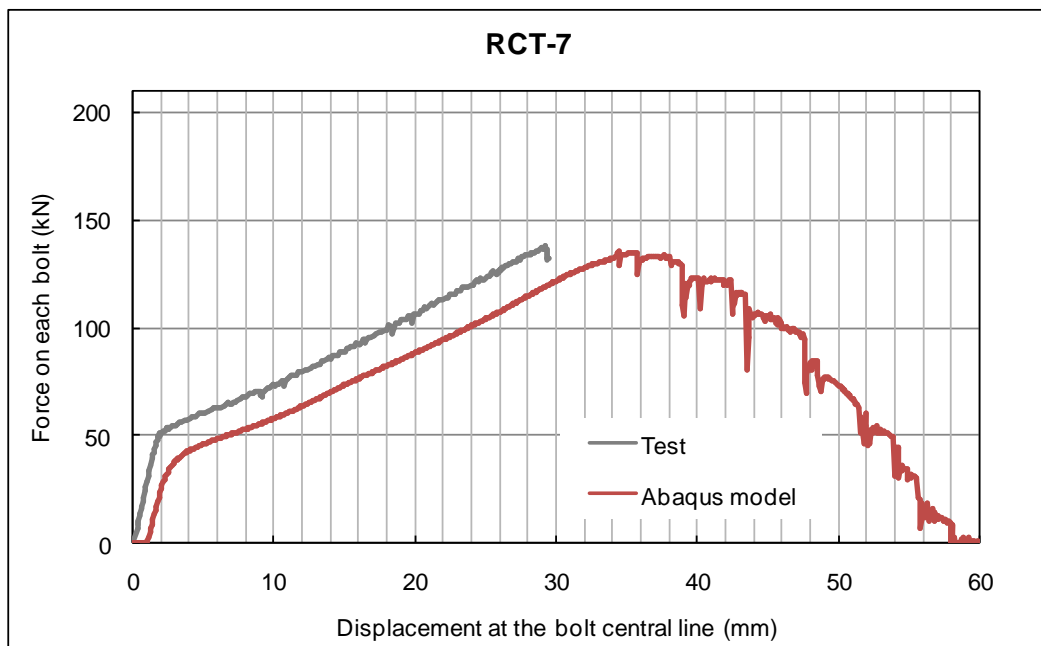
Figure 38: Mancheser RCT-7 test preliminary FE model .vs. test results

Figure 39 includes local deformation of the bolt hole at any applied force level. When the bolt is nearly pulled out, the local deformation contributes about two thirds of the component deformation. This can be seen from the test photograph (shown as Figure 40). The final deformed shape combines the straight-line plastic hinge mechanism and the cone model around the bolt hole, both of which are highlighted on Figure 40.
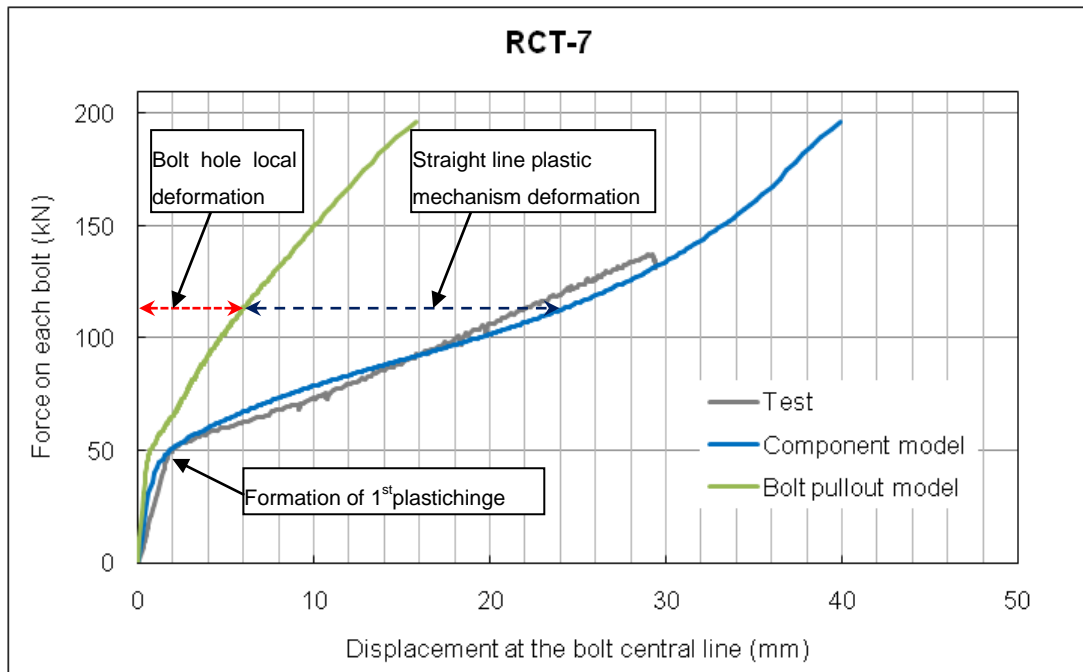
Figure 39: Component model for reverse channel under tension component model and bolt pull-out model validation against Manchester test RCT-7.
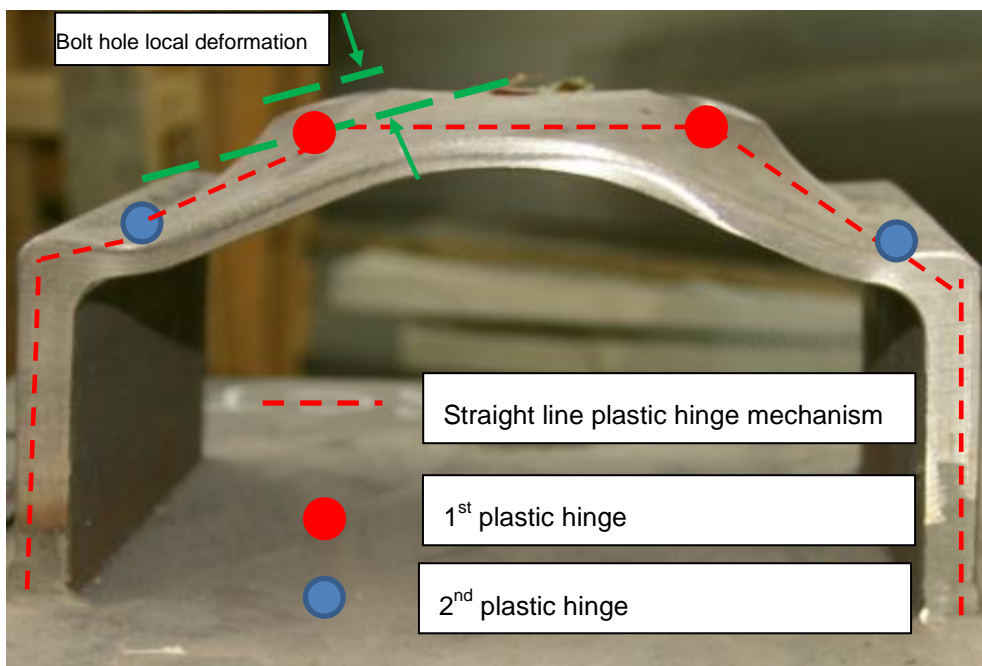
Figure 40: Post-test photograph of Manchester test RCT-7 (RFCS, 2012a).

3.4.3 Selected tests conducted at The University of Coimbra

The component model validation against a selection of the tests conducted by the University of Coimbra (defined in Table 5) uses the verified FEA simulation results from Luleå Technical University (RFCS, 2012a). The bolt pull-out model prediction is plotted in

Figure 41 to show the contribution that local bolt hole deformation makes at each applied force level.

Table 5: Reverse channel component tests conducted by the University of Coimbra

Test N.	Reverse channel section	section type	applied load	Test Temp (°C)	Steel grade	h(mm)	tw(mm)	tf(mm)
1	202x90x7	Welded	Tension	20	S275	202	7	15
2	202x90x10	Welded	Tension	20	S275	202	10	15
3	202x90x12	Welded	Tension	20	S275	202	12	15
15	200x90x8	Cut tube	Tension	20	S355	200	8	8
16	200x90x10	Cut tube	Tension	20	S355	200	10	10
17	200x90x12	Cut tube	Tension	20	S275	200	12	12
18	UPN200	Rolled	Tension	20	S275	200	8.5	11.5

In tests 1, 2, 3 and 18 (shown in Figure 41), the bolt pull-out model prediction is close to that of the component model, which means that the reverse channel is relatively stiff.

In the Coimbra component tests, the bolt separation was 85mm with M24 bolts. The reverse channels in tests 1, 2, 3 and 18 have thicker legs, Therefore, the bolt head is close to the reverse channel's root zone. As the result of this, the straight plastic hinge mechanism has barely formed, and the bolt pull-out model dominates.
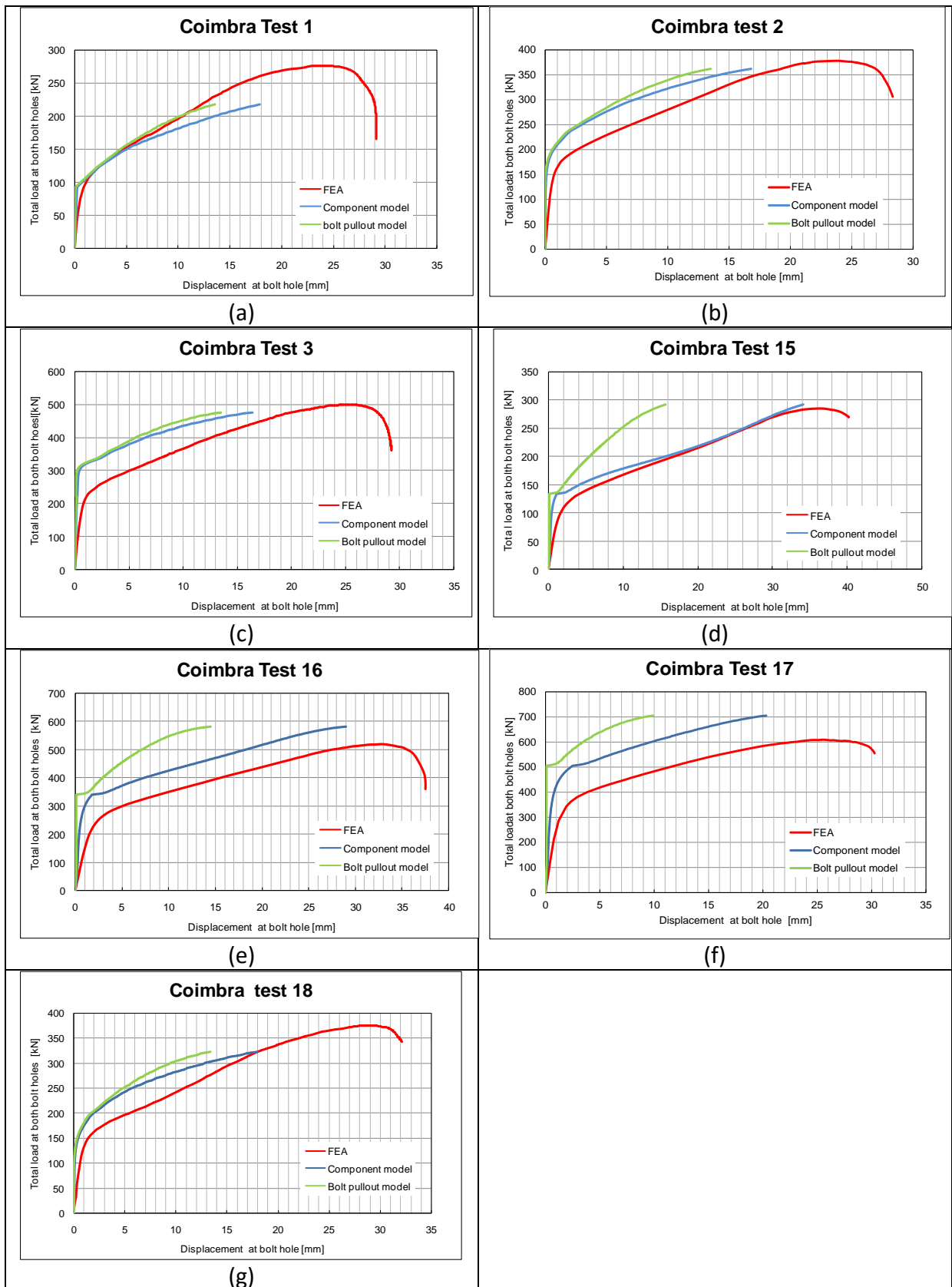
Figure 41: reverse channel under tension component model and bolt pull-out model validation against Coimbra tests.

3.4.4 Further parametric studies

The COMPFIRE component tests provide a good opportunity to validate the component model. The following parametric study aims to expand the component test data further to investigate the reverse channel behaviour at both ambient and elevated temperatures. All the parametric FEA analyses were conducted by Tim Heistermann from Luleå University of Technology.

Table 6 to Table 12 list the parametric study simulations. The SHS 350x8 cut-tube section, with leg length 90mm ('h' shown in Figure 42) is selected as a benchmark. Two general types of reverse channel (PFC and tube-cut) are considered. All the tests are analysed for both tension and compression cases.
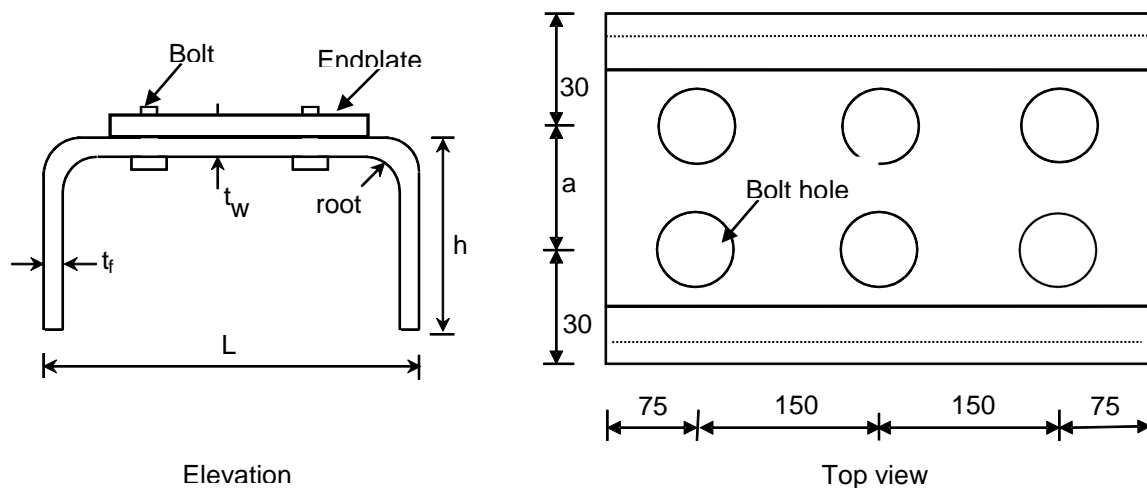
Figure 42: Reverse channel parametric studies layout (showing three bolt rows)

For the tension tests, analyses were intended to carry on up to bolt pull-out. As the bolt pull-out limit was beyond the specification of this parametric study, these FEA results do not necessarily show the maximum resistance, and were often stopped due to solution convergence problems. From this parametric study, the general locations and formation of plastic hinges in the reverse channel under tension/compression can be identified at intermediate stages of loading, using the strain contours. This identification is difficult to capture accurately from experimental component tests.

Table 6: Component model parametric study List 1

NO.	Section	Reverse Channel						Endplate Size			Bolt Size (mm)	Bolt rows	a^1(mm)	distance between bolt rows (mm)	temp (°C)	Note
		Flange Length L(mm)	Flange Thickness tw(mm)	Leg Length H(mm)	Leg Thickness tf(mm)	Root (mm)	Length beff(mm)	Width (mm)	Length (mm)	Thickness (mm)						
1	350X8 (cut)	350	8	60	8	12/8	150	150	150	20	20	1	90	150	20	one bolt row
2	350X8 (cut)	350	8	90	8	12/8	150	150	150	20	20	1	90	150	20	
3	350X8 (cut)	350	8	120	8	12/8	150	150	150	20	20	1	90	150	20	
4	350X8 (cut)	350	8	60	8	12/8	150	210	150	20	20	1	150	150	20	
5	350X8 (cut)	350	8	90	8	12/8	150	210	150	20	20	1	150	150	20	
6	350X8 (cut)	350	8	120	8	12/8	150	210	150	20	20	1	150	150	20	
7	350X8 (cut)	350	8	60	8	12/8	150	270	150	20	20	1	210	150	20	
8	350X8 (cut)	350	8	90	8	12/8	150	270	150	20	20	1	210	150	20	
9	350X8 (cut)	350	8	120	8	12/8	150	270	150	20	20	1	210	150	20	
10	350X8 (cut)	350	8	60	8	12/8	150	330	150	20	20	1	270	150	20	
11	350X8 (cut)	350	8	90	8	12/8	150	330	150	20	20	1	270	150	20	
12	350X8 (cut)	350	8	120	8	12/8	150	330	150	20	20	1	270	150	20	

Table 7: Component model parametric study List 2

NO.	Reverse Channel							Endplate Size			Bolt Size (mm)	Bolt rows	a^1(mm)	distance between bolt rows (mm)	temp (°C)	note
	Section	Flange Length L(mm)	Flange Thickness tw(mm)	Leg Length H(mm)	Leg Thickness tf(mm)	Root (mm)	Length beff(mm)	Width (mm)	Length (mm)	Thickness (mm)						
13	350X8 (cut)	350	8	90	8	12/8	300	150	300	20	20	2	90	150	20	two bolt rows
14	350X8 (cut)	350	8	90	8	12/8	300	210	300	20	20	2	150	150	20	
15	350X8 (cut)	350	8	90	8	12/8	300	270	300	20	20	2	210	150	20	
16	350X8 (cut)	350	8	90	8	12/8	300	330	300	20	20	2	270	150	20	
17	350X8 (cut)	350	8	90	8	12/8	450	150	450	20	20	3	90	150	20	three bolt rows
18	350X8 (cut)	350	8	90	8	12/8	450	210	450	20	20	3	150	150	20	
19	350X8 (cut)	350	8	90	8	12/8	450	270	450	20	20	3	210	150	20	
20	350X8 (cut)	350	8	90	8	12/8	450	330	450	20	20	3	270	150	20	
21	350X8 (cut)	350	8	90	8	12/8	150	210	150	20	20	1	150	150	450	one bolt row at elevated temperature
22	350X8 (cut)	350	8	90	8	12/8	150	270	150	20	20	1	210	150	450	
23	350X8 (cut)	350	8	90	8	12/8	150	210	150	20	20	1	150	150	550	
24	350X8 (cut)	350	8	90	8	12/8	150	270	150	20	20	1	210	150	550	

Table 8: Component model parametric study List 3

NO.	Section	Reverse Channel Flange Length L(mm)	Flange Thickness tw(mm)	Leg Length H(mm)	Leg Thickness tf(mm)	Root (mm)	Length beff(mm)	Endplate Size Width (mm)	Length (mm)	Thickness (mm)	Bolt Size (mm)	Bolt rows	a¹(mm)	distance between bolt rows (mm)	temp (°C)	note
25	350X8 (cut)	350	8	90	8	12/8	150	210	150	20	20	1	150	150	650	one bolt row at elevated temperature
26	350X8 (cut)	350	8	90	8	12/8	150	270	150	20	20	1	210	150	650	
27	350X8 (cut)	350	8	90	8	12/8	150	210	150	20	20	1	150	150	750	
28	350X8 (cut)	350	8	90	8	12/8	150	270	150	20	20	1	210	150	750	
29	350X8 (cut)	350	8	90	8	12/8	150	210	150	20	20	3	150	150	450	three bolt rows at elevated temperature
30	350X8 (cut)	350	8	90	8	12/8	150	270	150	20	20	3	210	150	450	
31	350X8 (cut)	350	8	90	8	12/8	150	210	150	20	20	3	150	150	550	
32	350X8 (cut)	350	8	90	8	12/8	150	270	150	20	20	3	210	150	550	
33	350X8 (cut)	350	8	90	8	12/8	150	210	150	20	20	3	150	150	650	
34	350X8 (cut)	350	8	90	8	12/8	150	270	150	20	20	3	210	150	650	
35	350X8 (cut)	350	8	90	8	12/8	150	210	150	20	20	3	150	150	750	
36	350X8 (cut)	350	8	90	8	12/8	150	270	150	20	20	3	210	150	750	

Table 9: Component model parametric study List 4

NO.	Section	Reverse Channel						Endplate Size			Bolt Size (mm)	Bolt rows	a^1(mm)	distance between bolt rows (mm)	temp (°C)	note
		Flange Length L(mm)	Flange Thickness tw(mm)	Leg Length H(mm)	Leg Thickness tf(mm)	Root (mm)	Length beff(mm)	Width (mm)	Length (mm)	Thickness (mm)						
37	350X8 (cut)	350	8	60	8	12/8	150	150	150	10	20	1	90	150	20	endplate thickness effect
38	350X8 (cut)	350	8	90	8	12/8	150	150	150	10	20	1	90	150	20	
39	350X8 (cut)	350	8	120	8	12/8	150	150	150	10	20	1	90	150	20	
40	350X8 (cut)	350	8	60	8	12/8	150	210	150	10	20	1	150	150	20	
41	350X8 (cut)	350	8	90	8	12/8	150	210	150	10	20	1	150	150	20	
42	350X8 (cut)	350	8	120	8	12/8	150	210	150	10	20	1	150	150	20	
43	350X8 (cut)	350	8	60	8	12/8	150	270	150	10	20	1	210	150	20	
44	350X8 (cut)	350	8	90	8	12/8	150	270	150	10	20	1	210	150	20	
45	350X8 (cut)	350	8	120	8	12/8	150	270	150	10	20	1	210	150	20	
46	350X8 (cut)	350	8	60	8	12/8	150	330	150	10	20	1	270	150	20	
47	350X8 (cut)	350	8	90	8	12/8	150	330	150	10	20	1	270	150	20	
48	350X8 (cut)	350	8	120	8	12/8	150	330	150	10	20	1	270	150	20	

Table 10: Component model parametric study List 5

NO.	Reverse Channel							Endplate Size			Bolt Size (mm)	Bolt rows	a^1(mm)	distance between bolt rows (mm)	temp (°C)	note
	Section	Flange Length L(mm)	Flange Thickness tw(mm)	Leg Length H(mm)	Leg Thickness tf(mm)	Root (mm)	Length beff(mm)	Width (mm)	Length (mm)	Thickness (mm)						
49	350X8 (cut)	350	10	60	10	15/10	150	150	150	20	20	1	90	150	20	RC Thickness 1
50	350X8 (cut)	350	10	90	10	15/10	150	150	150	20	20	1	90	150	20	
51	350X8 (cut)	350	10	120	10	15/10	150	150	150	20	20	1	90	150	20	
52	350X8 (cut)	350	10	60	10	15/10	150	210	150	20	20	1	150	150	20	
53	350X8 (cut)	350	10	90	10	15/10	150	210	150	20	20	1	150	150	20	
54	350X8 (cut)	350	10	120	10	15/10	150	210	150	20	20	1	150	150	20	
55	350X8 (cut)	350	10	60	10	15/10	150	270	150	20	20	1	210	150	20	
56	350X8 (cut)	350	10	90	10	15/10	150	270	150	20	20	1	210	150	20	
57	350X8 (cut)	350	10	120	10	15/10	150	270	150	20	20	1	210	150	20	
58	350X8 (cut)	350	10	60	10	15/10	150	330	150	20	20	1	270	150	20	
59	350X8 (cut)	350	10	90	10	15/10	150	330	150	20	20	1	270	150	20	
60	350X8 (cut)	350	10	120	10	15/10	150	330	150	20	20	1	270	150	20	

Table 11: Component model parametric study List 6

NO.	Section	Reverse Channel						Endplate Size			Bolt Size (mm)	Bolt rows	a^1(mm)	distance between bolt rows (mm)	temp (°C)	note
		Flange Length L(mm)	Flange Thickness tw(mm)	Leg Length H(mm)	Leg Thickness tf(mm)	Root (mm)	Length beff(mm)	Width (mm)	Length (mm)	Thickness (mm)						
61	350X8 (cut)	350	12	60	12	18/12	150	150	150	20	20	1	90	150	20	RC Thickness 2
62	350X8 (cut)	350	12	90	12	18/12	150	150	150	20	20	1	90	150	20	
63	350X8 (cut)	350	12	120	12	18/12	150	150	150	20	20	1	90	150	20	
64	350X8 (cut)	350	12	60	12	18/12	150	210	150	20	20	1	150	150	20	
65	350X8 (cut)	350	12	90	12	18/12	150	210	150	20	20	1	150	150	20	
66	350X8 (cut)	350	12	120	12	18/12	150	210	150	20	20	1	150	150	20	
67	350X8 (cut)	350	12	60	12	18/12	150	270	150	20	20	1	210	150	20	
68	350X8 (cut)	350	12	90	12	18/12	150	270	150	20	20	1	210	150	20	
69	350X8 (cut)	350	12	120	12	18/12	150	270	150	20	20	1	210	150	20	
70	350X8 (cut)	350	12	60	12	18/12	150	330	150	20	20	1	270	150	20	
71	350X8 (cut)	350	12	90	12	18/12	150	330	150	20	20	1	270	150	20	
72	350X8 (cut)	350	12	120	12	18/12	150	330	150	20	20	1	270	150	20	

Table 12: Component model parametric study List 7

NO.	Section	Reverse Channel						Endplate Size			Bolt Size (mm)	Bolt rows	a[1](mm)	distance between bolt rows (mm)	temp (°C)	note
		Flange Length L(mm)	Flange Thickness tw(mm)	Leg Length H(mm)	Leg Thickness tf(mm)	Root (mm)	Length beff(mm)	Width (mm)	Length (mm)	Thickness (mm)						
73	PFC 200x90x30	200	7	90	14	12	150	200	150	20	20	1	90	150	20	PFC .VS. tube-cut (all the tube-cut section are invented for comparison) [1]
74	200x7 (cut)	200	7	90	7	10.5/7	150	200	150	20	20	1	90	150	20	
75	PFC 230x90x32	230	7.5	90	14	12	150	200	150	20	20	1	90	150	20	
76	230x7.5 (cut)	230	7.5	90	7.5	11.25/7.5	150	200	150	20	20	1	90	150	20	
77	PFC 260x90x35	260	8	90	14	12	150	200	150	20	20	1	90	150	20	
78	260x8(cut)	260	8	90	8	8/12	150	200	150	20	20	1	90	150	20	
79	PFC 300x90x41	300	9	90	15.5	12	150	200	150	20	20	1	90	150	20	
80	300x9 (cut)	300	9	90	9	13.5/9	150	200	150	20	20	1	90	150	20	
81	PFC 380x100x54	380	9.5	100	17.5	15	150	250	150	20	20	1	90	150	20	
82	380x9.5(cut)	380	9.5	100	9.5	14.25/9.5	150	250	150	20	20	1	90	150	20	
83	PFC 430X100x64	430	11	100	19	15	150	250	150	20	20	1	90	150	20	
84	430x11(cut)	430	11	100	11	16.5/11	150	250	150	20	20	1	90	150	20	

This investigation includes the effects on strength, stiffness and failure mechanism of the following parameters:

- Leg length ('*h*' in Figure 42);

- Bolt separation ('*a*' in Figure 42);

- Endplate thickness;

- Reverse channel thickness (flange thickness 't_w' and web thickness 't_f' in Figure 42);

- Rolled channel (PFC) or constant-thickness channel cut from a tube;

- Group effects;

- Temperature.

The detailed results of the validation studies for the reverse channel under tension are presented in Figure 43 to Figure 55. Comparing the model with the tests and FEA analyses, the component model generally predicts the behaviour of the reverse channel under tension with an accuracy that is acceptable for simplified modelling.
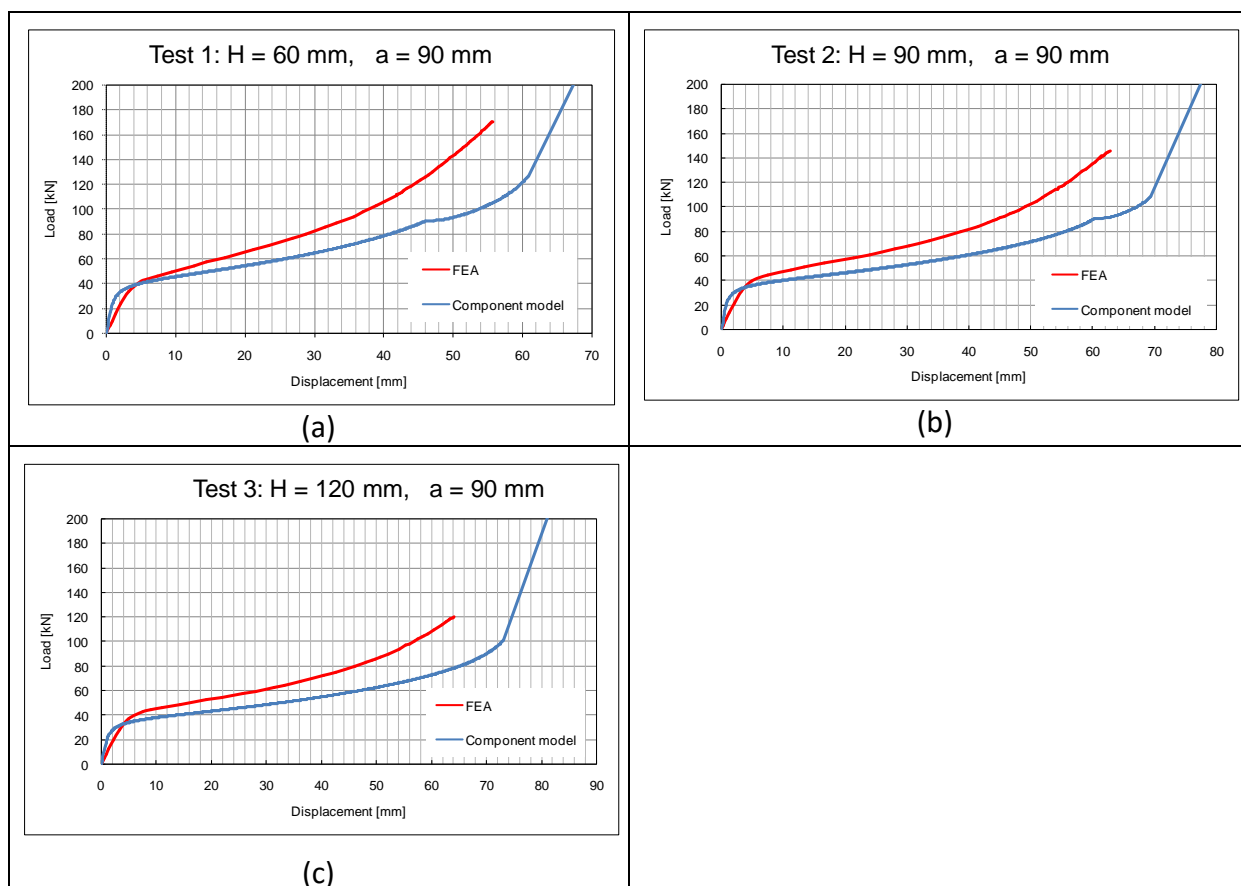
Figure 43: RC-in-Tension component model: parametric studies (Tests1-3)
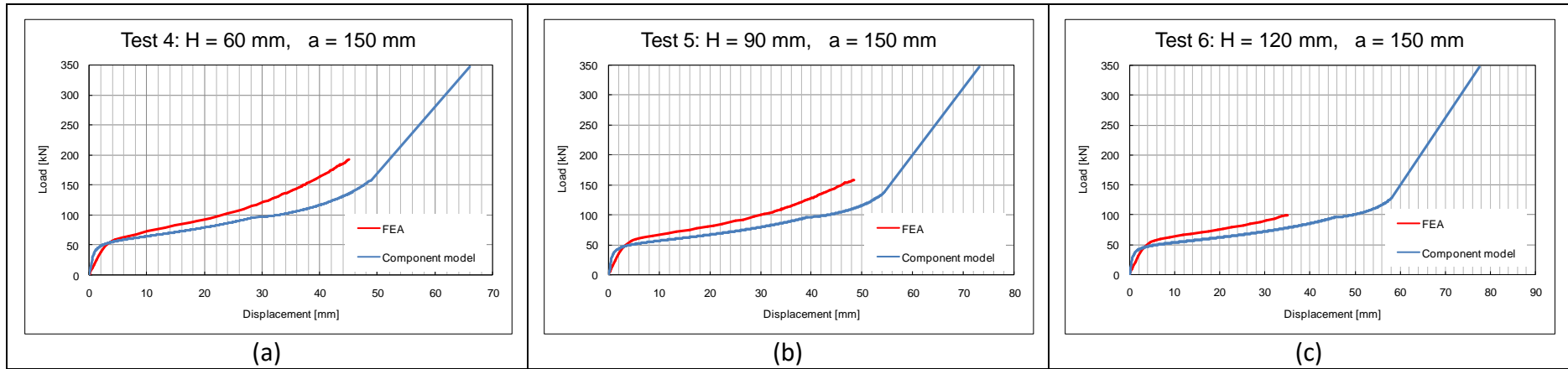
Figure 44: RC-in-Tension component model: parametric studies (Tests4-6)
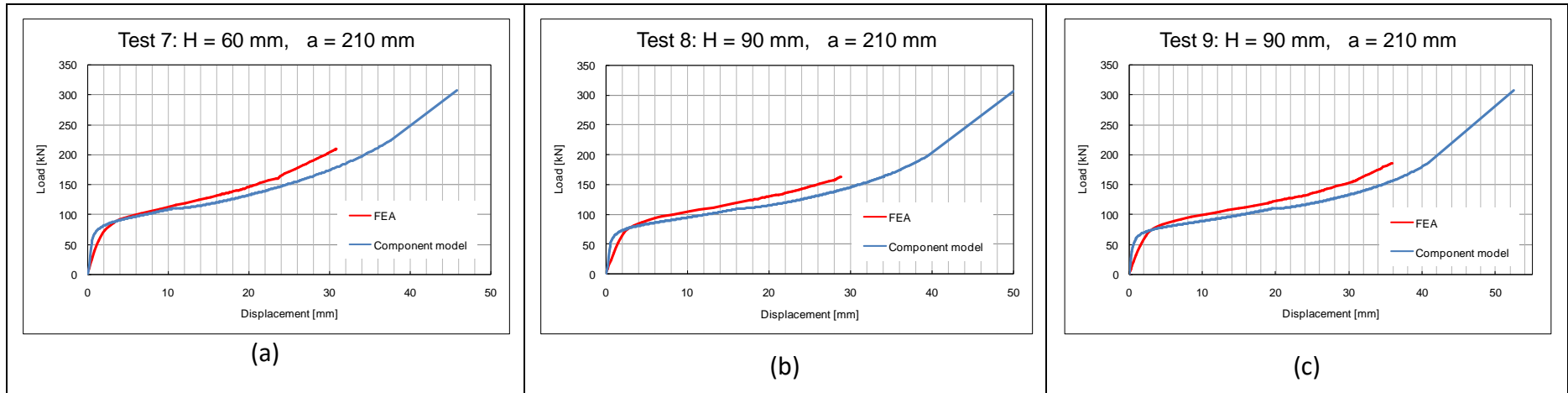
Figure 45: RC-in-Tension component model: parametric studies (Tests7-9)
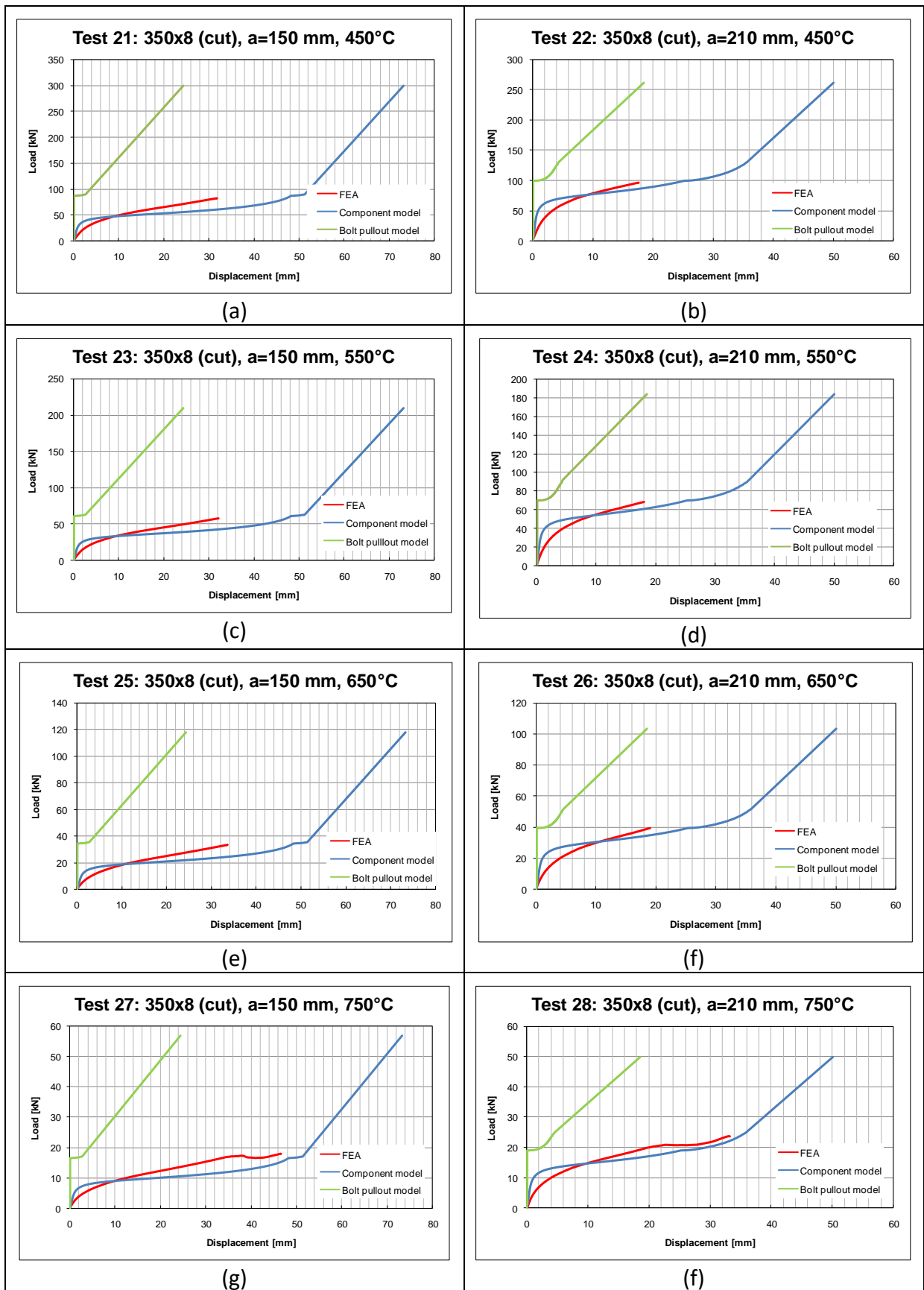
Figure 46: RC-in-Tension component model: parametric studies (Tests21-28)
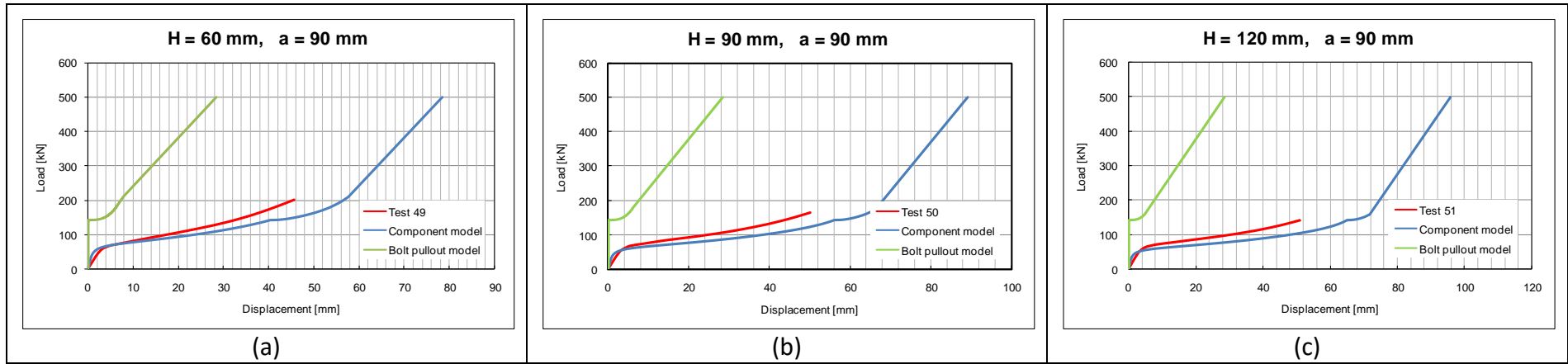
Figure 47: RC-in-Tension component model: parametric studies (Tests49-51)
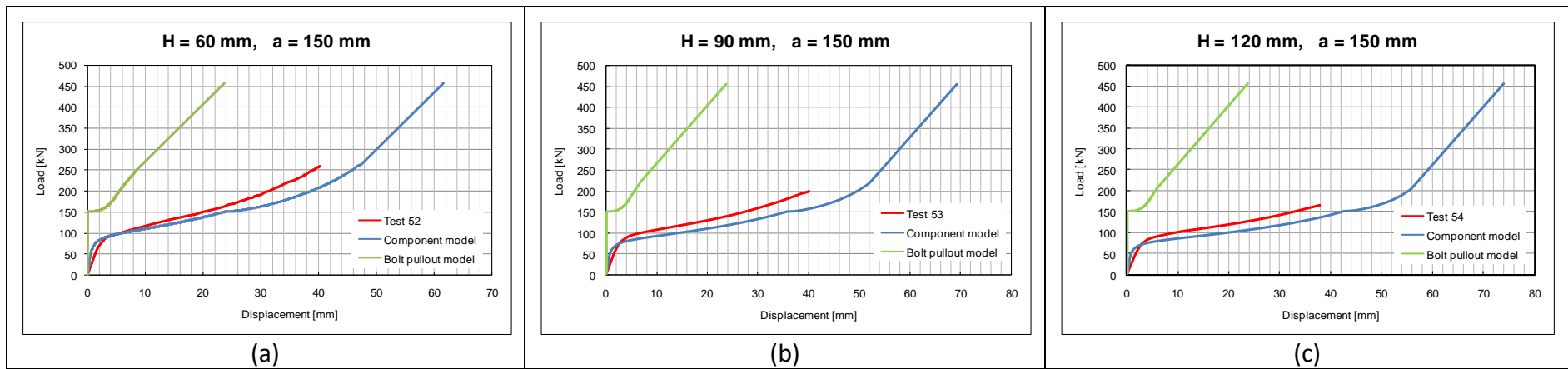
Figure 48: RC-in-Tension component model: parametric studies (Tests52-54)
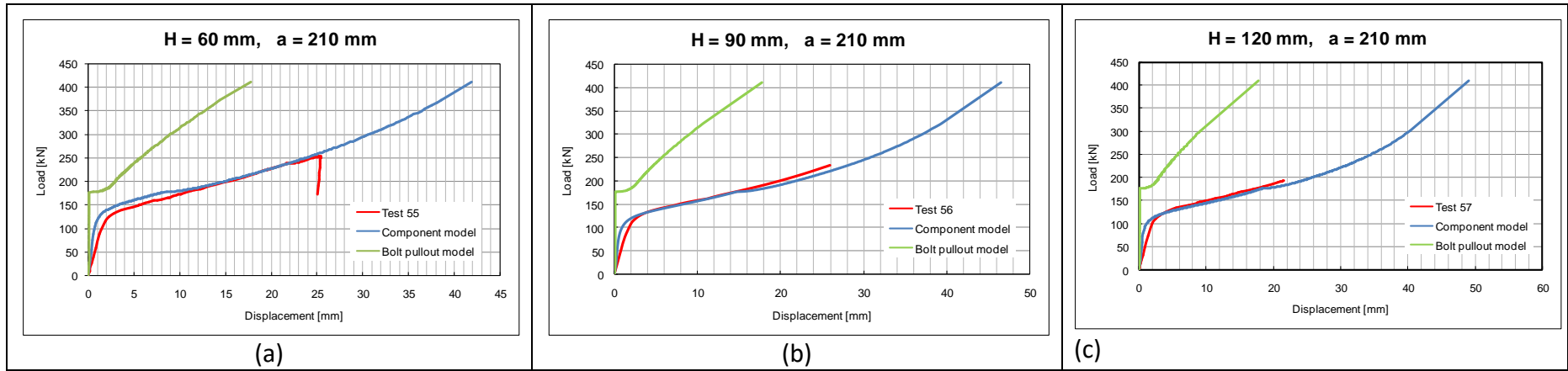
Figure 49: RC-in-Tension component model: parametric studies (Tests45-57)
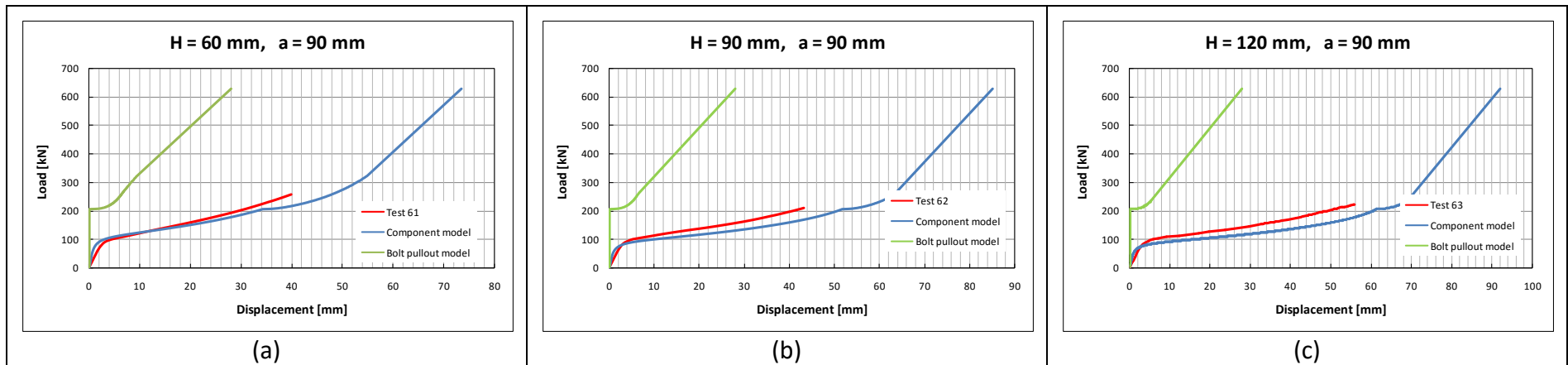
Figure 50: RC-in-Tension component model: parametric studies (Tests61-63)
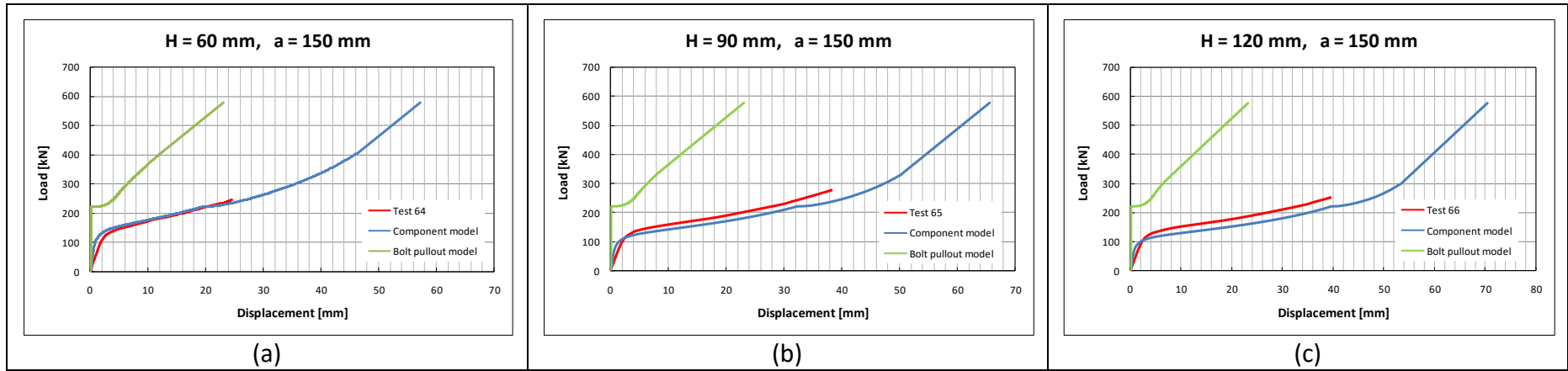
Figure 51: RC-in-Tension component model: parametric studies (Tests64-66)
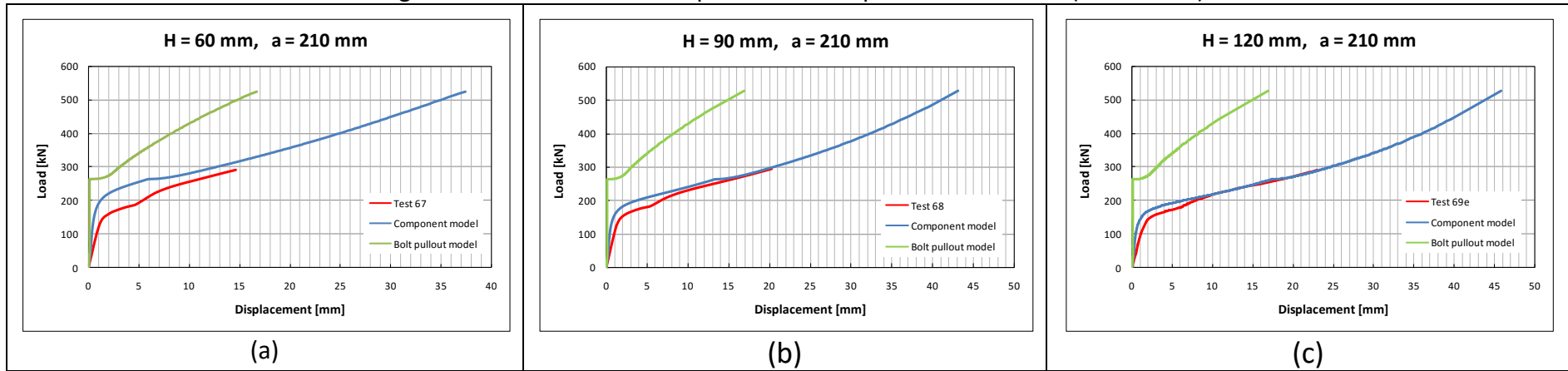
Figure 52: RC-in-Tension component model: parametric studies (Tests67-69)
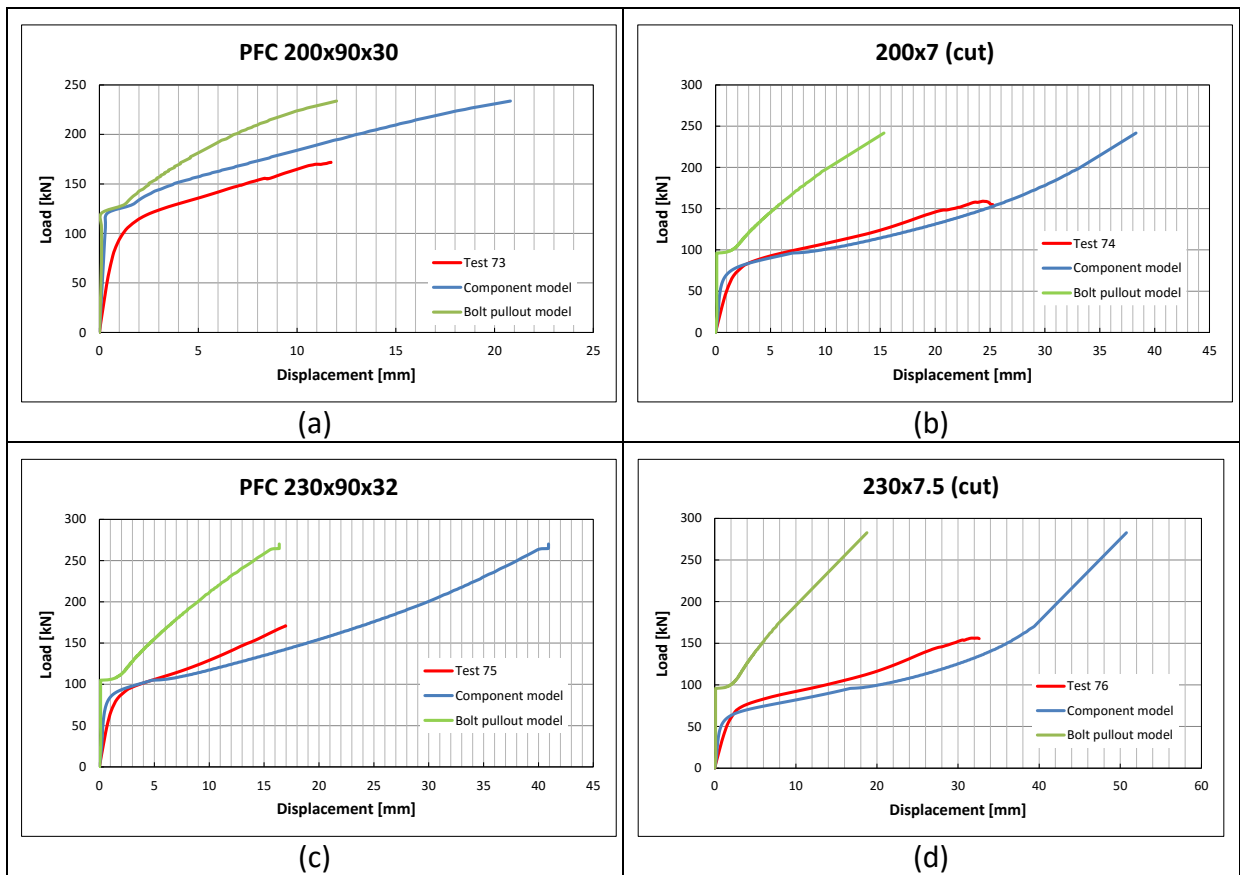
Figure 53: RC-in-Tension component model: parametric studies (Tests73-76)
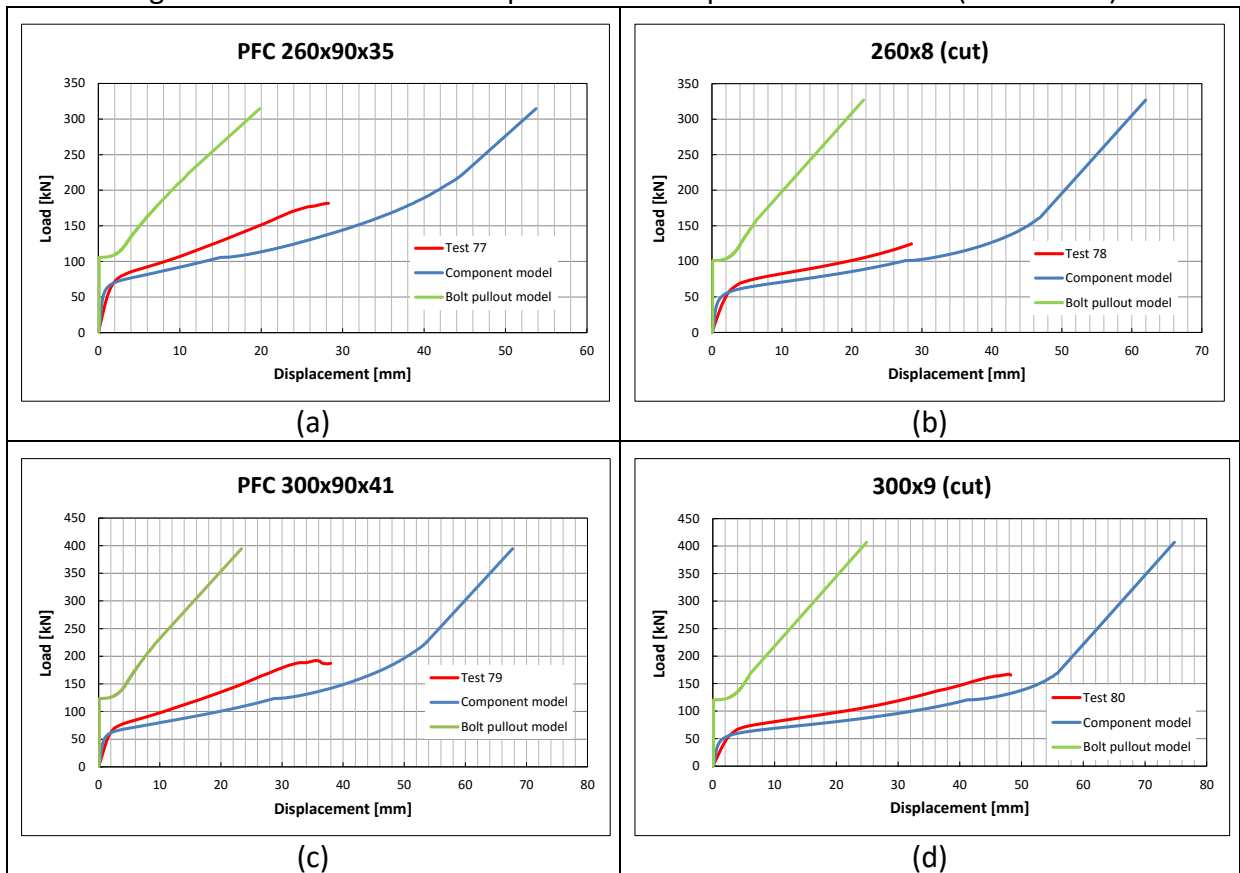
Figure 54: RC-in-Tension component model: parametric studies (Tests77-80)
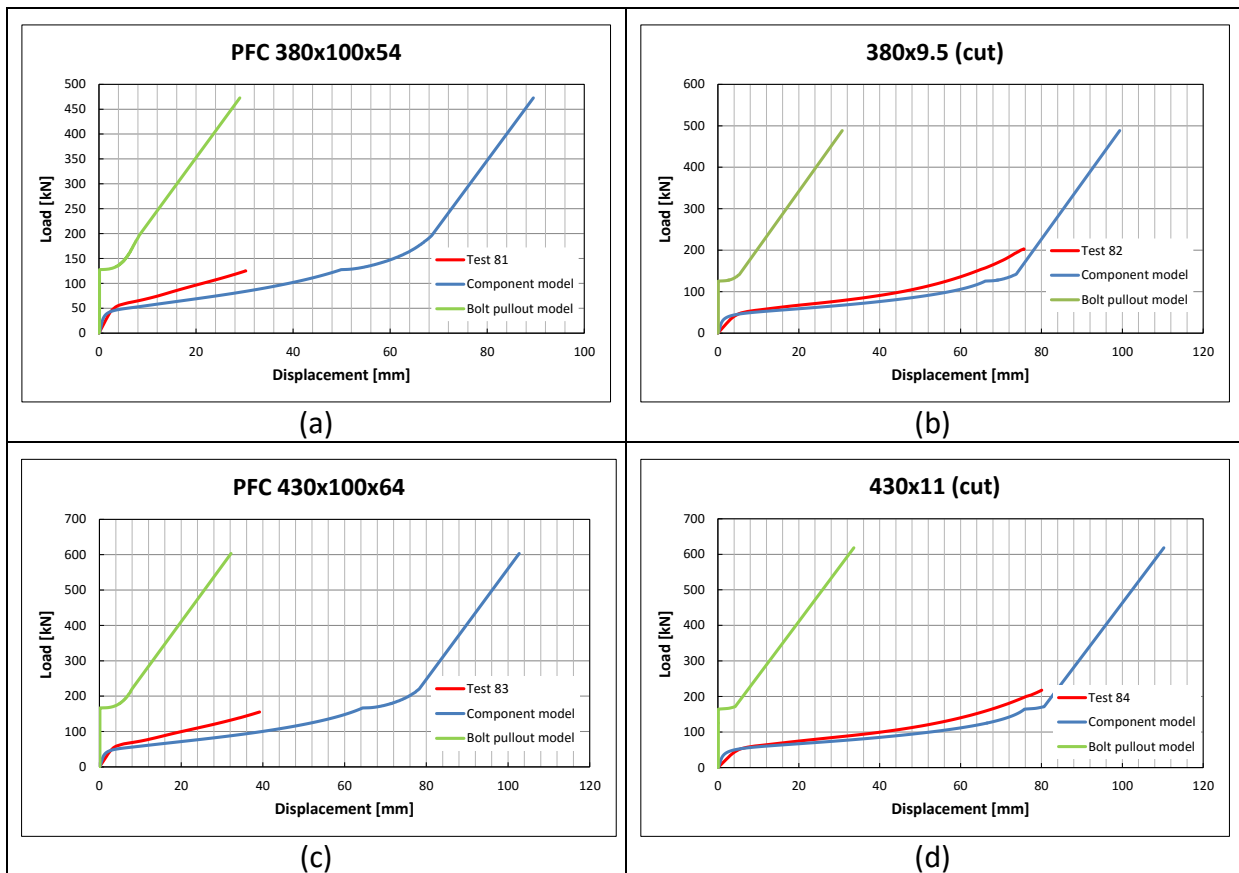
Figure 55: RC-in-Tension component model: parametric studies (Tests81-84)

3.4.4.1 Plastic hinge mechanism

Figure 56 shows the deformed shape from the tension parametric study based on Test 8. The FE analysis has supplied detailed data on the component behaviour. Figure 57 displays strain contours from this test, captured from an ABAQUS output video. These are the principal plastic strains in various parts of the reverse channel connections. The notation 11 indicates the principal bending strain, 22 is the strain in the orthogonal direction to 11. The video clearly shows how the plastic hinges form, and their locations. It is obvious that the three plastic hinges are located near to bolt holes, reverse channel roots, and legs.
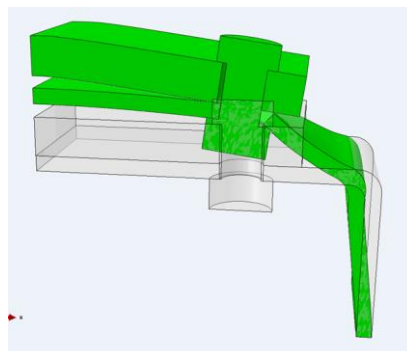
Figure 56: Tensile parametric Test 8 deformed shape by FEA

(a) leg Pe22 inner

(b) leg Pe22 outer

(c) max principal strain

(d) plate pe11 top

(e) web pe11 bottom

(f) web pe11 top
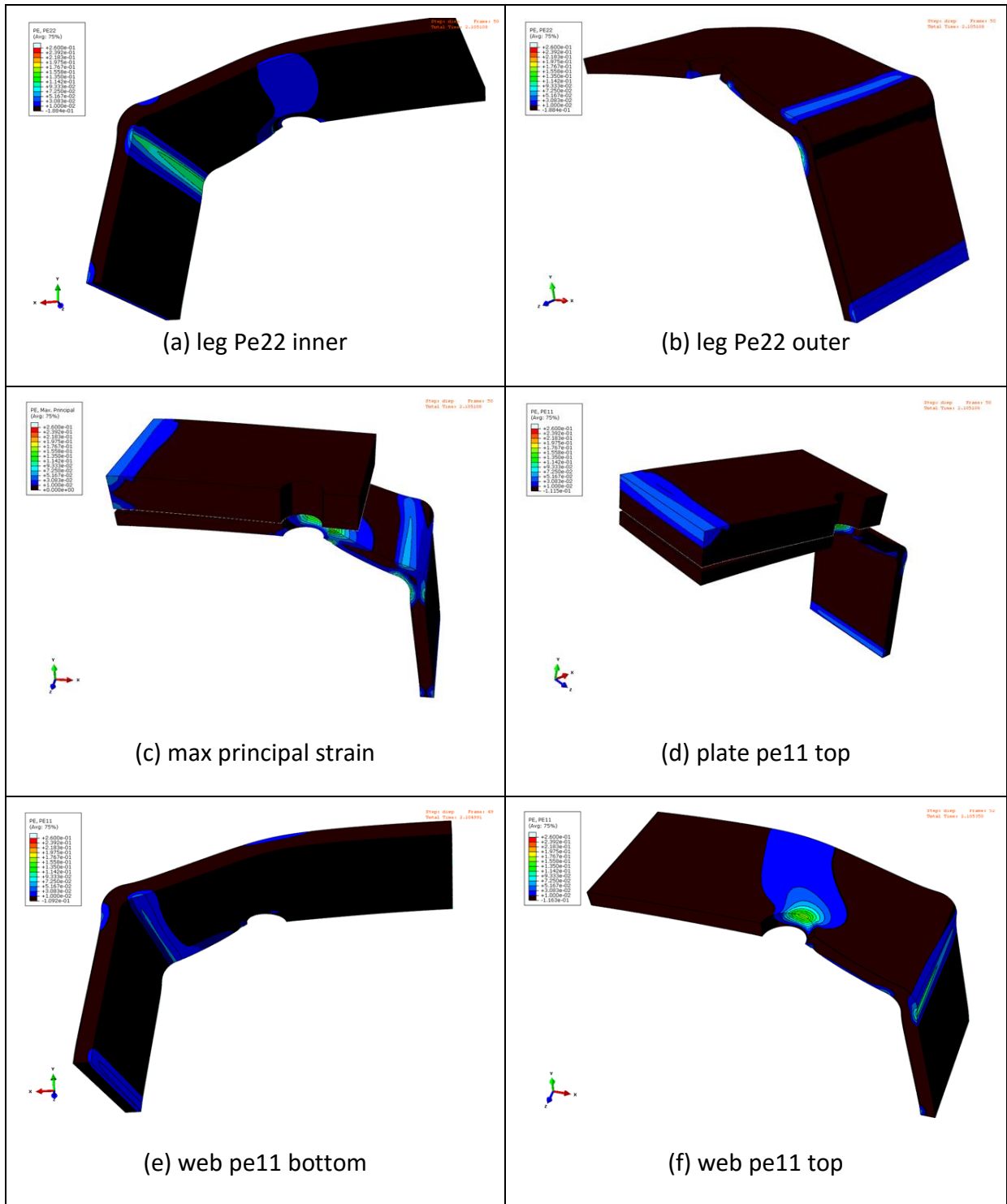
Figure 57: Tension parametric Test 8: strain contours by FEA

3.4.4.2 *Ambient temperature*

The ambient-temperature cases 1 to 9 are shown in Figure 43 to Figure 45. Generally, the force-displacement curve of the reverse channel (called the 'component model') shows the typical three stages (shown in Figure 58):

- Stage 1: The elastic stage, before the formation of the first plastic hinge;
- Stage 2: The reverse channel stiffness is reduced by plastic hinge formation;
- Stage 3: the reverse channel legs approach pure tension. The component becomes relatively much stiffer.

Not only does the component model capture the formation of the first pair of plastic hinges, but it also quite reasonably predicts the subsequent behaviour as new hinges form.
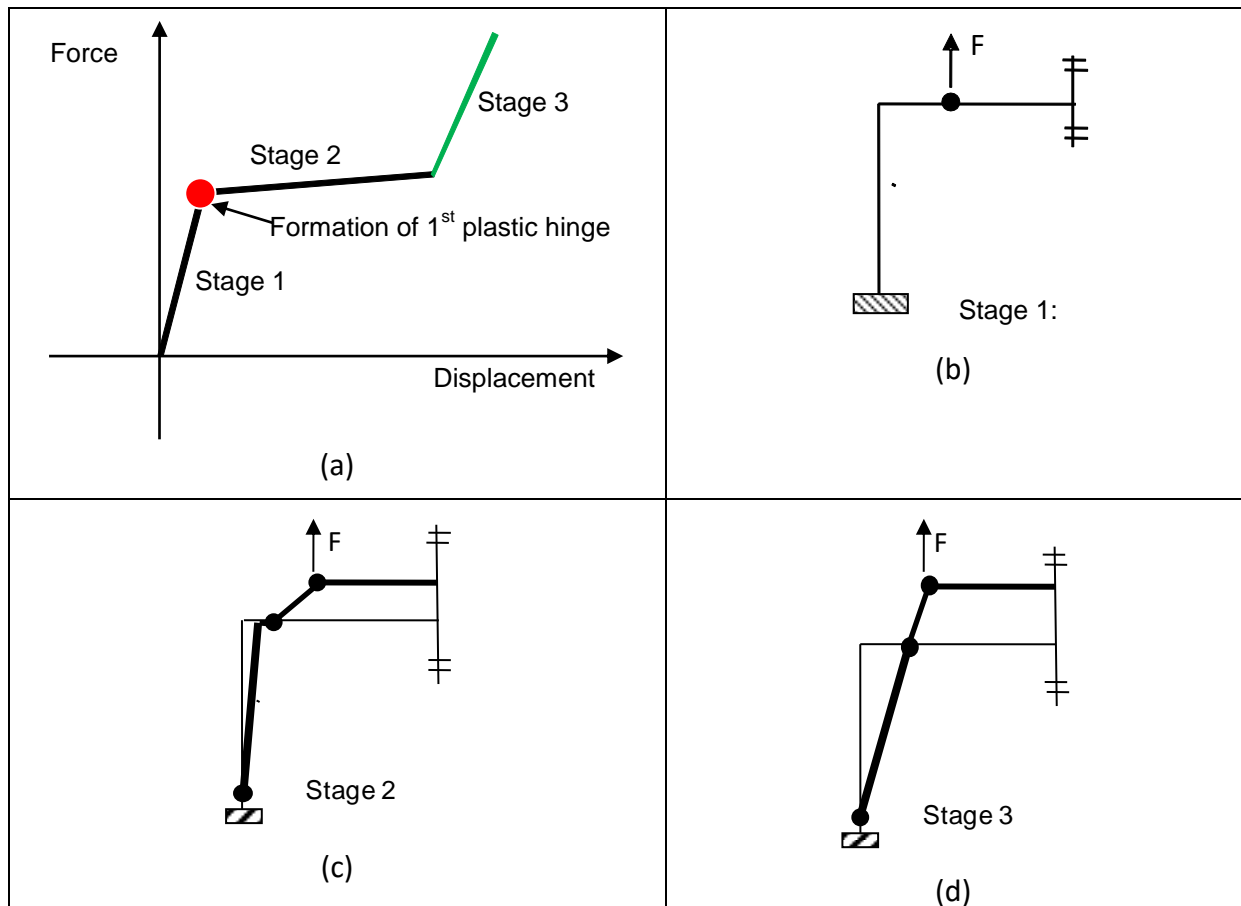
Figure 58: typical formation of straight line plastic hinge mechanism

3.4.4.3 Leg length

When the reverse channel is subject to tension, its legs will rotate inwards. For tests 1 to 9, the comparisons between the component model and FE results have been included in Figure 43 to Figure 45, which show that the component model is capable of predicting this trend as well. Figure 59 shows a comparison, taken from the component model, of the effects of different leg lengths on the behaviour. Generally, larger leg lengths increase the reverse channel's ductility. However, this effect is more obvious when the bolt separation is small (for example, when 'a' is 90mm).
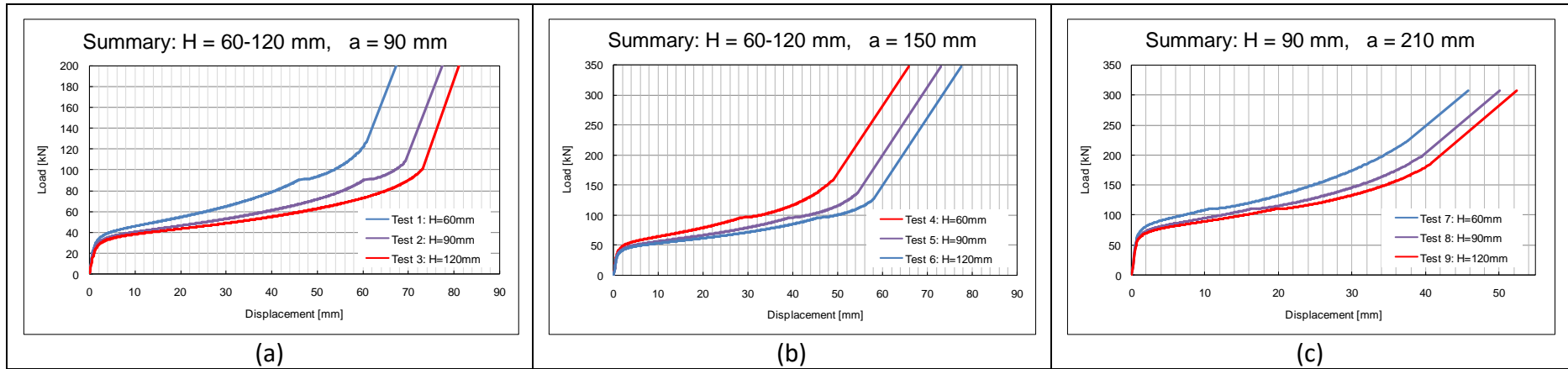
Figure 59: Comparison of leg length on RC-in-Tension component model
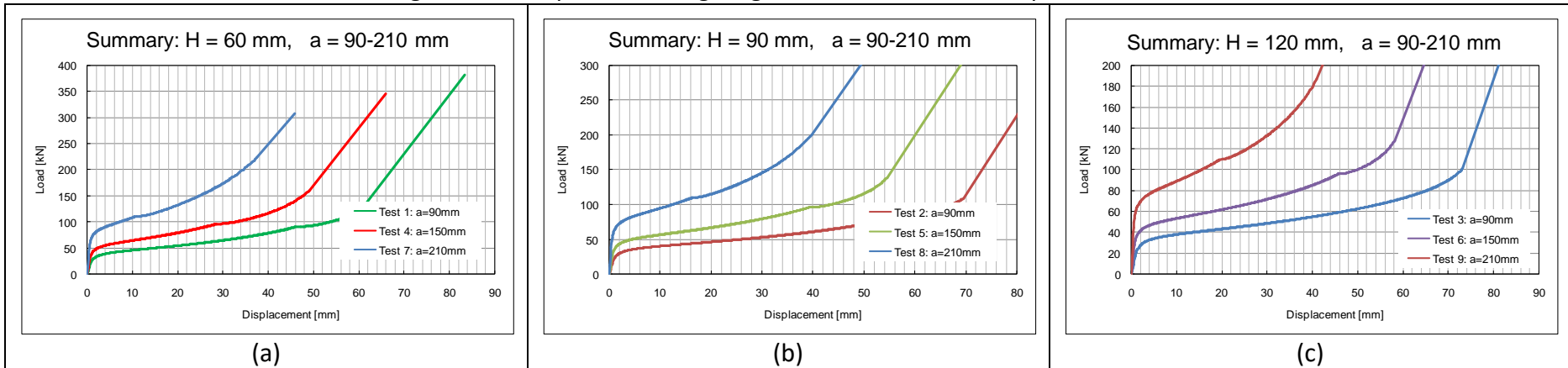
Figure 60: Bolt separation effects on one bolt row in tension; FEA results (Tests 1-12).

3.4.4.4   Bolt separation ('a' in Figure 42)

The detailing of the reverse channel web is the key to its ductility. The bolt separation defines the first plastic hinge location (shown in Figure 24) and the distance between the first and second plastic hinges. Figure 60 summarizes bolt separation effects on reverse channels under tension. In these figures, *'H'* is the leg length, and *'a'* is the bolt separation.

Generally, the reverse channel with the larger bolt separation has larger initial elastic stiffness. The tangent stiffness (Stage 2 in Figure 58) in the plastic range will generally also increase. This is because the space between the outer bolt and the channel leg controls the range of ductility. In the connection's design, a compromise value of bolt separation is necessary in order to give sufficient ductility without sacrificing ultimate capacity.

3.4.4.5   Reverse channel thickness

Figure 61 compares tube-cut reverse channels with different thicknesses (8mm in Test 1, 10mm in Test 49 and 12mm in Test 61), which are predicted by the component model. The validation of these component models have been presented in Figure 43, Figure 47 and Figure 50 . It is clear that thicker reverse channels have considerably greater capacities.
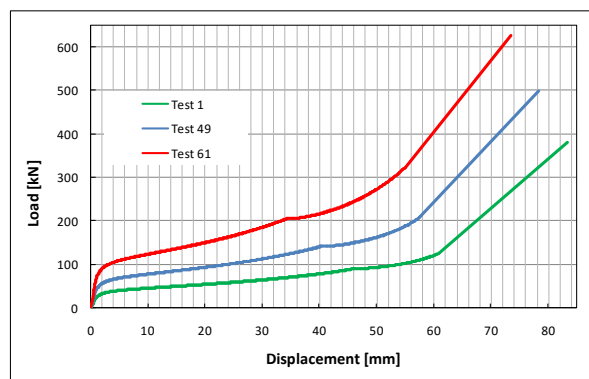
Figure 61: Effect of reverse channel thickness (tube-cut) in the parametric study (tension cases)

3.4.4.6   Rolled channel (PFC) or constant-thickness channel cut from a tube

Figure 62 shows comparisons of the rolled channel (PFC) and a constant-thickness channel cut from a tube with the same flange thickness. The main difference between these two types of section lies in their definition of leg thickness. Usually, the web thickness of a tube-cut channel is equal to its leg thickness, whereas for PFC the leg thickness is usually nearly twice the web thickness. Comparing these types, the tube-cut channel shows higher

68

ductility, due to its thinner legs. Therefore, in choosing between channels with the same capacity, the tube-cut section would be recommended.
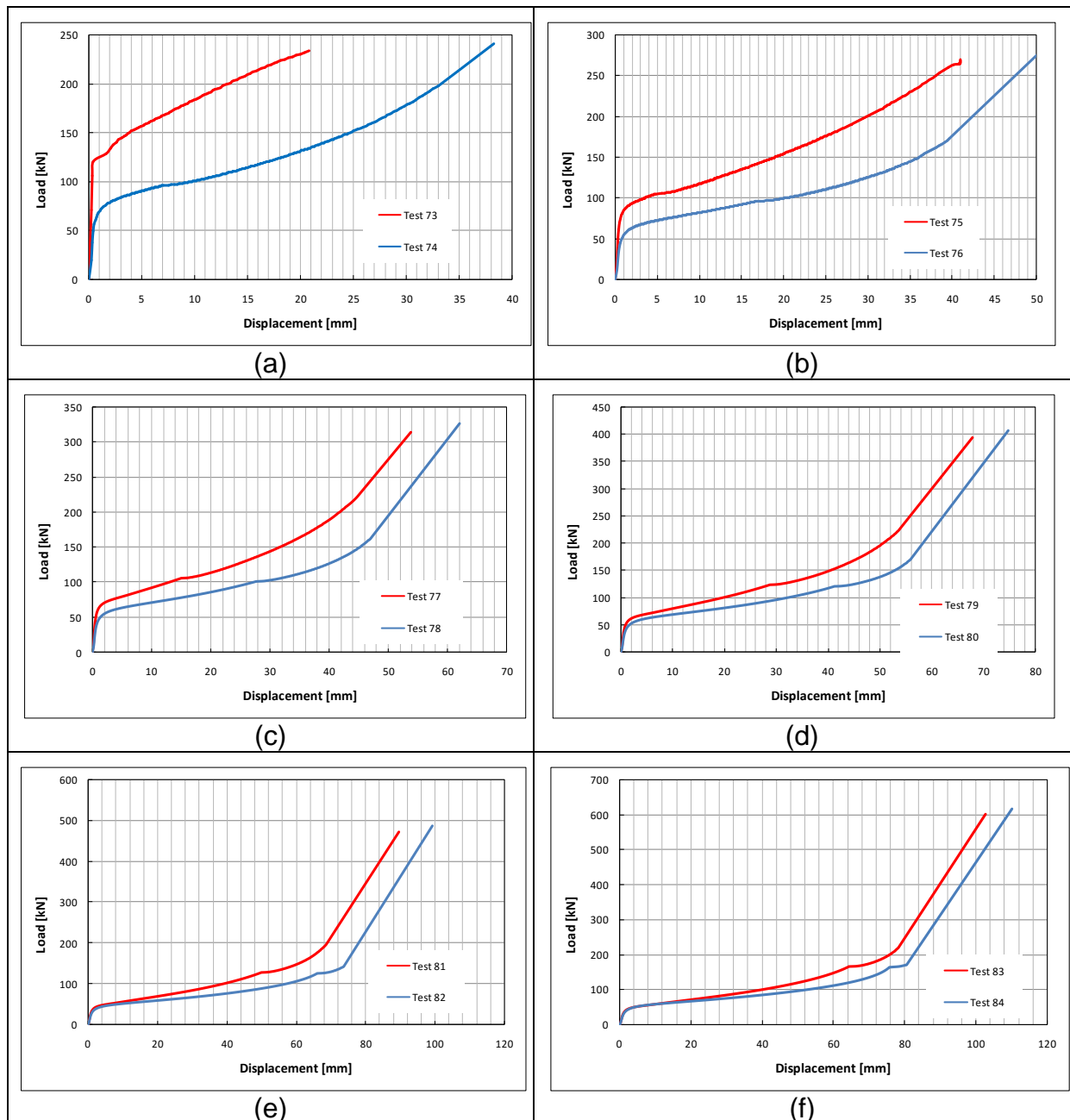
Figure 62: parametric study; PFC compared with tube-cut channels (tension).

3.4.4.7 Group effects

Figure 63 presents a comparison of group effects seen in the tensile parametric studies using detailed FE analysis. Tests 2, 5, 8 and 11 are single-bolt-row cases, Tests 14, 17, 20 and 23 are two-bolt-row cases and Tests 26, 29, 32 and 35 are three-bolt-row cases. The distance between multiple bolt rows is 150mm in all these tests. The force is the total reaction force at the bottom of the reverse channel. The deformation shown in Figure 63 for

two-bolt-row cases is that of any one of the bolt holes, and the deformation of three-bolt-row cases is that of any of the edge bolt holes. Due to symmetry, the deformations of the bolt hole in the two-bolt-row cases and of the edge bolt holes in three-bolt-row cases are the same. The FEA results also show that the edge and inner bolt-hole deformations in the three-bolt row cases match. At the same deformation level, Figure 63 shows that the forces in the two-bolt-row cases are twice their equivalents in the one-bolt-row cases, and those for three-bolt-row cases are three times those of the single-bolt-row cases. This indicates that the force distribution between the bolt rows is nearly uniform. Therefore, provided that there is a reasonable bolt row separation, it is practical to assume that the effective length of a reverse channel in tension is equal to the distance between bolt rows.
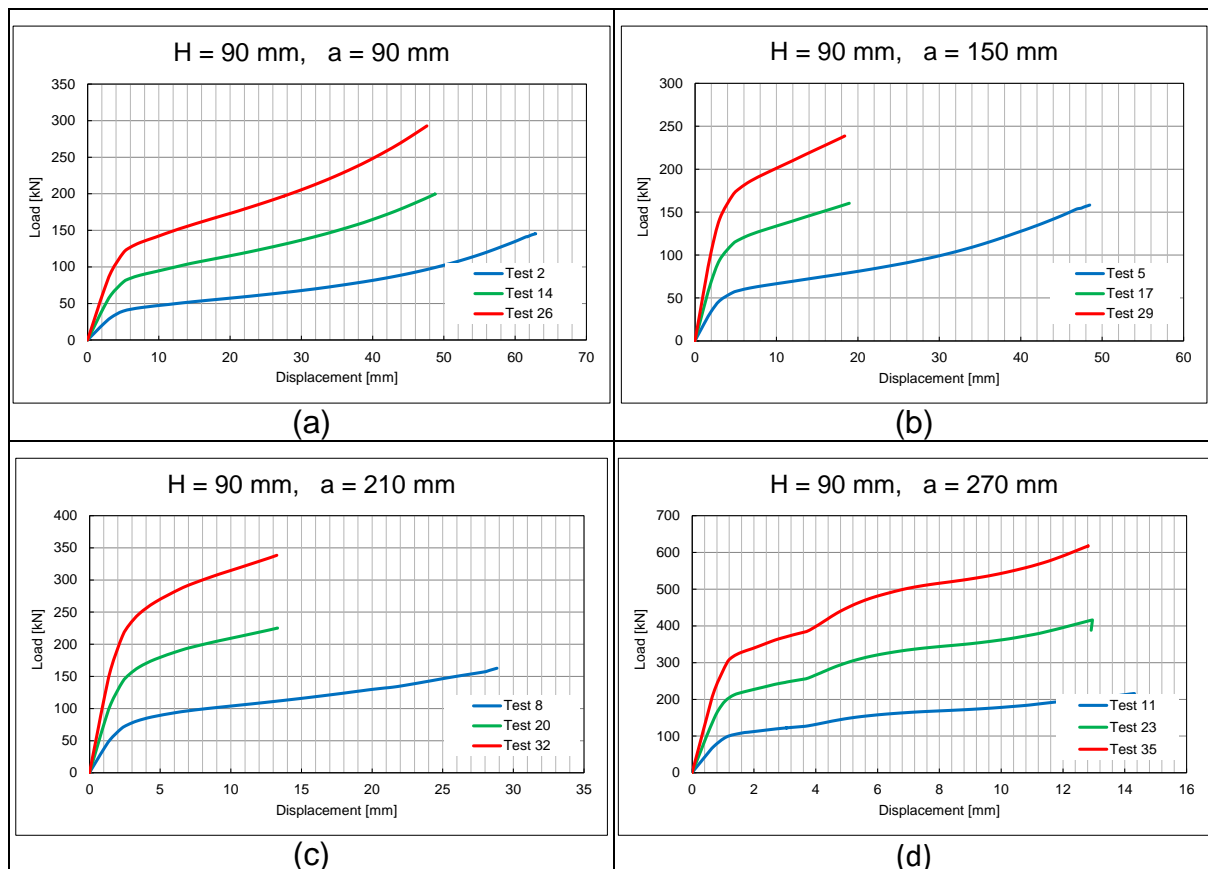
Figure 63: Parametric studies on group effect (tension, FE results).

3.4.4.8 Bolt pull-out model

The bolt pull-out model developed earlier is a sub-model, which is incorporated into the component model for the reverse channel under tension, to calculate the total local deformation at any force level, and to predict the limit at which the bolt hole deforms enough to allow the bolt to be pulled through.

The AISC limiting force (AISC, 2005) R_n for bolt pull-out through the wall of a hollow structural section is given by

$$R_n = 0.85 d_w t f_u$$

(3.49)

Where d_w is the average diameter of the bolt head, t is the tube wall thickness and f_u is the ultimate strength of the hollow structural section's steel.

The corresponding CIDECT limit (Jaspart, 2005) for punching of a single bolt through a tube wall, $F_{punch,cp}$, is:

$$F_{punch,cp} = \pi d_m \frac{t f_{yc}}{\sqrt{3} \gamma_{M0}}$$

(3.50)

Table 13 and Table 14 show the predicted bolt pull-out limits using the AISC, CIDECT and the current bolt pull-out models on the component tests. Figure 64 shows the comparison of these bolt pull-out limits. Generally, the CIDECT limit is the highest, and AISC is the most conservative for design purposes. With a proper design safety factor, the bolt pull-out model can be used safely in practical connection design.

3.4.4.9 Temperature

The component model is also tested for elevated-temperature situations (shown in Figure 46). The component model prediction is higher than the FE, especially at the kink created by the formation of first plastic hinge (refer to Figure 58) .This is because the component model only considers the energy absorbed by the yielding of the material at the plastic hinge locations, and neglects the gradual reduction of elastic stiffness with temperature. The mainly-elastic zones between plastic hinge locations also deform and store strain energy. Therefore, the component model's predictions will be stiffer, particularly in the early stages of deformation, and at elevated temperatures, when the modulus of steel degrades more quickly than the yield strength. However, the component model still predicts the higher-deflection and pull-out limit behaviour reasonably.

Table 13: RC-in-tension test bolt pull-out limit calculation by AISC & CIDECT

	test list	Test (kN)	Bolt head dia (mm)	Bolt shank dia (mm)	t_f (mm)	Yield strength (N/mm^2)	Ultimate strength (N/mm^2)	tem (°C)	AISC Limit (kN)	CIDECT (kN)
Manchester	RCT1	95	32.3	20	5.5	325	594	20	89.6	104.7
	RCT2	43	32.3	20	5.5	203	203	550	30.7	65.5
	RCT3	13	32.3	20	5.5	55	55	750	8.3	17.8
	RCT4	96	32.3	20	5.5	325	594	20	89.6	104.7
	RCT5	41	32.3	20	5.5	203	203	550	30.7	65.5
	RCT6	12	32.3	20	5.5	55	55	750	8.3	17.8
Coimbra	Test 1	135	38.8	24	7.0	287	581	20	134.1	141.4
	Test 2	174	38.8	24	10.0	287	581	20	191.6	202.0
	Test 3	251	38.8	24	12.0	287	581	20	229.9	242.4
	Test 7	78	38.8	24	10.0	179	179	550	59.2	126.2
	Test 8	97	38.8	24	12.0	179	179	550	71.0	151.5
	Test 11	20	38.8	24	10.0	49	49	750	16.1	34.3
	Test 12	23	38.8	24	12.0	49	49	750	19.3	41.2
	Test 15	140	38.8	24	8.0	347	420	20	110.8	195.4
	Test 16	238	38.8	24	10.0	516	592	20	195.2	363.1
	Test 17	295	38.8	24	12.0	471	540	20	213.7	397.8
	Test 18	200	38.8	24	8.5	344	605	20	169.6	205.8
	Test 19	67	38.8	24	8.5	215	215	550	60.3	128.6
	Test 20	21	38.8	24	8.5	58	58	750	16.4	35.0
	Test 21	100	37.0	20	6.0	96	255	550	48.1	38.6
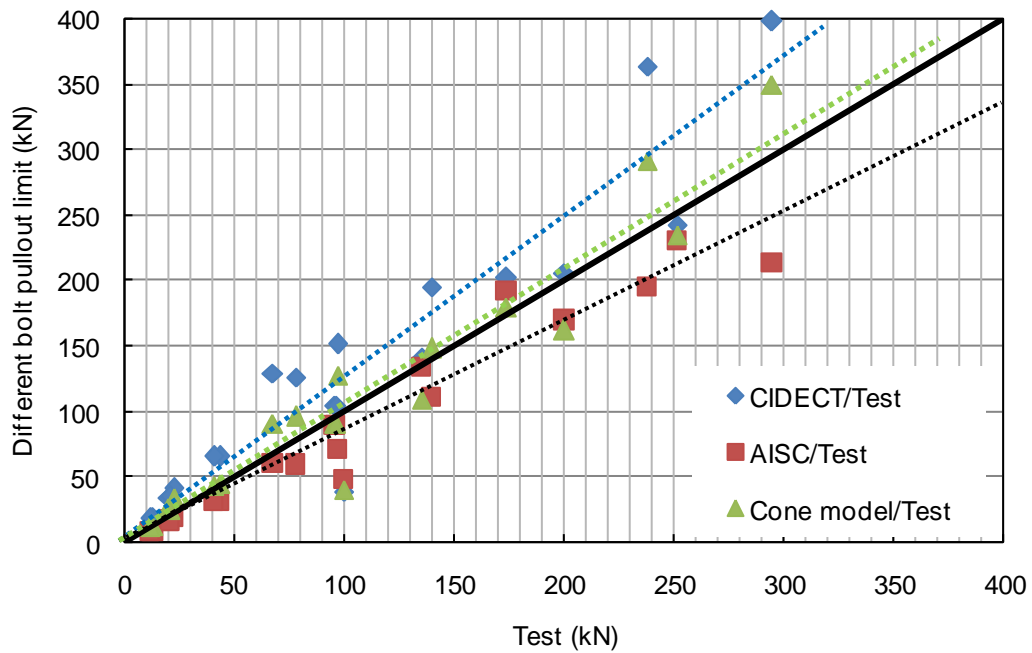
Figure 64: Comparison of bolt pull-out limits.

Table 14: RC-in-tension bolt pull-out limit calculation by bolt pull-out model

| | test list | Test (kN) | bolt pull-out model | | | | | | | | | | |
			R (mm)	θ	Δ	r_ave (mm)	ε_r	ε_y	ε_u	W_{strip}	W_θ	W_{total}	F (kN)
Manchester	RCT1	95	20.4	1.04	7.25	16.2	0.128	0.002	0.040	329834	327649	657483	91
	RCT2	43	20.4	1.04	7.25	16.2	0.128	0.002	0.002	121243	204780	326023	45
	RCT3	13	20.4	1.04	7.25	16.2	0.128	0.004	0.004	32811	55700	88511	12
	RCT4	96	20.4	1.04	7.25	16.2	0.128	0.002	0.040	329834	327649	657483	91
	RCT5	41	46.4	0.50	16.38	29.2	0.071	0.002	0.040	492728	222197	714925	44
	RCT6	12	46.4	0.50	16.38	29.2	0.071	0.003	0.003	133189	60438	193627	12
Coimbra	Test 1	135	33.8	0.76	13.59	23.9	0.113	0.001	0.155	918625	564519	1483143	109
	Test 2	174	36.3	0.71	14.55	25.15	0.107	0.001	0.155	1457339	1162596	2619935	180
	Test 3	251	36.3	0.71	14.55	25.15	0.107	0.001	0.155	1748807	1674138	3422944	235
	Test 7	78	36.3	0.71	14.55	25.15	0.107	0.002	0.002	672320	726622	1398943	96
	Test 8	97	36.3	0.71	14.55	25.15	0.107	0.002	0.002	806785	1046336	1853121	127
	Test 11	20	36.3	0.71	14.55	25.15	0.107	0.003	0.003	181949	197641	379591	26
	Test 12	23	36.3	0.71	14.55	25.15	0.107	0.003	0.003	218339	284603	502943	35
	Test 15	140	43.1	0.62	16.89	28.55	0.095	0.002	0.044	1576153	930269	2506423	148
	Test 16	238	39.5	0.66	15.69	26.75	0.101	0.002	0.049	2448107	2121136	4569243	291
	Test 17	295	35.9	0.72	14.40	24.95	0.108	0.002	0.067	2285664	2742991	5028656	349
	Test 18	200	34.3	0.75	13.79	24.15	0.112	0.002	0.178	1233626	999283	2232909	162
	Test 19	67	34.3	0.75	13.79	24.15	0.112	0.002	0.002	622708	624552	1247260	90
	Test 20	21	34.3	0.75	13.79	24.15	0.112	0.004	0.004	168392	169878	338271	25
	Test 21	100	44.2	0.65	19.40	28.1	0.116	0.001	0.137	629675	154984	784659	40

3.5   Development of the plastic hinge model for reverse channel under compression

When the reverse channel is subject to compression, its mechanical model is similar to that under tension. The flange is subject to bending. The legs are under compression, which is opposite to the channel under tension. Since the stiffness of flange under bending is less than the legs under compression, the two ends of flange will rotate inwards. The plastic hinges at the tops of the two legs are moved slightly away from each other by the bending deformation of the web (shown in Figure 65 and Figure 66). Since the legs are subject to compression, Plastic Hinges 2 (PH2 shown in Figure 68 and Figure 69) will move from the channel web to the reverse channel legs.
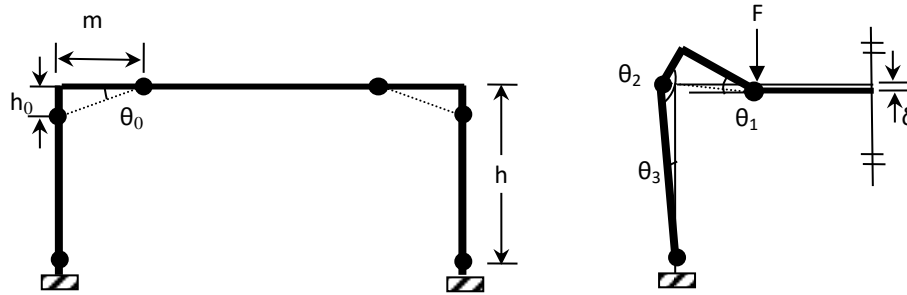
Figure 65: Plastic hinge rotations (I)
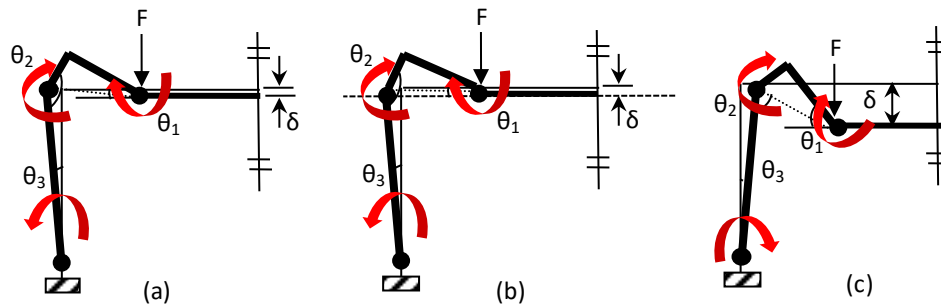
Figure 66: Plastic hinge rotations (II)

3.5.1 Failure modes

For a reverse channel under compression, there are four possible "failure" modes:

1. Large deformation of the reverse channel in a plastic hinge mechanism, leading to contact of the web of the reverse channel with the column flange/face. The detail of the plastic hinge mechanism is explained in 3.5.2.

2. Web fracture, by punching-through of the endplate (Figure 67). This can be estimated simply by applying the material shear strength over the punch perimeter area, although this assumes that failure is simultaneous around the perimeter.

$$F_{punching} = f_y \cdot c \cdot t_w / \sqrt{3} \tag{3.51}$$

Where f_y is the reverse channel yield strength, c is the perimeter of the punching shear area, and t_w is the reverse channel web thickness.

3. Leg buckling, in which the buckling force for a leg is based on the Perry-Robertson method (Coates, 1988) for an effective length factor of between 0.5 (fixed-fixed) and 0.7 (fixed-hinged). Conservatively, the latter is more reasonable. Since there is no information about the actual geometric imperfection level in the channel's flanges the original formula based on tests in the 1920s (Robertson 1925) seems as justifiable as the more recent formulae, for example those included in Eurocode 3 (CEN, 2005a).

$$\sigma_e = \frac{P_{cr}}{A} = \pi^2 E \left(\frac{r}{0.7L} \right)^2$$

(3.52)

$$\sigma = \frac{1}{2} \left[f_y + \left(1 + 0.003 \frac{L}{r} \right) \sigma_e \right] - \sqrt{\frac{1}{4} \left[f_y + \left(1 + 0.003 \frac{L}{r} \right) \sigma_e \right]^2 - f_y \sigma_e}$$

(3.53)

The buckling resistance is

$$F_{buckling} = \sigma A = \sigma l_{eff} t_f$$

(3.54)

Where l_{eff} is the reverse channel effective length, and t_f is the reverse channel leg thickness. For stocky legs this is equivalent to leg crushing.

a) Before test   b) After test

Figure 67: Test 13: welded reverse channel 202x200x10; compressive load; 750°C [University of Coimbra].

3.5.2   Plastic hinge mechanisms

Due to the variety of dimensions and stiffnesses of reverse channels and endplates which are possible, a reverse channel under compression has two possible plastic hinge mechanisms. When the endplate is so stiff that its bending is negligible, Plastic Hinge 1 (PH1 shown in Figure 68) will form in the channel web at the edge of the endplate. In cases where the endplate is relatively thin, a double plastic hinge (PH1) will be located near to the root of the weld connecting the beam web and endplate (Figure 69).

75
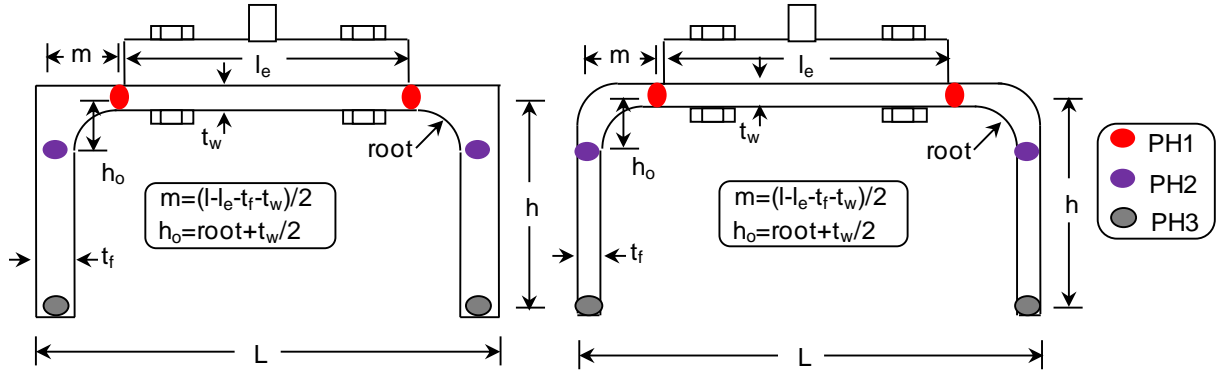
Figure 68: Reverse channel under compression (Plastic Hinge Mechanism 1).
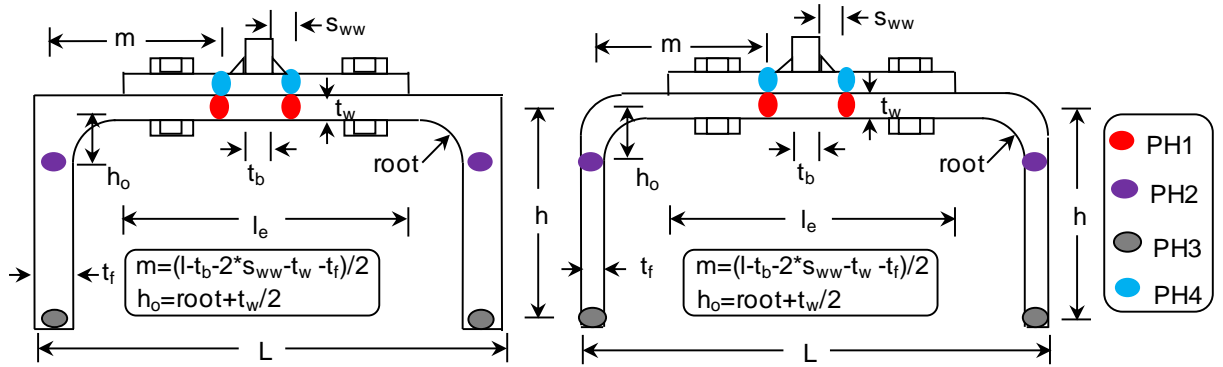
Figure 69: Reverse channel under compression (Plastic Hinge Mechanism 2).

The rotations in the two modes may be calculated (Figure 65 and Figure 66) from:

$$\theta_0 - \theta_1 = \arcsin\left(\frac{(h_0 - \delta) + (h - h_0)(1 - cos\theta_3)}{\sqrt{m^2 + h_0^2}}\right) \tag{3.55}$$

$$\theta_2 = \theta_1 + \theta_3 \tag{3.56}$$

$$\theta_3 = arcsin\left(\frac{\sqrt{m^2 + h_0^2}cos\theta_1 - m}{h - h_0}\right) \tag{3.57}$$

$$\theta_4 = \theta_1 \tag{3.58}$$

Figure 66 shows the rotation direction of each plastic hinge within the reverse channel. When θ_1 is less than θ_0, then θ_1, θ_2 and θ_3 increase with the displacement (δ) (Figure 66 a). When θ_1 is larger than θ_0, the θ_3 rotation will change direction. Accordingly, the mechanism will change and the channel resistance will enhance. In order to simplify the model, the component model will continue its analysis until θ_1 is equal to θ_0. The force is assumed to stay constant after this point, until the reverse channel reaches its maximum allowable deformation under compression.

3.5.3 Further parametric studies

During the COMPFIRE project, intensive parametric studies (listed in Table 6 to Table 12) were conducted by Luleå Technical University using ABAQUS. The aim was to expand the component test data, in order to investigate the reverse channel behaviour more extensively at both ambient and elevated temperatures. The detail of this parametric study is included in 3.4.4.

The detailed results of the validation studies for the reverse channel under compression are presented from Figure 70 to Figure 86. In general, by comparing the model with the tests and FEA analyses, the component model is seen to be able to predict the behaviour of the reverse channel under compression; the remainder of this section is a discussion of the parameters considered in this study:

- Plastic hinge mechanism
- Leg length
- Bolt separation
- Endplate thickness
- Reverse channel thickness
- Rolled channel (PFC) or constant thickness channel cut from a tube
- Post yield hardening in the reverse channel under compression
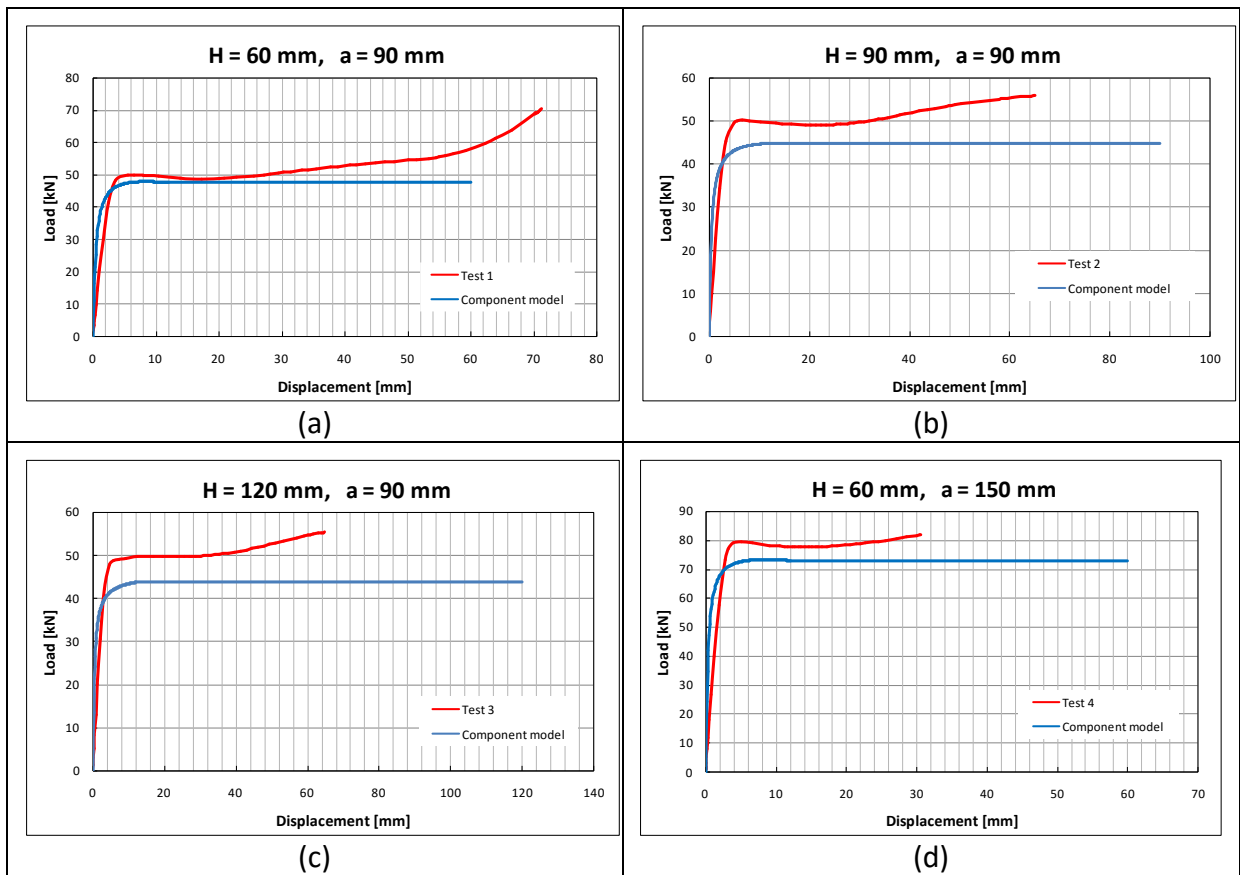
Figure 70: RC-in-Compression component model: parametric studies (Tests 1-4)
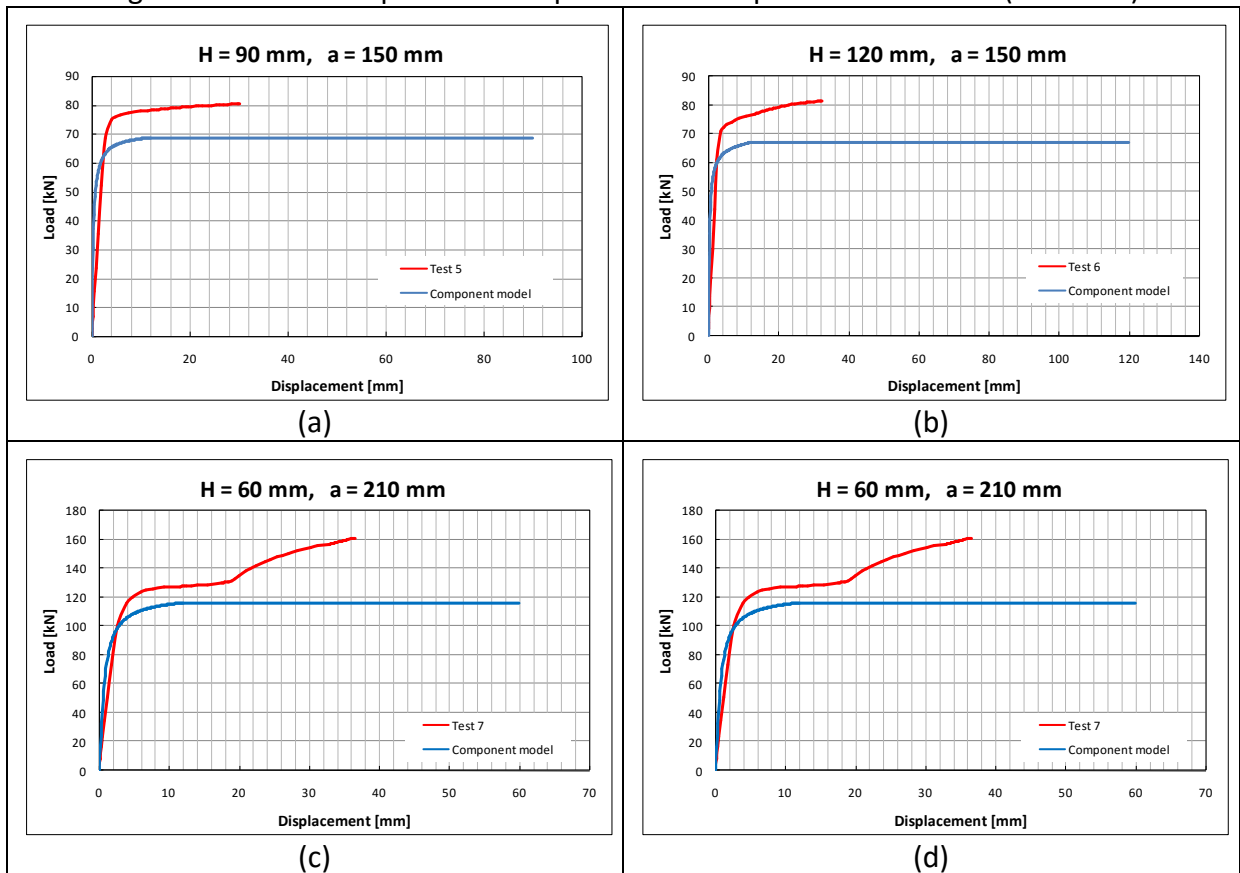
Figure 71: RC-in-Compression component model: parametric studies (Tests 5-8)
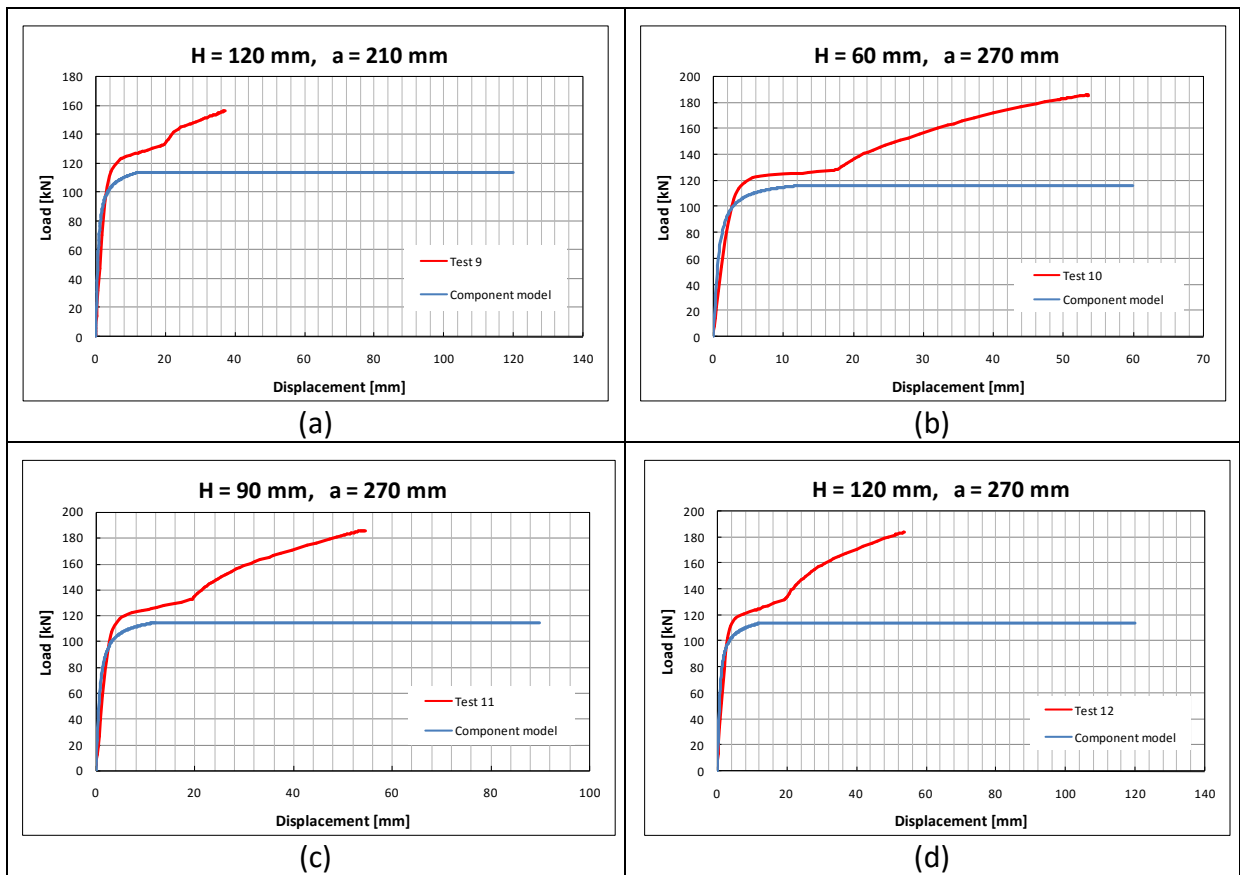
Figure 72: RC-in-Compression component model: parametric studies (Tests 9-12)
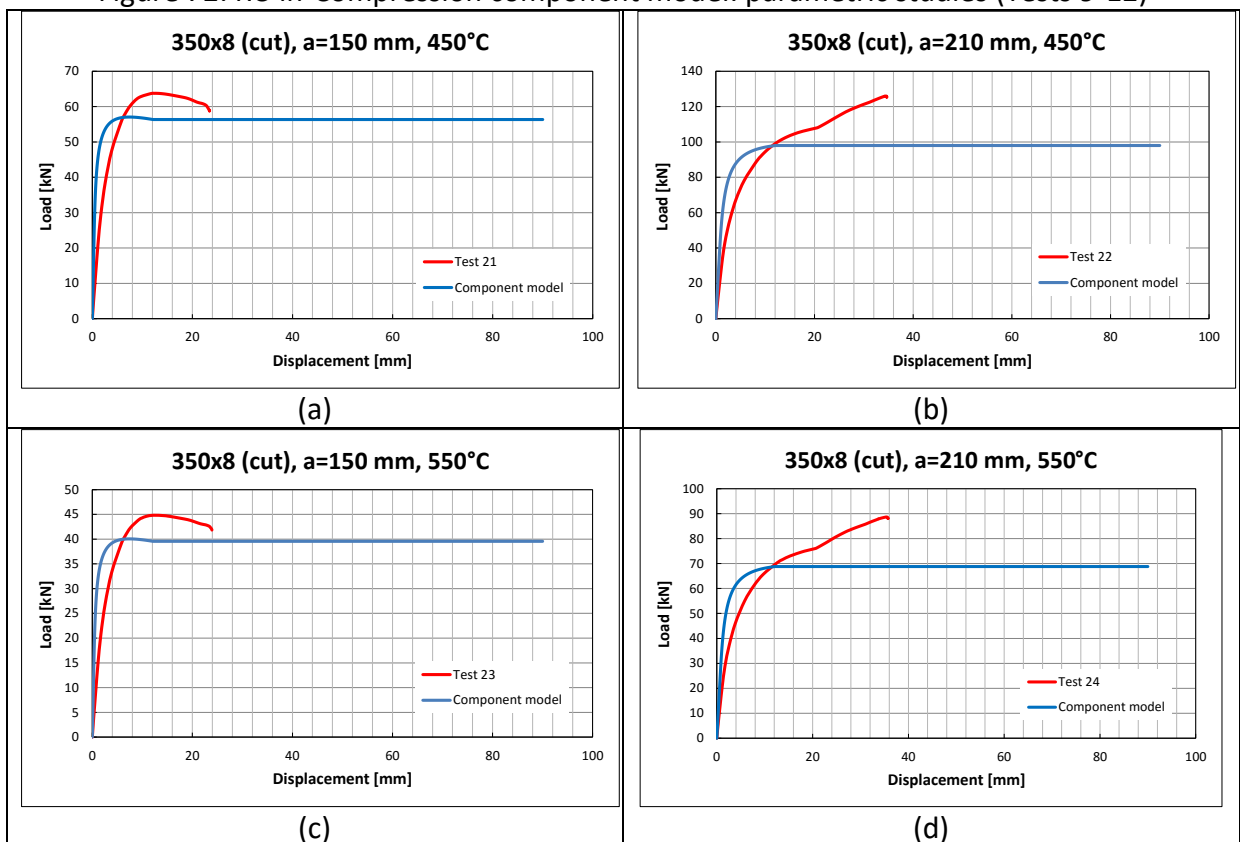
Figure 73: RC-in-Compression component model: parametric studies (Tests 21-24)
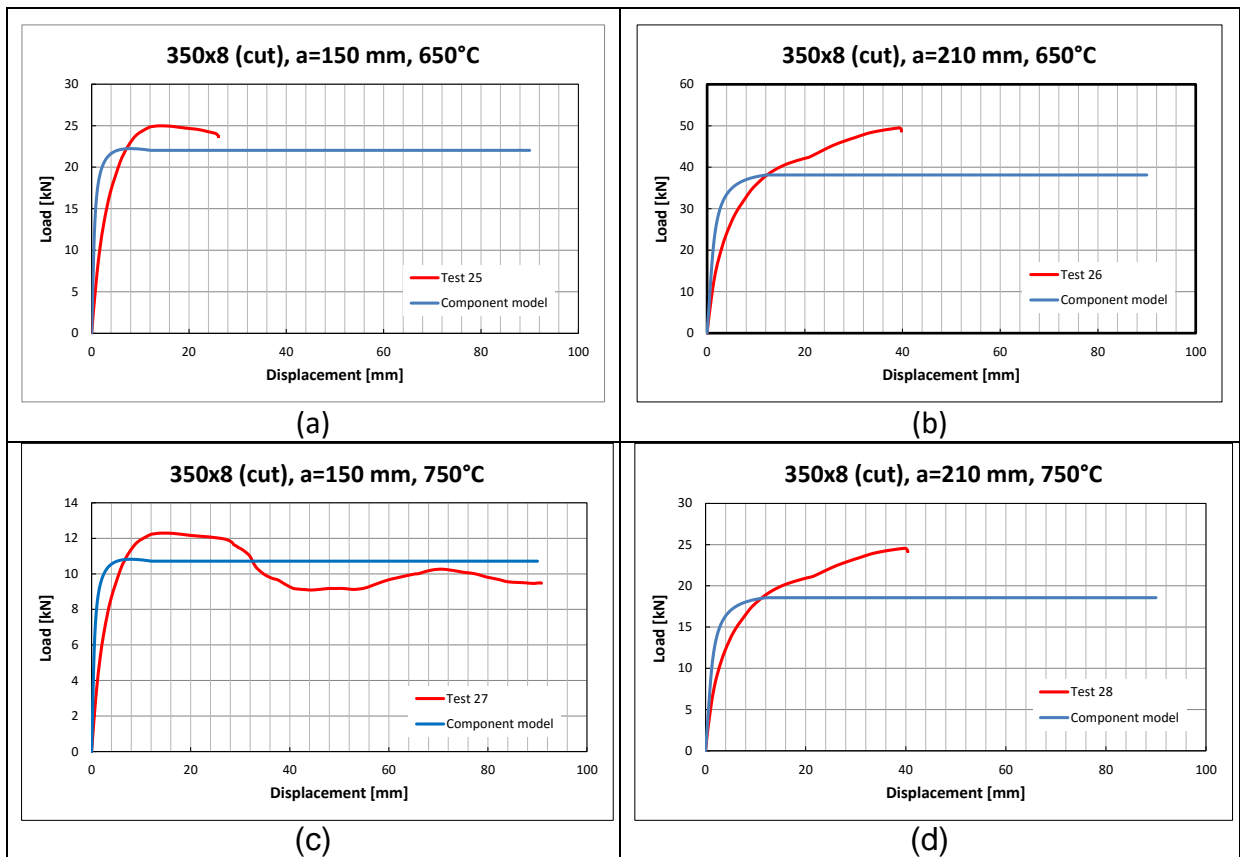
Figure 74: RC-in-Compression component model: parametric studies (Tests 25-28)
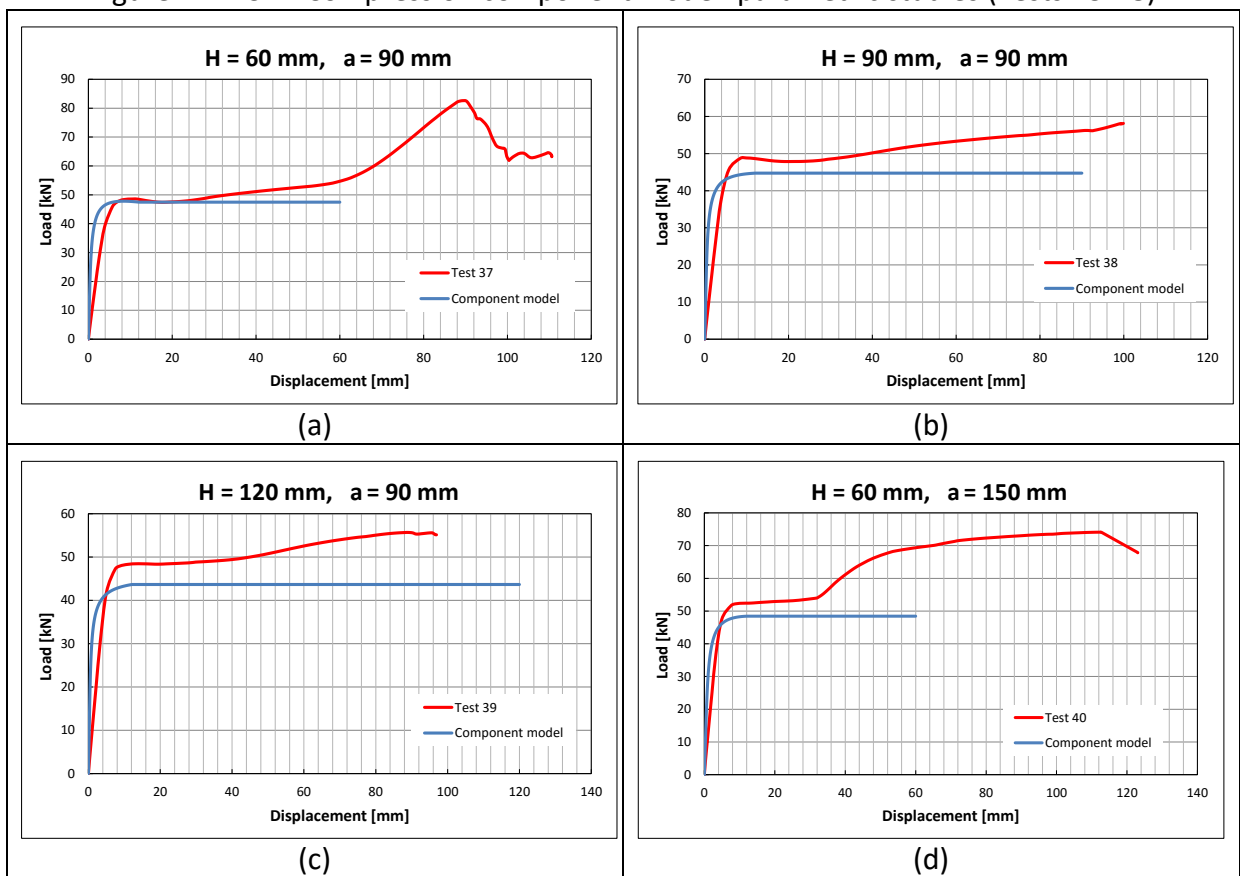
Figure 75:RC-in-Compression component model: parametric studies (Tests 37-40)
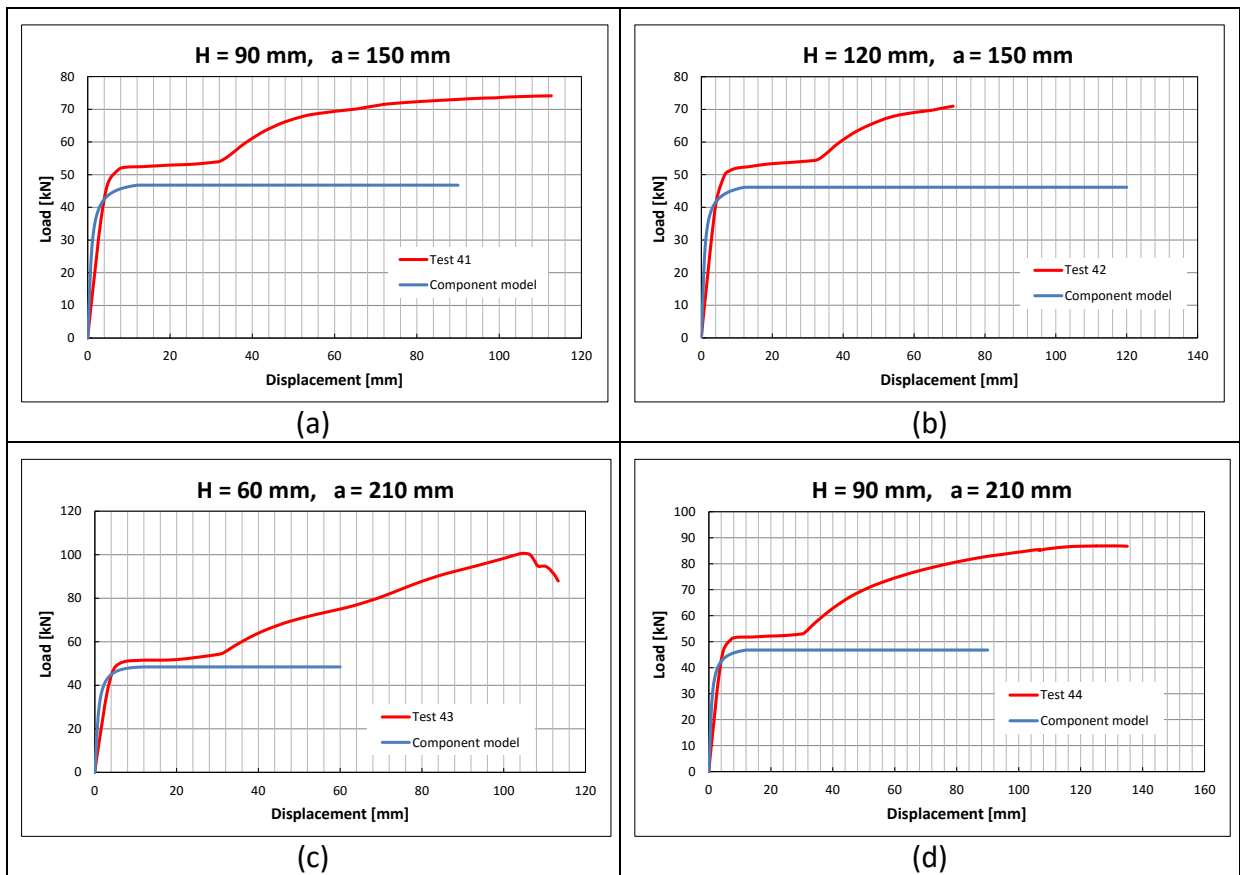
Figure 76:RC-in-Compression component model: parametric studies (Tests 41-44)
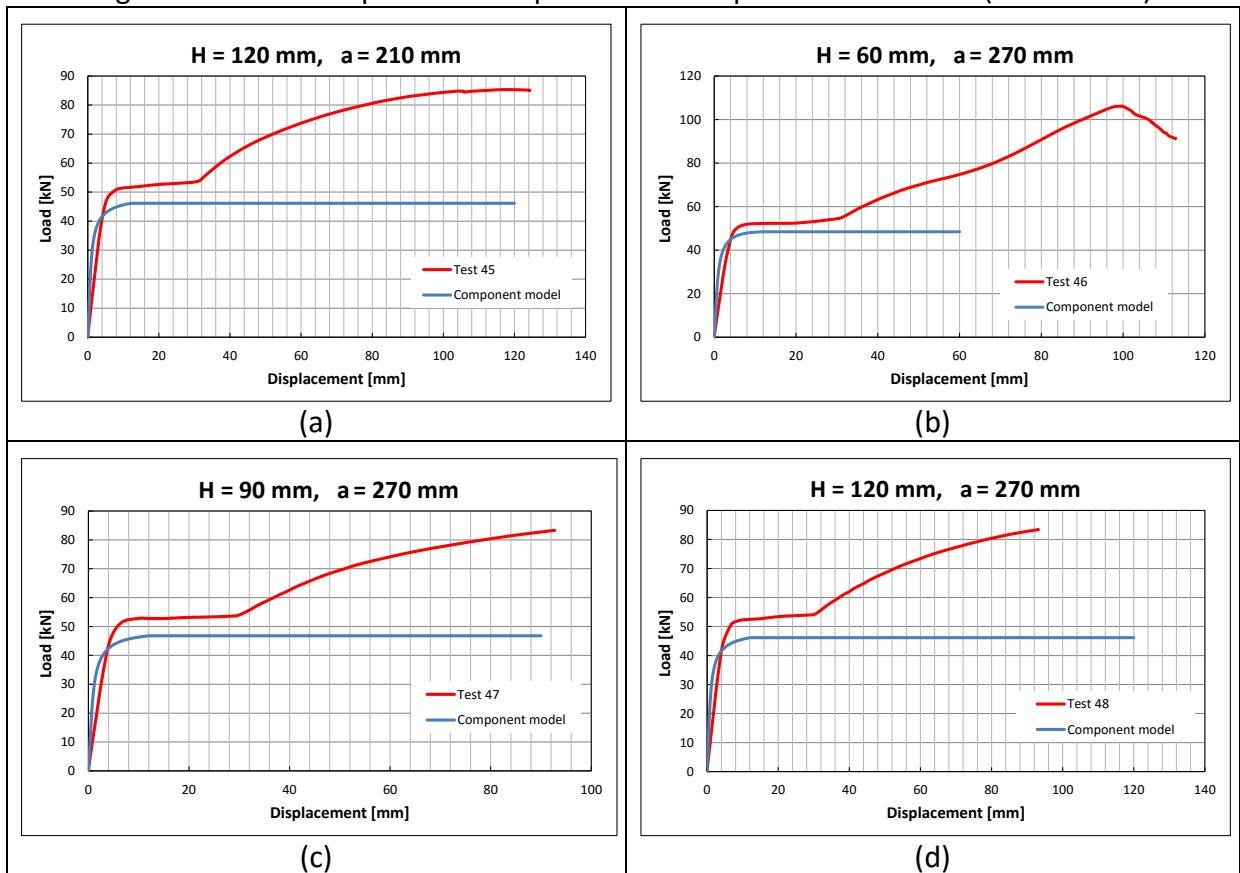
Figure 77: RC-in-Compression component model: parametric studies (Tests 45-48)
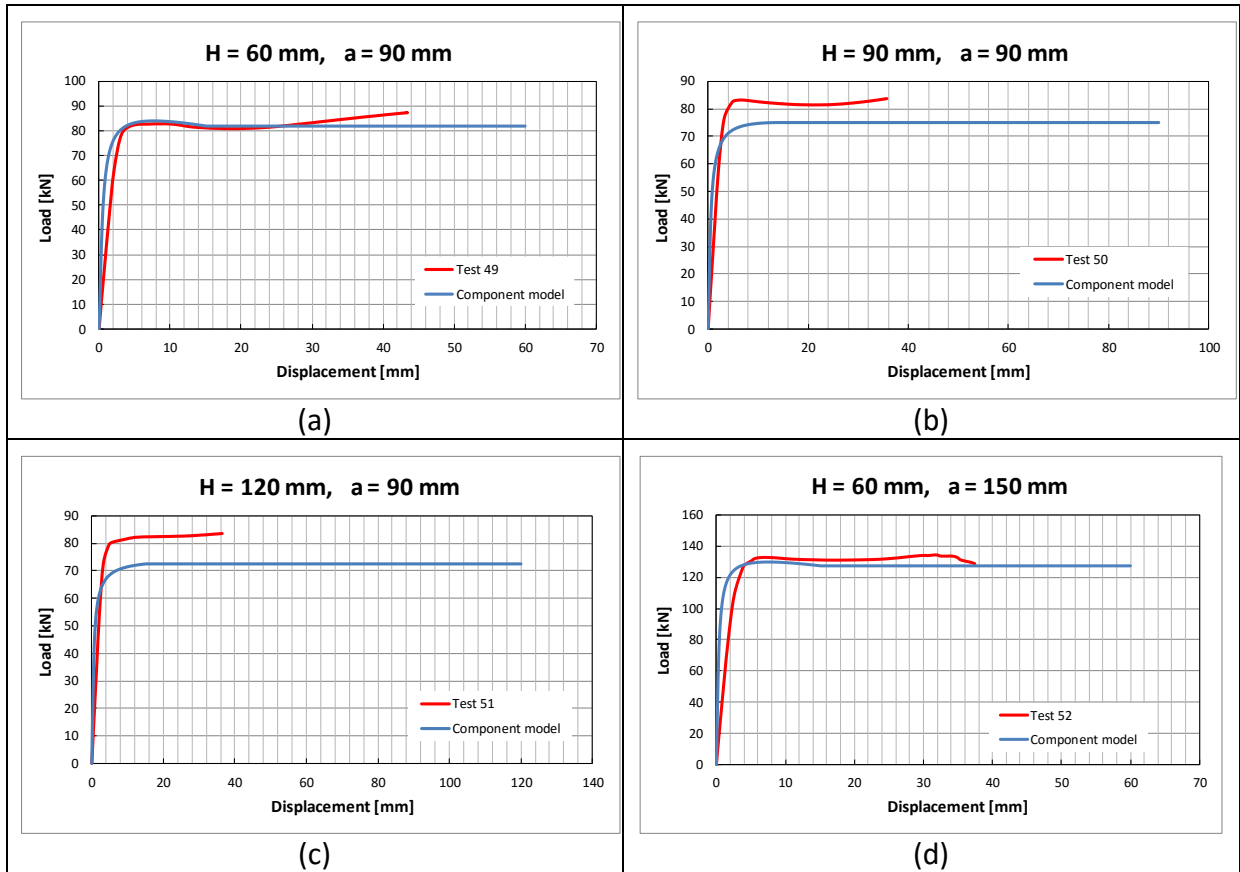
Figure 78: RC-in-Compression component model: parametric studies (Tests 49-52)
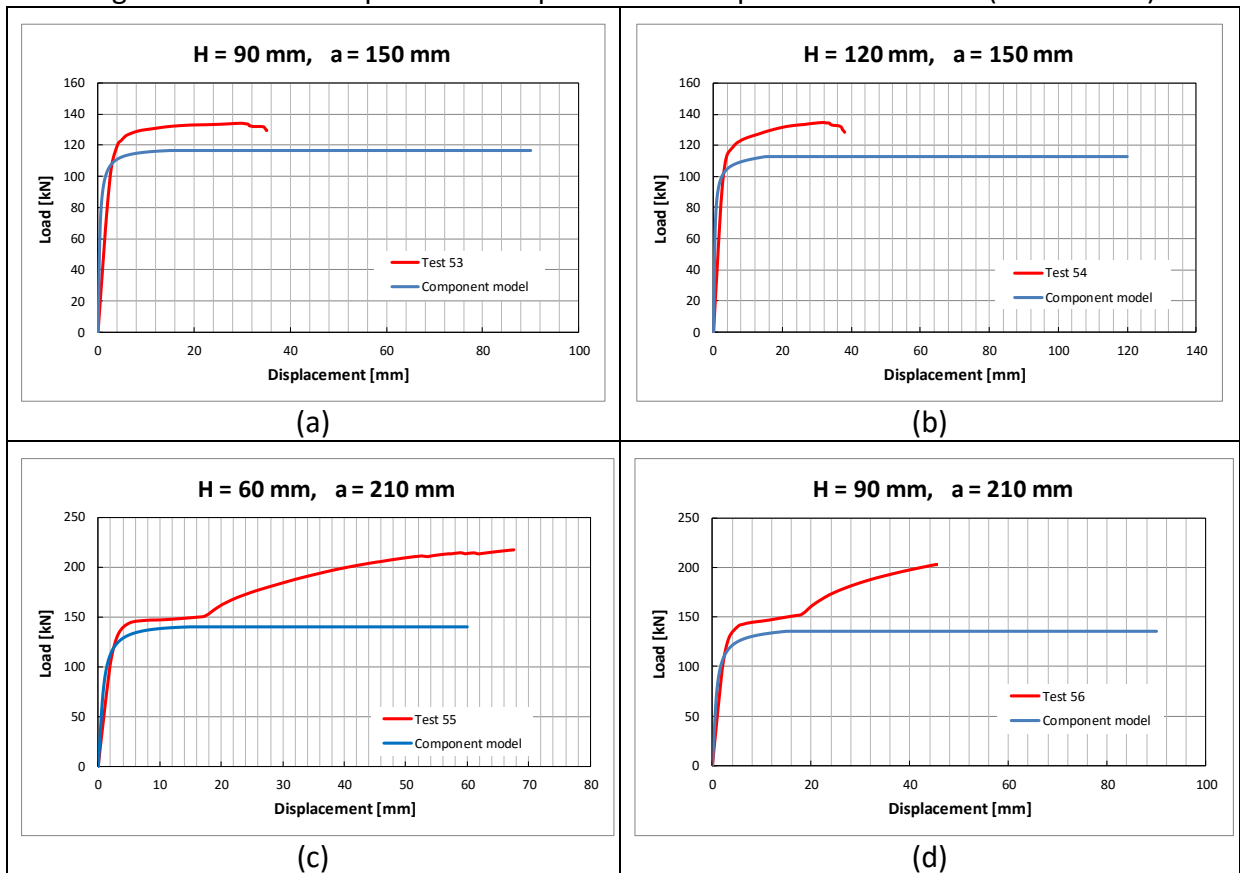
Figure 79: RC-in-Compression component model: parametric studies (Tests 53-56)
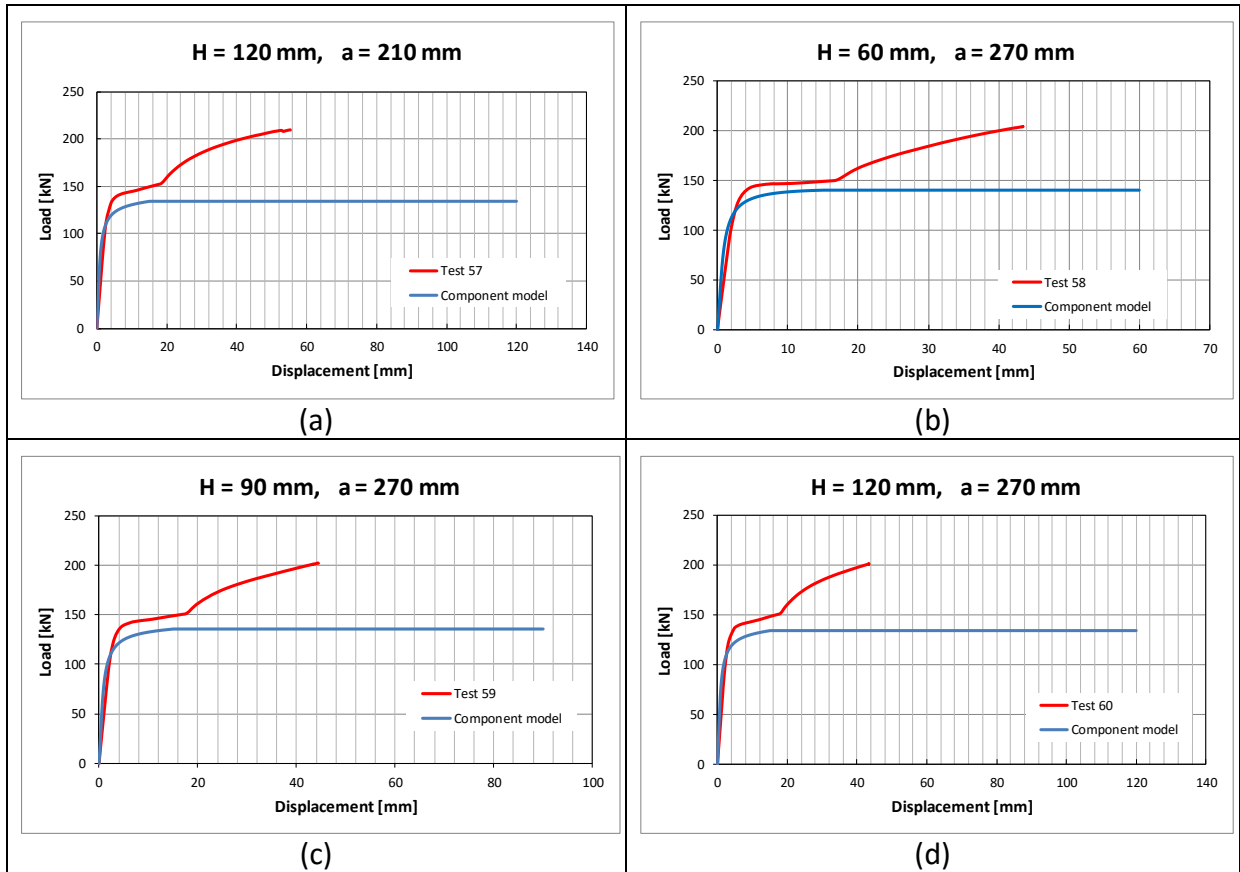
Figure 80: RC-in-Compression component model: parametric studies (Tests 57-60)
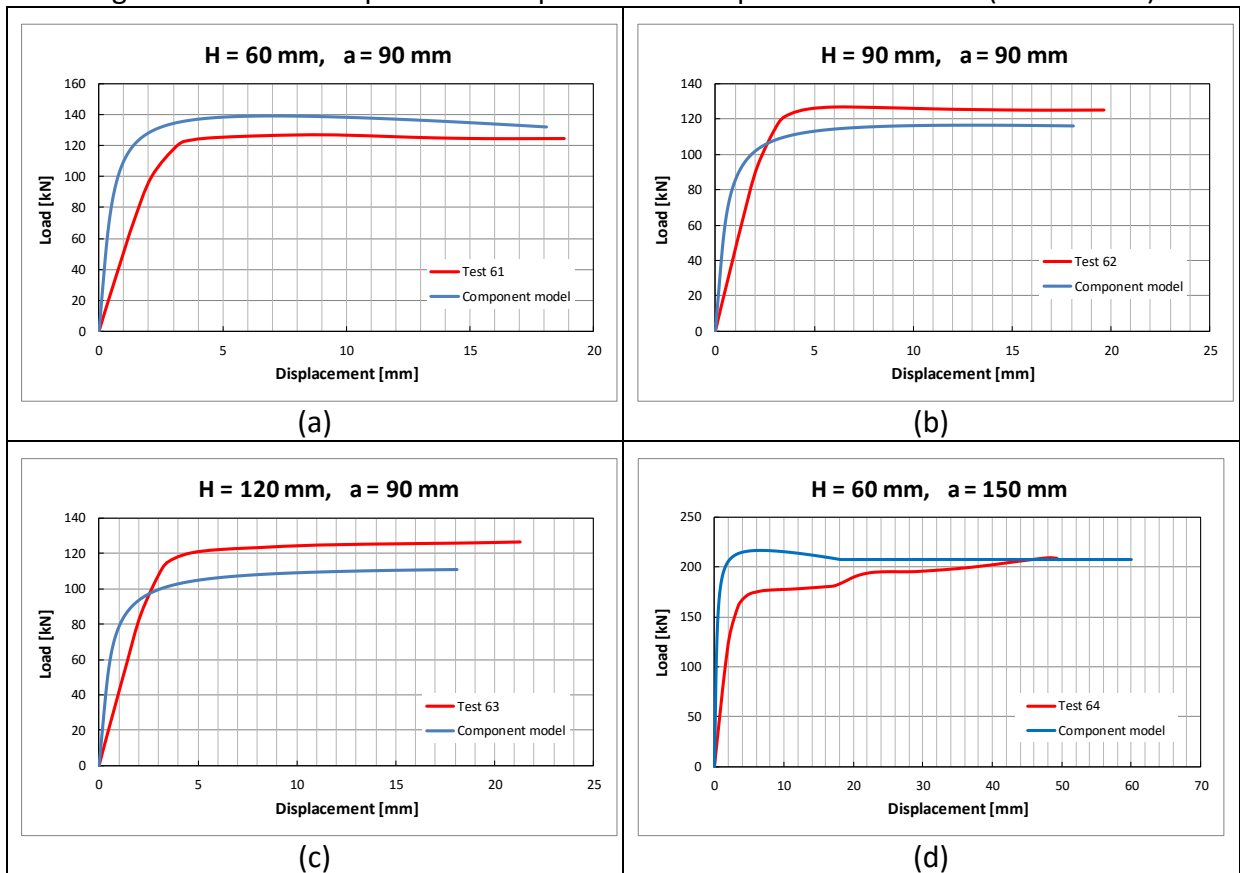
Figure 81: RC-in-Compression component model: parametric studies (Tests 61-64)
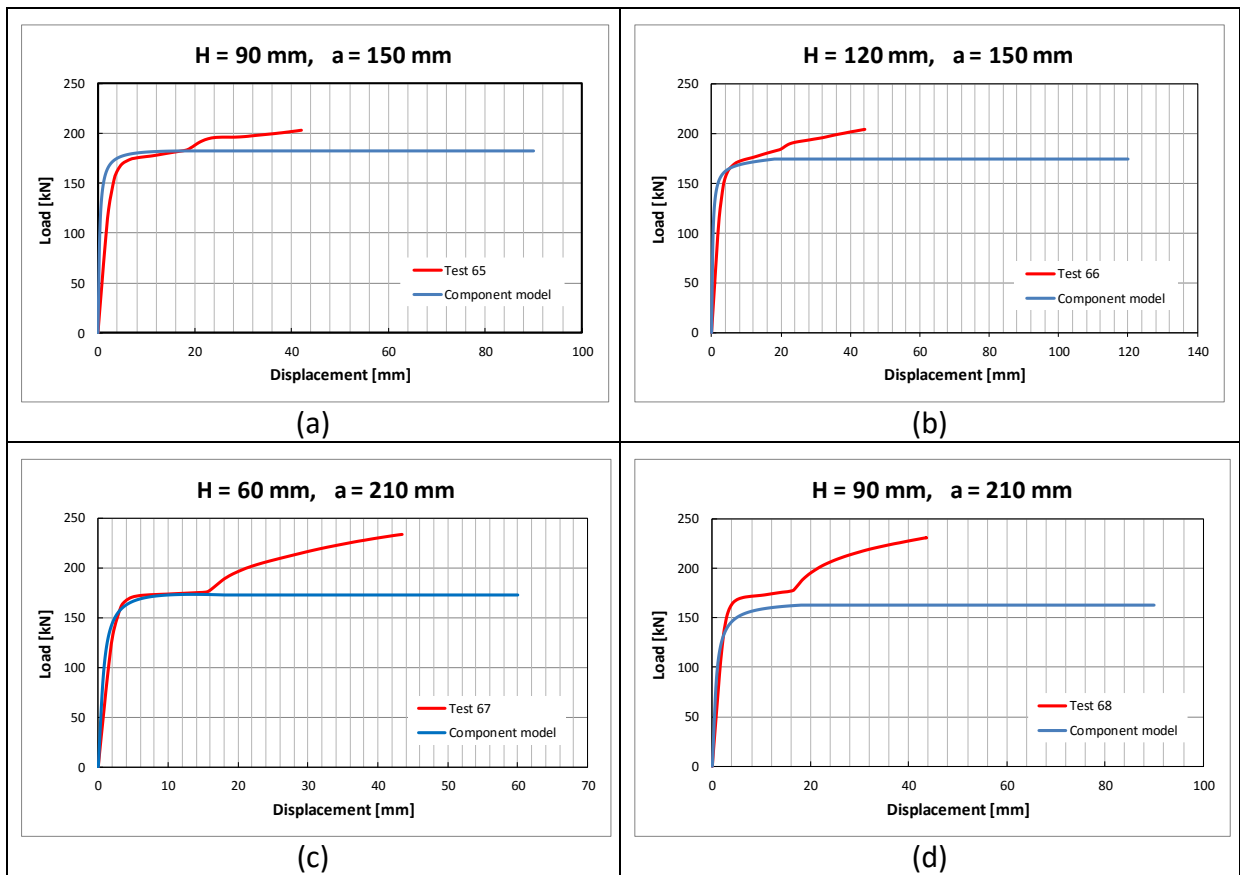
Figure 82: RC-in-Compression component model: parametric studies (Tests 65-68)
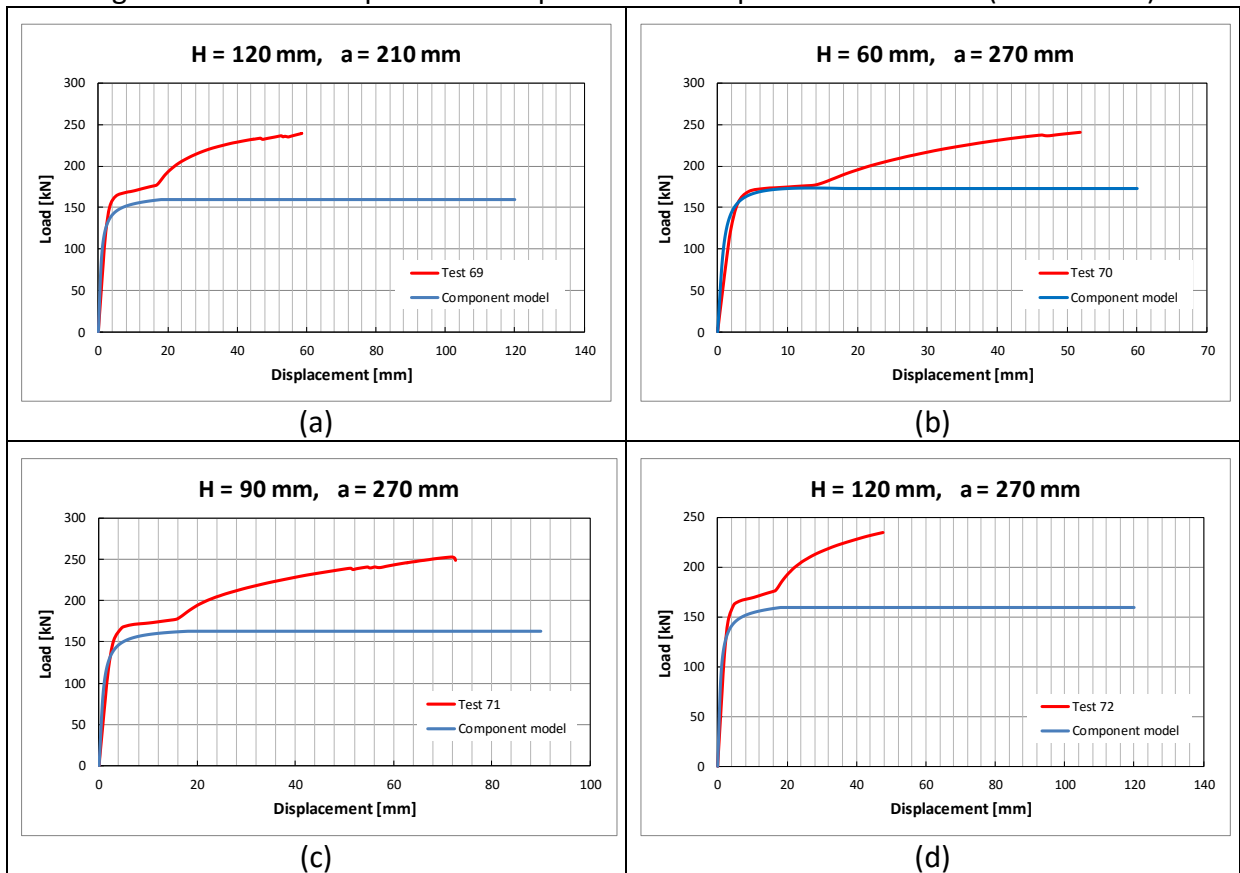
Figure 83: RC-in-Compression component model: parametric studies (Tests 69-72)
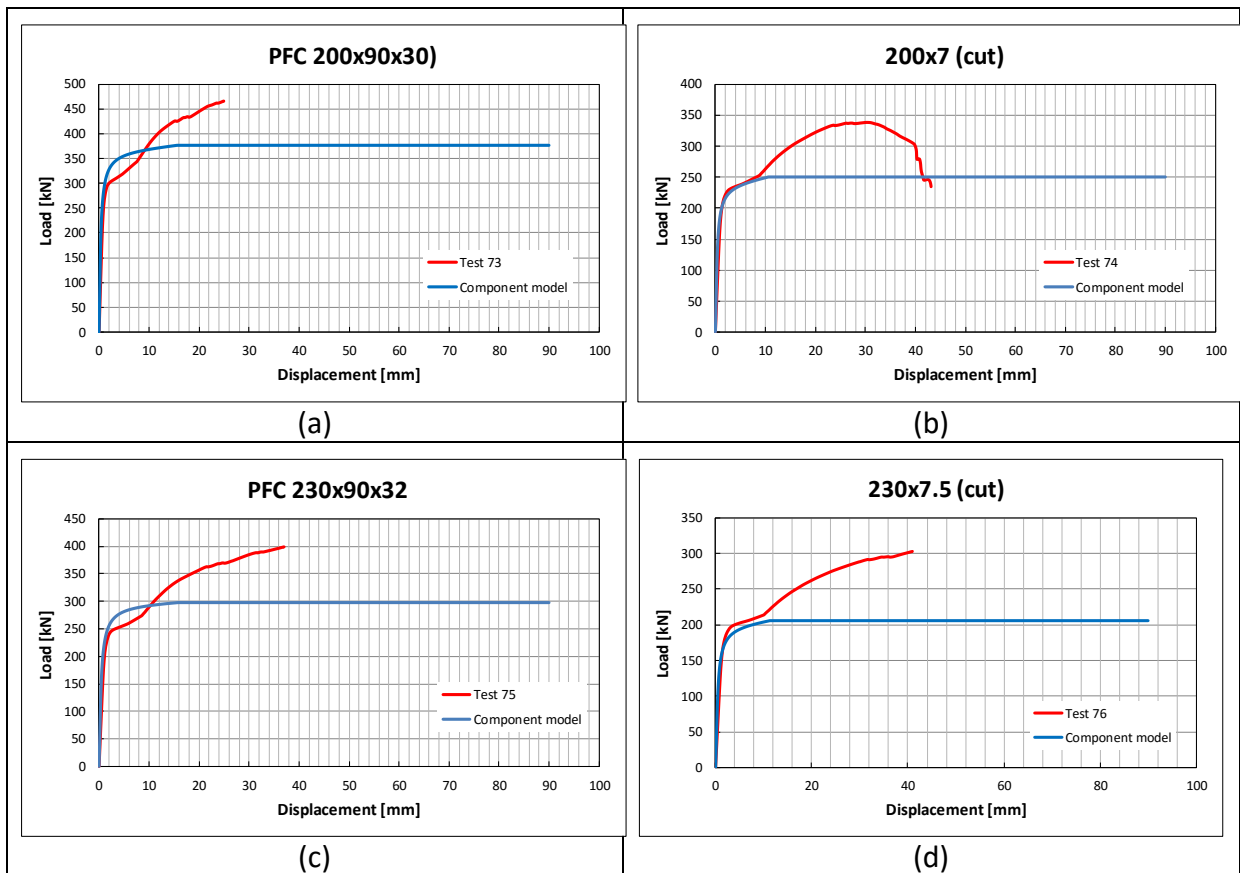
Figure 84: RC-in-Compression component model: parametric studies (Tests 73-76)
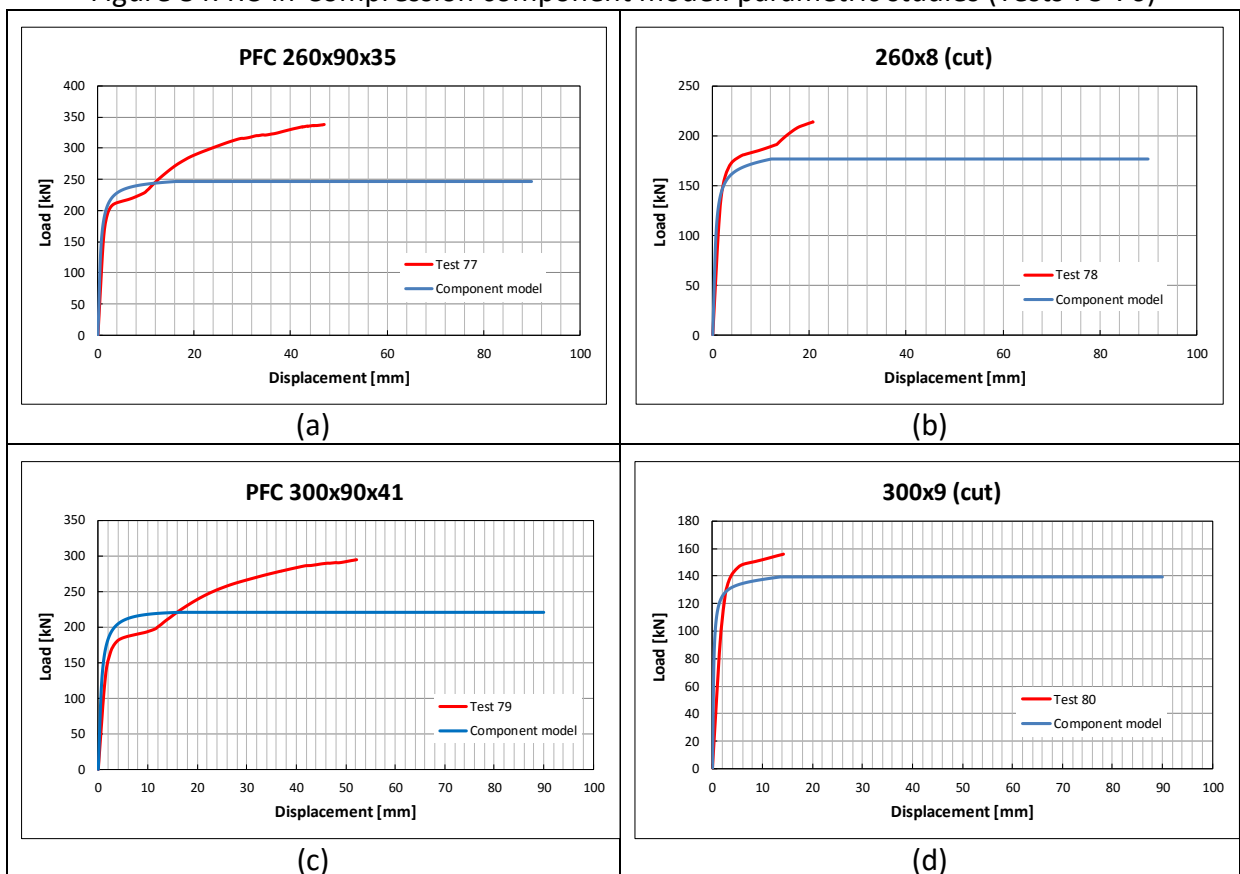
Figure 85: RC-in-Compression component model: parametric studies (Tests 77-80)
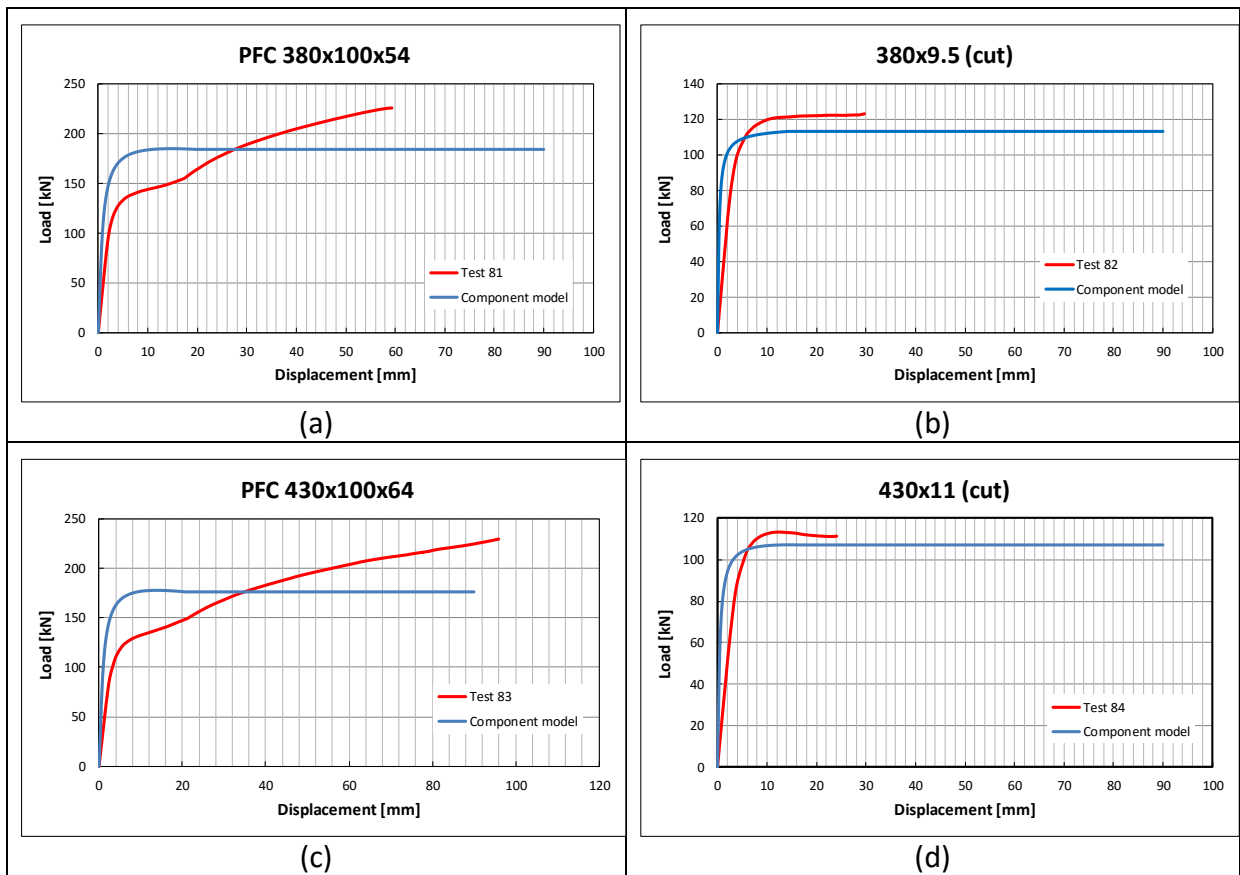
Figure 86: RC-in-Compression component model: parametric studies (Tests 81-84)

3.5.3.1 Plastic hinge mechanism

The FE analysis has supplied detailed data on the component behaviour. Figure 87 and Figure 89 show the deformed shapes for the parametric compression Tests1 and 48. Their strain contours are shown in Figure 88 and Figure 90; these clearly show the plastic hinge locations. They illustrate the two types of plastic hinge mechanism, which have been discussed in 3.5.2.
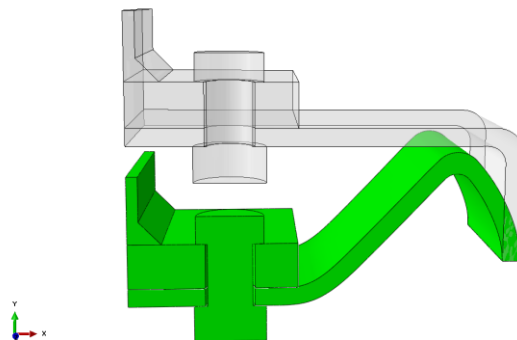
Figure 87: Compression parametric study Test 1 deformed shape by FEA.

86
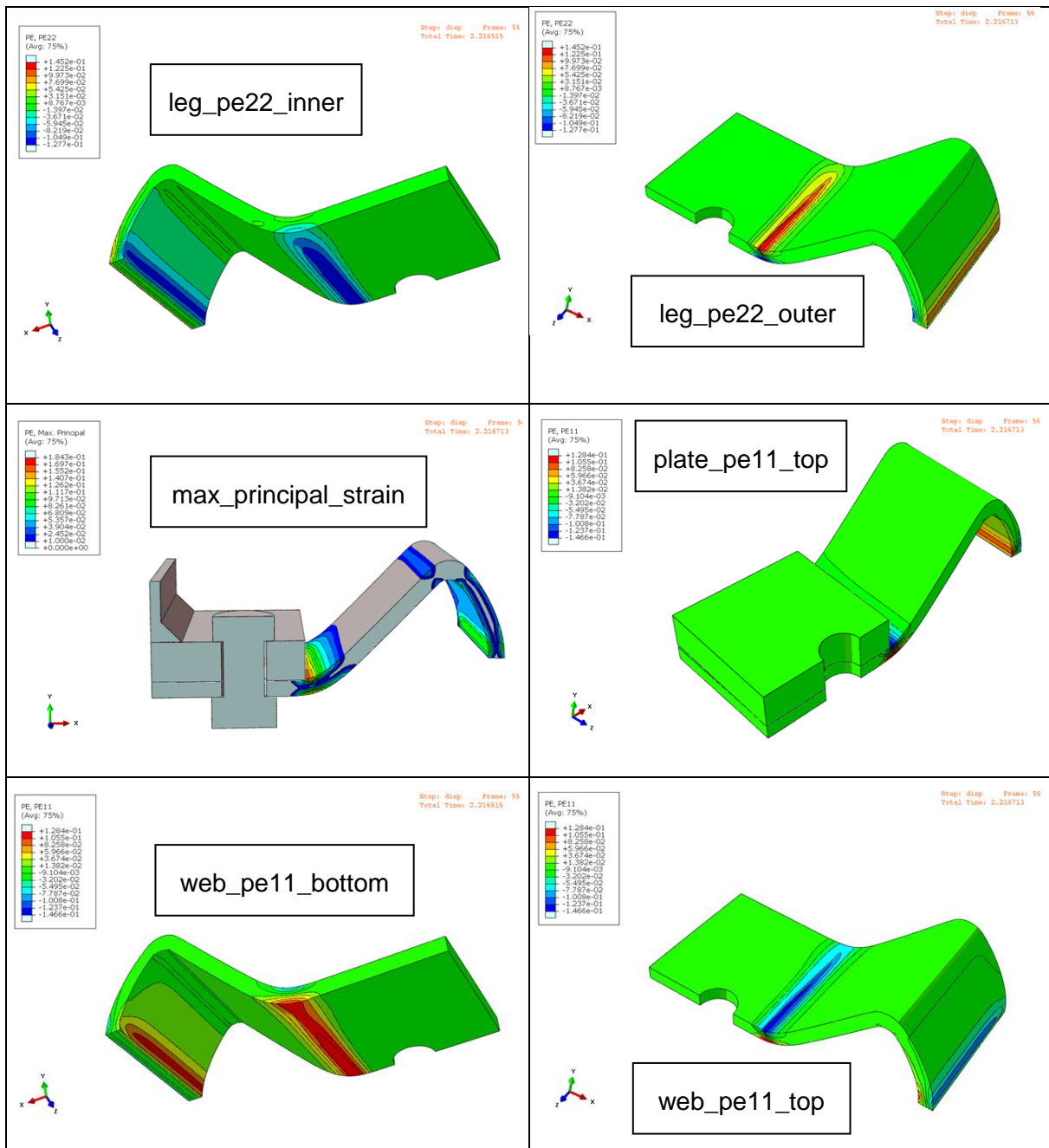
Figure 88: Compression parametric study Test 1 strain contours by FEA
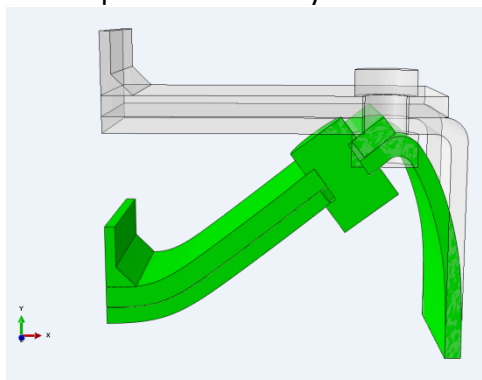
Figure 89: Compression parametric study Test 48 deformed shape by FEA
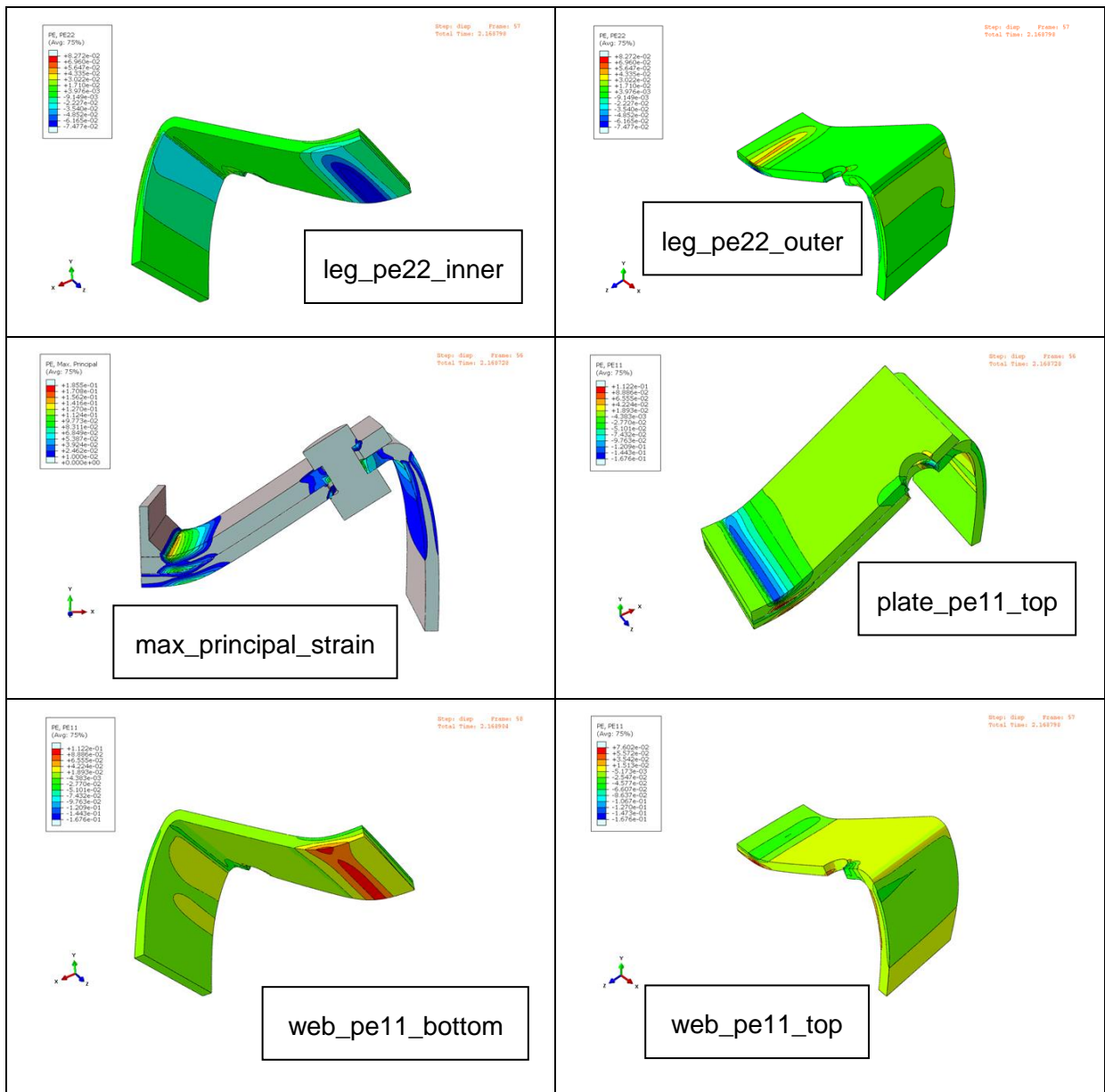
Figure 90: Compression parametric study test 48 strain contour by FEA

3.5.3.2 Leg length

Figure 91 presents summaries of FEA results 1 to 12 for compression. In these figures, 'H' is the leg length, and 'a' is the bolt separation. In the compression analysis, the effect of reverse channel leg length is not recognizable. This is because the analyses terminated early due to convergence problems. In fact, Test 1 (leg length 60mm) deviated from Test 2 (leg length 90mm) and Test 3 (leg length 120mm) after the deformation reached 60mm.
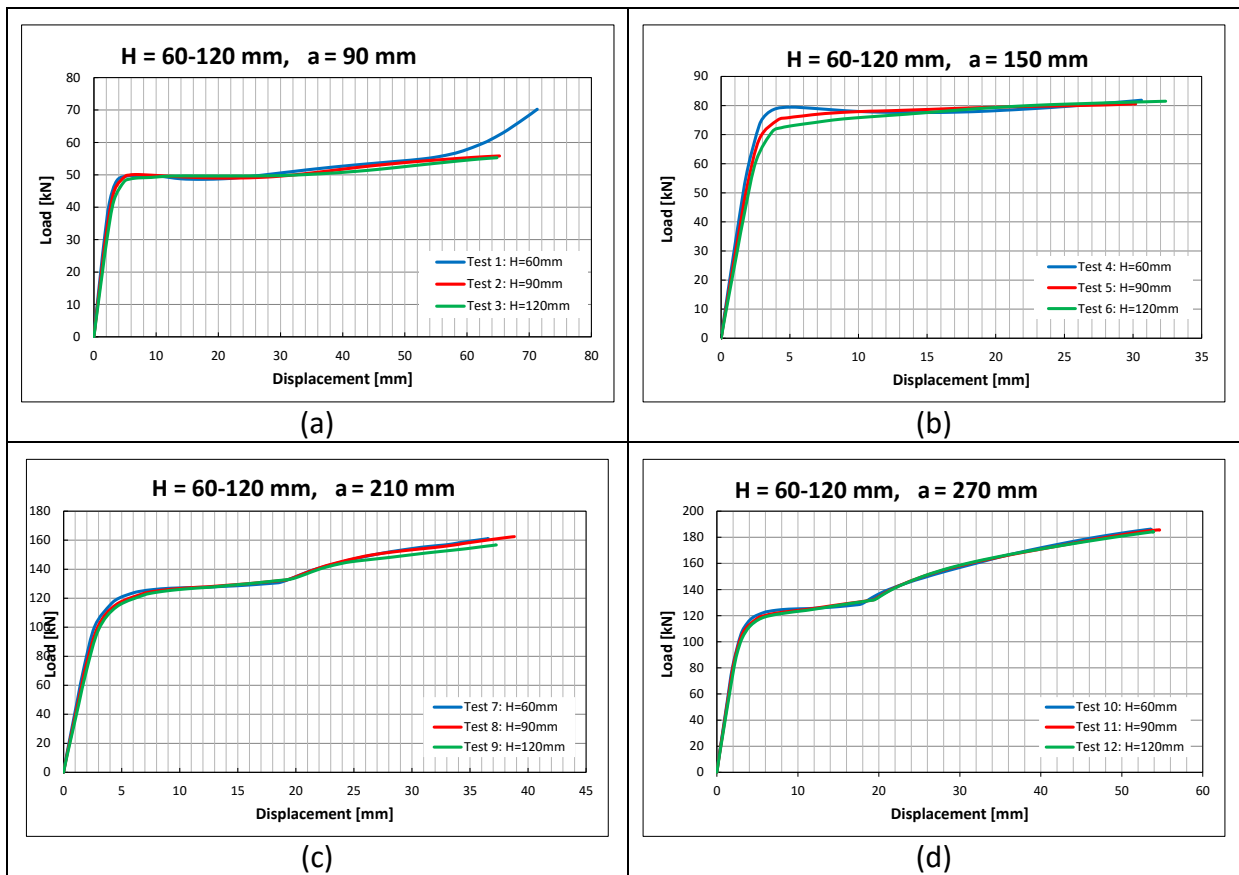
Figure 91: Leg length (H) effect on one bolt in compression parametric strudy: FEA results
(Tests 1-12)

3.5.3.3 Bolt separation ('a' in Figure 42)

Figure 92 shows a summary of bolt separation effects on reverse channels under both tension and compression. In these figures, 'H' is the leg length, and 'a' is the bolt separation. Since bolt edge distance is constant in this study, larger bolt separations imply larger endplate width. The larger bolt separation (wider endplate) will increase the elastic stiffness. This is similar to the tension cases, where the bolt separation defines the plastic hinge locations. Therefore, a reasonable bolt separation is necessary to increase the connection ductility.
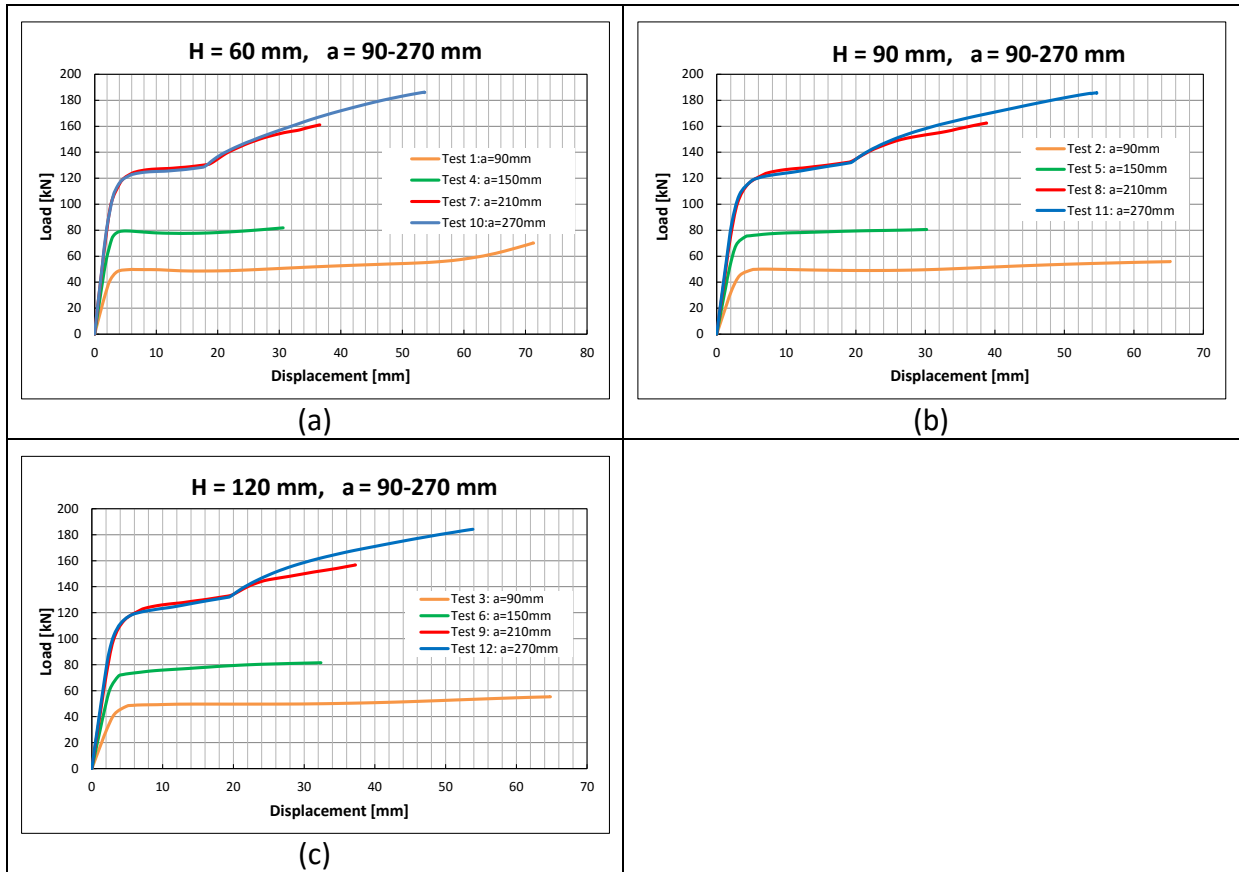
Figure 92: Bolt separation effect (a) on one bolt in compression parametric study FEA results (Tests 1-12)

3.5.3.4 Endplate thickness

Figure 93 shows a comparison of FEA results for one-bolt-row cases with different endplate thicknesses (10mm and 20mm). Except for cases with 90 mm bolt separation, the thinner endplate shows greater ductility. This is because the thinner endplate changes from plastic hinge Mechanism 1 to plastic hinge Mechanism 2 (shown in Figure 68 and Figure 69).Figure 94 shows the deformed shape and the different plastic hinge locations.

3.5.3.5 Reverse channel thickness

Figure 95 compares reverse channels with different thicknesses (8mm in Test 1, 10mm in Test 49 and 12mm in Test 61). Similarly to the tension cases, the stiffness will be increased considerably with a thicker reverse channel.
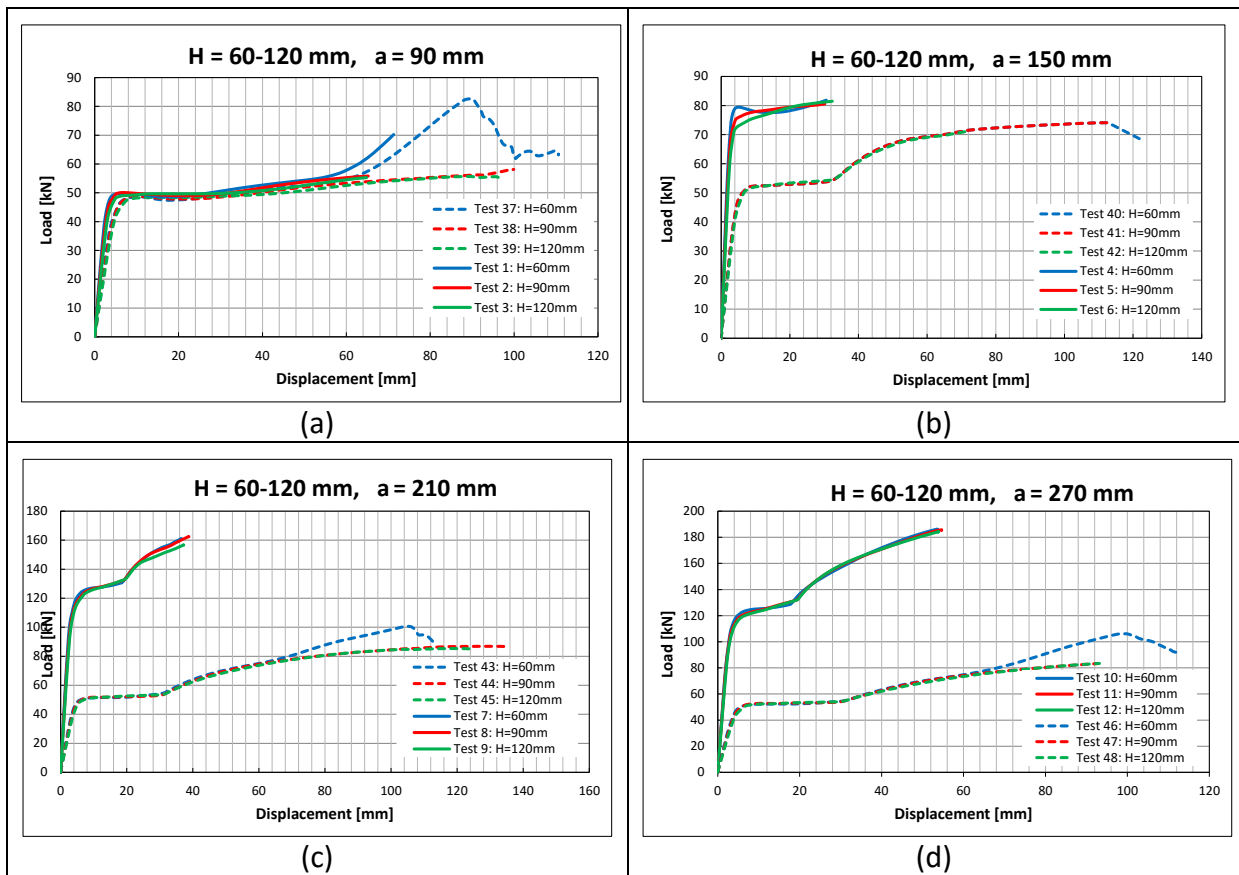
Figure 93: Endplate thickness effects on reverse channel in compression parametric study
FEA results (Tests 1-12 & 37-48)

| Test 4 | Test 40 |
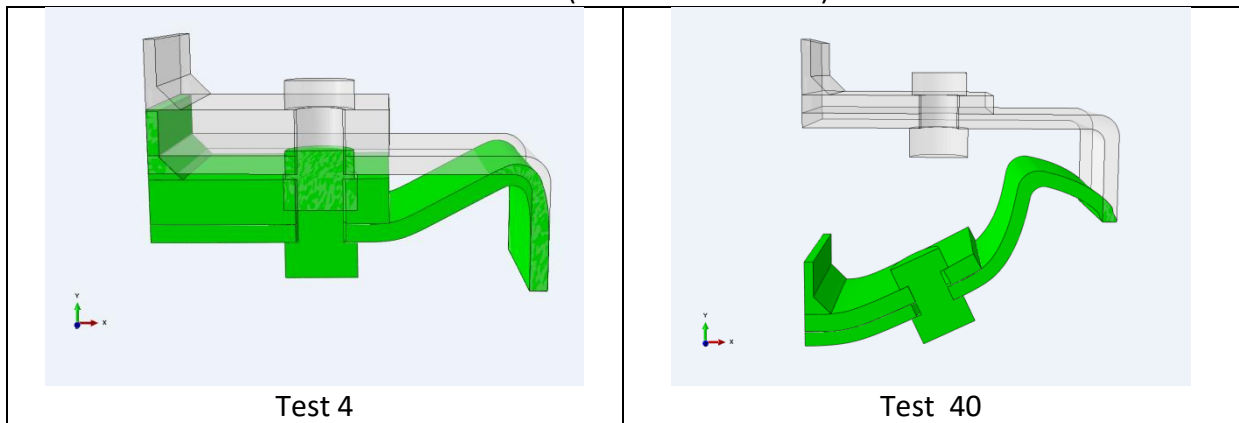
Figure 94: FEA images of compression parametric study tests 4 and 40

3.5.3.6   Rolled channel (PFC) or constant thickness channel cut from a tube

Figure 96 shows the comparison of the rolled channel (PFC) at a constant-thickness channel cut from a tube, which have different definition of leg thickness. Similar to the tension cases, the tube-cut section with thinner legs shows the higher ductility.
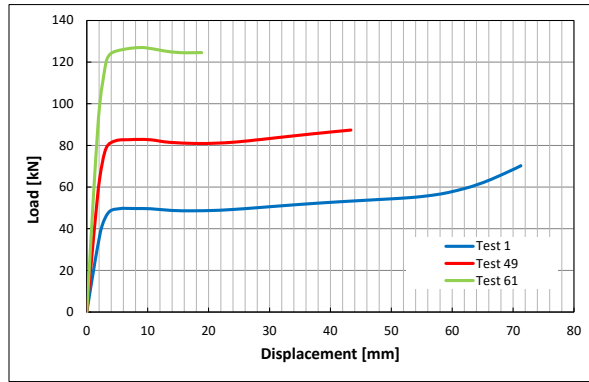
Figure 95: Effect of reverse channel thickness effect in the parametric study

(a)

(b)

(c)

(d)

(e)

(f)
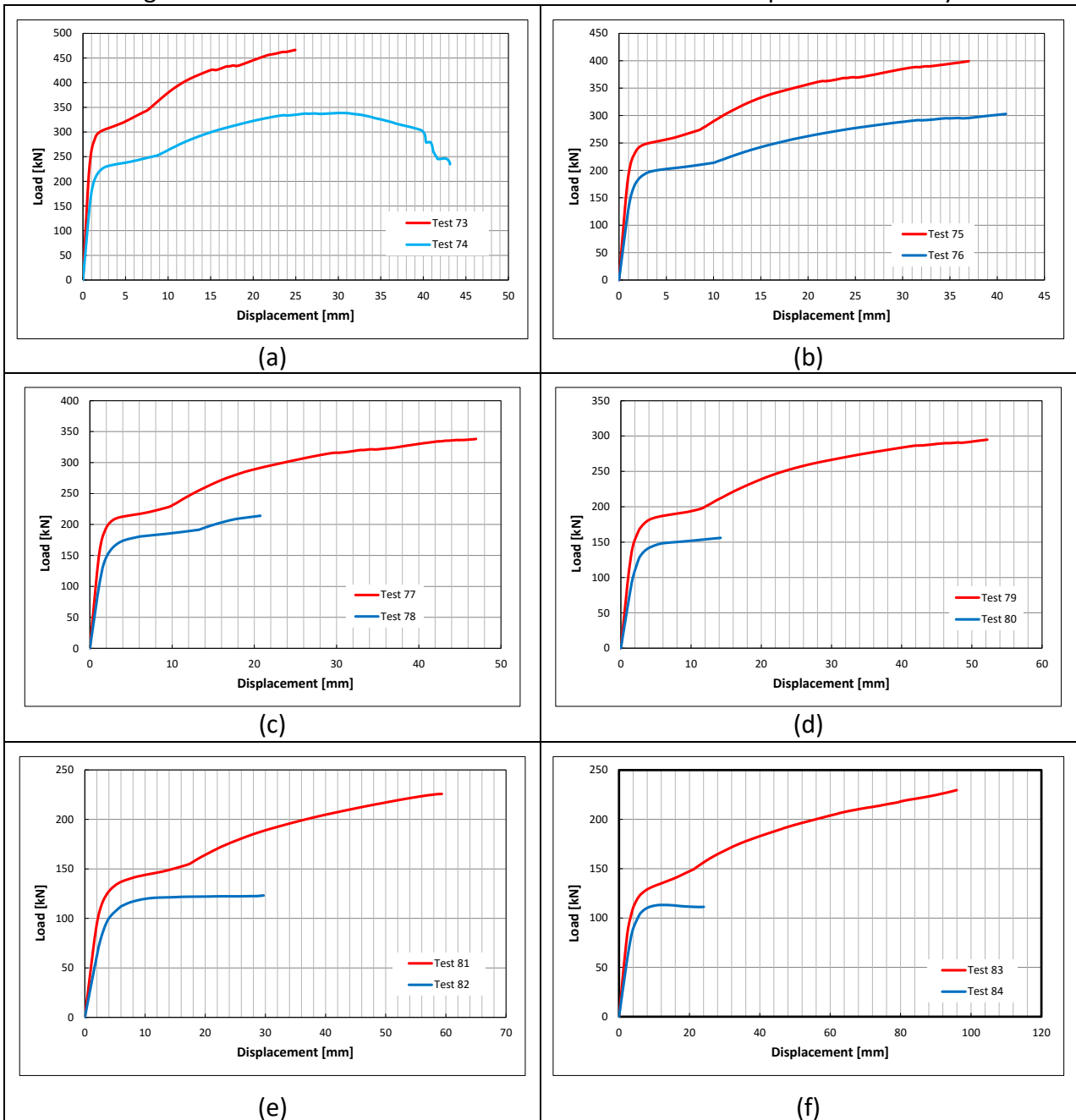
Figure 96: parametric study PFC VS. Tube-cut (compression)

3.5.3.7 Post yield hardening in the reverse channel under compression

Figure 97 presents the FE analysis results for the compression parametric study (single-bolt-row cases). The cases with wider endplate (a = 210 and 270 mm) show post-yield hardening after the plastic hinges form. This is because the reverse channel leg in compression is relatively stiff at the beginning. At large deformation it starts to show its contribution, as 'post-yield hardening' happens. In order to simplify the calculation, this post-yield hardening is excluded from this development.
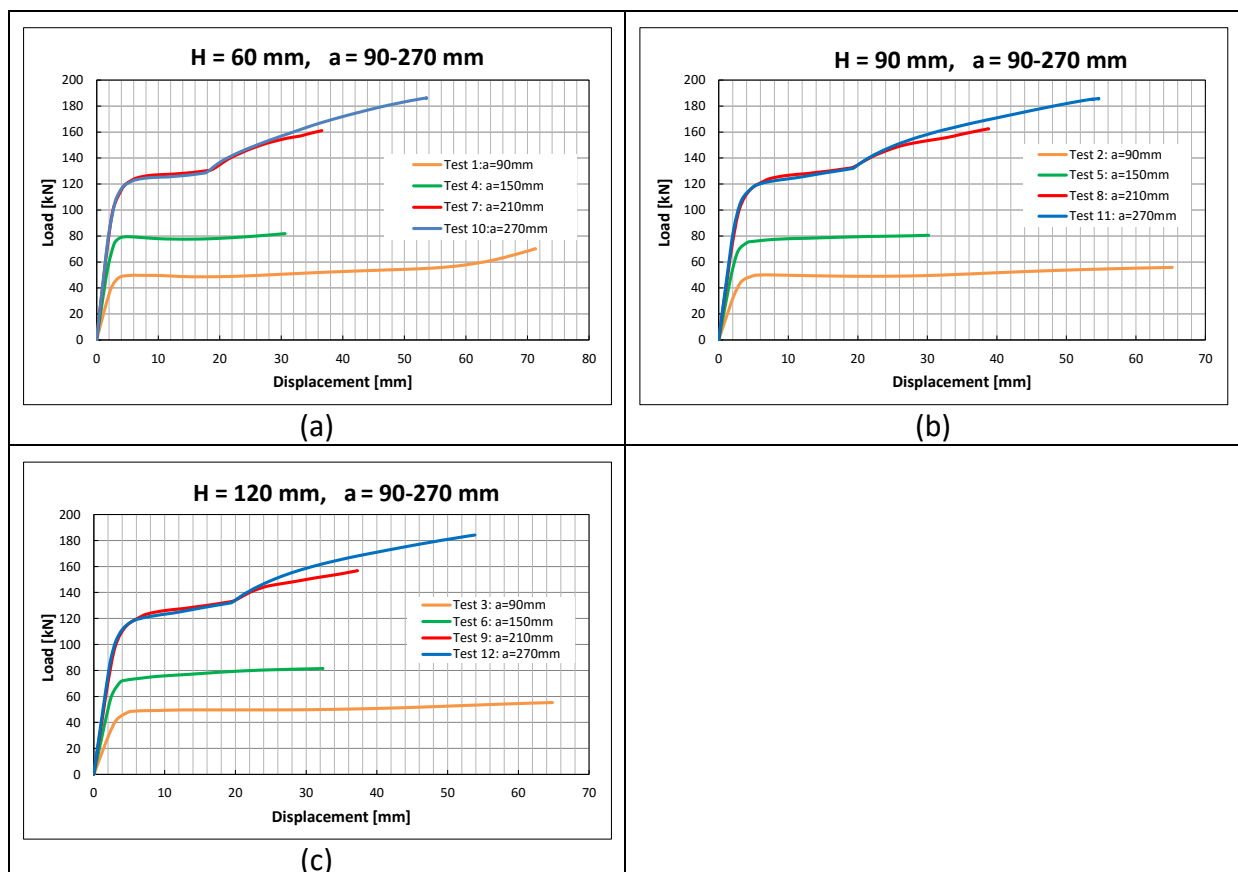
Figure 97: post-yield hardening in the compression parametric study

3.6 Conclusion

Based on the plastic hinge method, the component models for the reverse channel under tension and compression have been developed. In particular, a bolt pull-out limit has been derived from a 'cone model' (also called 'bolt pull-out model'). The COMPFIRE project has supplied comprehensive test and FE data to characterise the behaviour of the reverse channel under tension. Parametric studies are carried out hereafter to investigate the reverse channel behaviour. These studies will show that the component models are capable of reasonably representing the reverse channel behaviour, and that they are ready to be

implemented within the component based connection element, to model the reverse channel connection behaviour in fire.

Chapter 4. Development of a general-purpose component-based connection element

Over the past 30 years the components which can be assembled to represent ambient-temperature small-deflection moment-rotation behaviour of common connection types (mainly flush and extended endplate connections) have been investigated by researchers all around the world, and a number of component models have been developed. Figure 13 shows the component-based connection assembly by Simões da Silva (2001) for the flush endplate joint.

These researches have taken place in the context of the development of semi-rigid design principles (embodied in Eurocode 3 Part 8 (CEN, 2005b)) for steel and composite structural frameworks. Figure 98 shows another assembly which is consistent with Eurocode 3 Part 1.8, by Burgess (2009).
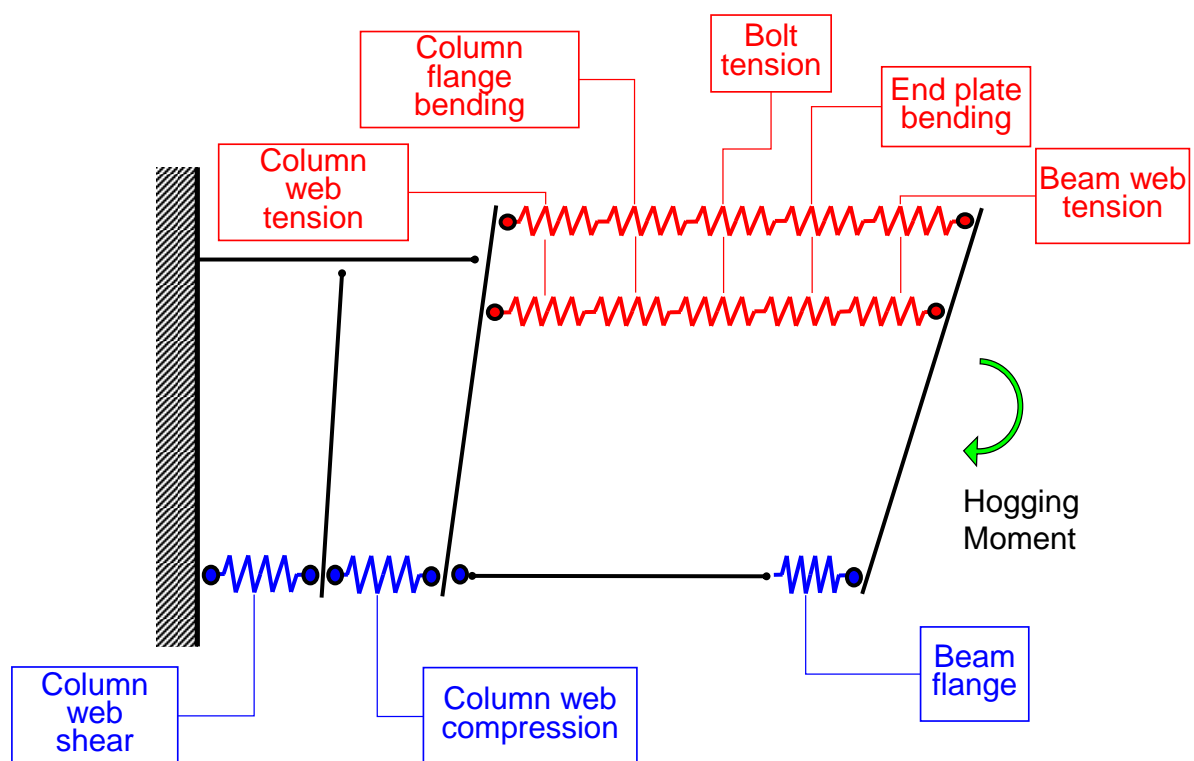
Figure 98: Component assembly for endplate connection (Burgess, 2009)

The previous research objectives have been rather limited. The component-based connection models have been used only to calculate the elastic rotational stiffnesses of connections, and their moment capacity; they do not need to include strain-reversal properties, fracture of individual components or the effects of elevated temperatures. In

contrast, the component-based connection models which are intended to be used in structural numerical modelling of framed building structures under fire conditions have to deal with the net compressive forces and distortions caused by restrained thermal expansion of beams, as well as the tensile forces and distortions caused by catenary action of the same beams at much higher temperatures, when the strength of steel has been greatly degraded.

Block (2006a) has summarized the procedure to develop a mechanical model into three steps, which are shown Figure 99Figure .

Step 1 Identification of the active components: Active components are those which either contribute to the deformation of a joint or limit its strength.

Step 2 Specification of the component characteristics: In order to extend material properties to the fire case, each component's behaviour needs to be analysed at elevated temperatures using F.E. studies and experiments, and described with a simplified analytical model.

Step 3 Assembly of the active joint components: If the behaviour of the individual components is known, it is possible to assemble them in a stiffness model and to represent the joint as a joint finite element. Each component is represented as a translational spring interconnected by rigid links. The joint's overall performance in fire will then be modelled.

This procedure is very flexible. It can consider any types of joint, either bolted or welded. In order to model the connection constitutive behaviour in fire, some specific effects such as component fracture, progressive failure of component can be introduced.

Component models which can be assembled to model both flush endplate and reverse channel connections under tension and compression at elevated temperatures, including their ultimate (or fracture) conditions, have been developed and characterized by the author as a part of the COMPFIRE project. These components can be assembled to model various connection specifications.
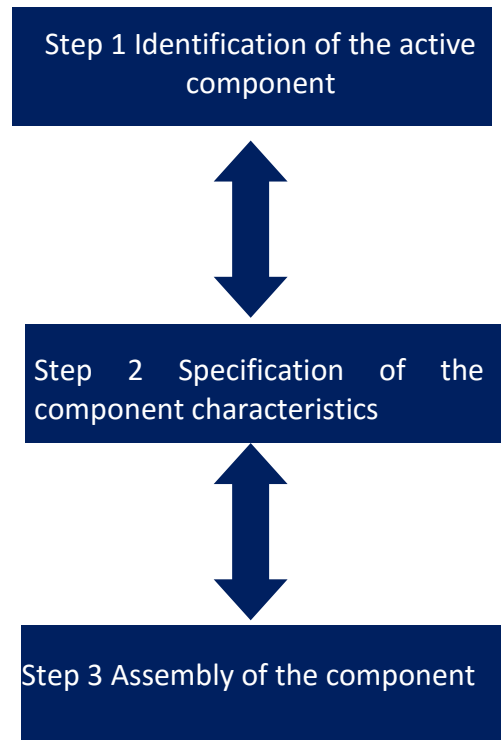
Figure 99: Component-based connection element development procedure.

In this chapter, the key components for flush endplate and reverse channel connections are identified. On the basis of the flush endplate connection, the assembly of an appropriate number of components within a general-purpose component assembly is generalized to represent connections of different specifications, and this is built into the *Vulcan* software. In this expandable assembly, the tension and compression components are represented using non-linear force/displacement curves, which are defined by the user. This is actually a component-based connection element with flexible access, and is called a user-defined connection element. Beyond this, several of the adopted component models are reviewed and incorporated into the general-purpose component assembly to form connection elements for both the flush endplate and the reverse channel connection types.

4.1 *Identification of the active components*

Table 6.1 in EC3 Part 1.8 lists the basic components for endplate joints:

- ➢ column web panel in shear
- ➢ column web in transverse compression
- ➢ column web in transverse tension

- column flange in bending,
- end-plate in bending,
- flange cleat in bending
- beam or column flange and web in compression,
- beam web in tension
- plate in tension or compression
- bolt in shear
- bolts in bearing
- Welds

These active components are also shown in Figure 100.
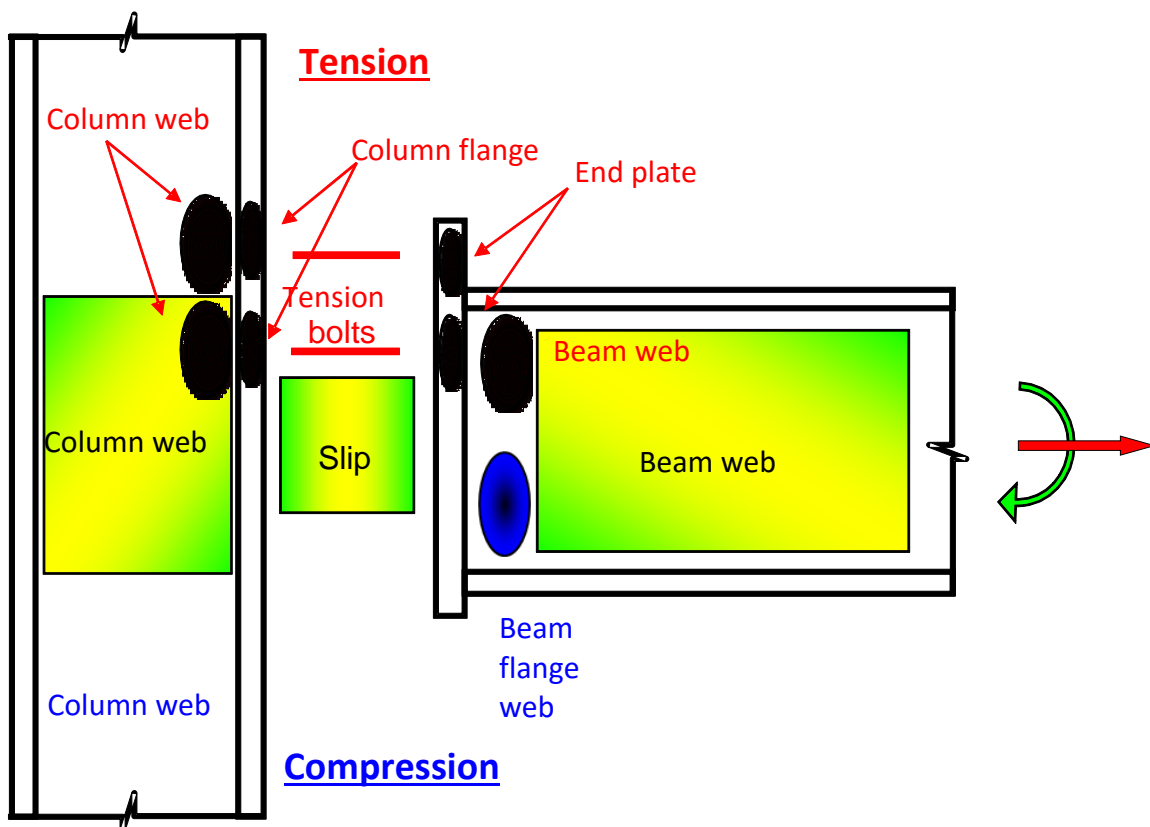
Figure 100: Endplate connection active component (Burgess, 2009)

Figure 101 lists the active components which are considered within the connection element under this development.
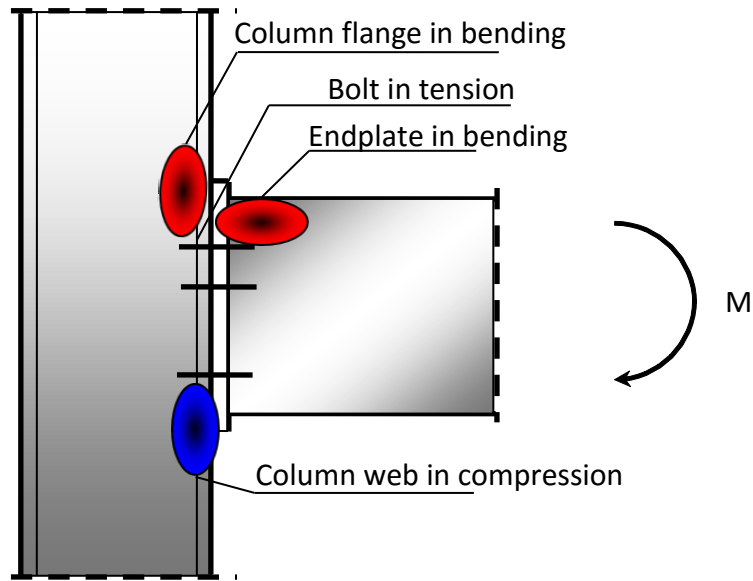
Figure 101: Zones of structural action in endplate joints (Spyrou, 2002).

Based on the experiments conducted in COMPFIRE (Huang, 2013a, 2013b) and FE studies (RFCS, 2012a), the zones of structural action for the reverse channel connection are identified in Figure 102.
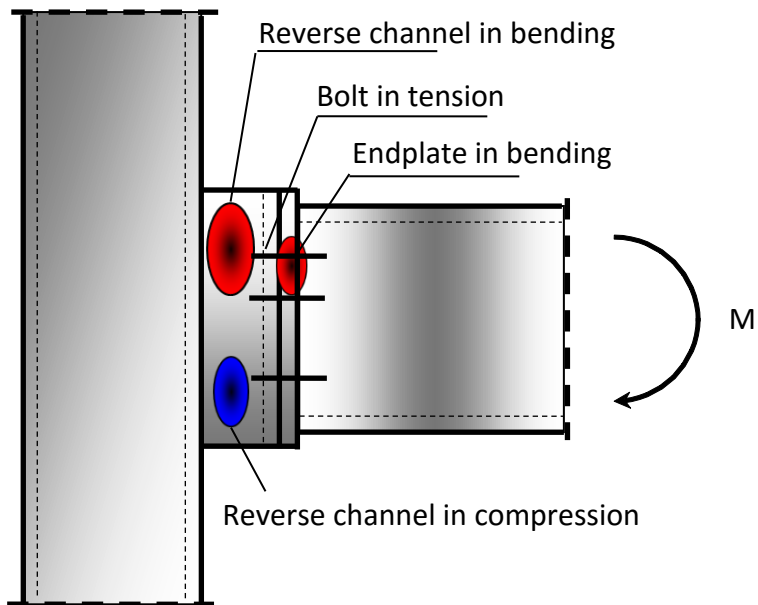
Figure 102: Active component in reverse channel joints.

4.2   Development of the user-defined connection element

The user-defined connection element is a component-based connection element developed from the assembly of a number of components, which follows the distribution of key components in the flush endplate connection (Figure 100). Users are allowed to define the

basic behaviour of all components at ambient temperature as non-linear force/displacement curves. Reduction factors are applied to the material properties of these in order to define the component behaviour at elevated temperatures. The following sections will cover:

➢ Basic assumptions for the structural properties of each tension/compression component,

➢ How to combine these tension components in series into one effective "bolt-row" spring,

➢ How to assemble these spring rows as a connection element,

➢ How to fit this connection element into *Vulcan* to deal with the structural behaviour of buildings at elevated temperatures, including progressive collapse.

4.2.1 Assembly of components

Figure 103 depicts the general-purpose component assembly of a simple two-bolt-row endplate connection, together with the action of the adjacent shear panel towards the end of the beam. Figure 104 illustrates how this component-based connection element and shear panel can deform in response to the combination of axial force, shear force and moment which can happen during a fire.

In order to tackle the changing force combination during a fire, gaps (shown in Figure 105) are utilised in Figure 103 and Figure 104. Figure 106 uses a reverse channel connection as an example to illustrate the function of these gaps. The gap between a compression spring row and a rigid face is designed to represent the space between the reverse channel and the beam endplate. Once these are in contact, the compression spring row is activated, which ensures that it only works under compressive force. The gaps between the rigid links above bolt springs in tension (explained in detail in 4.2.5) are formed and increased when the bolt's plastic deformation breaks the contact between the mating plate surfaces. However, the bolt does not act in compression, which is transferred directly by the contact between the reverse channel (or column) face and endplate springs.
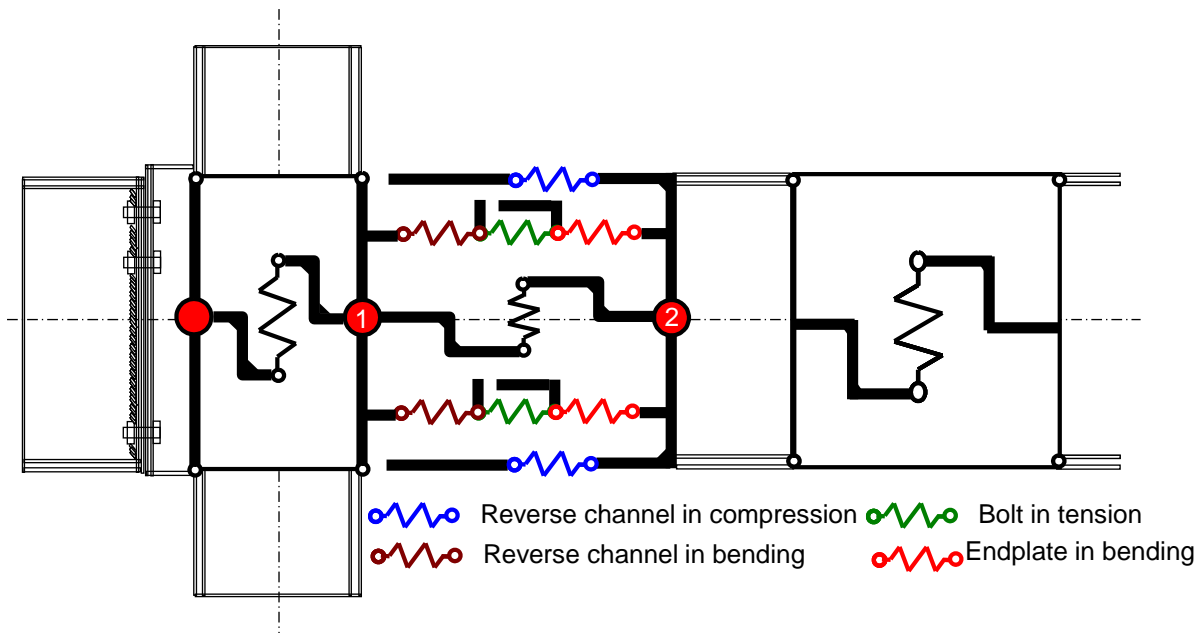
Figure 103: Component assembly and beam-end shear panel (Block, 2006)
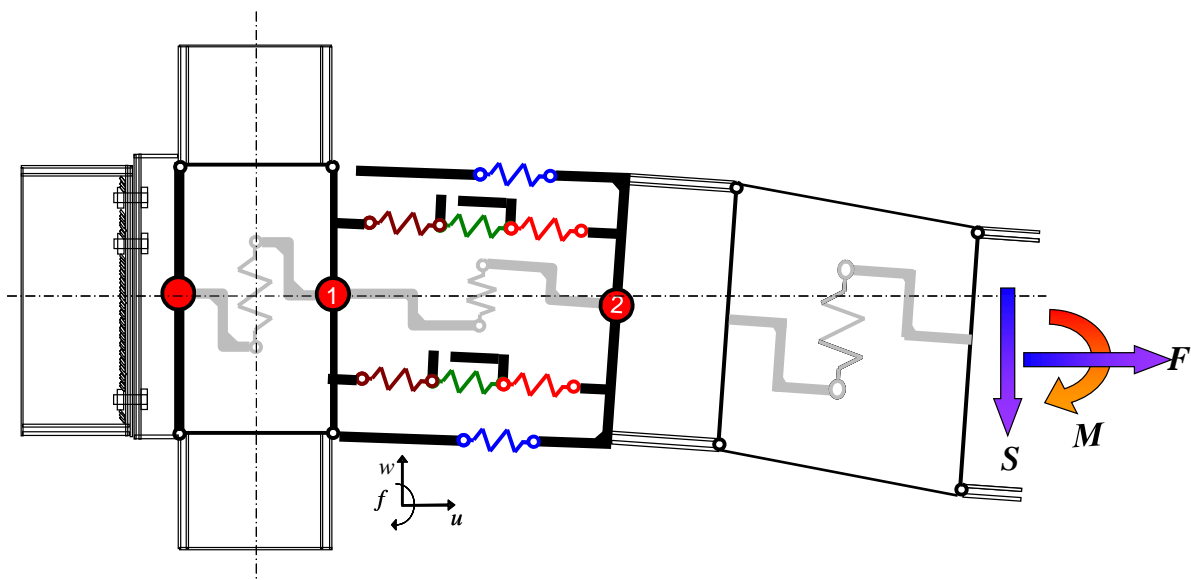
Figure 104: Deformation of component assembly and beam-end shear panel (Block, 2006)

The column-face connection (shown in Figure 106), removing the shear panel from these, is assumed to have its components assembled between rigid surfaces. In its implementation the connection assembly has been designed to include a maximum of five tension spring (bolt) rows and two compression spring rows. Node 1 is located at the intersection between the beam and column reference axes. Node 2 is the end-node of the beam. The vertical shear behaviour, representing slip between the column face and the beam end, has not so far been included in this assembly, and the connection is therefore assumed to be rigid in the vertical shear direction (as shown in Figure 106).

Figure 105: Illustration of gaps in a reverse channel connection

Compression component
Tension component
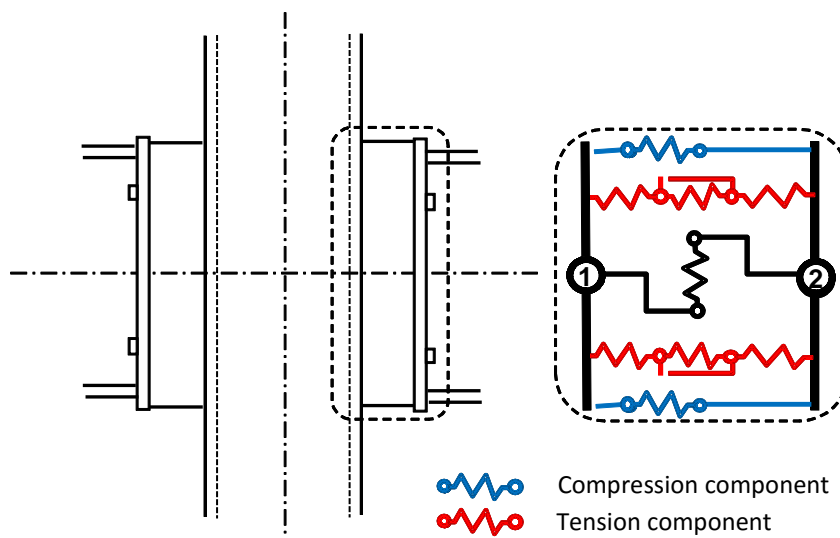
Figure 106: Schematic component assembly for the column-face
connection (Block 2006).

The column-face connection element is assumed to have no physical length. According to Li *et al*. (1995), the length of a modelled connection is so trivial compared to the length of the attached beam that its influence on frame behaviour is negligible.

4.2.2   Tension component

In the general-purpose component assembly, each tension bolt row includes three tension components, which work in series. The middle component in each series is designed to

represent the bolt in tension, and how this is represented will be explained in detail later. The other two tension components in a bolt row represent the column flange in tension and the endplate in tension for flush endplate connections, or the reverse channel in tension and endplate in tension for reverse channel connections. Each tension component's Force/Displacement behaviour is represented by a multi-linear curve without any 'descending' (negative stiffness) part. A typical multi-linear curve (Figure 107) consists of 5 intersections, which can be expanded if more are required, to plot relevant aspects of the component behaviour. In Figure 107, Point 5 represents the 'ultimate strength', at which point the component has its maximum resistance and deformation. Beyond the ultimate strength, the component is deemed to be fractured. If Point 5 is reached, the whole spring row in which this component is located will be 'switched off', and is not recoverable. It will not contribute to the joint's stiffness or robustness in the subsequent analysis.
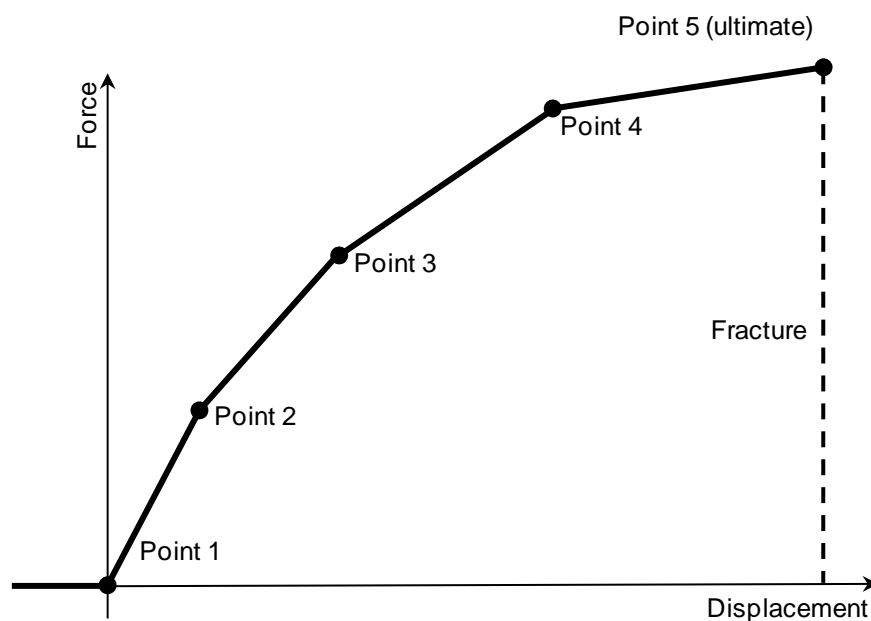
Figure 107: Typical tension component force/displacement behaviour

4.2.3   Effective Force/Displacement curve of a component at constant temperature

When a component carries a force it may become inelastic, and will then have irreversible deformation ('residual deformation') when its force is reduced to zero. In this development, the classic Masing rule (Gerstle, 1988) is employed for this 'memory effect'. Based on the Masing rule the unloading curve is the original loading curve doubled in scale and rotated by 180°.

If the initial loading curve (Block, 2006) is represented by:

$$D = f(F)$$

(4.1)

then the unloading curve can be described as

$$\frac{(D_A - D)}{2} = f\left(\frac{F_A - F}{2}\right)$$

(4.2)

where D_A and F_A (shown in Figure 108) are respectively the displacement and force at which unloading was initiated. In Figure 108, the node (F_A, D_A) is called the Intersection Point, and the intersection of the unloading curve with the zero-force axis is called Reference Point 1, which represents the permanent deformation caused. The intersection of the unloading curve with the zero-displacement axis is called Reference Point 2, and defines the point at which the component is pushed back to its original position by compression force. If the applied force, or the component's displacement, lies beyond its current intersection point, its displacement and applied force lie on the loading curve, and its permanent displacement will increase accordingly. On the other hand, if they lie below the intersection point, then they are on the unloading curve, and the permanent deformation will not change. Therefore, the bold solid line in Figure 108, incorporating the loading and unloading curves, has become the 'effective' *F/D* curve to represent the component's behaviour.
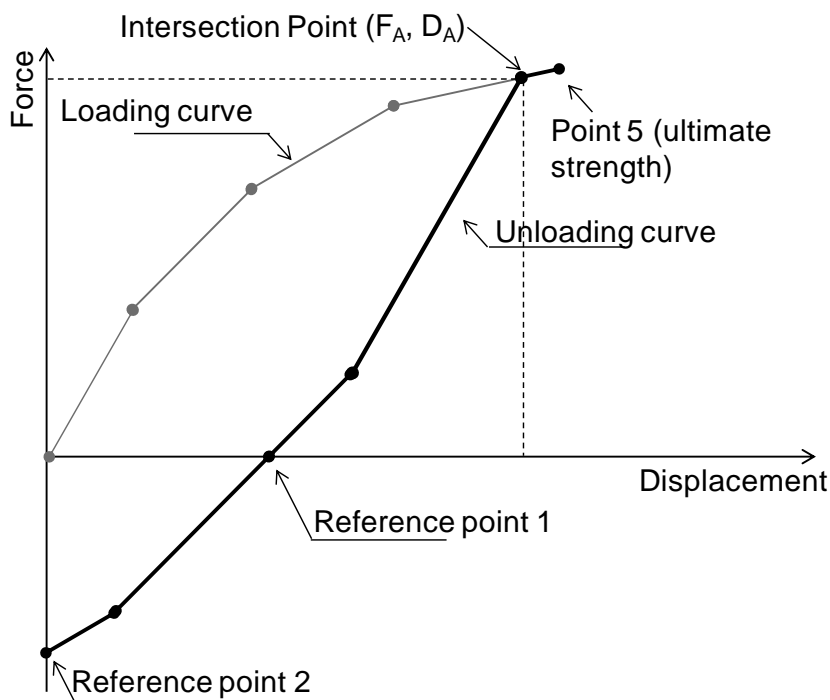
Figure 108: Typical tension component F/D curve

4.2.4   Unloading with changing temperatures

When a component is heated in a fire, its *F/D* curve is temperature-dependent and the temperature is continuously changing during the fire. Therefore, the 'Reference Point' concept is introduced to locate the unloading curve. Block (2006) describes the principle of the 'Reference Point' concept as 'plastic strain which is not affected by a temperature variation'.   Therefore, the component's permanent deformation is assumed not to change when only its temperature changes. When moving to the next temperature step, the component's current permanent deformation is that saved from the last step, and will be updated at the end of each calculation step.
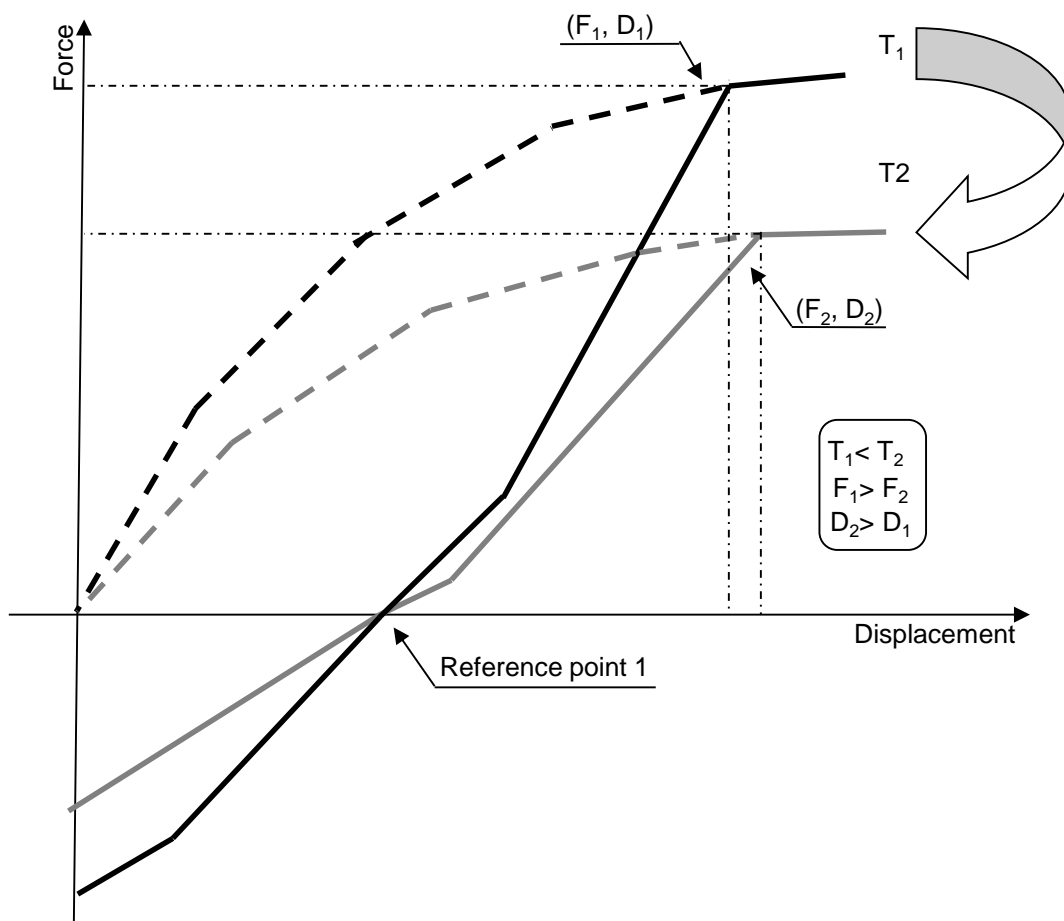
Figure 109: Unloading at changing temperatures

Figure 111 explains how this concept is implemented in *Vulcan*.   Reference Point 1 is updated at the end of the step at temperature T_1, on the basis of the applied force and the component's Force/Displacement (F/D) curve. When moving to the next step (temperature T_2), the unloading curve will be plotted on the basis of the component's new F/D curve. Therefore the new unloading curve will be located by starting from a point on the new

loading curve, passing through Reference Point 1 from the previous step (temperature T_1). Finally, the effective *F/D* curve is formed for this temperature T_2.

4.2.5 Typical tension bolt row

In the calculation process for this connection element, the three components in each tension bolt row are combined into one effective spring at each temperature step (Figure 110). The force-displacement curves of the tension bolt rows are used to define the connection's local force and stiffness. After the global analysis reaches a converged stable equilibrium (explained in 4.2.7), the forces in the tension bolt rows are established, and the displacements of each tension component are calculated; these are then output in order to help the user to evaluate the state of the connection. The related information, such as each component's permanent deformation, is then updated.

In accordance with the principle of springs working in series, the force stays the same in each spring within a spring row. The maximum resistance of the effective spring is defined by the weakest spring in this series. The forces at all the points in all the components' F/D curves are sorted in increasing order, and any force above the weakest component's ultimate resistance is ignored. At each force level, the effective spring's displacement is the aggregate of all the components' displacements under the corresponding force level. When calculating each component's deformation, the unloading curve will be used if the force is below that at the previously established intersection point.
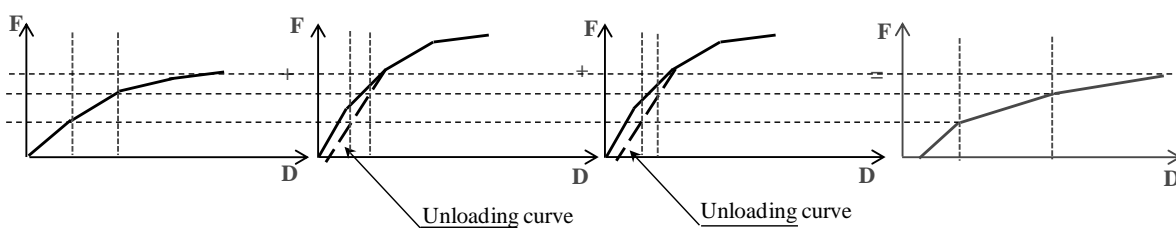
Figure 110: Assembly of the individual tension components in a tension bolt row

The middle component in each tension bolt row is allocated to the bolt in tension. This is only able to transfer tension force. Figure 111 illustrates the typical effective force/displacement curve for a bolt in tension, for which there is no Reference Point 2 (Figure 108). This is because the bolt does not take compression force in either the flush endplate connection or the reverse channel connection. In compression, the left- and right-hand components will contact directly to transfer the force.

The endplate connection is now used to explain this principle. In this connection, the three tension components in each tension bolt row include the column flange under bending, the bolt in tension and the endplate in bending, are represented by two T-stub components. Figure 112 illustrates this as a picture of a T-stub tension test.
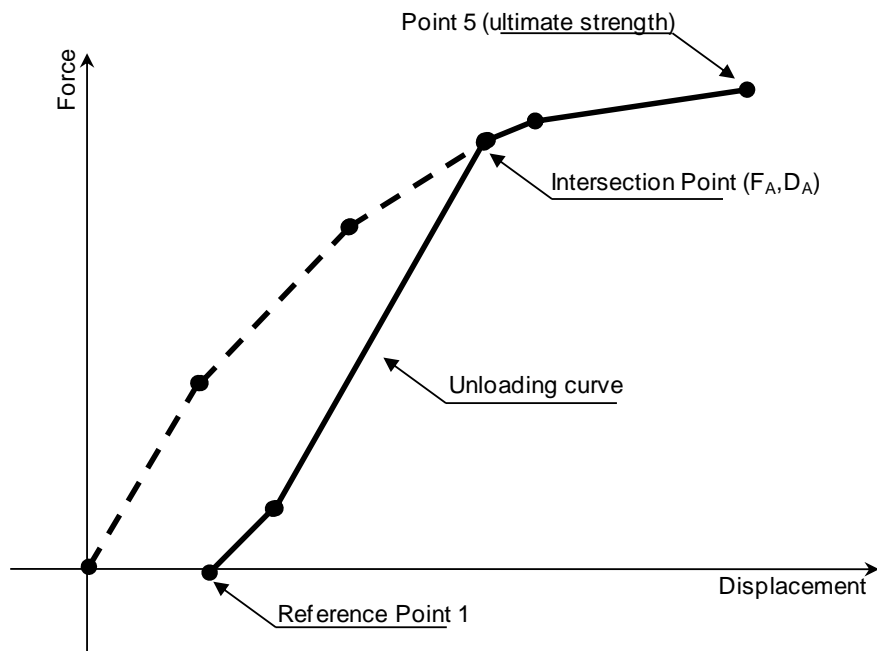
Figure 111: Typical tension component F/D curve for bolt in tension

Figure 112: T-stub test picture (Spyrou, 2002)

Figure 113 shows the deformed shapes of the T-stub at various stages of a sequence of axial force. The applied force starts with increasing tension, which reduces to zero, changes to compression, reduces to zero again, and finally changes to tension.
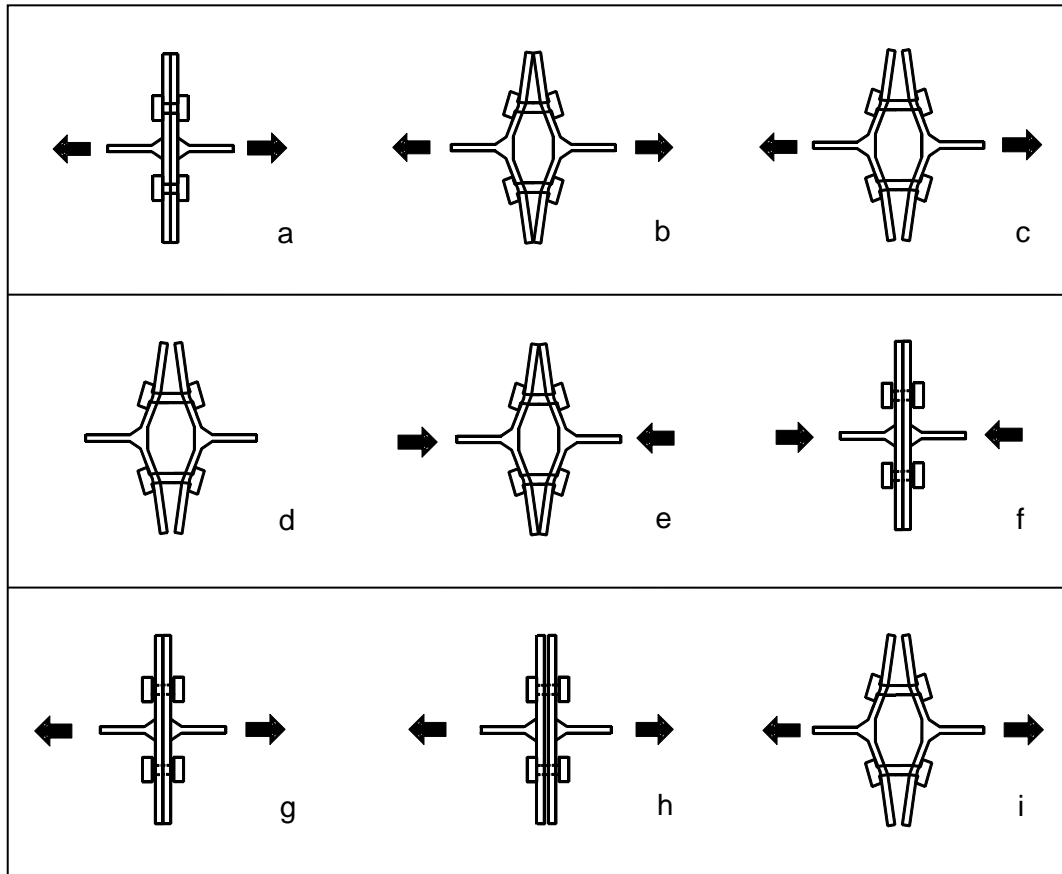
Figure 113: T-stub deformed shapes at different testing stages

The typical tension bolt row Force/Displacement (*F/D*) curve consists of four parts (Figure 114): tension, bolt plastic deformation, compression, and residual compression. Each part may be used at different stages of a fire.

The 'tension part' (Figure 113 a, b and c) shows all three components in parallel under tension. Two T-stub flanges are subject to bending, while two bolts are under tension.

The 'bolt recovery of plastic deformation part'(Figure 113 d) represents the stage between the 'tension' and 'compression' parts, during which the applied tension reduces to zero, and the deformed endplate and column flange have not yet come into contact. As the bolt-in-tension component does not work under compression, the tension spring row's stiffness is zero after this. The plastic deformation of the bolt is residual and irrecoverable, even during the reloading which is shown in Figure 113 g, h and f.

The 'compression part' (Figure 113 e and f) represents the state when the plastically deformed endplate and column flange are pushed back until their centres come into contact.

The 'residual compression' part (Figure 113 f) is based on the assumption that the tension bolt row can transfer a certain amount of compression force. However, as the parts of the connection represented by the compression spring group are much stiffer than this, most of the compression force will be transferred by the compression spring group.
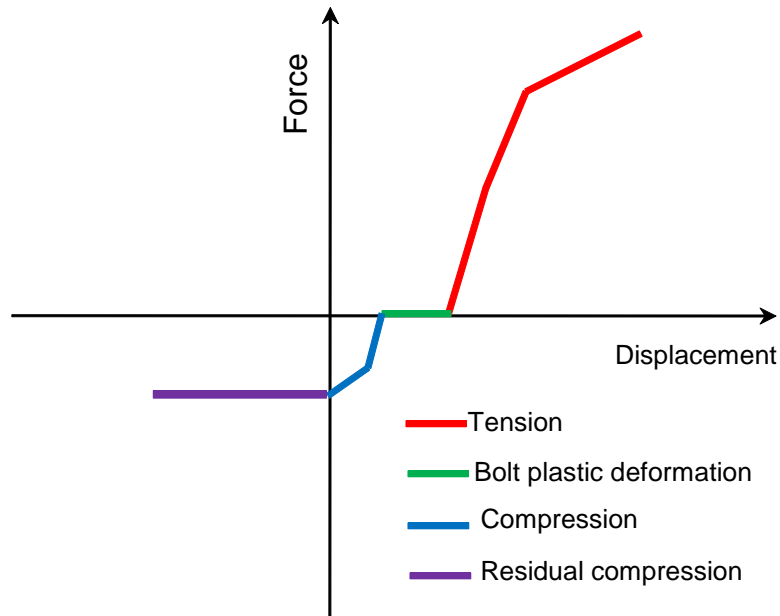
Figure 114: Typical tension bolt row force/displacement curve

4.2.6   Compression spring row

A compression component characteristic is represented by 3 intersection points, which can be increased if necessary (Figure 115). A compression component will be 'switched off' under tension force, when its stiffness contribution is zero and it transfers zero tension force. Point 3 is the ultimate strength point beyond which no change of force occurs.
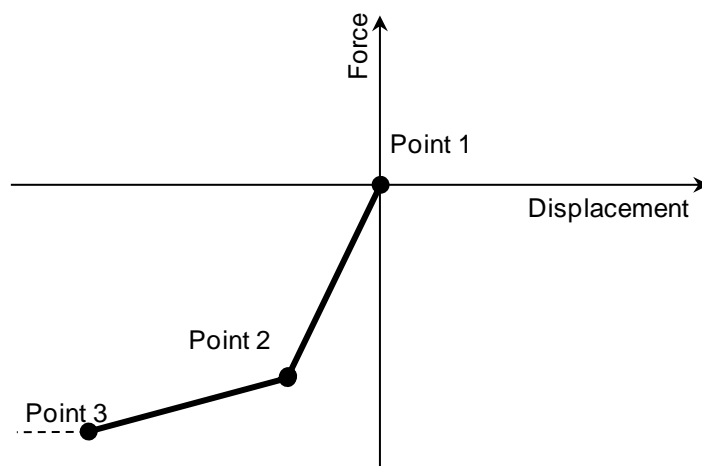
Figure 115: Typical compression component force/displacement behaviour

4.2.7 Solution process of Vulcan

Since the general-purpose component assembly has now been developed, consideration of the effects of interaction at connections within frames under elevated temperatures can be addressed, once it has been incorporated into the global nonlinear finite element software *Vulcan*. The principles and procedure are also applicable to other type of connection and can be incorporated into other finite element packages.

Vulcan is a nonlinear finite element analysis software for structural fire engineering. When modelling a discrete structure, the whole structural system is represented with a large number of elements. A joint will be modelled as a 2-noded connection element. The whole structure forms a global system with global coordinates, while each element forms an internal system with its own local coordinates.

After applying loadings, such as temperature, force and/or deformation, a structure may stay stable, or lose its stability and collapse. A stable structure retains equilibrium of internal and external forces, compatibility of internal and external deformations, and its defined constitutive relationships between internal force and deformation (Izzuddin, 2005). *Vulcan* is intended to track the equilibrium, while retaining its compatibility and constitutive relationships, which are represented by the following three equations:

$$\{P\} = [T]^T\{f\}$$

(4.3)

This equation represents the equilibrium of internal and external forces. {*P*} is the vector of applied forces based in global coordinates, and {*f*} is the vector of internal forces based in local coordinates. [*T*] is the geometric transformation matrix between the global and local coordinates.

$$\{d\} = [T]\{U\}$$

(4.4)

This equation matches the internal and external deformations. {*d*} is the internal deformation vector based in local coordinates, and {*U*} is the external deformation vector based in global coordinates

$$\{f\} = [k]\{d\}$$

(4.5)

This equation relates the internal force to deformation using the constitutive relationships. $\{f\}$ is the vector of internal forces based in local coordinates. The local stiffness matrix $[k]$ is variable, due to both geometrical and material nonlinearities.

For linear elastic analysis, the unknown $\{U\}$ can be determined for a given $\{P\}$:

$$\{P\} = [K]\{U\} \tag{4.6}$$

where

$$[K] = [T]^T[k][T] \tag{4.7}$$

The commonly used Newton-Raphson iterative technique (Sun, 2012) is adopted to achieve a converged solution. In the load control method, equilibrium states are hunted for various load levels defined by (λ_1,.., λ_i...., λ_n). An unknown equilibrium state corresponding to λ_i is obtained through an iterative procedure, which starts from the last known equilibrium state in the load level λ_{i-1} and consisted of steps. It should be noted that *Vulcan* has both static and dynamic solvers; the following is an illustration of procedure on the basis of static solver. In the static solver, the rates of inertial effects from the change of loading and temperature are ignored. The relationship between static and dynamic solver will be included in 4.2.9. The following is the calculation process to find the equilibrium at load level "P_1" on the basis of load level "P_0". This procedure is also shown in Figure 116.
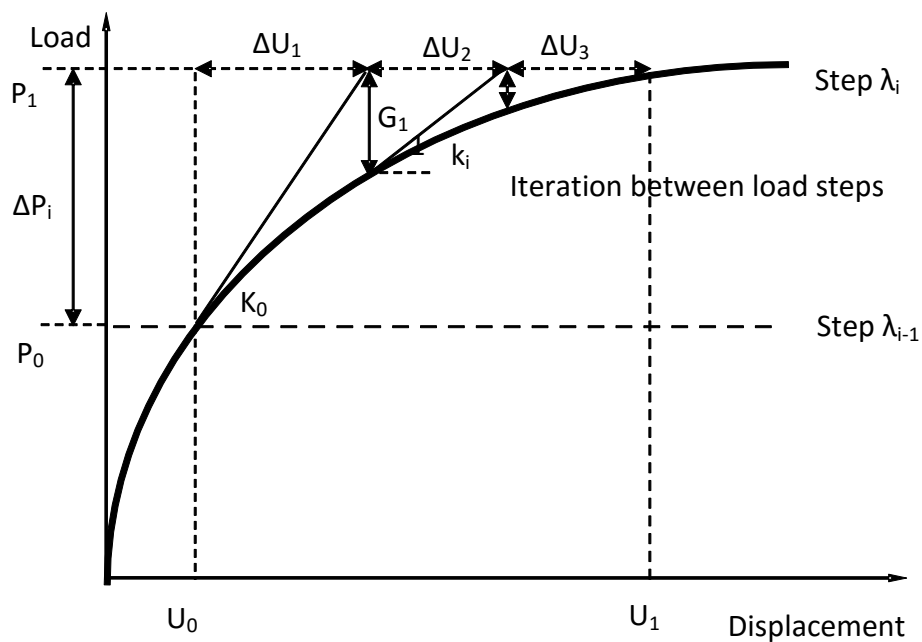
Figure 116: Newton-Raphson iterative procedure

1. Calculate incremental $\{\Delta P\}$ from load level P_0 to load level P_1.

2. Using the stiffness $[K_0]$ on the last step, solve the incremental global displacement

$$\{\Delta U_i\} = [K_0]^{-1}\{\Delta P\} \tag{4.8}$$

3. Update the global nodal displacement

$$\{U_1\} = \{U_0\} + \sum\{\Delta U_i\} \tag{4.9}$$

4. Update the global nodal forces

$$\{P_1\} = \{P_0\} + \{\Delta P\} \tag{4.10}$$

5. Update the local element displacement

$$\{d_1\} = [T]\{U_1\} \tag{4.11}$$

6. Calculate the global internal force

$$\{R_1\} = [T]\{f_1\} \tag{4.12}$$

7. Calculate the out of balance forces $\{G_i\}=\{R_i\}-\{P_i\}$

$$\{G_1\} = \{R_1\} - \{P_1\} \tag{4.13}$$

8. If G_1 does not meet with the convergence criteria, the above calculation will repeat. The stiffness will be calculated for the next step. The iteration will be carried on, until the convergence criteria is met.

4.2.8   Incorporation of the user-defined connection element into Vulcan

Within *Vulcan*, this new connection element is attached to the existing subroutine, called SEMIJO, which is specified for the existing simpler spring elements and which Block (2006a) also used for his connection element. In each calculation step (or load/displacement step), the connection element receives the necessary incremental displacement vector from SEMIJO and returns the tangent stiffness matrix and force vector (shown in Figure 117).
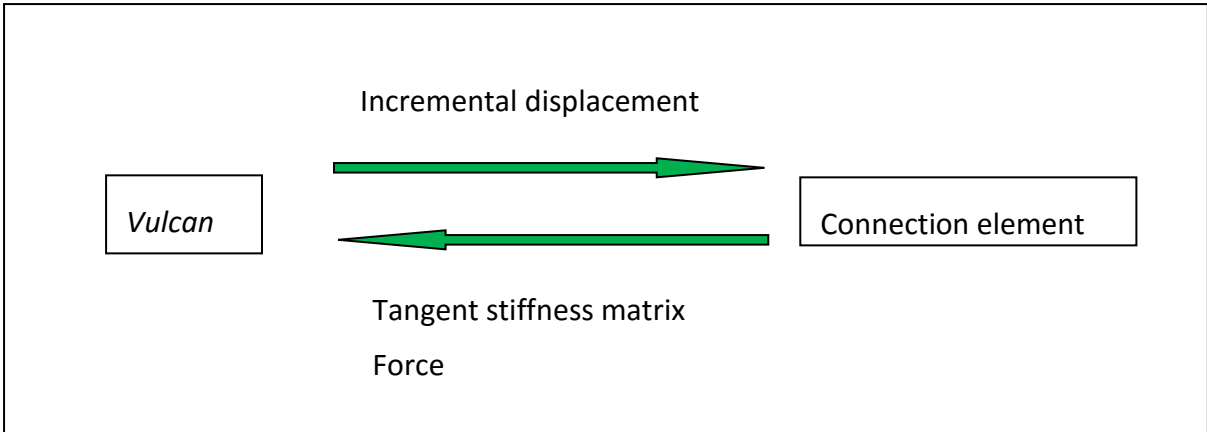
Figure 117: interaction between connection element and *Vulcan*

Block (2006) first derived the tangent stiffness matrix ($K_c^{'}$) of the connection element, shown as Equation 4.14. Based on the element local axis, a node has total six Degrees of Freedom (DOF), including x, y, z, xx (rotation about x-axis), yy (rotation about y-axis) and zz (rotation about z-axis). The x-axis is the axial direction of the connection. The y- and z-axes are the shear directions of the connection. The connection element local coordinate system is also illustrated in Figure 118. Accordingly, the tangent stiffness matrix will be 12x12. The out-of-plane and torsional DOF are assumed to be connected rigidly and without interaction, because these are currently under development and are in any case of relatively minor importance in steel or composite building structures.
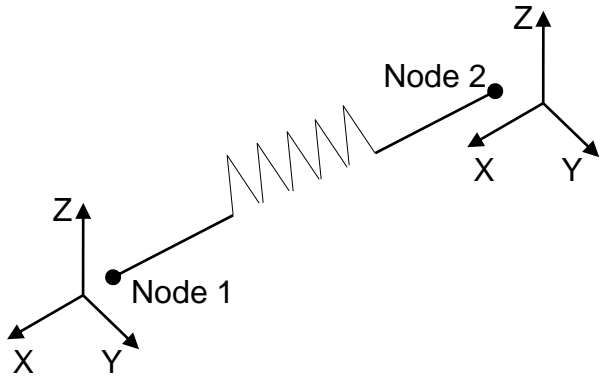
Figure 118: Connection element local coordinate system

$$K_C' = \begin{bmatrix} K_{11}' & 0 & 0 & 0 & K_{15}' & 0 & -K_{11}' & 0 & 0 & 0 & -K_{15}' & 0 \\ 0 & \infty & 0 & 0 & 0 & 0 & 0 & -\infty & 0 & 0 & 0 & 0 \\ 0 & 0 & K_{33}' & 0 & 0 & 0 & 0 & 0 & -K_{33}' & 0 & 0 & 0 \\ 0 & 0 & 0 & \infty & 0 & 0 & 0 & 0 & 0 & -\infty & 0 & 0 \\ K_{51}' & 0 & 0 & 0 & K_{55}' & 0 & -K_{51}' & 0 & 0 & 0 & -K_{55}' & 0 \\ 0 & 0 & 0 & 0 & 0 & \infty & 0 & 0 & 0 & 0 & 0 & -\infty \\ -K_{11}' & 0 & 0 & 0 & -K_{15}' & 0 & K_{11}' & 0 & 0 & 0 & K_{15}' & 0 \\ 0 & -\infty & 0 & 0 & 0 & 0 & 0 & \infty & 0 & 0 & 0 & 0 \\ 0 & 0 & -K_{33}' & 0 & 0 & 0 & 0 & 0 & K_{33}' & 0 & 0 & 0 \\ 0 & 0 & 0 & -\infty & 0 & 0 & 0 & 0 & 0 & \infty & 0 & 0 \\ -K_{51}' & 0 & 0 & 0 & -K_{55}' & 0 & K_{51}' & 0 & 0 & 0 & K_{55}' & 0 \\ 0 & 0 & 0 & 0 & 0 & -\infty & 0 & 0 & 0 & 0 & 0 & \infty \end{bmatrix}$$

(4.14)

in which

$$K_{11}' = \sum_{i=1}^{n} k_{T,i}' + \sum_{i=1}^{2} k_{C,i}'$$

(4.15)

$$K_{15}' = K_{51}' = \sum_{i=1}^{n} l_{T,i} k_{T,i}' + \sum_{i=1}^{2} l_{C,i} k_{C,i}'$$

(4.16)

$$K_{33}' = k_s'$$

(4.17)

$$K_{55}' = \sum_{i=1}^{n} l_{T,i}^2 k_{T,i}' + \sum_{i=1}^{2} l_{C,i}^2 k_{C,i}'$$

(4.18)

In which the subscripts $_T$ and $_C$ represent components working in tension or compression, and n is the number of bolt rows. The subscript $_S$ denotes a shear component.

K_{11} represents the axial stiffness under the axial force in axis-x shown in Figure 118. K_{15} is the axial stiffness in axis x under the bending about the y-axis. K_{33} is the shear stiffness in axis z under shear in z direction. K_{55} is the bending stiffness about axis y under the bending about axis y.

However, the static solver only converges on the ascending part (positive stiffness) of the force-displacement curve. The change to a descending part, with negative stiffness or unstable equilibrium, will lead to a numerical singularity and is beyond the static solver's

capacity. It will stop the analysis without accurately predicting the failure of the whole structure. At that time, a dynamic solver is necessary, which is included in 4.2.9.

4.2.9 *The static/dynamic Vulcan solver.*

As a key part of performance-based structural design, the structural engineering should ensure that the possibility of disproportionate structural collapse in fire is avoided. Scenario-based non-linear finite element modelling of the structure is necessary for the performance-based structural fire engineering building design, particularly for large and complex buildings. Therefore, the numerical modelling must be capable of predicting the real structural behaviour, not only before the first loss of structural stability, but also from the local instability to total collapse.

The following takes the connection as an example. One component failure in a connection, such as fracture of a bolt, may indeed trigger a progressive structural collapse, but does not in itself constitute failure of the whole structure. Generally, a component failure will cause the structure to lose its stability temporarily, as other components and members of the structure share the redistributed internal forces. After the load path is re-formed in this way, it is possible for the structure to re-stabilize. This is a common phenomenon in experimental testing under load-control, where the force-deflection trace is saw-toothed because of a sequence of releases of internal force as local fractures occur. When equilibrium cannot be achieved between the external loading and the redistributed internal forces, a more widespread structural collapse occurs.   Figure 119 shows schematically the situation in terms of applied force and deflection when part of the structure reaches its peak load capacity.   Since the load level remains constant the deflection accelerates dynamically, and will become extremely high unless a re-stabilized configuration is found. The figure shows the initial quasi-static equilibrium path, followed by a dynamic phase which re-stabilizes and once again becomes quasi-static. Figure 120 shows the alternative (or eventual) situation, when no re-stabilization is found and a real structural collapse occurs.
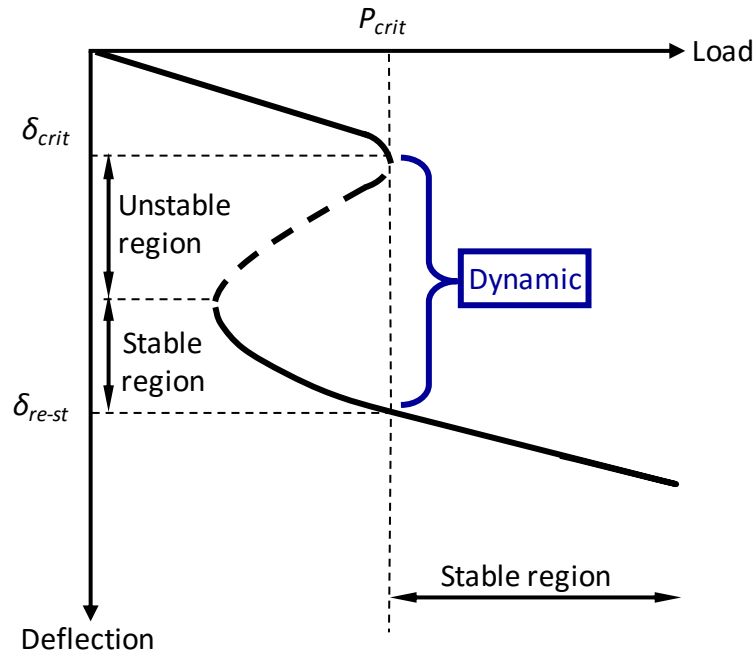
Figure 119: Loss of stability and re-stabilization of structure.
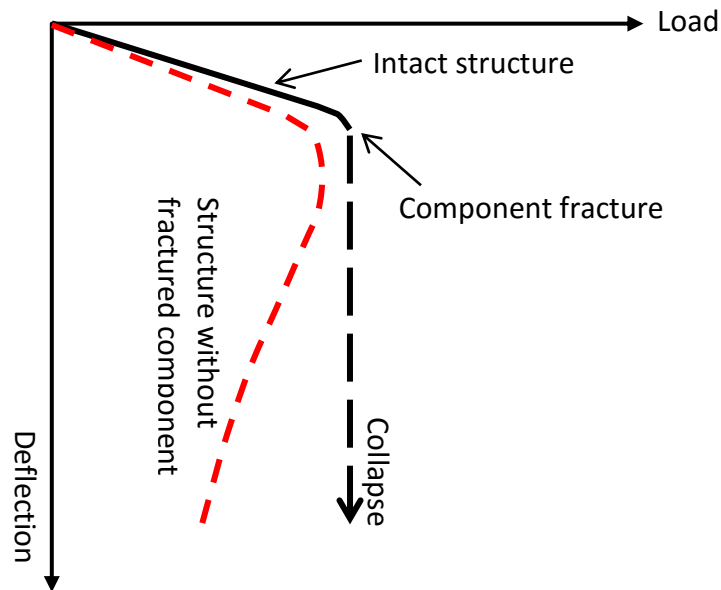
Figure 120: component failure causing structural collapse

Figure 121 shows the general flowchart for modelling of a structure and its connections, including its failure sequence. Generally a quasi-static analysis solver is used, up to the point at which the first component fails. From this point the dynamic solver is activated to track the motion of the structure. If stability is not regained, this initiates a cascade of failures of the other components, leading to complete detachment of the members.
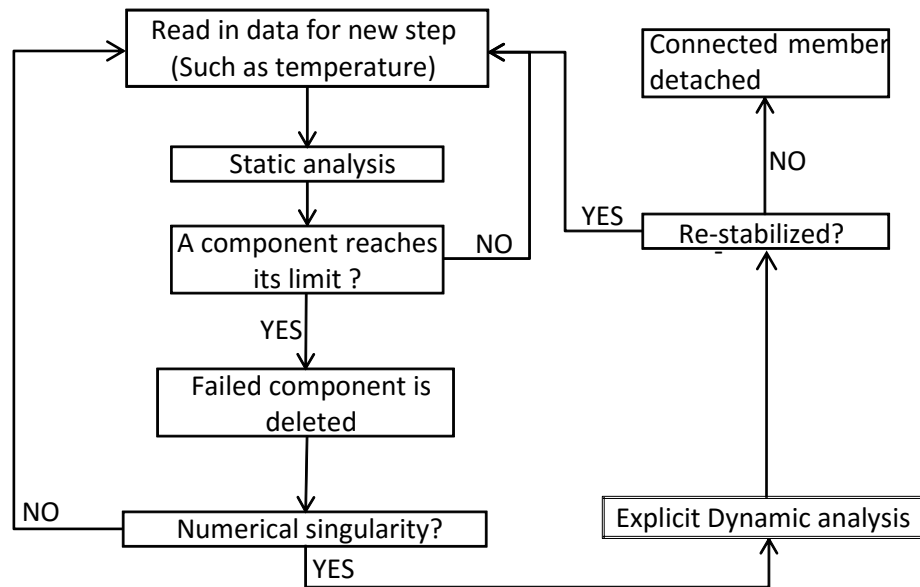
Figure 121: procedure of connection failure modelling

4.2.10 Preliminary application of the user-defined connection element in examples

The development of the general-purpose connection element was intended to cope with reverse channel and flush endplate connections, in which the component characterizations will be defined internally on the basis of connection geometries, temperature development and temperature-dependent material properties. However, the connection element also allows the definition of component behaviour by users, which is called the user-defined connection element. The force-displacement curves and the temperature-dependent strength and modulus reduction factors for the components are required for the input. The element provides a tool to investigate the interaction between connections and the adjacent connected structure, and to understand the demands posed by the structure on its connections.

The user-defined connection element has been successfully incorporated into *Vulcan*. In order to test its functioning in limited subframe examples rather than in more extensive structural frames, four cases were created to test the element:

➢ Case 1:   Isolated beam with connection elements, without axial restraint (Figure 122)

➢ Case 2:   Isolated beam with connection elements, with axial restraint (Figure 123)

➢ Case 3:   2D subframe (Figure 124)

➢ Case 4:   2D "rugby goal-post" frame (Figure 125)

All these cases were analysed with the static-dynamic solver, using different connection details, and the results were compared with those obtained using idealized rigid and pinned connections. The connection behaviour in the cooling phase of the fire has also been examined.

In all of these test cases the beam section was 254x102UKB22, and the column was 203x203UKC71. The beam endplate thickness was 12mm and the steel grade was S275. No out-of-plane deflection was allowed. The joint details (Figure 127) were designed to test the connection elements' full capacity for 3 and 5 bolt rows, of which the lowest would normally be considered to act only in shear.

The component behaviour (Figure 127) for both arrangements was based on a set of derivations from earlier studies (Hu *et al.*, 2007 and Yu *et al.*, 2009). In order to consider the components' behaviour at elevated temperatures, reduction factors and ductility factors (Figure 128, Figure 129 and Figure 130 respectively) were temporarily introduced to reduce the ambient-temperature resistance and to increase the ductility at high temperatures.
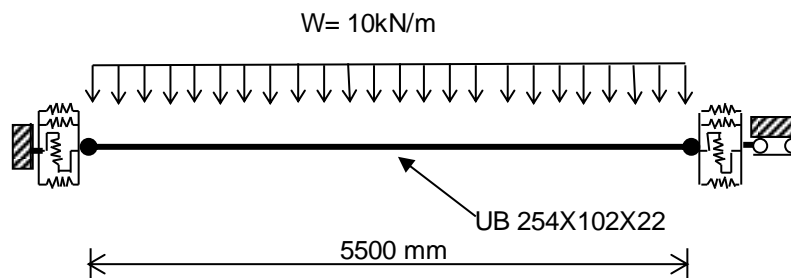
Figure 122: Isolated beam with connection elements, without axial restraint.
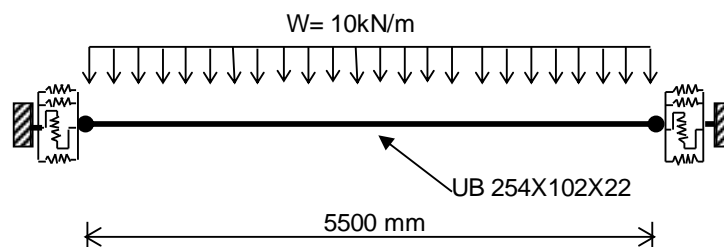
Figure 123: Isolated beam with connection elements, with hinged end, fixed in position.

Figure 124: 2D subframe.

UB 254X102X22

3500 mm

3500 mm

2750 mm 5500 mm 2750 mm
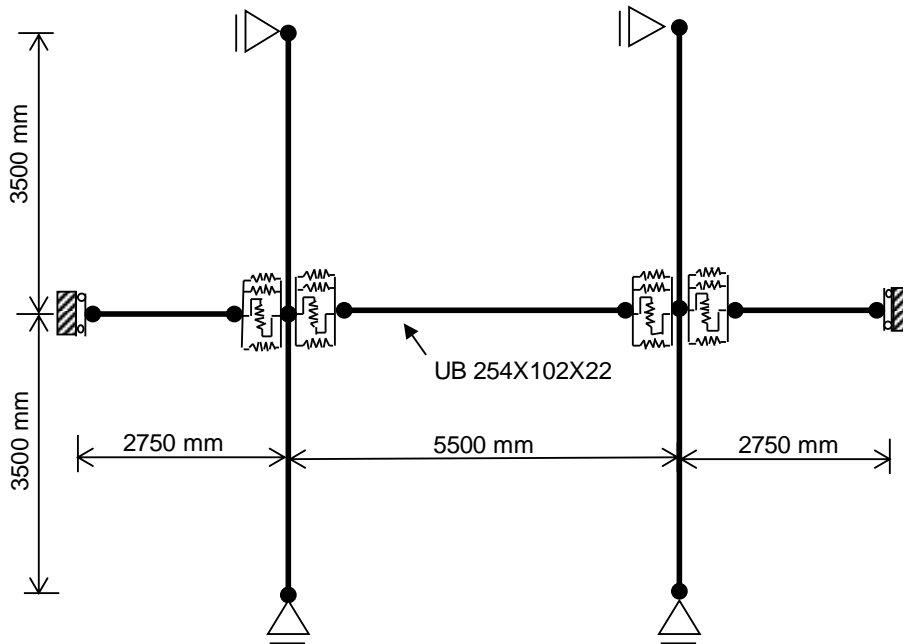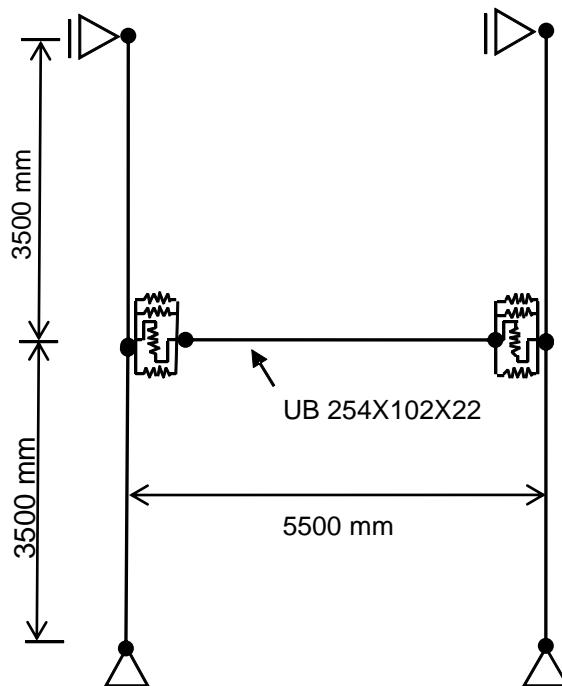
Figure 125: 2D "rugby goal-post" frame.

UB 254X102X22

3500 mm

3500 mm

5500 mm
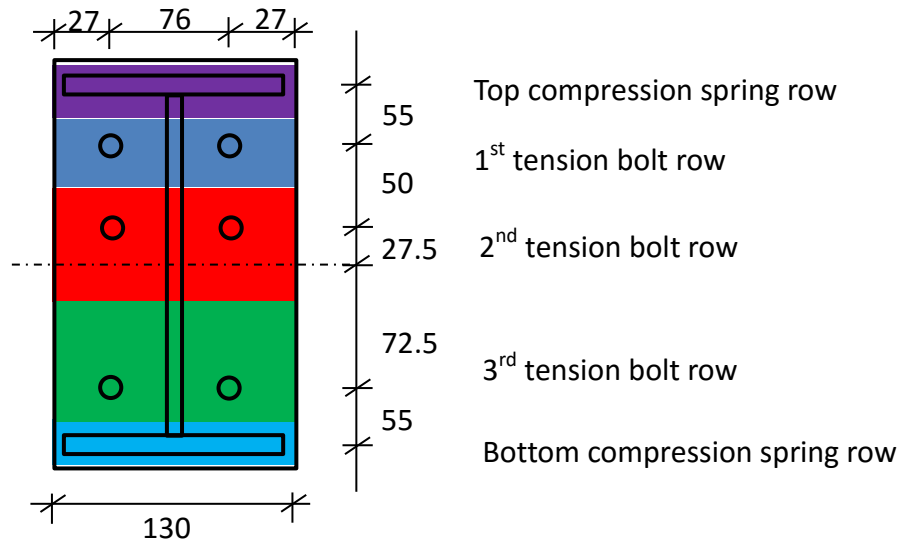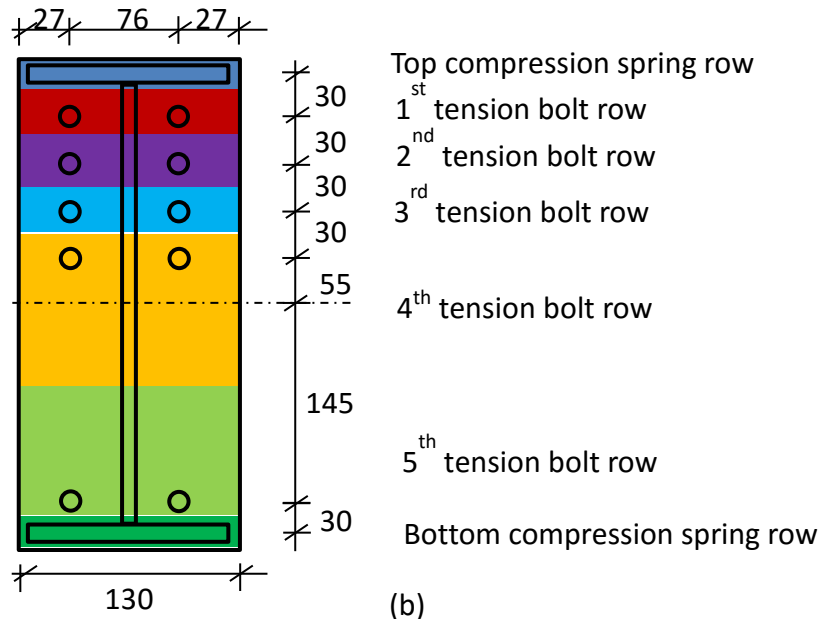
Figure 126: Analysed endplate connection details.
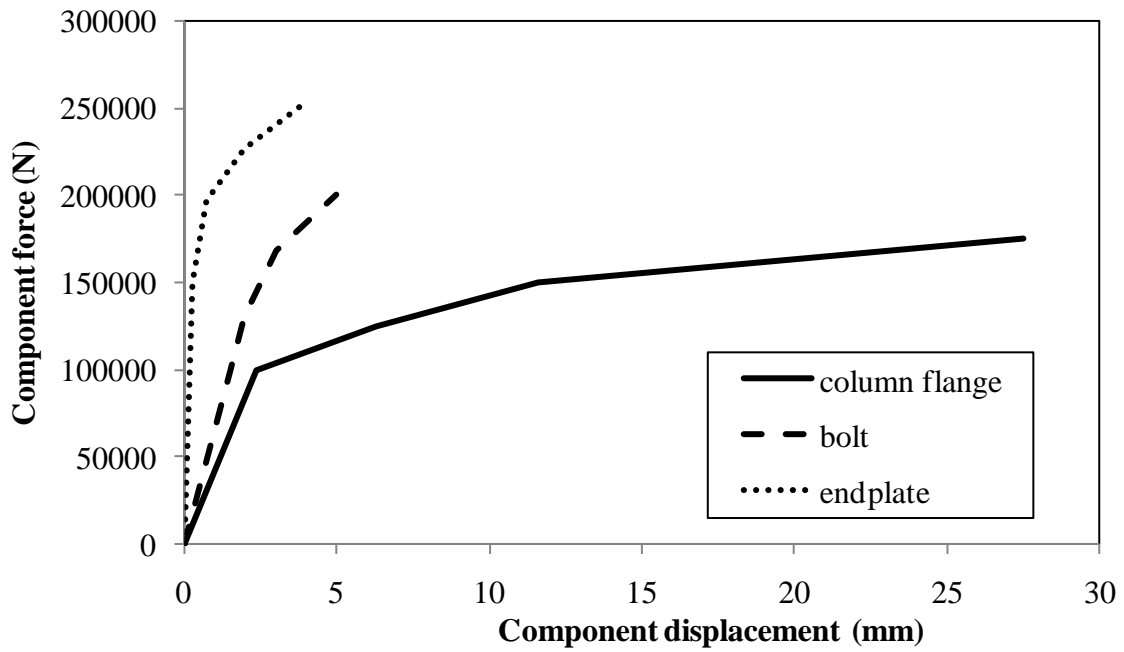
Figure 127: Typical tension component Force/Displacement (F/D) curve -assumptions at 20°C.
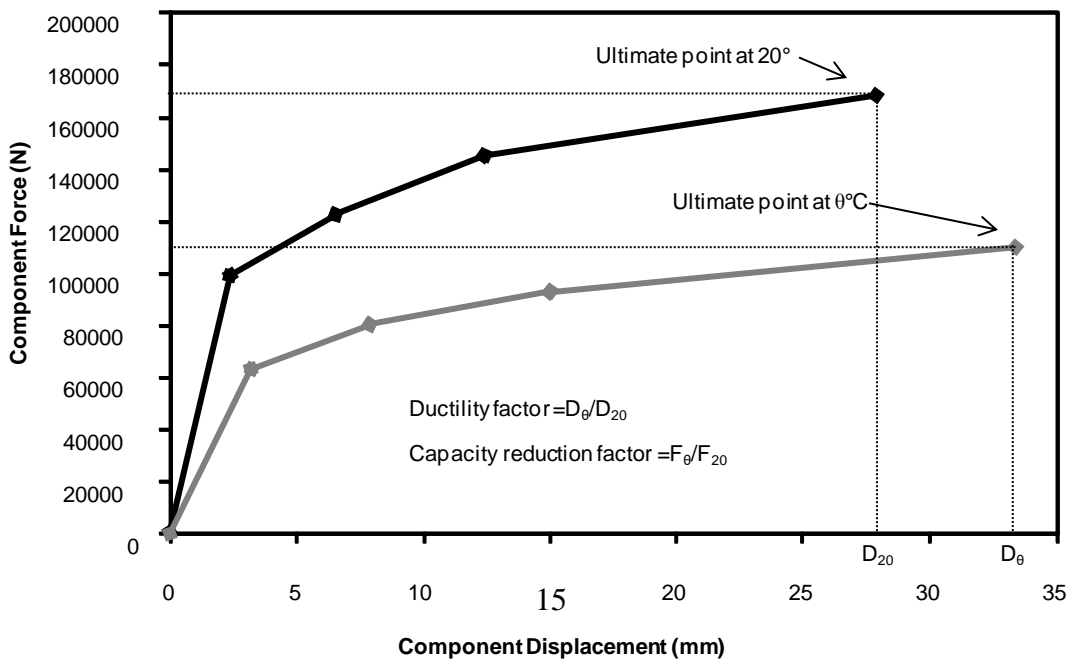
Figure 128: Typical Component F/D curves at different temperatures.
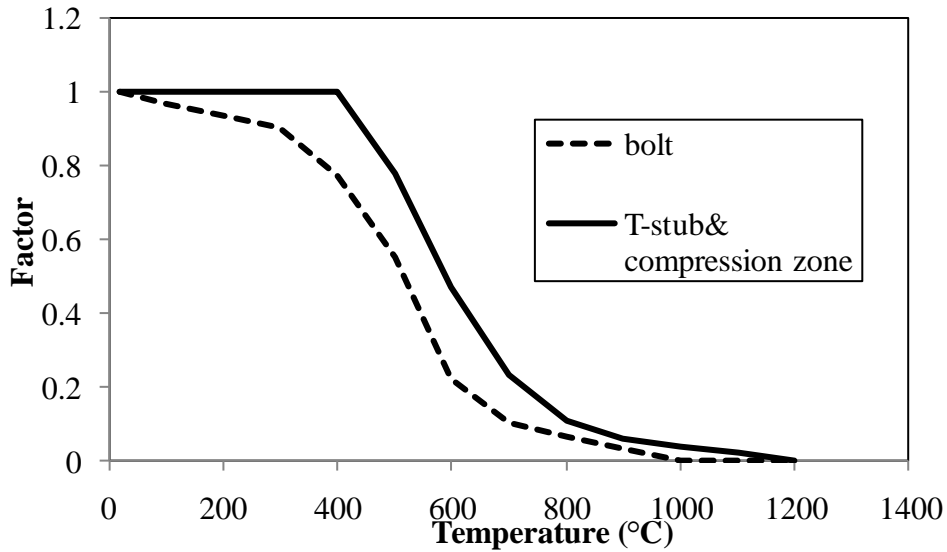
Figure 129: Capacity reduction factors for all the components.
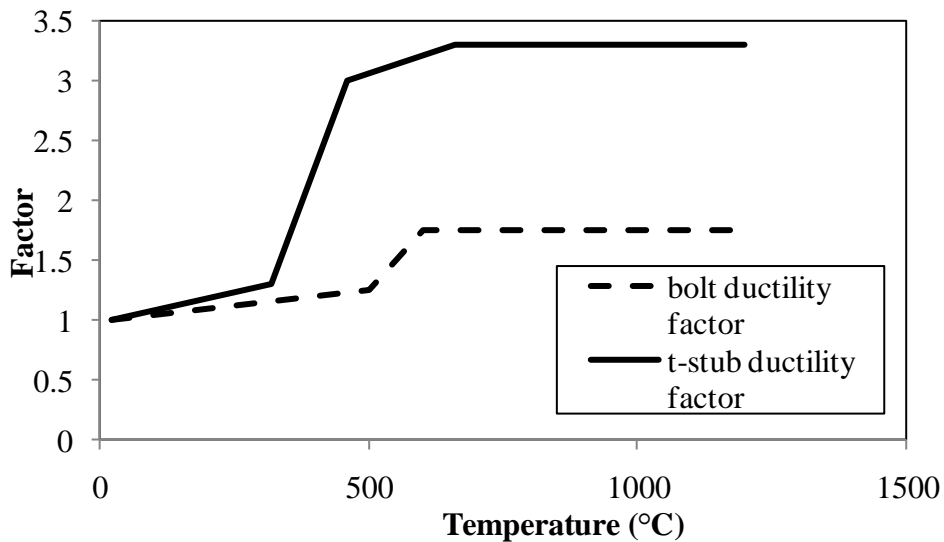
Figure 130: Ductility factor for tension component.

Case 1: Isolated beam with connection elements, without axial restraint

Case 1 was tested for mid-span deflections against cases with the ends both perfectly restrained laterally, but allowed to move axially and unrestrained against rotation. Figure 131 plots the bolt row forces against steel temperature for the 5-bolt-row case. The forces in the bolt rows all start reducing beyond 500°C, while the spring row deformations are noticeably increasing in Figure 132. From the output file, the fracture of the first tension bolt row triggers a progressive structural failure, since the remaining components cannot resist the applied load.
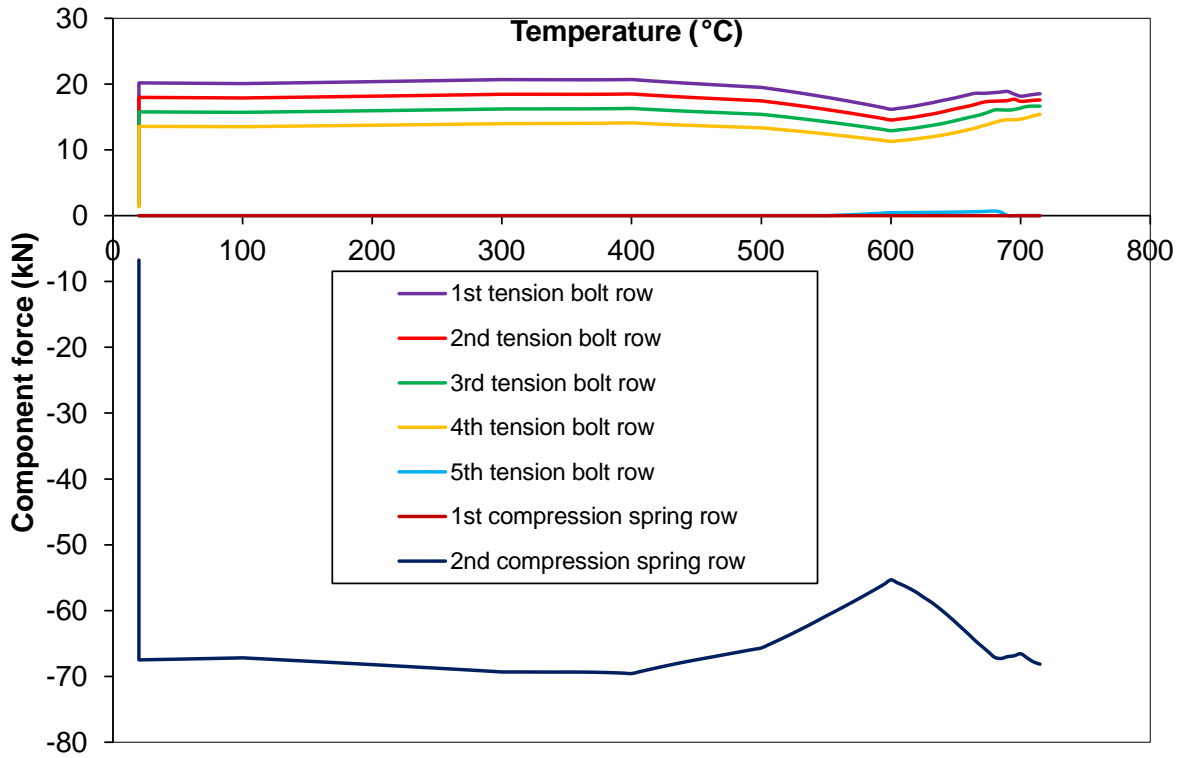
Figure 131: Bolt row forces for Case 1 (5-bolt-row case) [load 10kN/m].
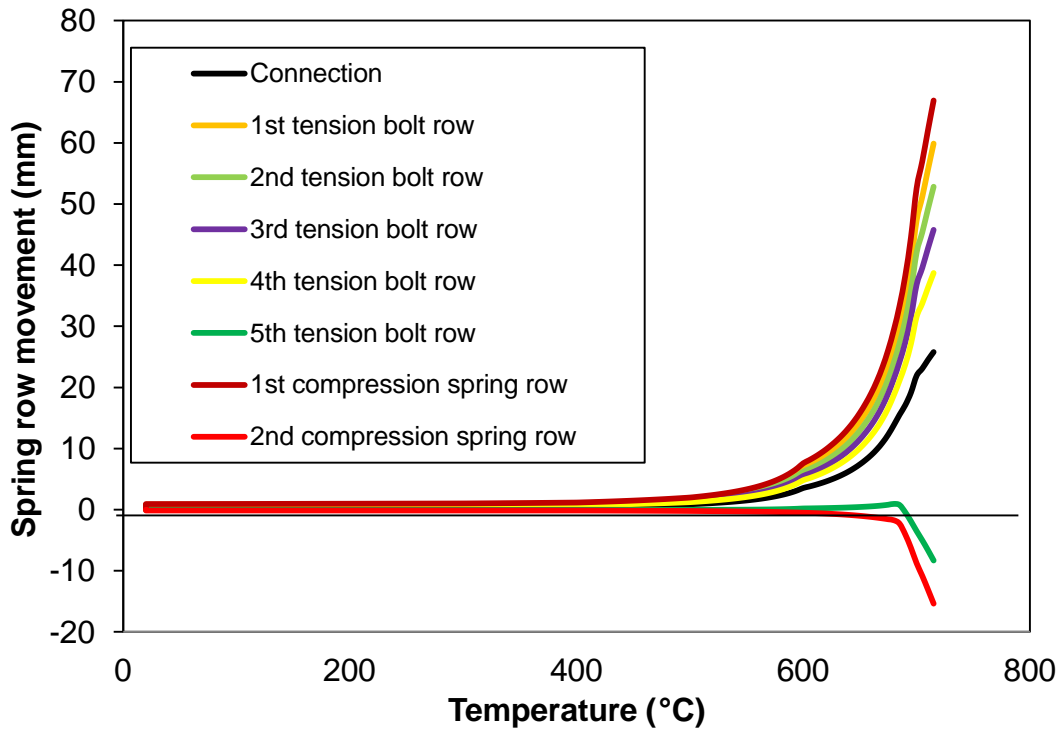
Figure 132: Spring row and connection horizontal movements for Case 1 (5-bolt-row case) [load 10kN/m].

Figure 133 and Figure 134 respectively show the bolt row forces and spring row deformations against temperature for 3-bolt-row case, in which the force starts to reduce

beyond 400°C, while the spring row deformation starts increasing sharply. It can also be seen from Figure 135 that, in both of the connection element cases, deflections lie between those for the perfectly rigid and pinned cases. Logically, the 5-bolt-row connection is stiffer than the 3 bolt row connection and also has higher resistance.
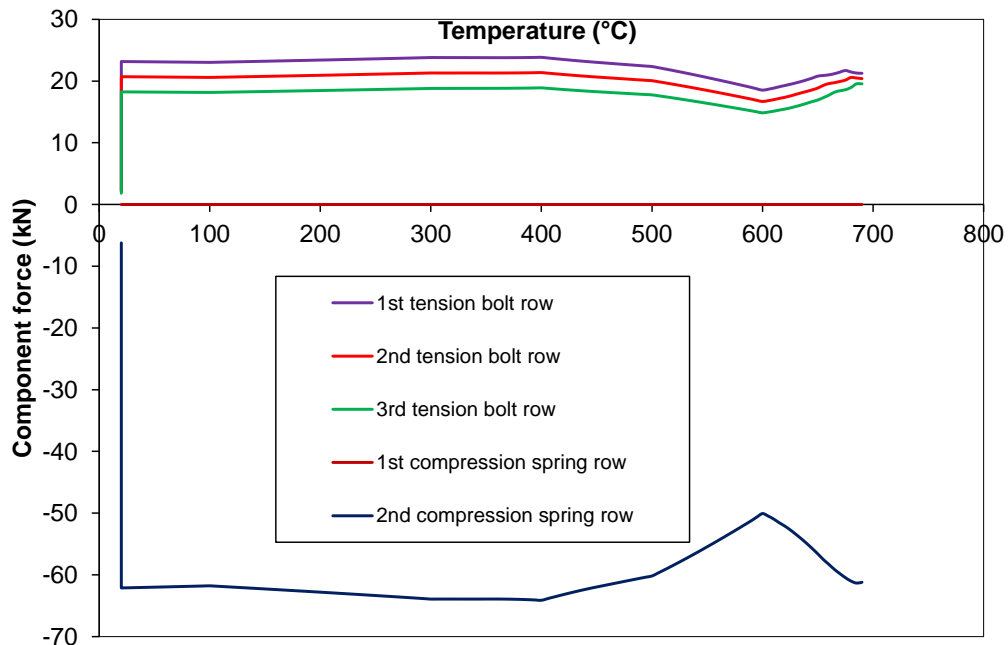
Figure 133: Bolt row force for case 1 (3-bolt-row case) [load 10kN/m].
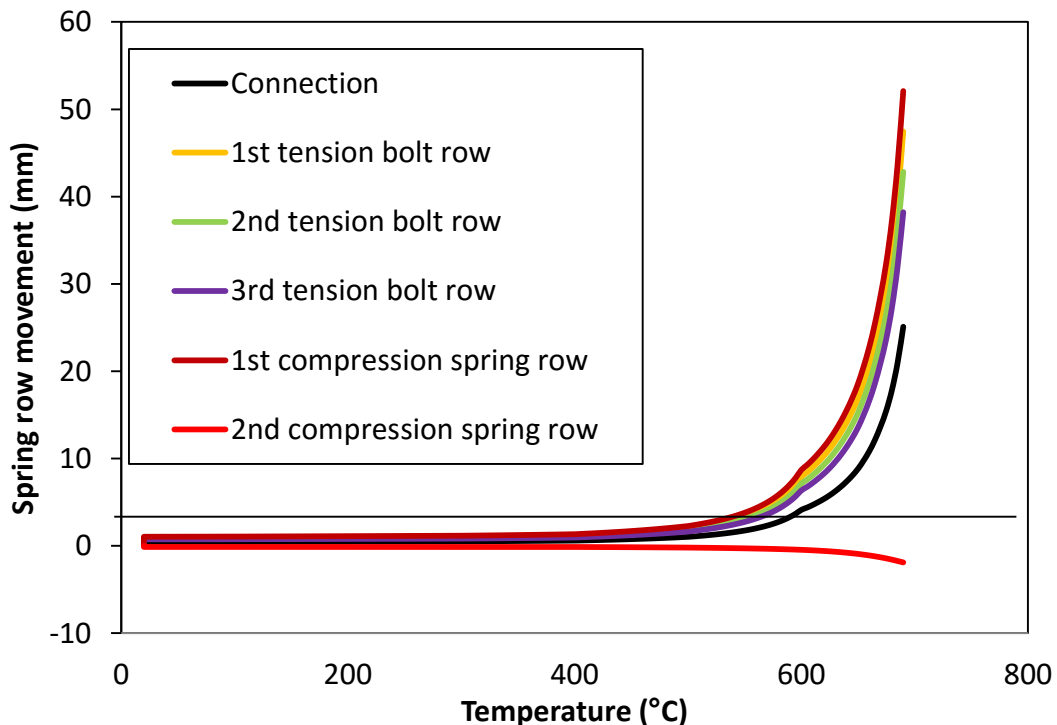
Figure 134: Spring row and connection horizontal movement Case 1 (3-bolt-row case) [load 10kN/m].

124
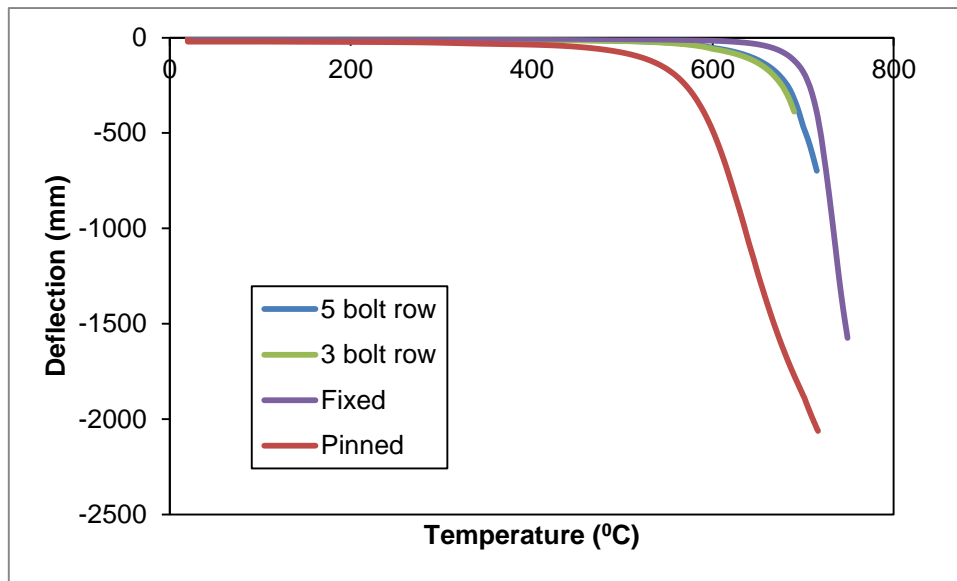
Figure 135: Beam mid-span deflections for Case 1 [load 10kN/m].

Case 2: Isolated beam with connection elements, with axial restraint

In Case 2, the deflections for the rigid and pinned connections (Figure 136) come very close at high temperatures (above 600°C), when the beam is in the catenary stage and is under nearly pure tension; this is logical for a case with fixed ends. It is also noticeable that the deflection of the beam with connection elements initially lies between those of the beams with rigid and pinned connections. Above 685°C, the beam with connection elements has a larger deflection than either of the rigid or pinned cases. This happens because catenary action causes a net shortening of the beam which is greater than the thermal expansion, and some of this net shortening can be accommodated by extension of the bolt rows. The bolt row deflections, together with the net movement of the beam end, are shown in Figure 137, and illustrate this point.
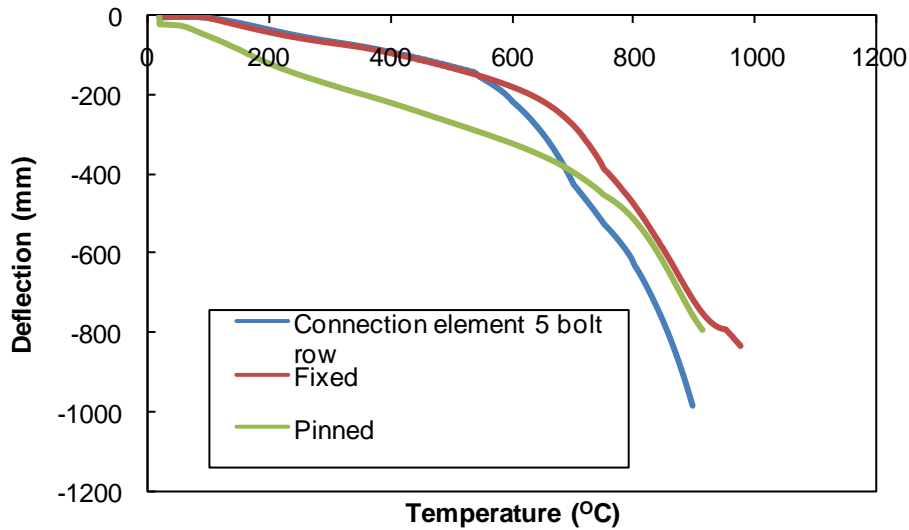
Figure 136: Beam mid-span deflections for Case 2 [load 10kN/m].
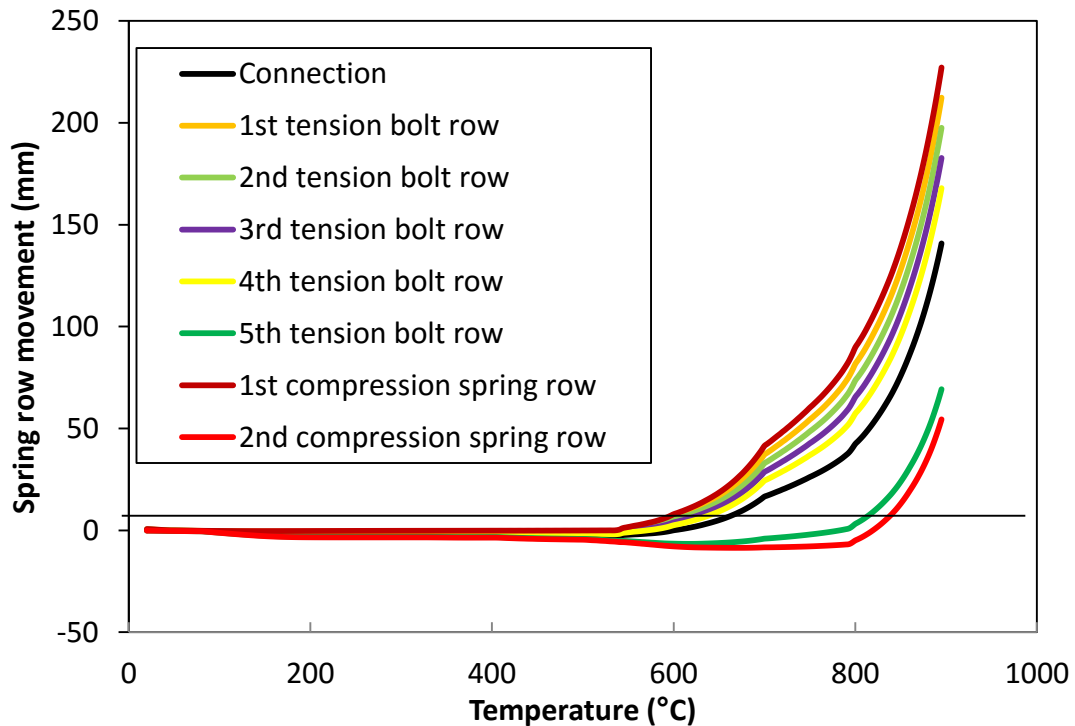
Figure 137: Spring row and connection horizontal movement Case 2 [load 10kN/m].

Figure 138 shows how the connection element deals with the combination of forces in the joint when the beam is heated in Case 2. In the initial stage, the top 4 tension bolt rows and the bottom (2nd) compression spring row work to resist the beam-end rotation due to the applied load. After the beam is heated it starts to expand, and the connection experiences a combination of compression and bending, at which stage all the top 4 tension bolt rows are gradually 'switched off' as the tension force in the top of the section is offset by the thermal

expansion. Once all the tension bolt rows have temporarily stopped working, the top compression spring row starts to work together with the bottom compression spring, and the whole section is under compression. With the temperature increasing further, the beam's deflection increases sharply and the top 4 tension bolt rows progressively replace the top compression spring row in resisting the combination of compression force and moment. Above 600°C, the beam progressively develops catenary tension and reduces its bending action. Eventually all the 5 tension bolt rows are working and both of the compression spring rows are 'switched off'. The initial failure is at the first tension bolt row, and the remaining components cannot then resist the applied load.
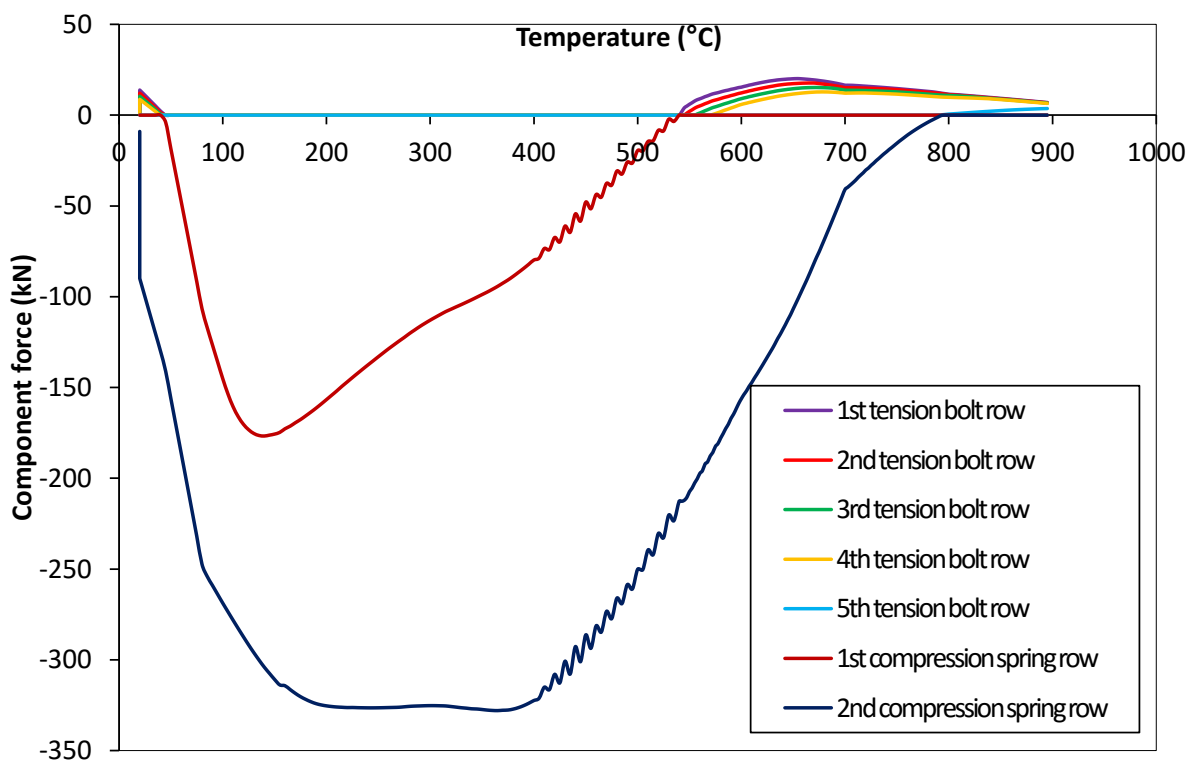
Figure 138: Component force for Case 2 [load 10kN/m].

In Case 2, the assembly was examined during cooling (Figure 139 and Figure 140). In Figure 140 the simulation was stopped due to the fracture of the bolt in the first tension bolt row, which was determined from the *Vulcan* output file.
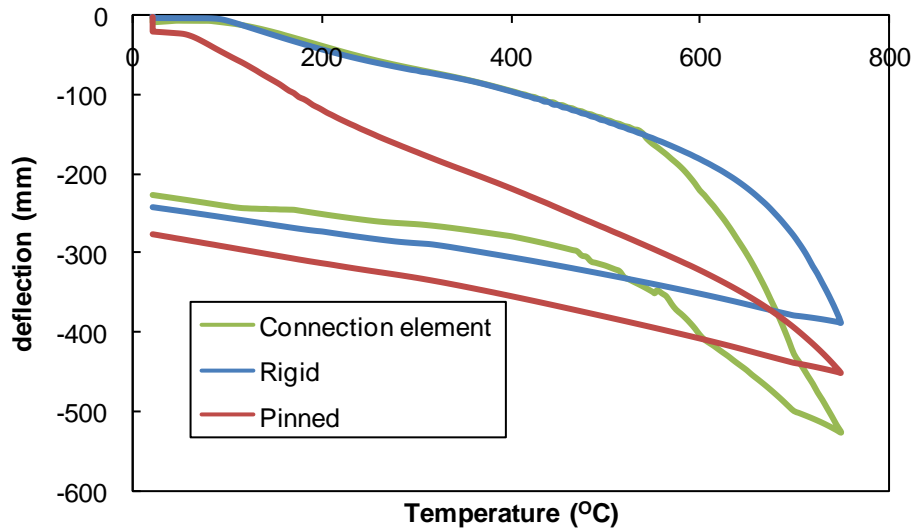
Figure 139: Beam deflection with cooling from 750°C for Case 2 [load 10kN/m].
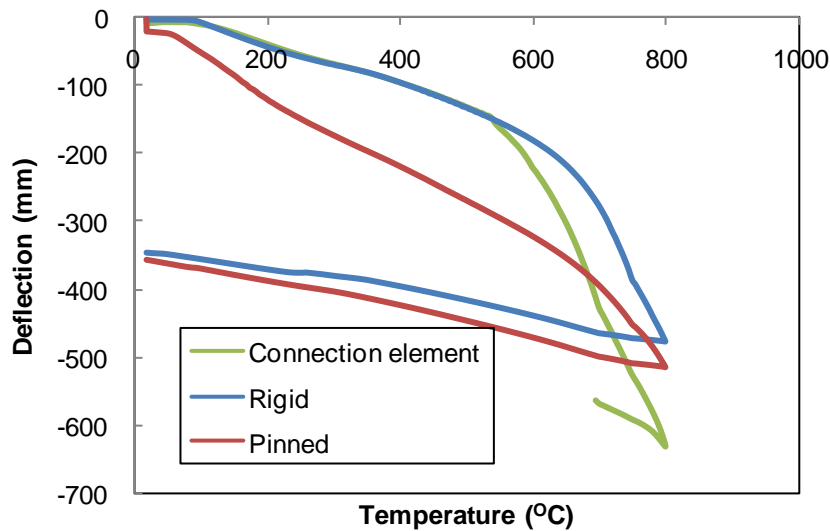
Figure 140: Beam deflection with cooling from 800°C for Case 2 [load 10kN/m].

Case 3:   2D subframe

Figure 141 and Figure 142 respectively show component forces and displacements in Case 3. It follows the same trend as Case 2, in which the 5 tension bolt rows and 2 compression spring rows switch on/off in sequence while the beam is heated up and expands. About above 550°C, the beam progressively develops catenary tension and reduces its bending action. Eventually all the 5 tension bolt rows are working, and both of the compression spring rows are 'switched off'. The first failure is at the first tension bolt row, after which the remaining components cannot resist the applied load.
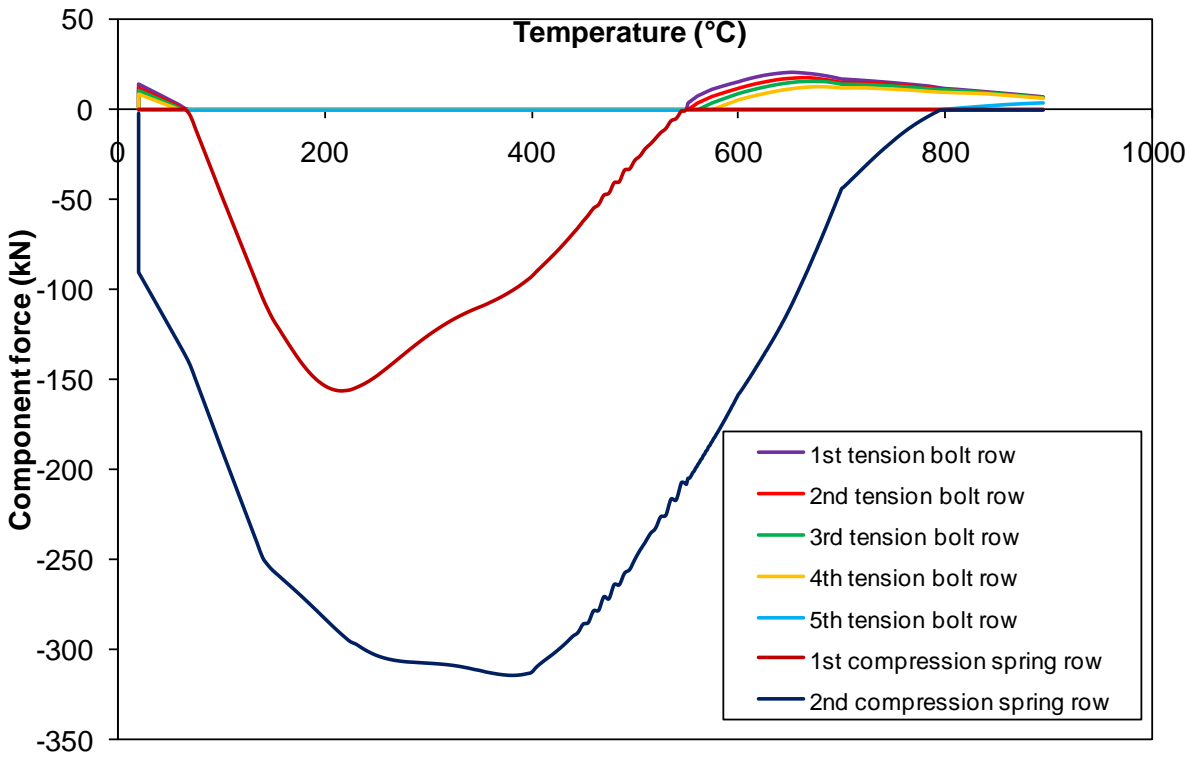
Figure 141: Component force for Case 3 [load 10kN/m].
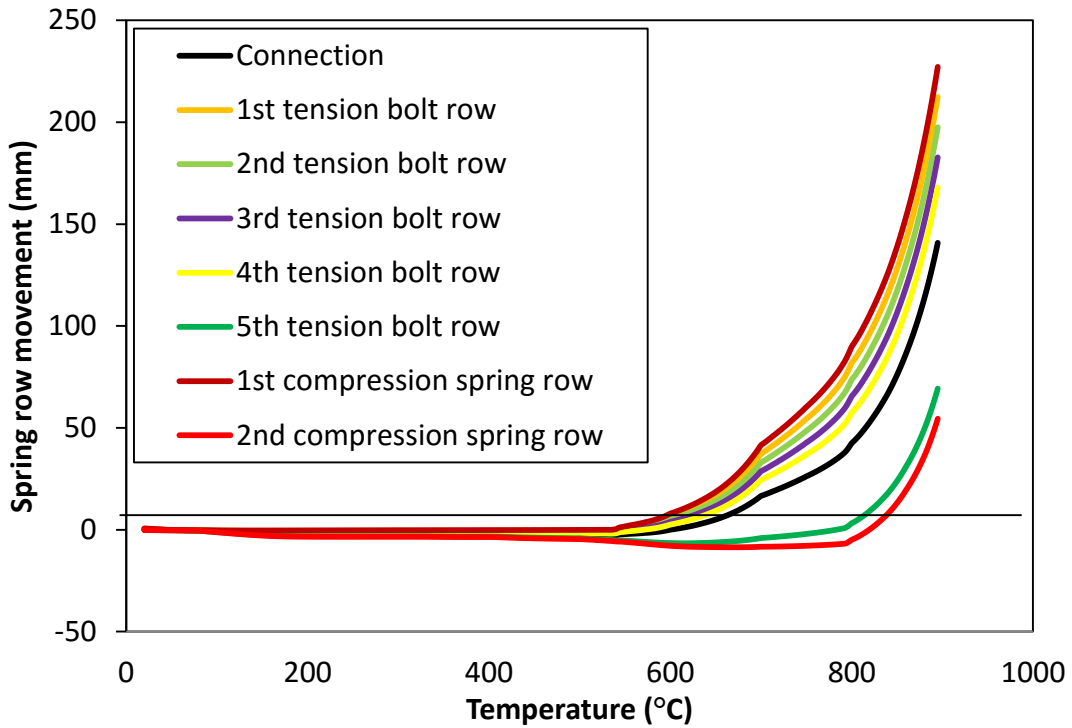
Figure 142: Spring row and connection horizontal movement for Case 3 [load 10 kN/m].

Case 4: 2D "rugby goal-post" frame

Figure 143 and Figure 144 respectively show the component forces and displacements in Case 4. Case 4 is similar to case 1. The top four tension bolt rows work until the first tension bolt fails, triggering the connection failure.
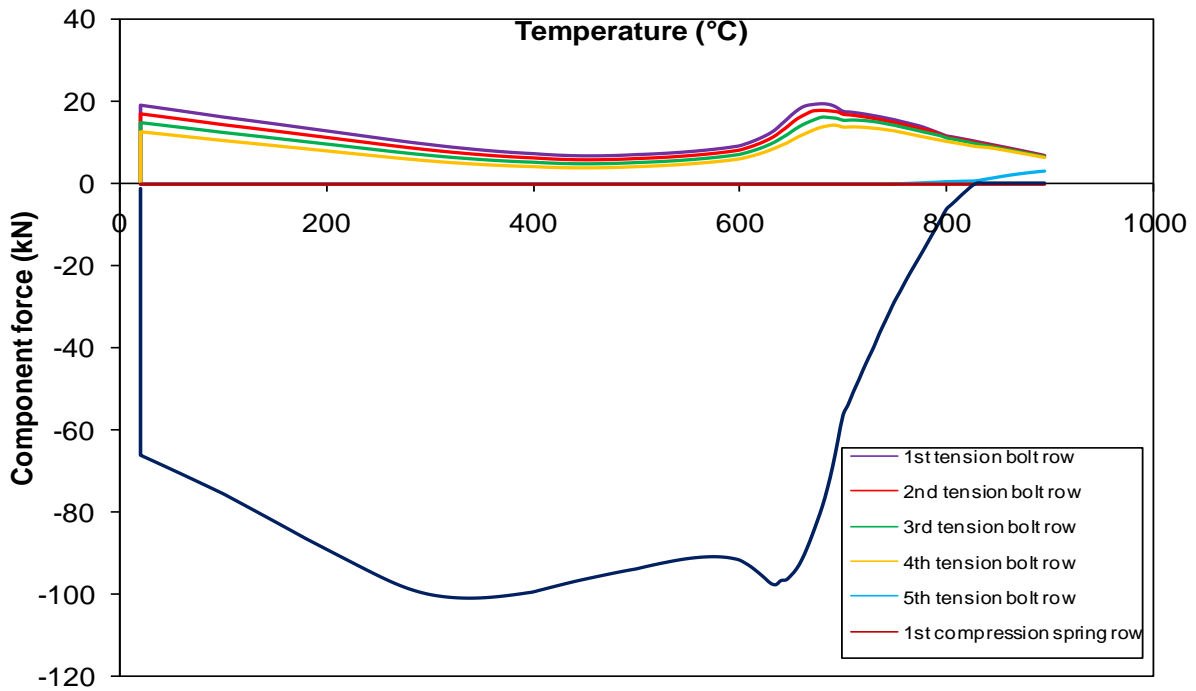
Figure 143: Component force for Case 4 [load 10 kN/m].
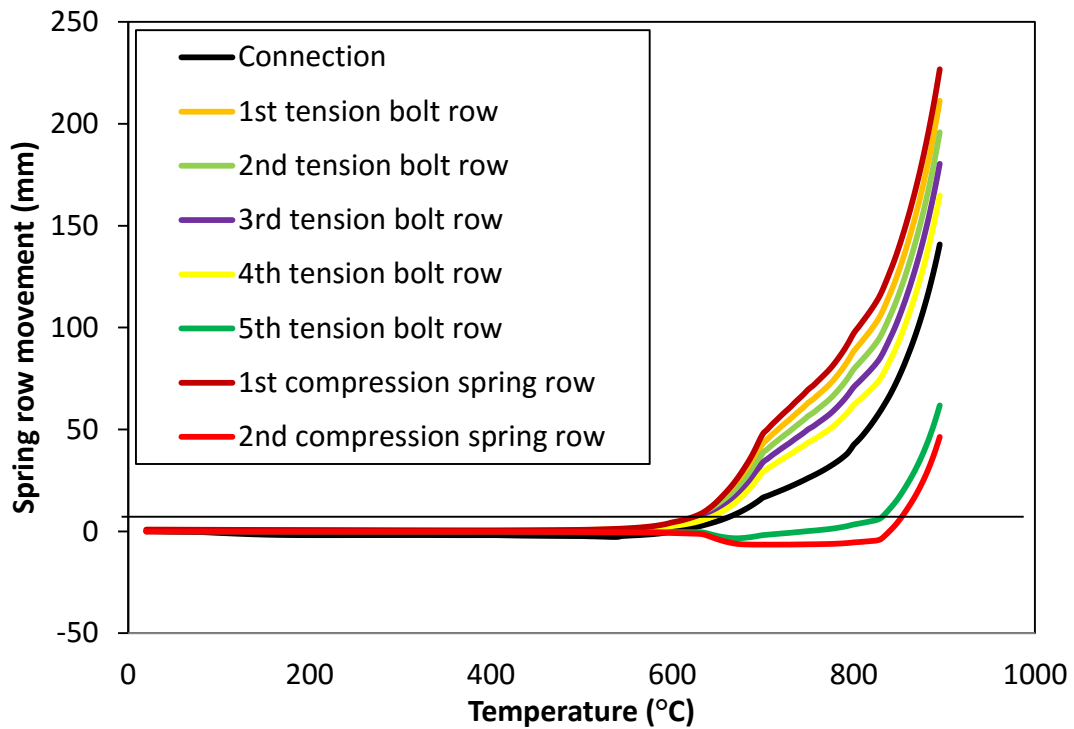
Figure 144: Spring row and connection horizontal movement Case 4 [load 10 kN/m].

Summary

The main differences and similarities shown by the four cases outlined above lie in their degrees of beam-end restraint in the axial and rotational degrees of freedom. In particular, Cases 1 and 4 have limited axial restraint stiffness, whereas Cases 2 and 3 have very high axial restraint. Figure 145 shows one aspect (the mid-span deflection) of the effects of these boundary conditions in the 4 cases. The mid-span deflections of Cases 2 and 3 are nearly overlapped. The deflections of the isolated beam without axial restraint (Case 1) and the 2D "Rugby goal-post" frame (Case 4) are close, and increase sharply above 600°C. Both Cases 1 and 4 initially deflect very little, since very low axial forces do not induce thermal buckling of the beam, whereas the cases with high axial restraint very rapidly induce sufficient axial force because of their restraint to thermal expansion. However, the same axial restraint equilibrates catenary tension, which acts to control the deflections at high temperatures, when the less restrained cases are capable of "run-away" deflection because their mechanisms mainly consist of bending. Case 4 can generate some axial tension at high deflections because of the elastic and plastic resistance to pull-in of the two columns, and it can be seen that the "run-away" is much less rapid than that of the simple beam in Case 1.
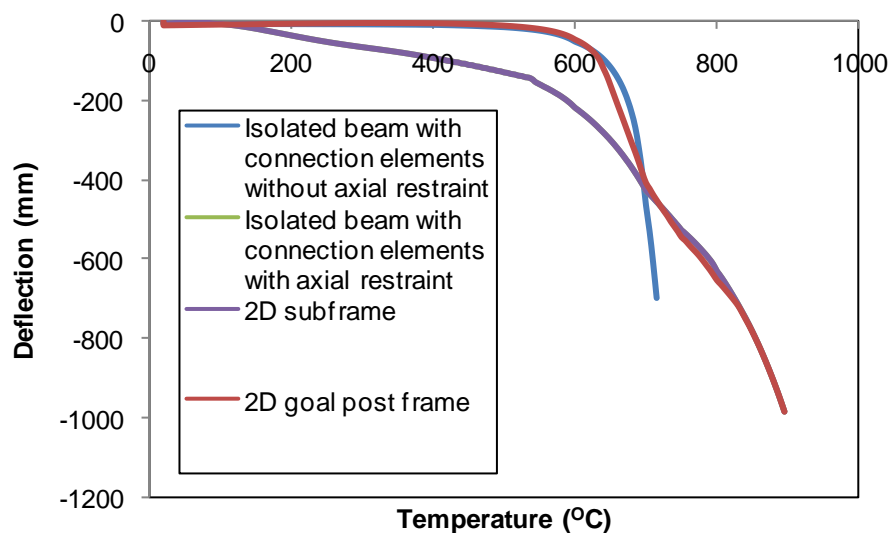
Figure 145: The heated beam's mid-span deflection for 4 cases [load 10 kN/m]

4.3 Development of the connection element for flush endplate connection

The preliminary applications of the user-defined connection element have shown that it is feasible to use component-based connection elements in numerical modelling of structural

frames in fire. Once the component models for the column flange in bending, endplate in bending, bolt in tension and column flange in compression are fitted into a general-purpose component assembly, the connection element will be capable of modelling the flush endplate connection.

4.3.1 Adopted component model

As connections are subject to large deformations in fire, each component spring model must be developed not only to consider the initial stiffness and failure modes for ambient-temperature design, but also to include the plastic resistance and ductility over a range of elevated temperatures. Component models have been intensively developed by researchers from the University of Sheffield, who have spent some years on the characterization of component behaviour at elevated temperatures. The current component-based connection element mostly adopts the component characteristics (listed in Table 15) which have been developed at the University of Sheffield.

Table 15: list of characterized component models

Component	Adopted component model	Reference
End plate in bending	T-stub model	Spyrou (2002), Yu *et al* (2009)
Column flange in bending	T-stub model	Spyrou (2002), Yu *et al* (2009)
Bolt in tension	T-stub model	Spyrou (2002), Yu *et al* (2009)
Column web in compression	Column web in compression	Spyrou (2002), Block (2006)
Reverse channel in tension	Reverse channel in tension	RFCS (2012a)
Reverse channel in compression	Reverse channel in compression	RFCS (2012a)

The component model for the column web in compression has been well documented by Spyrou (2002) and Block (2006), and this work is not repeated here. The details of component models for the reverse channel are included in Chapter 3. The T-stub model was originally developed by Spyrou (2002), and developed further by Yu *et al.* (2009). It has

been validated against a series of component tests. In order to fit into the component assembly, these T-stub models were combined.

4.3.1.1 Previous development of the T-stub model

In the endplate connection's tension zone, the three tension components (*bolt in tension*, *endplate in bending* and *column flange in bending*) are equivalent to the two T-stubs (shown in Figure 146), connected by bolts.

The behaviour of the T-stub has been widely investigated over the past thirty years, both experimentally and theoretically, even if most of this research has been for relatively small deflections. Coelho (2004) summarised the earlier works by Zoetemeijer (1974), Packer *et al.*(1977), Yee *et al.* (1986), Jaspart (1991), Bursi *et al.* (1997), Faella *et al.* (1998), Gebbeken *et al.* (1999), Swanson *et al.* (2000) and Piluso *et al.*(2001). These works have been selectively included in EC3 Part 1.8 (CEN, 2005b). In particular, the development by Zoetemeijer includes the basic principles of the component methods. It is the most important among these developments and is even now broadly applied throughout Europe.
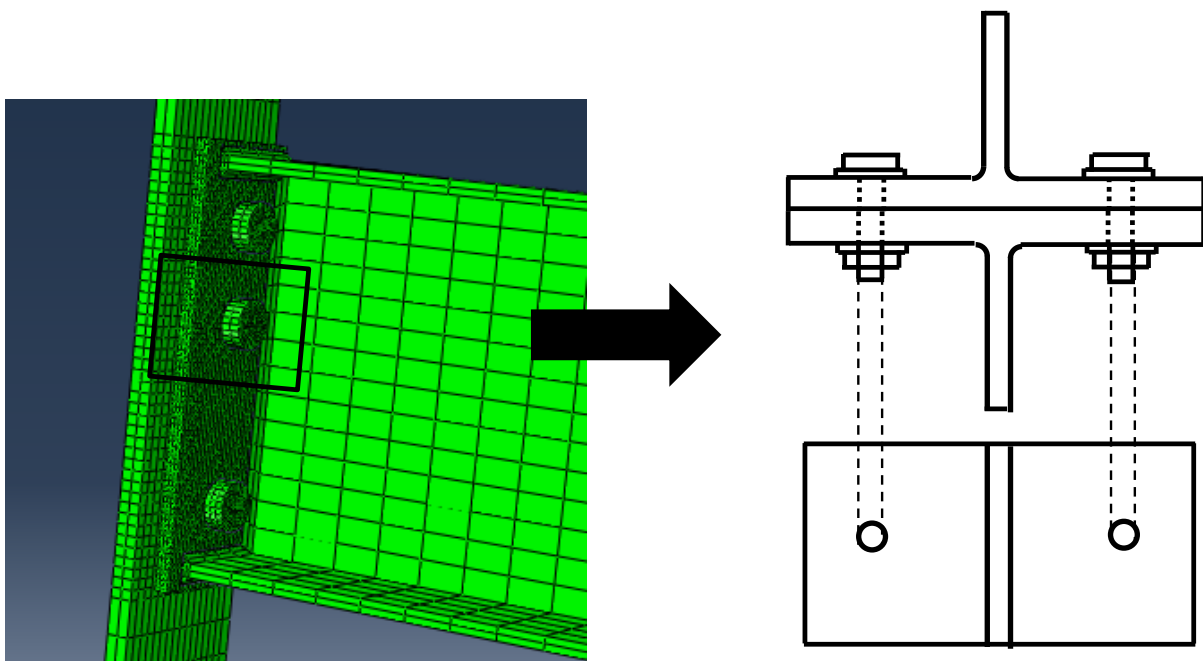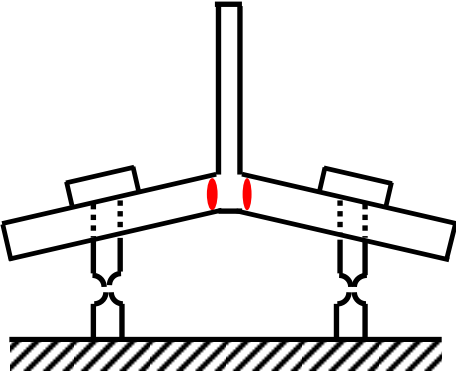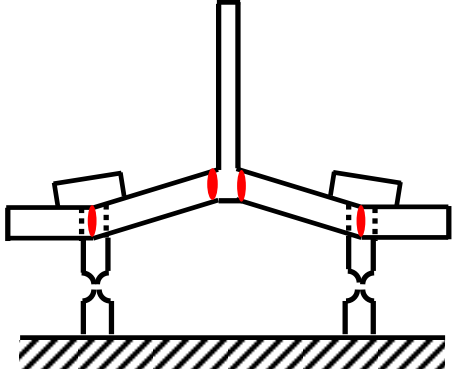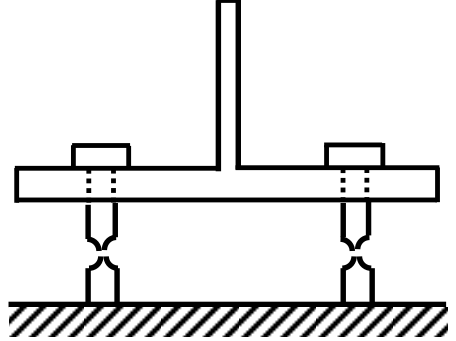
Figure 146: Equivalent T-stub (one bolt row)

Zoetemeijer (1974) derived his T-stub model based on the yield-line principle; this can be used to assess the ultimate plastic resistance of the T-stub. It assumed that the plastic deformation is large enough to allow the adoption of the most favourable static equilibrium condition. The three classic failure mechanisms considered are illustrated in Table 16. For

each collapse mechanism, the resistance can be calculated from the equilibrium in the plastic condition, taking into account any prying force which exists. The resistance of the T-stub is the smallest of those from these collapse mechanisms. Zoetemeijer also successfully introduced the concept of effective length (of the T-stub in the dimension perpendicular to the plane of the "T") for design purposes. The effective length is the equivalent length of the flange plate which contributes to load transmission; it does not have to be the physical length of the plate, or the inter-bolt-row spacing.

Table 16: Failure modes for the T-stub (Spyrou, 2002)

	<u>Failure mode 1:</u> • First plastic hinge forms in the T-stub flange • Bolt yielding • Bolt fracture
	<u>Failure mode 2:</u> • First plastic hinge forms in the T-stub flange • Second plastic hinge forms in the T-stub flange • Bolt yielding • Bolt fracture
	<u>Failure mode 3:</u> • Bolt yielding • Bolt fracture

4.3.1.2 The development of the T-stub model at the University of Sheffield

Two component models have been verified against tests, and can be used to represent the tension component behaviour at elevated temperatures.

Spyrou (2002) tested a large number of bolted T-stub assemblies at elevated temperatures, and their force-displacement characteristics were measured. Spyrou developed a simplified analytical model on the basis of classic beam theory, corresponding to the three possible collapse mechanisms (Table 16). In Block's (2006) connection element, Spyrou's formulations were used to simulate separately the endplate in tension and the column flange in tension. The T-stub's effective length was defined as shown in 'Joints in Steel Construction: Moment connections' (SCI, 1997).

Spyrou's derivation included two identical T-stubs with four bolts. The model gives acceptable results, and is straightforward to use for the prediction of the tension zone behaviour at elevated temperatures. However, in Spyrou's model the prediction of the formation of the second plastic hinge is slightly conservative, because the location of the second plastic hinge is considered to be at the bolt centre line. In reality, the T-stubs can be held together by sufficiently stiff bolts, and can only form a hinge at the edge of the bolt head or nut. On the other hand, in the case of one sufficiently thick T-stub flange, working with a relatively small bolt, the bolt can also rotate due to the very stiff and strong T-stub flange. Therefore, the second plastic hinge's location is dependent upon the relative strengths of the plate and bolt.

Yu (2009a) developed a yield-line model in accordance with the plastic work principle (Figure 19).

$$F\delta = W_{PH1} + W_{PH2} + W_{bolt} \tag{4.19}$$

In the above equation, the work ($F\delta$) done by the applied force F is equal to the sum of the rotational plastic work of the two plastic hinges plus the tensile work in distortion of the bolts. In Yu's model, three-phase elastic-plastic material models are assumed for both the T-stub flange and the bolt. The bolt reaches necking after it has reached its ultimate strength. The model considers material and geometric nonlinearities (**Error! Reference source not found.**), which enable the component failure to be precisely captured. The validations against both finite element models and tests at ambient and elevated temperatures have

shown that this model represents the behaviour of T-stubs very well. Yu's model is also easy to implement within the component assembly for endplate connections.

4.3.1.3 Revised component model for T-stub

This section will focus on how the tension component T-stub is characterised and built into the assembly. The general assembly (**Error! Reference source not found.**) considers the three tension components in a row to be working in series, and consequently the same force is present in all the components in a bolt row. The active tension components in the endplate connection are the *column flange in bending*, the *bolt in tension* and the *endplate in bending,* which are represented by the T-stub model (discussed in 4.3.1.2). However, due to prying action, the force in the bolt can differ from that which it applies to either of the two flanges. In order to implement the T-stub model in the general component assembly (Figure 103), the *bolt in tension* is included in the weaker side of two T-stubs (that with lower maximum resistance). Figure 147 shows typical force/displacement curves for both the T-stub flanges and whole T-stub. The plotted force is the applied force, and the displacements for the column flange and the pair of T-stub flanges are (δ-δ_b) and δ respectively (as illustrated in Figure 19). Therefore, the effective *F/D* curve for each tension bolt row (Figure 148) consists of the sum of the deflections from an effective *F/D* curve for the weaker side of the whole T-stub and an effective *F/D* curve from its stronger side.
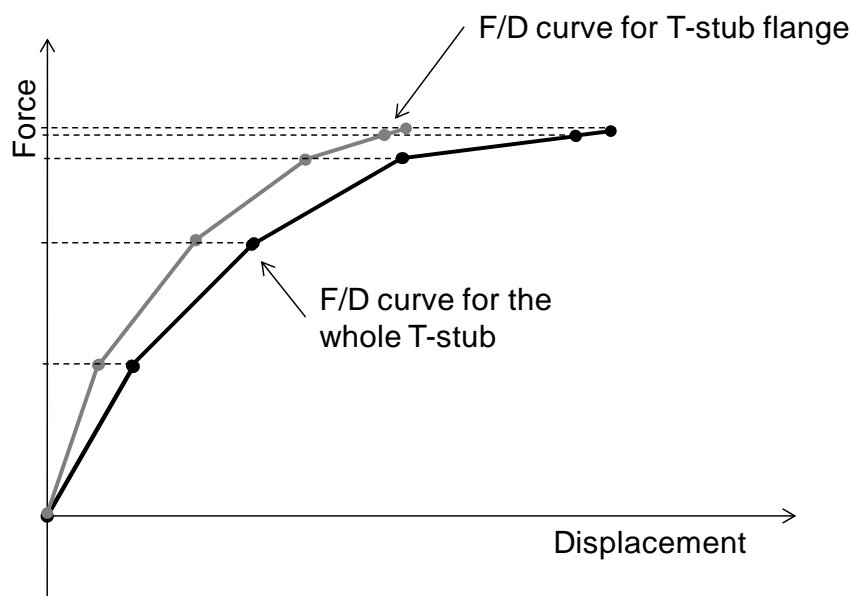
Figure 147: Force/displacement curves plotted by the T-stub model
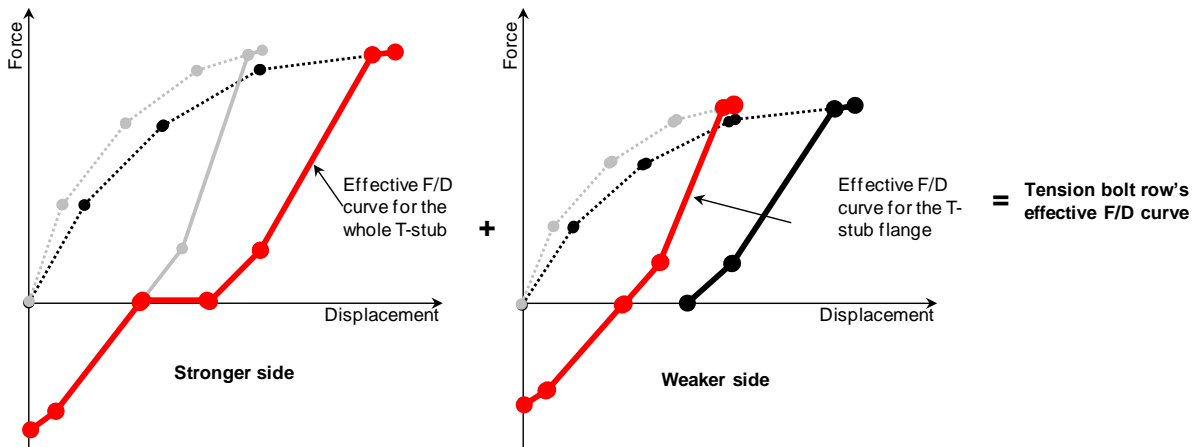
Figure 148: Effective tension bolt row F/D curve in an endplate connection

In order to efficiently model component behaviour and capture the failure, the component-based connection element adopted to represent the T-stub is a combination of Spyrou's and Yu's component models. Yu's yield line model is used to compute the Force/Displacement curve and to capture the failure point. As it is time consuming to consider such a detailed *F/D* characteristic in each component within the connection element, the *F/D* curve (shown in Figure 149) has been simplified and divided uniformly to be represented by just 5 points (nodes 1 to 5) connected by straight lines. As the initial stiffness is a basic element of the component-based connection element's prediction, this is calculated on the basis of Spyrou's T-stub model. Figure 150 shows that Node 2 is relocated at the intersection between the line representing the initial stiffness and the extended Line 2. A typical simplified curve is shown in Figure 151.
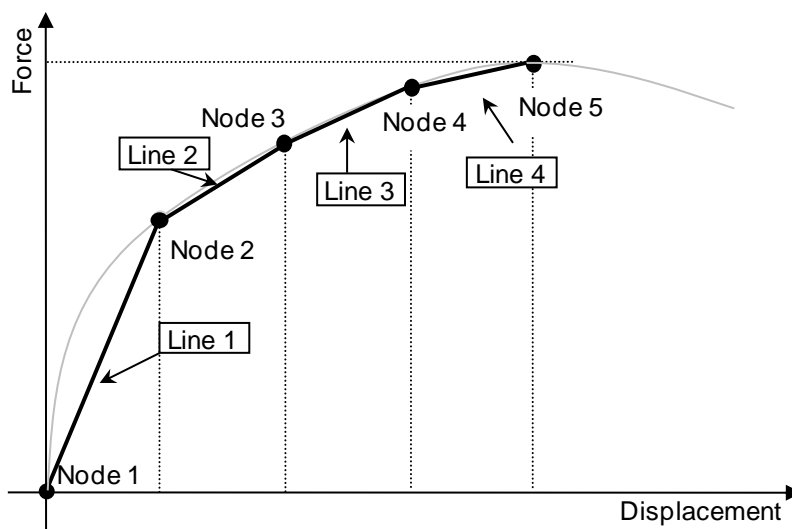
Figure 149: Simplification of component model F/D, curve (a)
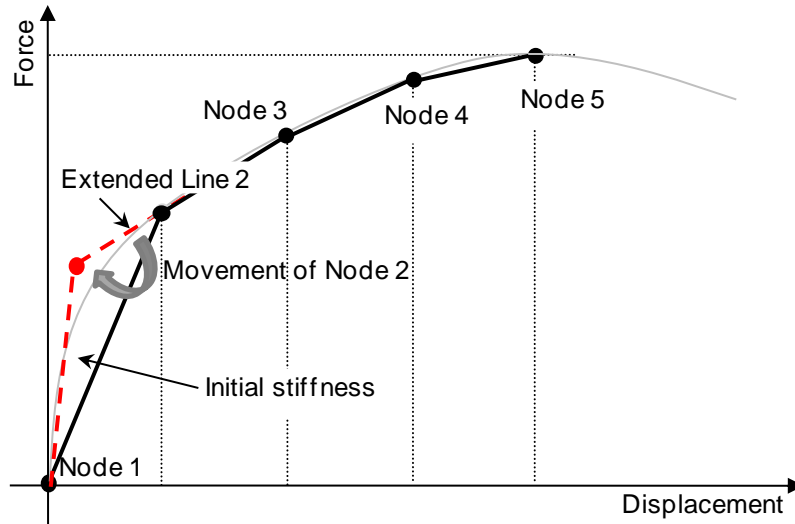
Figure 150: Simplification of component model F/D, curve (b)
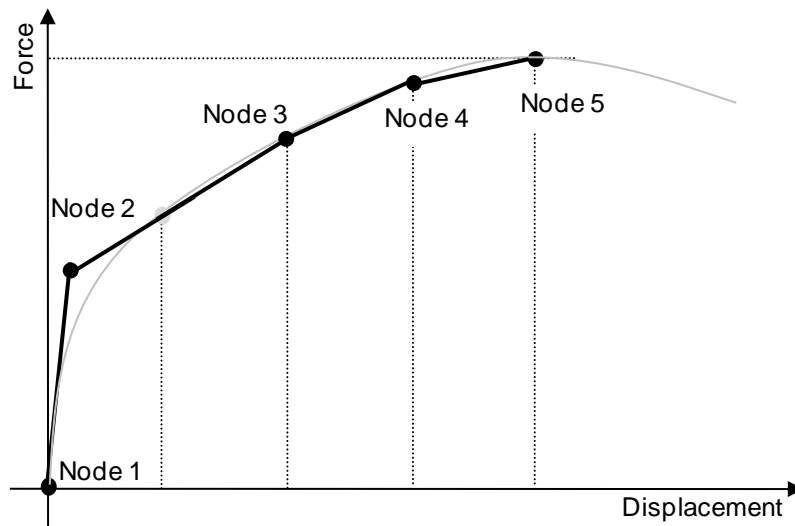
Figure 151: Simplification of component model F/D, curve (c)

The geometry of a T-stub is shown in Figure 152.

The initial bolt stiffness (K_b) is given by:

$$K_b = \frac{E_b A_s}{L_b}$$

(4.20)

Where L_b is the effective bolt length, E_b is the Young's modulus of the bolt, and A_s is the bolt shank area.
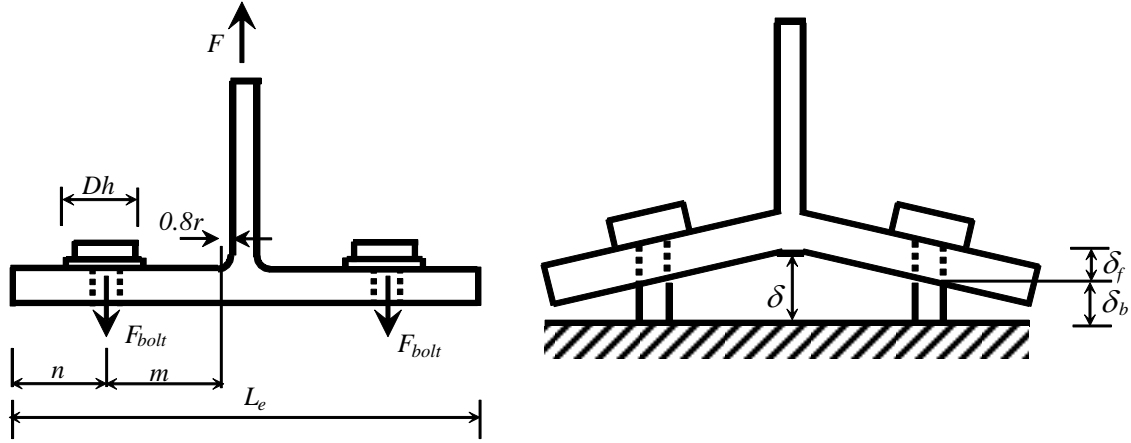
Figure 152: T-stub geometry

The whole T-stub deformation (δ) is:

$$\delta = \delta_f + \delta_b \tag{4.21}$$

Where δ_f is the T-stub flange deformation and δ_b is the bolt deformation. The ratio of bolt force (F_{bolt}) to the total T-stub force (F) is developed by Spyrou (2002) and given by:

$$\rho = \frac{F_{bolt}}{F} = \frac{\dfrac{1}{EI}\left(\dfrac{nL_e^2}{16} - \dfrac{n^3}{12}\right)}{K_b - \dfrac{1}{EI}\left(\dfrac{n^3}{6} + \dfrac{Dh^2 n}{24} + \dfrac{nm^2}{2} - \dfrac{nl2_e}{8} - \dfrac{Dh^3}{384}\right)} \tag{4.22}$$

Where E is the T-stub Young's modulus; $I = 2L_e t_f^3 /12$, L_e is the effective width of the T-stub flange and t_f is the T-stub flange thickness. F is the tension force applied to the T-stub, and F_{bolt} is the bolt tension force.

The initial stiffness of the T-stub (Spyrou,2002) is

$$K = \frac{1}{\dfrac{L_e^3}{48EI} - \dfrac{\rho}{EI}\left(\dfrac{L_e^3}{24} + \dfrac{m^3}{6} - \dfrac{m^2 L_e}{4} - \dfrac{Dh^2 n}{24}\right)} \tag{4.23}$$

The initial stiffness of the T-stub flange (Spyrou,2002) is

$$K_f = \frac{1}{\dfrac{1}{K} - \dfrac{\rho}{K_b}} \tag{4.24}$$

4.3.2   Comparison with flush endplate joint tests

The connection element was validated (Table 17) against the flush endplate joint tests, which were conducted by Yu in the collaborative EPSRC project (EP/C5109841/1) conducted by the Universities of Sheffield and Manchester. This project investigated the robustness of connections in fire conditions (Yu *et al.*, 2008a, 2008b, 2009a, 2009b, 2009c, 2009d and 2011; Hu *et al.*, 2009, Dai *et al.*, 2009a, 2009b, 2010a and 2010b). Yu's connection tests focused on high-temperature structural behaviour of components and assemblies under combined tying and shearing forces. A large number of connections (shown in Figure 153 and Figure 154) were tested to destruction under inclined forces, at temperatures up to 650°C. The tested connections cover four typical beam-column connection types, including the flush endplate connection (listed in Table 17).
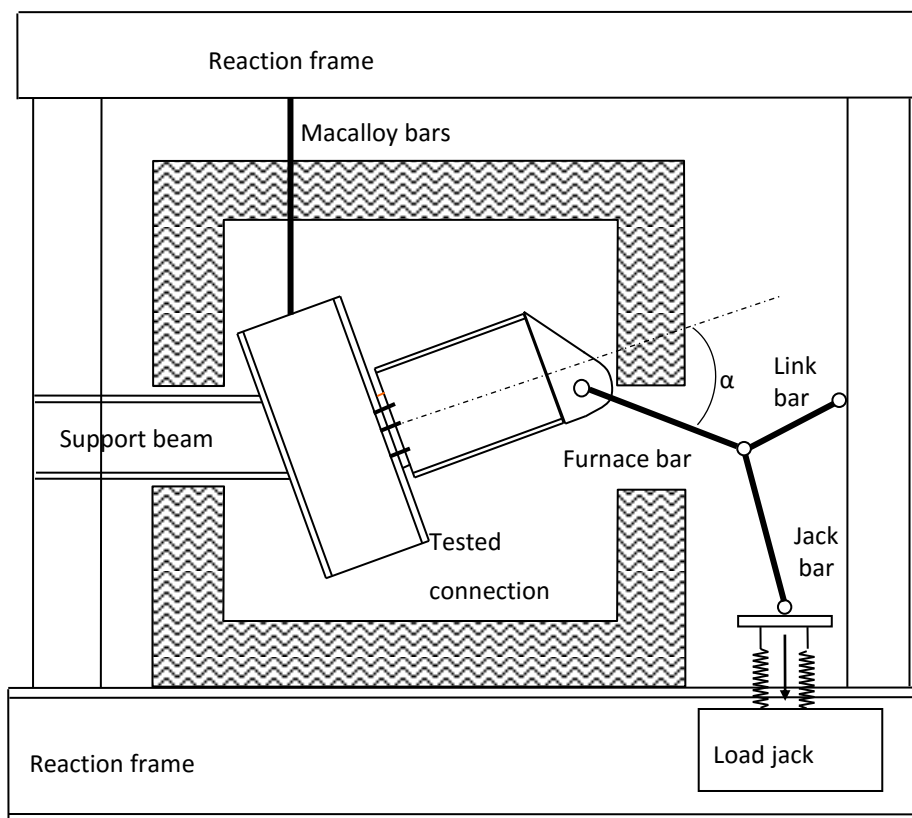
Figure 153: Joint test setup by Yu (2011)

Figure 154: Joint test side view by Yu (2011)

Table 17: Selected list of isolated flush endplate joint tests

Test ID	Endplate thickness (mm)	Initial angle	Number of bolt rows	Temperature (°C)
EP_20_35_04-02-08_8mm	8	35	3	20
EP_20_35_05-02-08	20	35	3	20
EP_20_55_28-02-08	20	55	3	20
EP_450_35_23-11-07	20	35	3	450
EP_450_45_23-10-07	20	45	3	450
EP_450_55_19-02-08	20	55	3	450
EP_550_35_11-12-07_8mm	8	35	3	550
EP_550_35_17-12-07_15mm	15	35	3	550
EP_550_35_27-11-07	20	35	3	550
EP_550_45_16-10-07	20	45	3	550
EP_550_55_13-02-08	20	55	3	550
EP_650_35_30-11-07	20	35	3	650
EP_650_45_19-10-07	20	45	3	650
EP_650_55_15-02-08	20	55	3	650

4.3.2.1   Material properties

The material properties of the endplate connection tests at ambient and elevated temperatures were summarized by Yu *et al.* (2011), and are listed in Table 18.

141

Table 18: Simplified material properties for endplate tests

	Temperature (°C)	20	450	550	650
Column and beam	Yield stress (N/mm^2)	357	176	106	63
	Ultimate stress (N/mm^2)	568	300	211	105
	Young's modulus (N/mm^2)	176000	82900	63050	32450
	Second modulus (N/mm^2)	1062	532	398	137
Endplate	Yield stress (N/mm^2)	293	145	87	52
	Ultimate stress (N/mm^2)	492	297	173	86
	Young's modulus (N/mm^2)	149000	70150	53350	27450
	Second modulus (N/mm^2)	1002	768	432	170
Bolt	Yield stress (N/mm^2)	677	341	135	49
	Ultimate stress (N/mm^2)	998	519	285	128
	Young's modulus (N/mm^2)	210000	157000	111850	54500
	Second modulus (N/mm^2)	1629	899	751	397

4.3.2.2   Model setup

Figure 155 shows how the tests were set up, and the form in which they were modelled in *Vulcan*. The bars (heavy black lines between hinges) were assumed to be rigid.
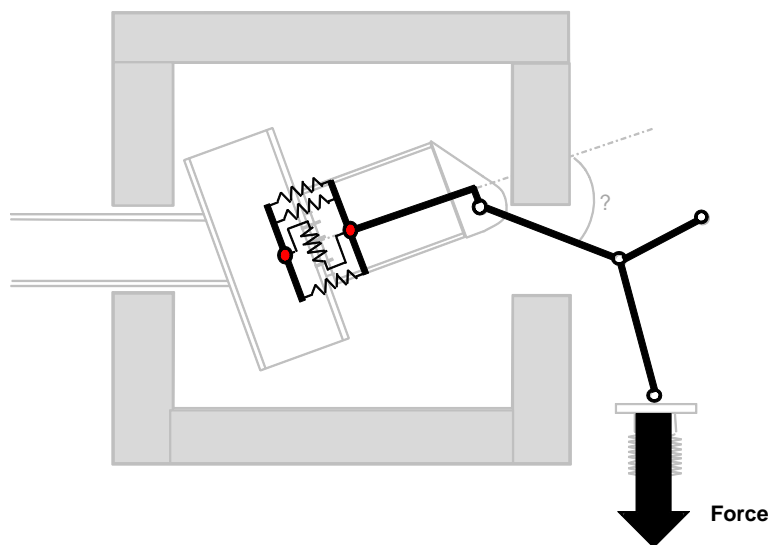
Figure 155: Model setup

4.3.2.3   Results

Comparison between the component-based connection element and tests (furnace-bar force versus the connection rotation) are presented in Figure 156 to Figure 169. In general, the connection element is in satisfactory agreement with the test results, especially if its simplicity compared with comparable Finite Element models is recalled. The prediction of

initial stiffness given by the element matches that from the tests. More importantly, in the context of robustness analysis, the element also captures the maximum resistance conditions well enough, and in most cases conservatively. The modelling results have been plotted until one component is predicted to fracture, so that the curves show the peak capacities; the experimental curves show the full extent of each test. In some tests failure occurred; others were stopped in order to protect the furnace from damage.
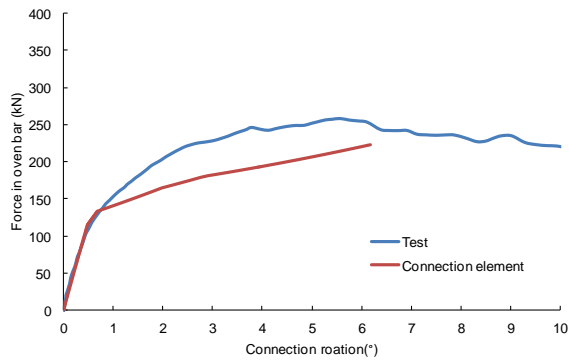
Figure 156: EP_20_35_04-02-08_8mm
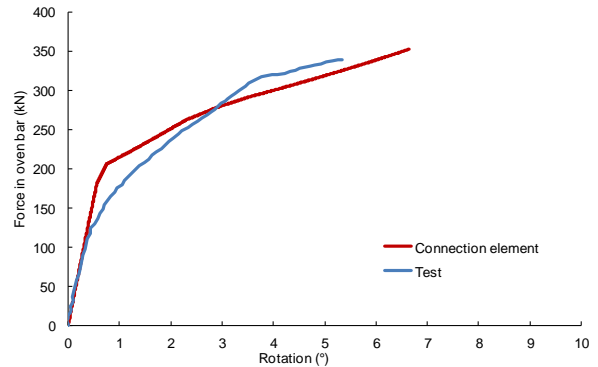
Figure 157: EP_20_35_05-02-08
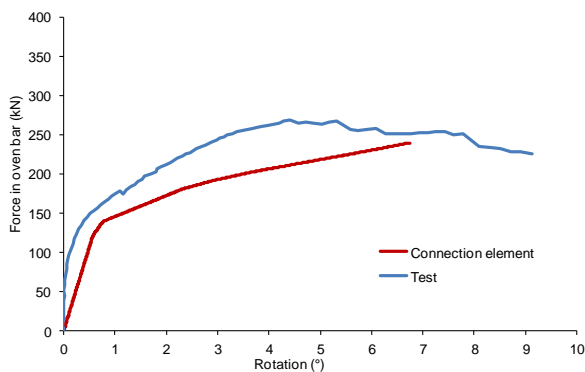
Figure 158:EP_20_55_28-02-08
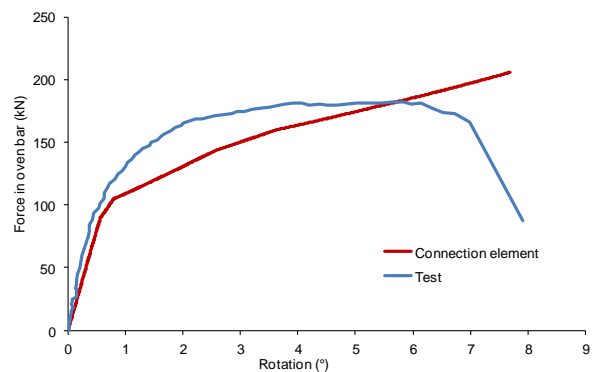
Figure 159: EP_450_35_23-11-07
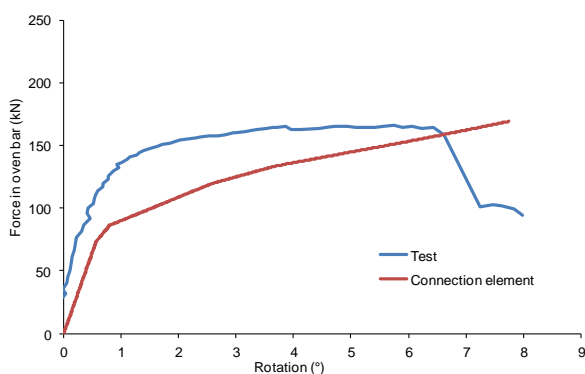
Figure 160: EP_450_45_23-10-07
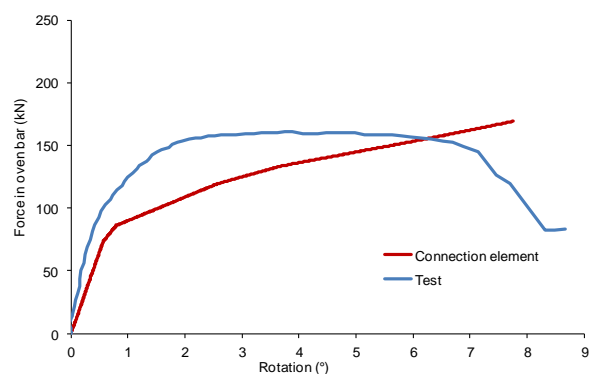
Figure 161: EP_450_55_19-02-08
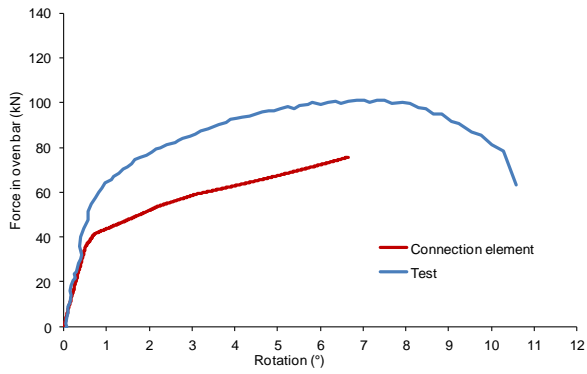
Figure 162: EP_550_35_11-12-07_8mm
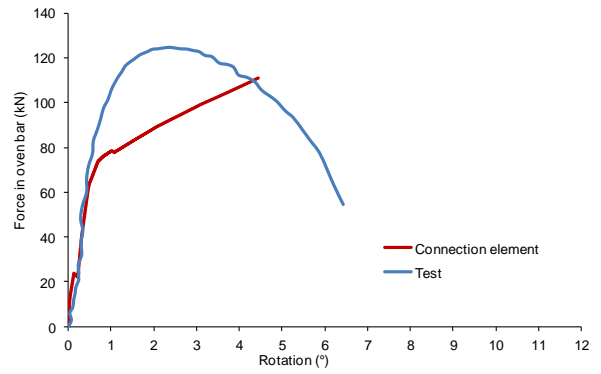
Figure 163: EP_550_35_17-12-07_15mm
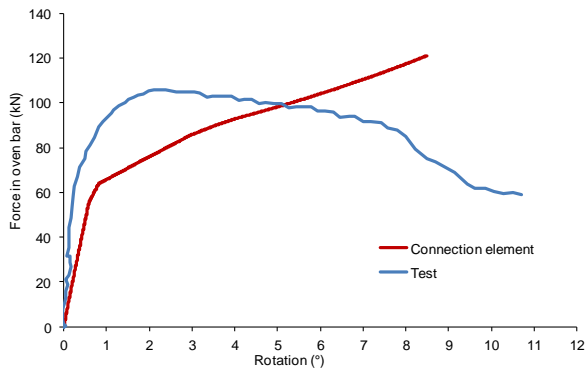
Figure 164: EP_550_35_27-11-07
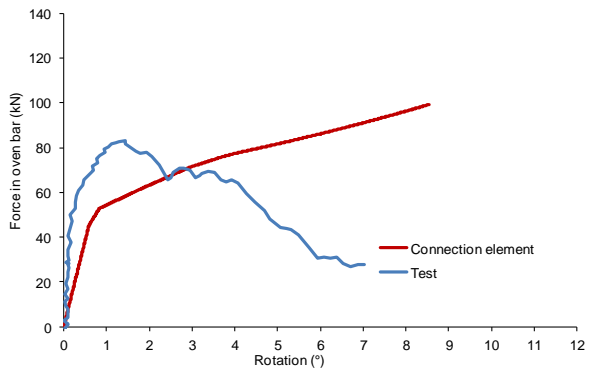
Figure 165: EP_550_45_16-10-07
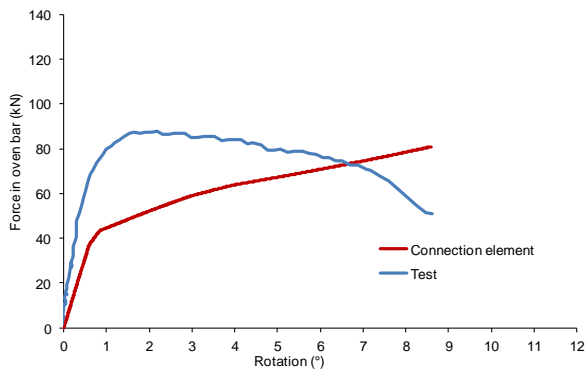
Figure 166: EP_550_55_13-02-08
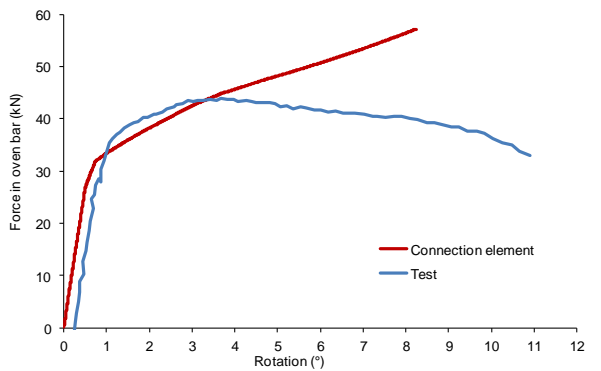
Figure 167: EP_650_35_30-11-07
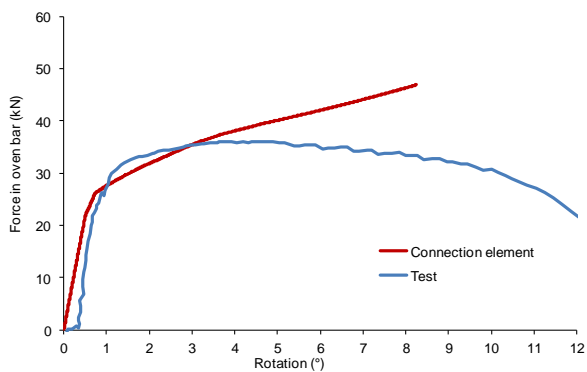
Figure 168: EP_650_45_19-10-07
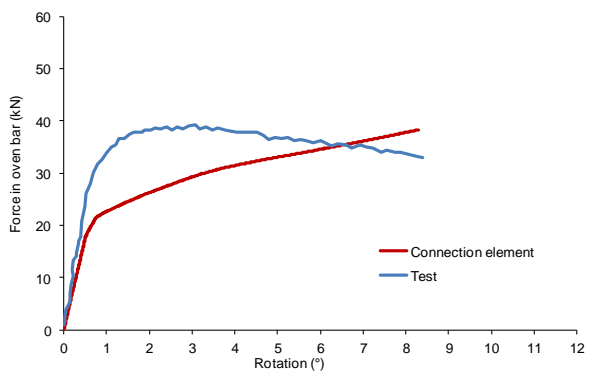
Figure 169: EP_650_55_15_02_08

144

4.4 Development of the connection element for reverse channel connection

The component characterizations reported previously in Chapter 3 have been built-into *Vulcan,* and are accessible to the general-purpose element model. The component model for reverse channel connections was developed in the COMPFIRE project, and this enabled 20 tests under axial force and moment to be carried out and compared with analysis. It is therefore possible to validate the connection element for reverse channel connections against the joint tests conducted in the COMPFIRE project.

4.4.1 Comparison with reverse channel joint tests

As part of COMPFIRE, the University of Sheffield performed 20 constant-temperature tests on isolated joints to Concrete-Filled-Tube (CFT) and Partially-Encased (PE) H-section columns under different combinations of axial and shear forces and moments. These isolated joint tests provided valuable experimental data to identify the behaviour of the composite joint and validate the component-based element under conditions which combine a number of bolt rows, working together in the context of a fairly general form of joint distortion, in contrast to the isolated bolt-row tests carried out at Manchester and Coimbra. Table 19 shows the list of 14 of the Sheffield joint tests which have been used in the following validation.

The test setup was similar to the flush endplate tests (shown schematically in Figure 155). Selected test photos are shown from Figure 170 to Figure 174. The geometry of the individual test specimens is well documented in RFCS (2009) and is therefore not repeated here.

Table 19: Isolated joint tests performed at Sheffield within COMPFIRE.

No	ID	Column	Temp	Connection type
1	CCFT-RC200_550_55_10-01-2011	O CFT	550	RC cut from SHS 200X6
2	SCFT-RC200_550_55_04-01-2011	□ CFT	550	RC cut from SHS 200X6
3	CCFT-RC250_550_55_1-10-2010	O CFT	550	RC cut from SHS 250X8
4	SCFT-RC250_550_55_15-09-2010	□ CFT	550	RCcut from SHS 250X8
5	CCFT-UKPFC230_550_55_06-08-2010	O CFT	550	UKPFC230x90x32
6	SCFT-UKPFC230_550_55_02-07-2010	□ CFT	550	UKPFC230x90x32
7	CCFT-UKPFC230_20_55_03-03-2011	O CFT	20	UKPFC230x90x32
8	SCFT-UKPFC230_20_55_24-01-2011	□ CFT	20	UKPFC230x90x32
9	CCFT-UKPFC200_550_55_17-09-2010	O CFT	550	UKPFC200x90x30
10	SCFT-UKPFC200_550_55_08-07-2010	□ CFT	550	UKPFC200x90x30
11	CCFT-UKPFC180_550_55_23-09-2010	O CFT	550	UKPFC180x90x26
12	SCFT-UKPFC180_550_55_13-07-2010	□ CFT	550	UKPFC180x90x26
13	PE-UKPFC150_550_55_13-01-2011	P/E*	550	UKPFC150x75x18
14	PE-UKPFC150_650_55_19-01-2011	P/E*	650	UKPFC150x75x18

*Partially-encased H-section column

Figure 170: CCFT-RC200_550_55_10-01-2011 side view after test

Figure 171: CCFT-RC200_550_55_10-01-2011 top view after test

Figure 172: SCFT-RC200_550_55_04-01-2011 side view after test

Figure 173: SCFT-RC200_550_55_04-01-2011 side view 2 after test

Figure 174: SCFT-RC200_550_55_04-01-2011 top view after test

4.4.1.1 Material properties

The component characterizations used within the component-based connection element use three-stage elastic-plastic material properties at ambient temperature, defined by the "yield" and "ultimate" strength points. After the ultimate strength point is reached, the stress values are assumed to stay constant, and the strain is allowed to increase without limit from this point.

The bolt material properties are the same as those in the endplate joint tests (shown in Table 18). The steel material properties (Table 20) at ambient temperature use the average values from the coupon test results. The temperature-dependent yield strength and elastic modulus reduction factors given in EC3 part 1-2 are employed to partially define the material properties at elevated temperatures. The ultimate strength is assumed to be reached at a strain of 0.04 at both ambient and elevated temperatures. In order to calculate the ultimate strength at elevated temperature (above 400°C), the tangent modulus is assumed to be100N/mm^2 at all temperatures.

Table 20: Material properties for isolated reverse channel joint tests.

		Test ID	Yield stress (N/mm^2)	Ultimate stress (N/mm2)	Young's modulus (N/mm^2)	Tangent modulus (N/mm^2)	Temp. (°C)
Reverse channel	1	CCFT-RC200_550	247	251	125557	100	550
	2	SCFT-RC200_550	245	249	125612	100	550
	3	CCFT-RC250_550	247	251	125557	100	550
	4	SCFT-RC250_550	245	249	125612	100	550
	5	CCFT-UKPFC230_550	225	228	84964	100	550
	6	SCFT- UKPFC230_550	225	229	108401	100	550
	7	CCFT-UKPFC230_20	365	543	114333	4691	20
	8	SCFT- UKPFC230_20	368	546	189685	4674	20
	9	CCFT-UKPFC200_550	186	190	98448	100	550
	10	SCFT- UKPFC200_550	186	190	98448	100	550
	11	CCFT-UKPFC180_550	183	187	126501	100	550
	12	SCFT- UKPFC180_550	174	178	98339	100	550
Endplate	1	CCFT-RC200_550	269	273	97659	100	550
	2	SCFT-RC200_550	269	273	97659	100	550
	3	CCFT-RC250_550	269	273	97659	100	550
	4	SCFT-RC250_550	269	273	97659	100	550
	5	CCFT-UKPFC230_550	269	273	97659	100	550
	6	SCFT- UKPFC230_550	269	273	97659	100	550
	7	CCFT-UKPFC230_20	430	617	214635	4905	20
	8	SCFT- UKPFC230_20	430	617	214635	4905	20
	9	CCFT-UKPFC200_550	269	273	97659	100	550
	10	SCFT- UKPFC200_550	269	273	97659	100	550
	11	CCFT-UKPFC180_550	269	273	97659	100	550
	12	SCFT- UKPFC180_550	269	273	97659	100	550
Beam	1	CCFT-RC200_550	359	512	234268	4041	550
	2	SCFT-RC200_550	359	512	234268	4041	550
	3	CCFT-RC250_550	359	512	234268	4041	550
	4	SCFT-RC250_550	359	512	234268	4041	550
	5	CCFT-UKPFC230_550	359	512	234268	4041	550
	6	SCFT- UKPFC230_550	359	512	234268	4041	550
	7	CCFT-UKPFC230_20	359	512	234268	4041	20
	8	SCFT- UKPFC230_20	359	512	234268	4041	20
	9	CCFT-UKPFC200_550	359	512	234268	4041	550
	10	SCFT- UKPFC200_550	359	512	234268	4041	550
	11	CCFT-UKPFC180_550	359	512	234268	4041	550
	12	SCFT- UKPFC180_550	359	512	234268	4041	550

4.4.1.2 Results

The plots of the furnace-bar force against connection rotation for Tests 1 to 10 are shown in **Error! Reference source not found.** to **Error! Reference source not found.**.

Table 21 shows the failure mode in each case. Both the adopted AISC limit and the current bolt pull-out model limit are seen to be safe for design purposes. The connection element

using the CIDECT limit reasonably predicts the maximum resistance against the test results. It also successfully predicts the failure mode, except in Tests 9 and 10. However, since the predicted maximum resistance is close to that in the test, the prediction of failure mode can be sensitive to various factors, such as material properties and test specimen dimensions.

The validation summary plot (Figure 185) also shows that the connection element with the bolt pull-out model is capable of modelling the reverse channel connection failure capacities for design purposes.

Table 21: Failure modes in the validations against joint tests.

No	Name	Test Failure mode	Connection element prediction		
			Pull-out model	AISC	CIDECT
1	CCFT-RC200_550_55_10-01-2011	No failure (Technical limitation)	Pull-out	Pull-out	Tensile fracture
2	SCFT-RC200_550_55_04-01-2011	Pull-out	Pull-out	Pull-out	Pull-out
3	CCFT-RC250_550_55_1-10-2010	No failure (Technical limitation)	Tensile fracture	Pull-out	Tensile fracture
4	SCFT-RC250_550_55_15-09-2010	Tensile fracture	Tensile fracture	Pull-out	Tensile fracture
5	CCFT-UKPFC230_550_55_06-08-2010	Tensile fracture	Pull-out	Pull-out	Tensile fracture
6	SCFT-UKPFC230_550_55_02-07-2010	Tensile fracture	Pull-out	Pull-out	Tensile fracture
7	CCFT-UKPFC230_20_55_03-03-2011	Technical limitation	Pull-out	Pull-out	Pull-out
8	SCFT-UKPFC230_20_55_24-01-2011	Pull-out	Pull-out	Pull-out	Pull-out
9	CCFT-UKPFC200_550_55_17-09-2010	Tensile fracture	Pull-out	Pull-out	Pull-out
10	SCFT-UKPFC200_550_55_08-07-2010	Tensile fracture	Pull-out	Pull-out	Pull-out
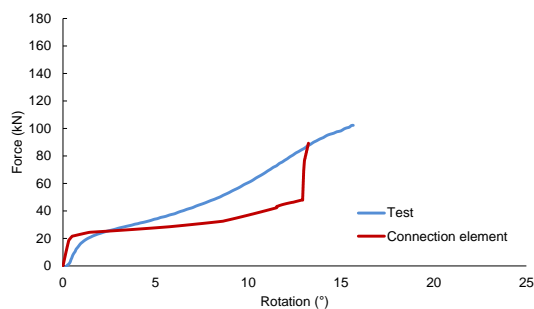
Figure 175: CCFT-RC200_550_55_10-01-2011.
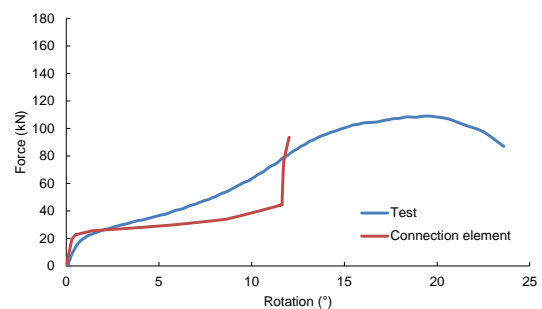
Figure 176: SCFT-RC200_550_55_04-01-2011.
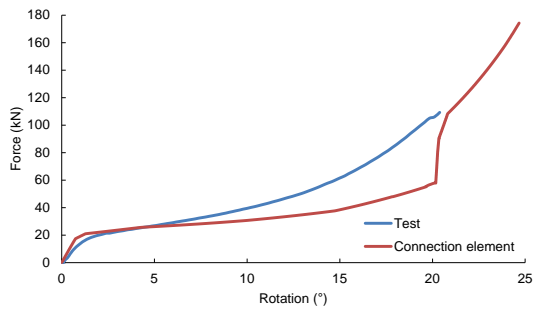
Figure 177: 3. CCFT-RC250_550_55_1-10-2010.
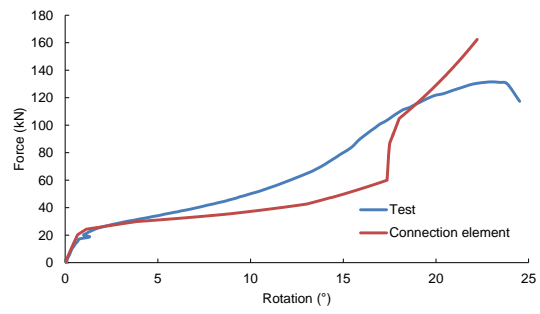
Figure 178: 4. SCFT-RC250_550_55_15-09-2010.
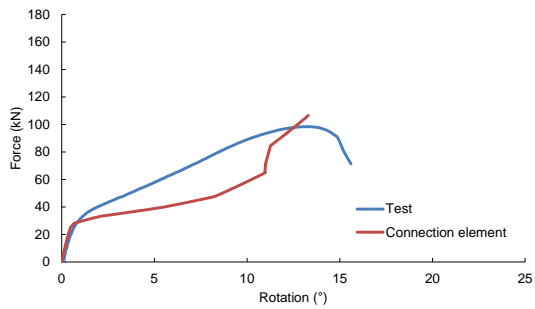
Figure 179: 5. CCFT-UKPFC230_550_55_06-08-2010.
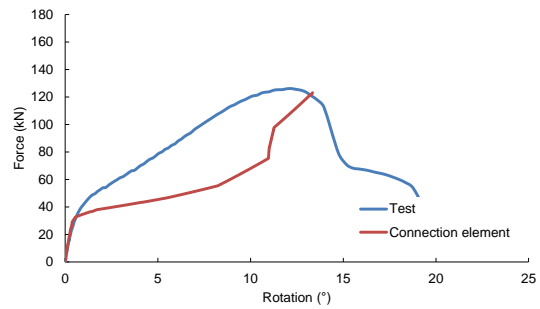
Figure 180: 6. SCFT-UKPFC230_550_55_02-07-2010.
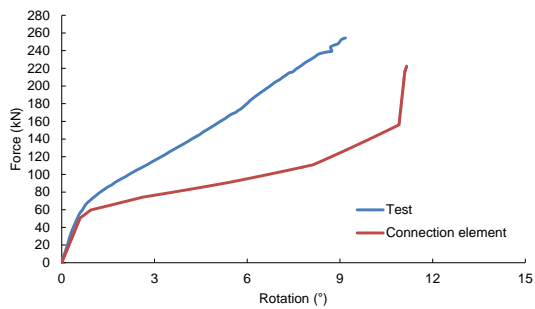
Figure 181: 7. CCFT-UKPFC230_20_55_03-03-2011.
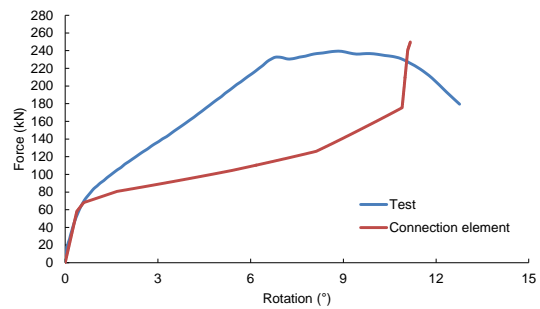
Figure 182: 8. SCFT-UKPFC230_20_55_24-01-2011.
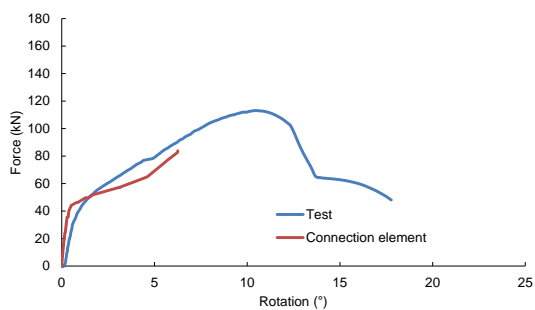
Figure 183: 9 .CCFT-UKPFC200_550_55_17-09-2010.
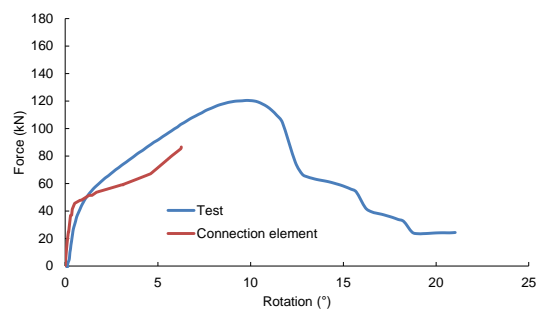
Figure 184: 10. SCFT-UKPFC200_550_55_08-07-2010.

152
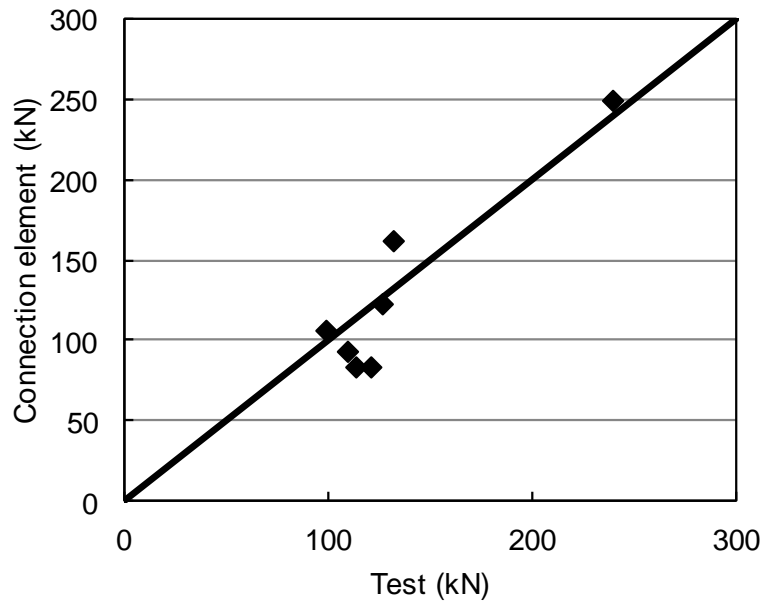
Figure 185: Comparison of predicted failure loads against test results.

4.5 Conclusion

The component-based connection element has been developed. The approach is consistent with EC3 Part 1-8, in which the connection is divided into several effective lateral non-linear springs, which are assembled with rigid links to represent the semi-rigid connection. The reduced material properties at elevated temperature are also taken into account. The proposed connection element has been implemented within *Vulcan* to model joints at elevated/cooling temperatures. Validation against experimental results at ambient and elevated temperature has been carried out. The connection element has shown that it can model with adequate accuracy the nonlinear temperature-dependent response of two connection types (endplate and reverse channel connection) under generalised loading conditions, including unloading (deflection reversal) whenever this occurs. For the reverse channel connection, the predictions of the component model, including the simple sub-model representing bolt pull-out, are close to the test results, and can be used for practical design analysis. Due to the simplification of component model, the force/rotation curves do not match as perfectly as general detailed finite element modelling, and there may be scope for improvements particularly to the pull-out model. Some factors, such as the precise locations of plastic hinges, are at present too complicated for the component model to take into account accurately, and some further development may be able to optimize these.

However, as an intermediate method at the present time, the component-based connection element balances reasonable accuracy with great advantages in computing and setup time costs. It allows engineers to model the connection in fire efficiently without losing too much accuracy.

Chapter 5.   Application of the component-based element to COMPFIRE connections

This chapter concerns the use of the general-purpose component-based connection element in the analysis of steel-framed buildings in fire. It is firstly applied in the modelling of a subframe test conducted at Manchester as part of the COMPFIRE project. A 2D model will be used to show how, when used in combination with the static-dynamic solver, the connection element is capable of modelling the progressive failure of connections in a plane multi-storey frame. The results show how the behaviour of steel joints in fire conditions can be modelled using component-based joint models.

5.1   Small-scale fire test

Within the scope of the COMPFIRE project, researchers at the University of Manchester completed four fire tests (RFCS, 2012). These were intended to investigate the complex behaviour of reverse channel connections within simple structural frameworks under different fire scenarios, including their behaviour during the cooling phase. The tests were designed to investigate the effects of both rotational and axial restraint on the rotations and thermal expansions and contractions of the beam, including local yielding and buckling, and overall catenary action. Comparing the results from modelling against the subframe test results shows that the component-based connection element is capable of modelling the whole range of joint behaviour.

The Manchester experimental layout is shown Figure 186. Two hydraulic jacks, manually pumped, were used with the objective of applying equal constant vertical forces to the beam. The target was to maintain a 40kN load at each jack; this was generally achieved, as shown in Figure 187. The reaction forces were measured by load cells installed at the bases of the columns. A total of 34 thermocouples (shown in Figure 188) were used to monitor the temperature development during and after the tests.
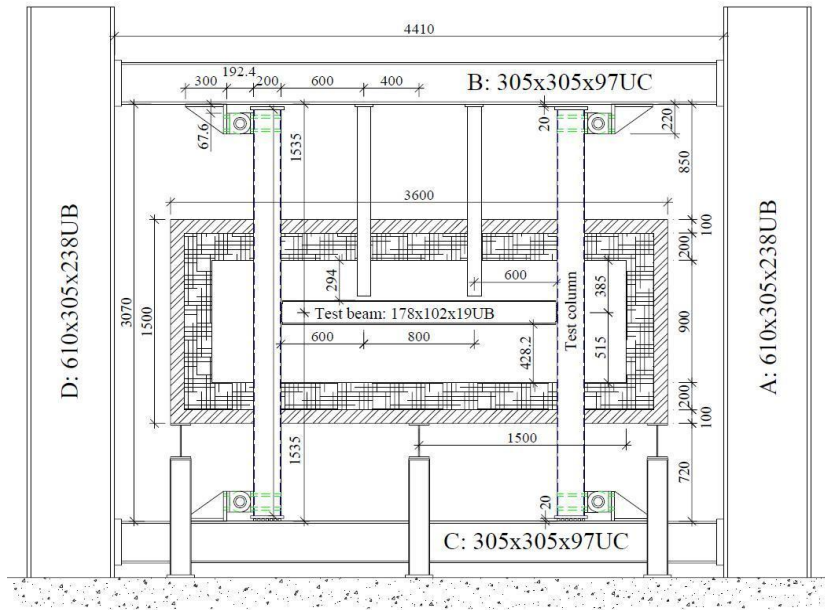
Figure 186: Setup of the subframe tests at Manchester
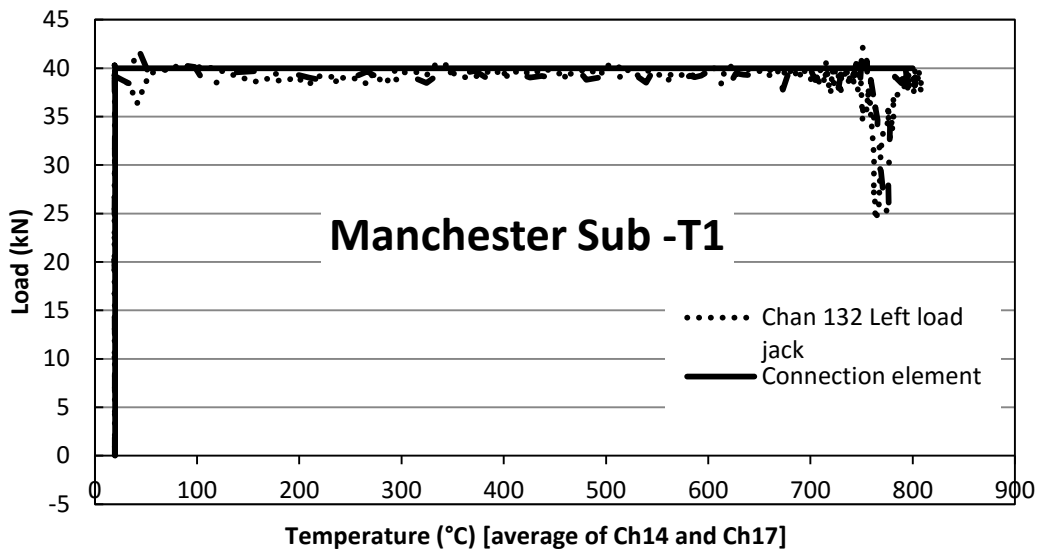
Figure 187: Applied loading in subframe test
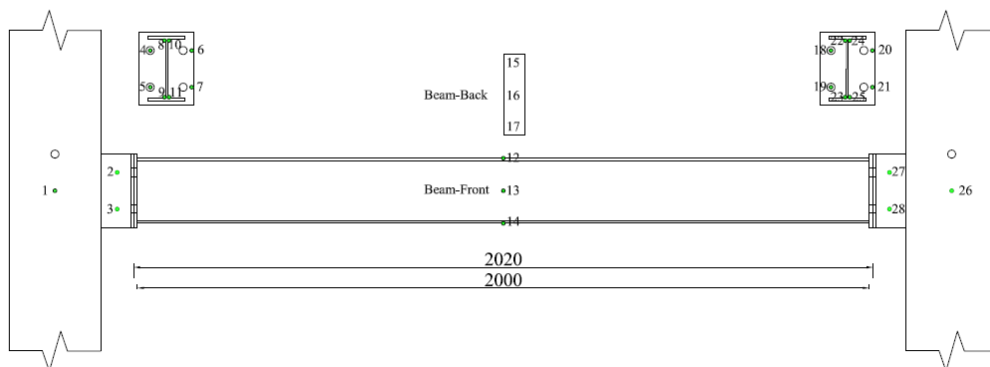
Figure 188: Thermocouple locations in tests TD1 (RFCS, 2012)

Test TD1 is selected for this investigation. Using symmetry, only one half of the frame (shown in Figure 189) needs to be modelled, and this saves considerable computing time.

The top and bottom ends of the column are restrained from horizontal movement, although the vertical movement of the column's top end is allowed.

Table 22 shows how the temperature curves are simplified for modelling, and the test curves are illustrated in Figure 190.
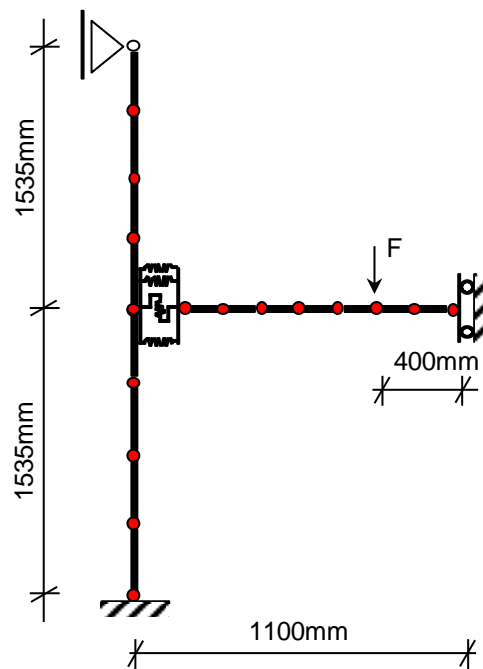
Figure 189: Subframe model of Manchester test TD1.

Table 22: simplification of temperature curves

No	Location	Temperature curve
1	Column (heated part)	Average of CH1 and CH26
2	Beam top flange	Average of CH12 and CH15
3	Beam web	Average of CH13 and CH16
4	Beam bottom flange	Average of CH14 and CH17
5	Connection	CH2

The temperature distribution over the connection region is assumed to be uniform, which is in accordance with the observations from the tests. The material properties used in the modelling are listed in Table 23. The bolt pull-out limit is defined from the pull-out model described in 3.3.2. Since the loads applied in the test were released during cooling, the thermos-structural analysis does not consider the cooling stage.
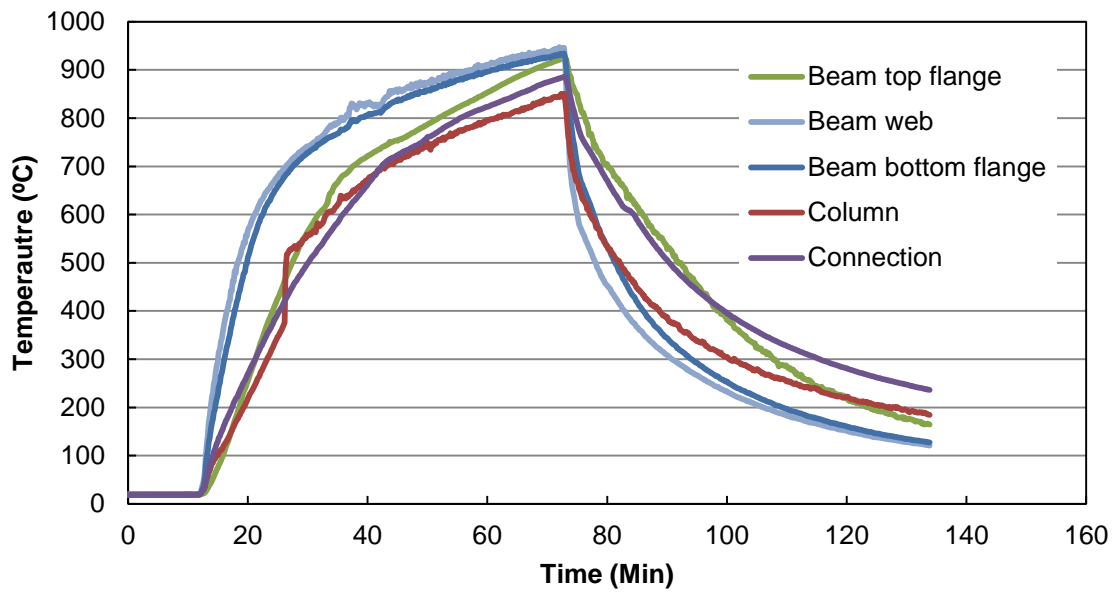
Figure 190: TD1 temperatures

Table 23: Material properties

	End plate & beam	Bolt	Tube section
Yield stress (N/mm2))	293	677	357
Ultimate stress (N/mm2)	492	998	568
Young's modulus (N/mm2	149000	210000	176000
Tangent modulus (N/mm2)	1002	1629	1062

Figure 191 shows the beam mid-span deflection-temperature curve; the temperature shown is the average test value in the beam's bottom flange (average of Channels 14 and 17, shown in Figure 188).
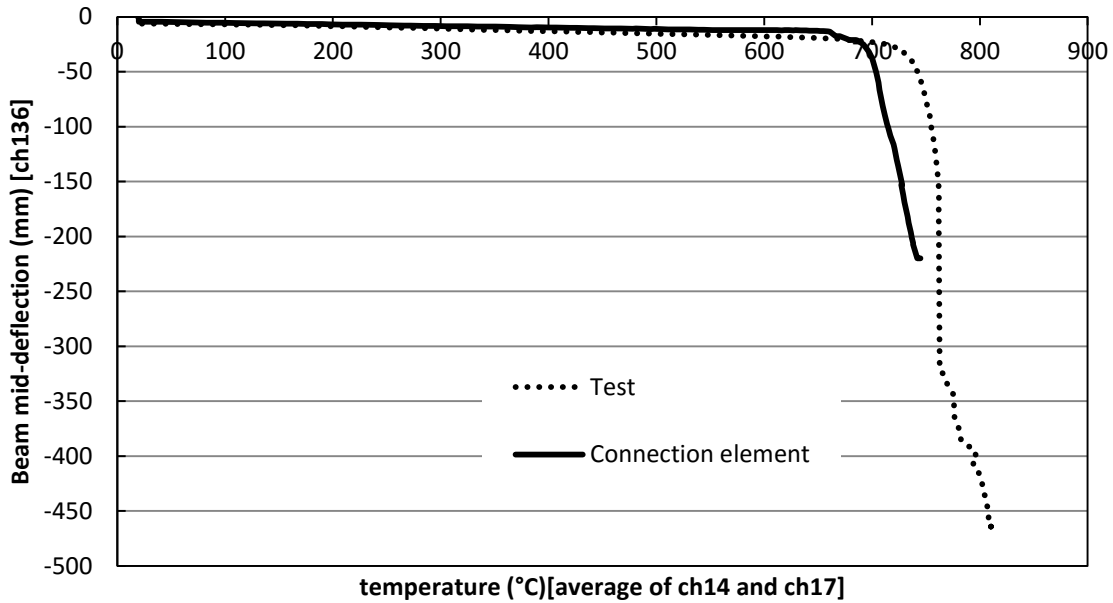
Figure 191: TD1 beam mid-span deflection.

The deflection of the beam predicted by *Vulcan* modelling including the connection element initially lies close to the test result. Above 700°C, this deflection begins to rise sharply. At 745°C, both of the tension bolt rows failed, due to reaching the bolt pull-out limit (170kN) defined by the pull-out model. The maximum deflection is 220 mm at 745°C. If the bolt pull-out limit is that defined by CIDECT (Jaspart, 2005) it fails at the same temperature, but due to bolt fracture, given a maximum bolt tensile resistance of 190kN. The failure type actually identified in the test was bolt thread-stripping, which is one of the ways in which bolts can fail in tension.

Figure 192 presents the connection axial force-temperature results; again the temperature shown is the average test value in the beam bottom flange. The axial force shown for the test results is the sum of the reaction forces recorded by the load cells. The left-hand load cells are Channels 128 and 129, and the right-hand load cells are Channels 130 and 131. Figure 192 shows that the beam's axial compression force initially increases, due to the restraint provided by the connections and columns to thermal expansion of the beam, but gradually reduces and changes to tension as the beam's deflection increases sharply and enters the catenary stage. The axial force given by the modelling is generally slightly higher than the test results.

159

Manchester Sub -T1
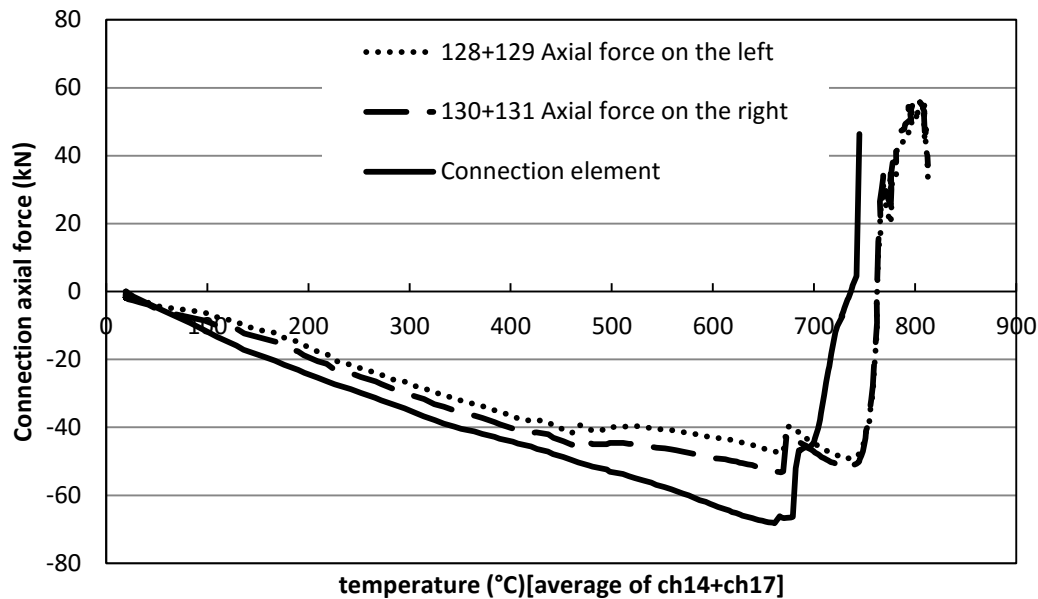
Figure 192: Connection axial force-temperature relationships

5.2 Dynamic modelling of failure process in connection

As described above, the connection element has been implemented within the *Vulcan* research code with the static-dynamic solver. The progressive failure of a connection can therefore be simulated. In order to demonstrate the capacity of the procedure, a progressive collapse analysis of a 2-D structural frame is carried out in the following section.

The geometry of the 3-span composite 2D subframe can be seen in Figure 193. The beam span (L) is 6 metres, and the floor height is 3.5 metres. It is assumed that the fire happens in the middle bay. The temperatures of the heated connections are assumed to be the same, and identical to that of the beam, and the temperatures of the heated columns are each half of that of the heated beam. The beam size is 305x165x40UB. The column is SHS400x400x16 concrete-filled with C30 concrete. The uniform line load on the beam is 27.8 kN/m. The effect of upper floors is represented by an axial compression force of 8000kN per column. The connections used are reverse channel connections, one of which is shown in Figure 194. The reverse channel is a cutting from a 250x10 tube, cut with a 90 mm leg length. The M20 bolts used are Grade 8.8. The leg length of the fillet welds is 8mm. The structural steel generally used is S355, except for the endplates which are S275. Because of the symmetry of the model, only half of the structure needs to be modelled.

160
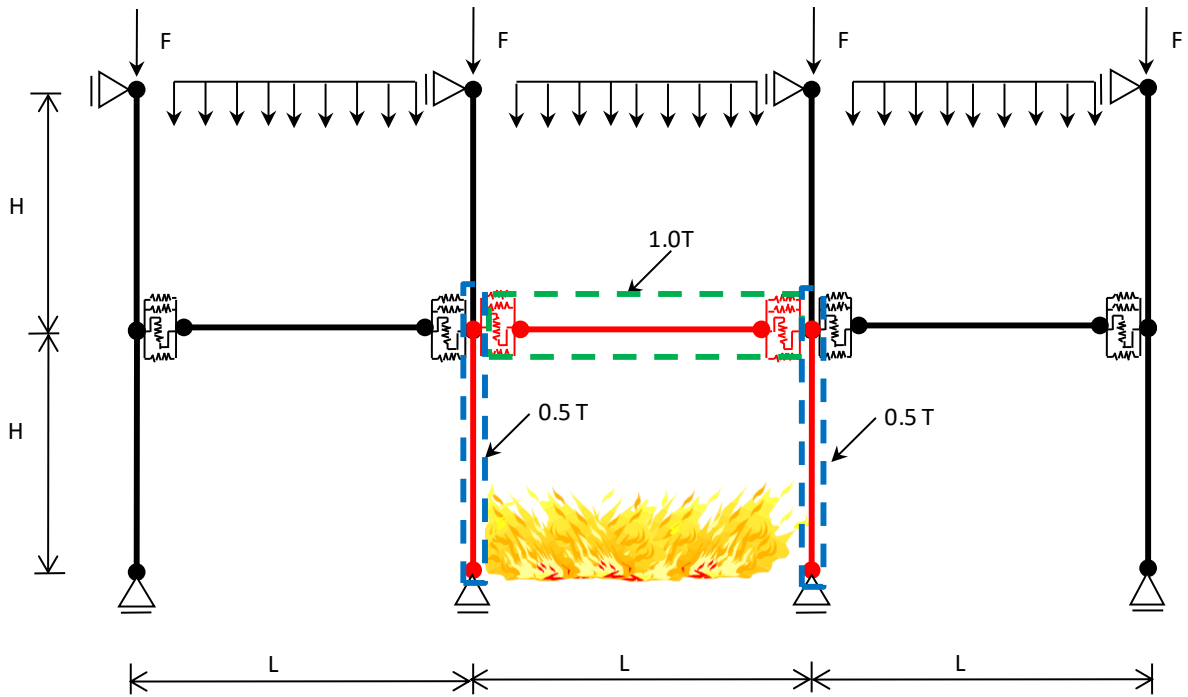
Figure 193: Subframe in parametric study.

Top compression spring row

1st tension bolt row

2n tension bolt row

3rd tension bolt row

Bottom compression spring
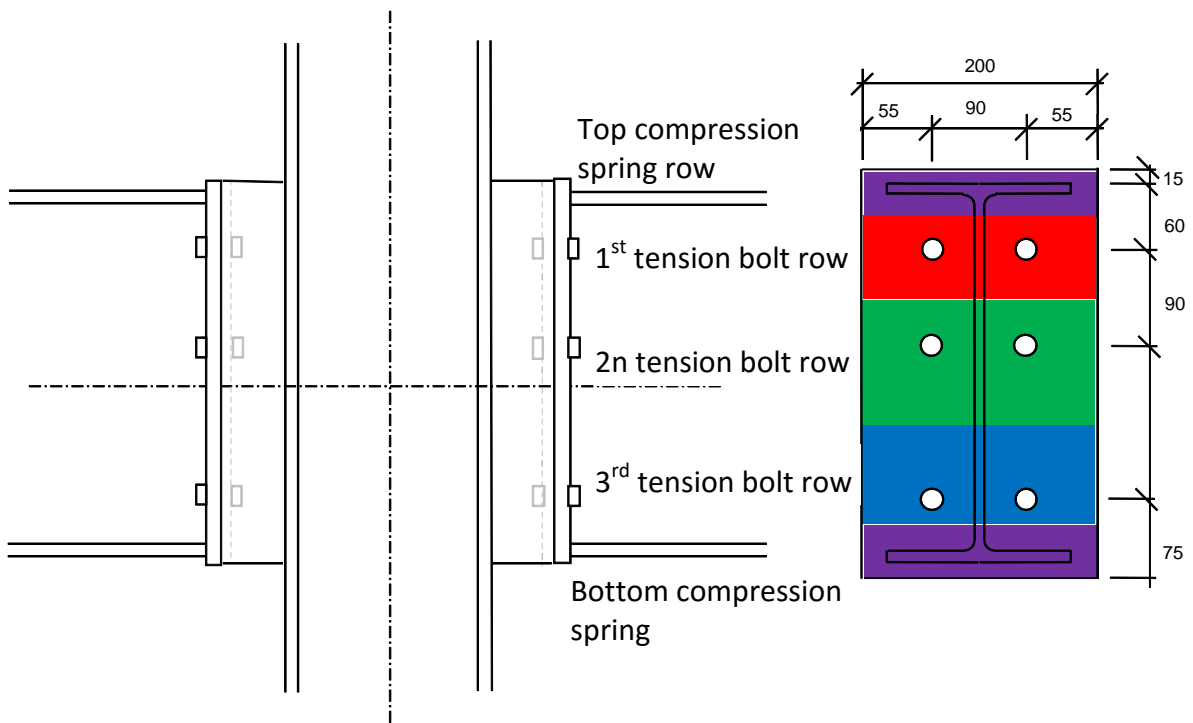
Figure 194: Reverse channel connection used in the parametric study.

Figure 195 shows the axial forces, generated by the *Vulcan* analysis, in the different component spring rows within the heated connections against the connection temperatures. The heated connections fracture at 710°C.
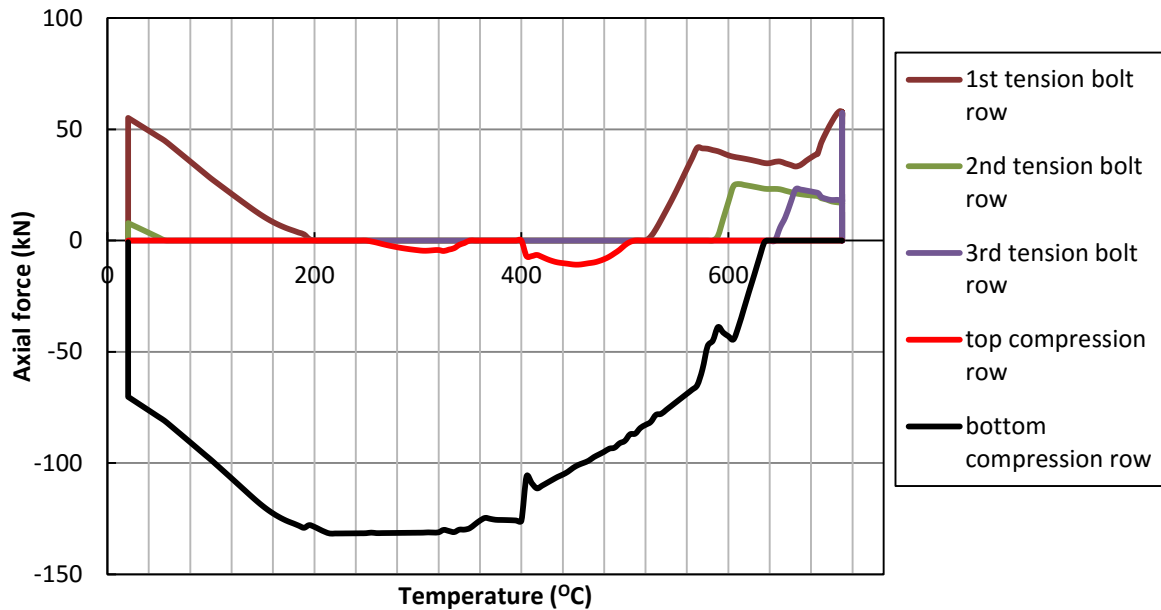
Figure 195: Axial forces of spring rows against connection temperature

Figure 196 plots the heated connections' component axial (normal) forces against their equal beam end rotations. It can be seen that the sequence of fracture of the tension bolt rows starts from the top tension bolt row and ends with the bottom row.
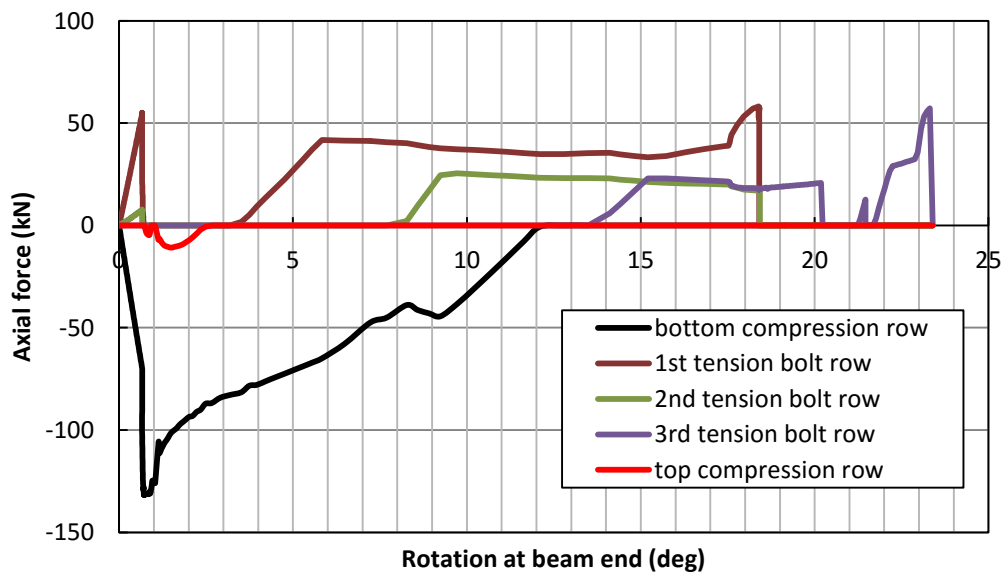
Figure 196: Axial forces of spring rows against beam end rotation

These three tension bolt rows fracture when the beam end rotation reaches 18.61°, 19.41° and 24°. After all the bolt rows have fractured, the beam is completely detached from the columns.

Figure 197 plots the beam rotation against the heated connection's temperature. The analysis continues until buckling of the column occurs at a higher temperature.
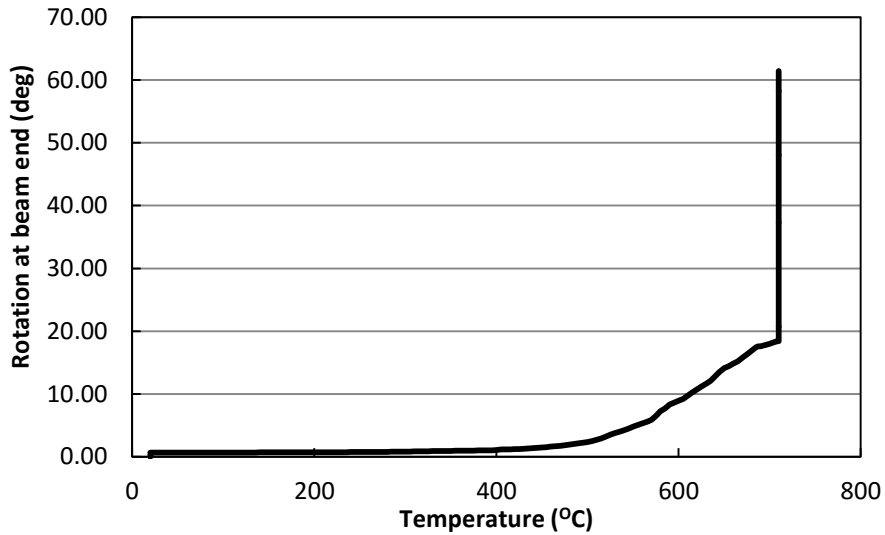
Figure 197: Beam end rotation against connection temperature.

Figure 198 shows the shows the vertical displacement at the top of the heated column. In the end, the column top deflection reaches the floor height of 3.5 metres, which means that the structure collapses.
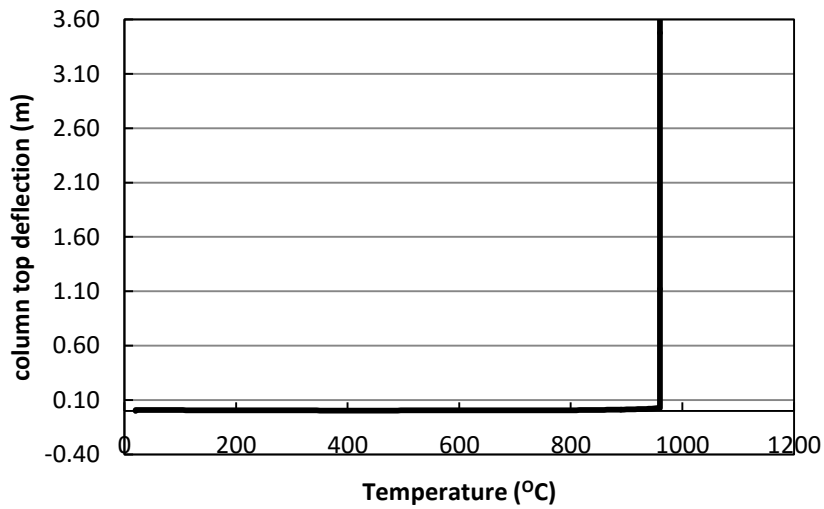
Figure 198: Column top deflection against connection temperature.

The eventual column buckling denotes the failure of the whole structure. This failure sequence is illustrated schematically in Figure 199 to Figure 201.
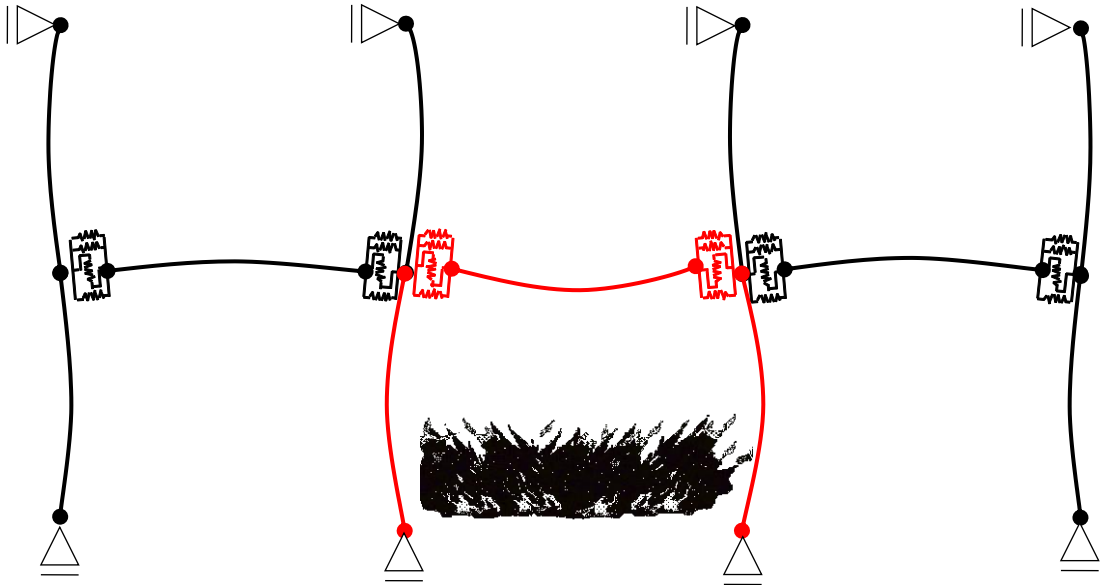
Figure 199: Heated structure – initial stage.
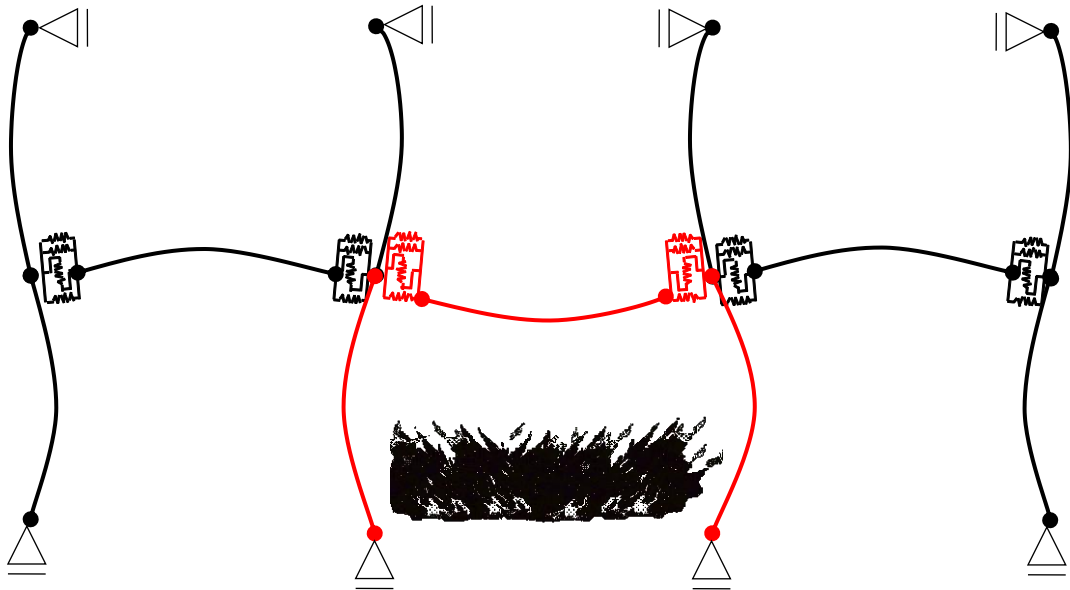
Figure 200: Connection fractured (710°C).
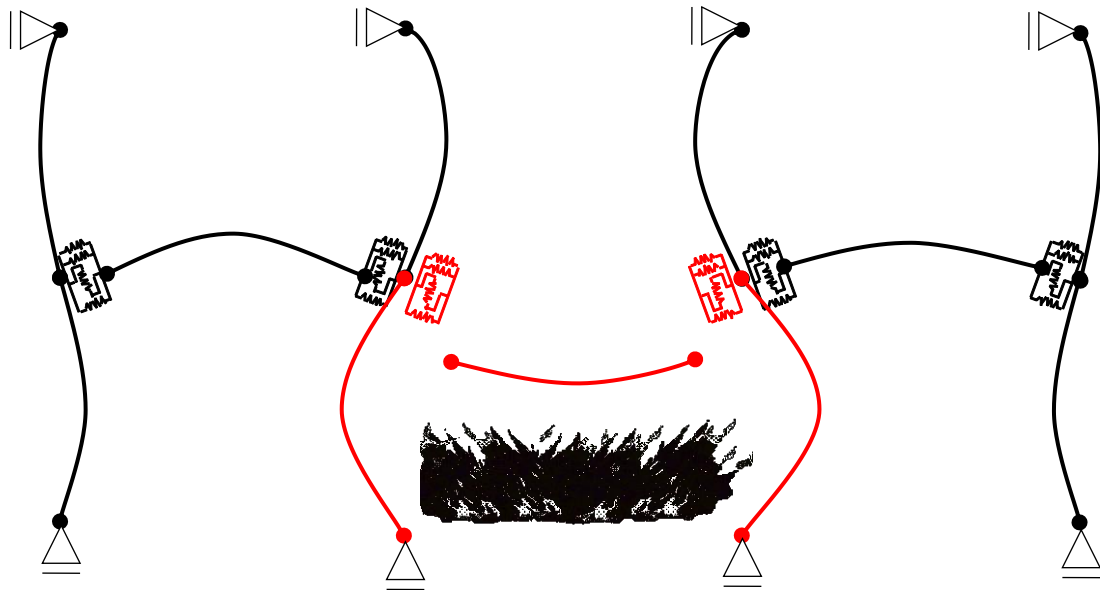
Figure 201: Column buckling at 960°C .

This modelling has demonstrated that analysis with a combination of the component-based connection element with the static-dynamic solver is capable of simulating the progressive fracture of spring rows within connections as temperatures rise. It also shows the structural behaviour beyond connection fracture until final structural collapse occurs.

Chapter 6.   Discussion, Conclusion and Further Recommendations

6.1   Summary

The traditional idealizations of joints in steel frames, as either 'pinned' or 'rigid', were for many years assumed to describe their actual behaviour in fire. It was only after observations from the Cardington fire test series, followed by very prominent fire-induced events such as the collapse of three of the World Trade Centre buildings in 2001, which engineers and researchers realized fully that the connections could be the most vulnerable parts of a structure when fire happens. Connections can be seen to behave differently in fire and at ambient temperature. The material properties of steel plate and bolts both degrade with increasing temperature. However, because of the combination of this weakening with the partially restrained thermal expansions and contractions, particularly of long-span beams, the connections can be subjected to large axial forces. Taking into account the large rotations to which the connections are subjected at high temperatures, the senses of these axial forces may change during the fire. Therefore, it is necessary for designers to comprehend how structures can really behave, when deciding how to analyse them with acceptable accuracy and reasonable efficiency in terms of time and cost.

The component-based method is an intermediate and efficient way of modelling the behaviour of connections, within the framework of a global finite element analysis which is computationally efficient compared with detailed FE modelling. This thesis has addressed the creation of a general-purpose component-based representation of the column-face "connection" zone, as an element which has two external nodes but can internally contain any number of rows of components with temperature-dependent properties, including both force-reversal and failure. The principles of its development are applicable to different connection types and to implementation in different software packages.

The development began with the creation of a flush endplate connection element, and was then extended to the reverse channel connection. For both connection types the key components, which limit the connection capacity or contribute to the joint deformation, were identified at the start. The component characterization for endplate connections has generally adopted the models previously developed by Spyrou (2002), Block (2006), and Yu (2009a). The component models for the reverse channel were developed by the author

during the course of the COMPFIRE project. The assembled component-based connection elements were also validated against the isolated joint tests carried out by Yu in a previous Sheffield project.

In the course of this work the general-purpose connection element has been implemented within the software Vulcan, which has been equipped with a static-dynamic solution process in a parallel project. The coming-together of these two development threads has created a software tool, albeit still at the level of research code, which should allow engineers to identify the local failures of the joints, and to predict the subsequent failure sequence of the remaining structure. Engineers should henceforward be able to identify the vulnerable parts of a structure in scenario-based analyses, and to modify their designs in order to produce a building which will perform robustly in different fire cases.

6.2   Recommendations for further work

Due to the limited amount of time available for postgraduate research, this PhD study cannot cover everything. The advantages of the component-based connection element have been shown above. The following are issues which follow-on from the work done, which should be considered in future research work.

6.2.1   Generalization of the component model

Specific component-based models have been applied to various types of connection: web-cleat, fin plate and flush endplate etc. Although these connections are different, the application of the component-based element principle is the same. This has been well-established during this development process, in which the basic assumptions were made in the context of flush endplate connections and subsequently extended to the reverse channel. This is an illustration that the connection element can be generalized further, and it is apparent that all bolted connections have certain common features; "tension" components (which may act in compression under some circumstances) tend to be chained in series at the levels of bolt-holes, with additional compression components which never act in tension, generally located where the top or bottom flange of the beam member contacts the column face, possibly through an endplate. In order to develop the generalized component-based connection element, it is necessary for the component assembly to

accommodate different component characteristics, and to have the capability to switch on/off any component or spring rows under certain conditions.

Firstly, the component behaviour needs to be generalized, and then the deflections of the number of components in each spring row can easily be added. Figure 202 is a sketch showing the proposed generalized component behaviour, across all four tension and compression quadrants. The unloading follows the Masing rule (Gerstle, 1988). Each component has descending (negative-stiffness) parts from both the tension and compression zones.
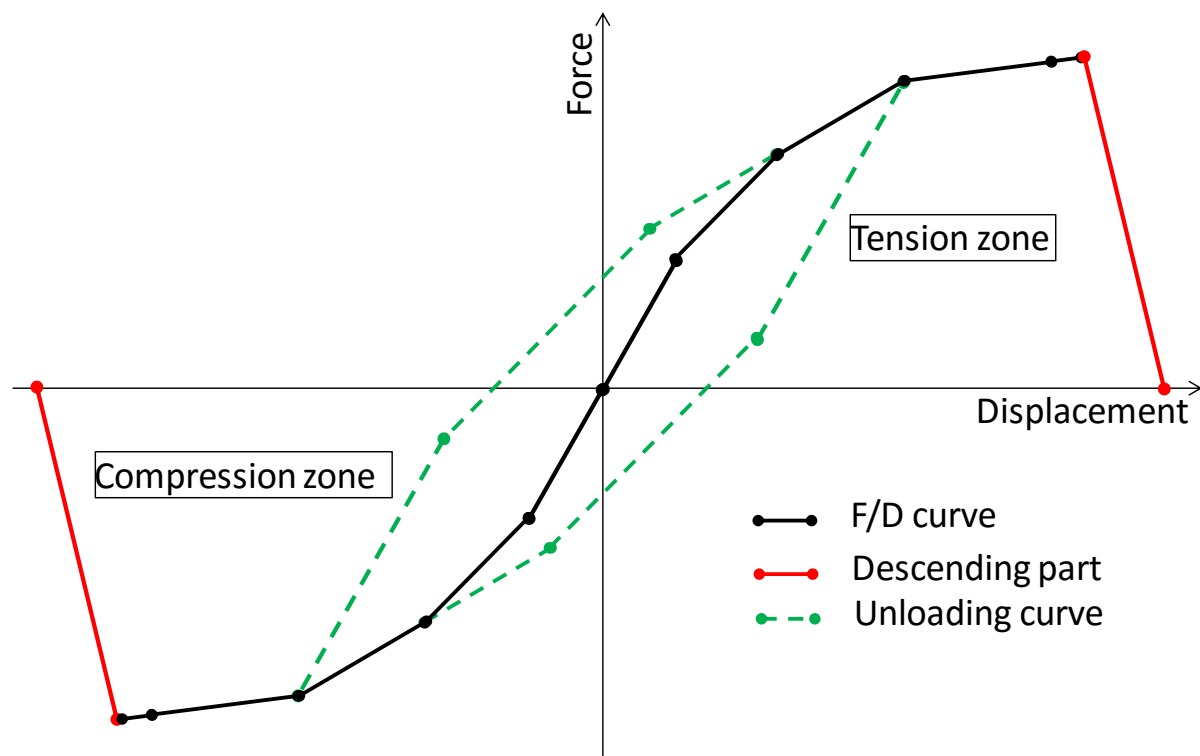
Figure 202: Generalized component assumption.

Figure 203 shows the concept of 'stops' within a component; there can be limits to the permissible ranges of both tension and compression. When a limit is reached, the component can become completely rigid.

Figure 204 illustrates the concept of 'stops' for a complete spring row. These can make the spring row switch on/off according to certain limits, and can cope with both tension and compression. Therefore, the extra spring rows can be easily built up.
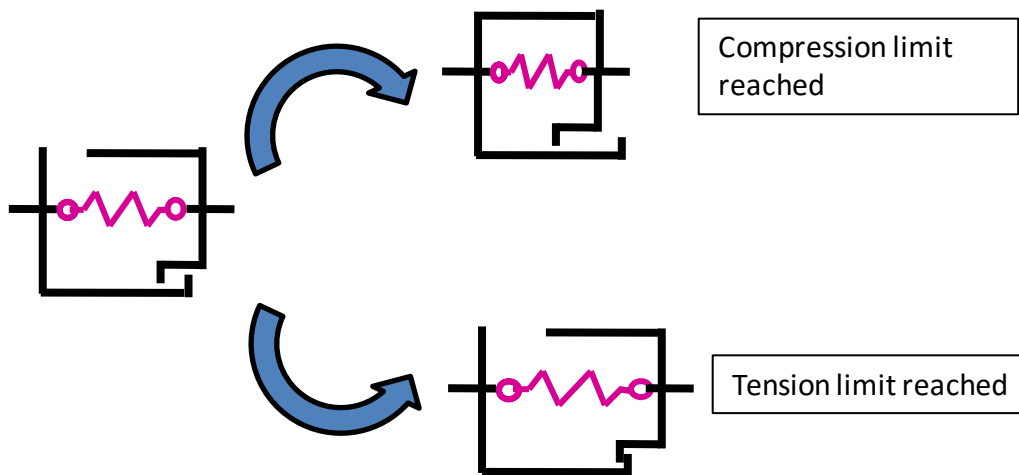
Figure 203: Stops for a component.
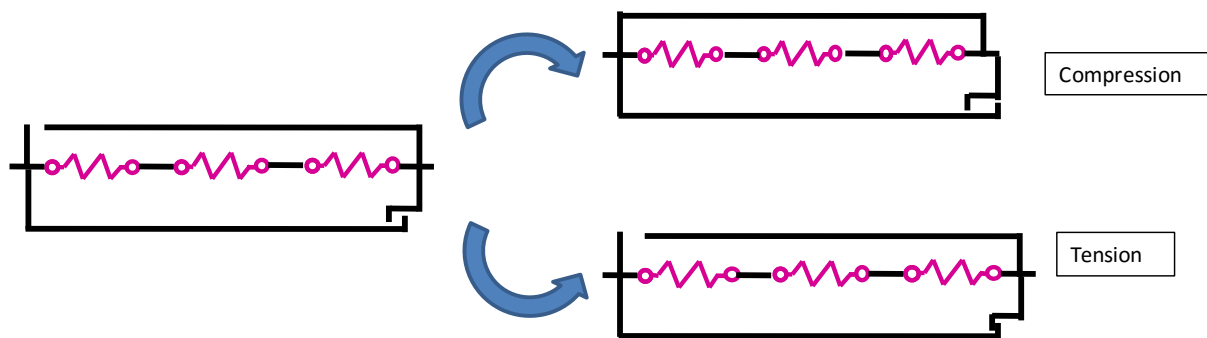
Figure 204: Stops for a complete spring row.

6.2.2 Joint zone

EC3 Part 1.8 points out that it is necessary to take into account not only the rotational deformation of a connection but also the shear deformation of the web panel. EC3 1.8 also requires classification of both the connection (at the column-face) and joint (the whole region near a beam-end). A 'joint' therefore logically includes the connection plus web shear panels. Web shear panels may exist within both the column web in the region of the beam connections, and in the beam web near to the end of the beam.

A 4-noded shear panel element can be proposed to represent the column web behaviour, whereas the beam web naturally forms a 2-noded shear panel element (Figure 205). The column-face connection element defined in this thesis is then located between the column web shear panel and the beam shear panel elements. The column web element connects to

the upper and lower beam-column elements representing the continuous column. The beam web shear panel element is located between the column-face connection element and the end of the beam element.
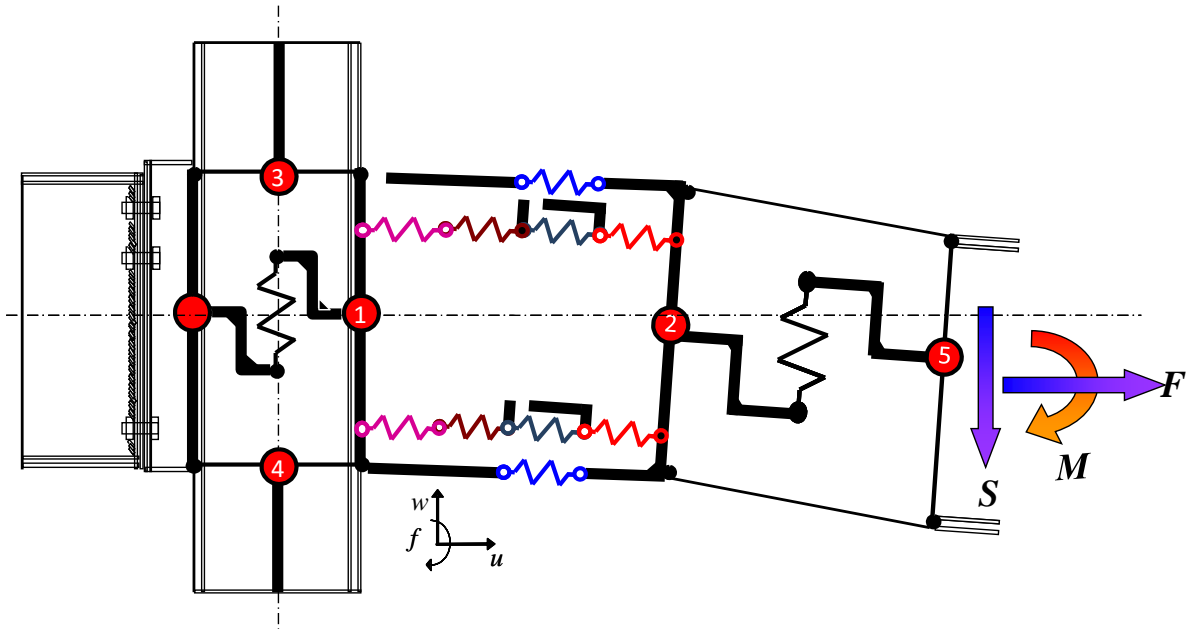
Figure 205: Component based joint array.

References

Al-Jabri K.S. (1999), "The behaviour of steel and composite beam-to-column connections in fire", PhD Thesis, University of Sheffield.

Al-Jabri K.S., Davison J.B. and Burgess I.W. (2008), "Performance of Beam-to-Column Joints in Fire-A Review", Fire Safety Journal, 43 (1), pp. 50-62.

AISC (2005) Steel Construction Manual.American Institute of Steel Construction INC.

Astaneh A. (1989). "Demand and Supply of Ductility in Steel Shear Connections", Journal of Constructional Steel Research 14, pp.1-19.

Bailey C.G. and Moore D.B. (2000a), "The Structural Behaviour of Steel Frames with Composite Floor Slabs Subjected to Fire: Part1: Theory", The Structural Engineer, 78(11), pp. 19-27.

Bailey C.G. and Moore D.B. (2000b), "The Structural Behaviour of Steel Frames with Composite Floor Slabs Subjected to Fire: Part 2: Design", The Structural Engineer, 78(11), pp. 28-33.

Bailey C.G. (2002), "Holistic Behaviour of Concrete Buildings in Fire", Proceedings of the Institution of Civil Engineers, 152(3), pp.199-212.

Bhatt, P (1999). 'Structures'. Longman Group United Kingdom.

Block, F.M., Burgess, I.W. and Davison, J.B.(2004a), 'Numerical and Analytical Studies of Joint Component Behaviour in Fire', Paper S7-4, Third International Workshop on Structures in Fire, Ottawa, Canada, (May) pp 383-395.

Block, F.M., Davison, J.B., Burgess, I.W. and Plank, R.J. (2004b), 'A Component Approach to Modelling Steelwork Connections in Fire: Behaviour of Column Webs in Compression', Proc. ASCE Structures Congress, Nashville, (May)) ISBN 0-7844-0700-2.

Block, F.M., Davison, J.B., Burgess, I.W. and Plank, R.J.(2005a),'High-Temperature Experiments on Joint Components', 4thEuropean Conference on Steel Structures, Maastricht, Netherlands.

Block, F.M., Davison, J.B., Burgess, I.W. and Plank, R.J.(2005b),'High-Temperature Experiments on Joint Component Behaviour', ICASS '05, Shanghai, China.

Block, F.M. (2006a), 'Development of a Component-Based Finite Element for Steel Beam-to-Column Connections at Elevated Temperatures',PhD thesis, University of Sheffield.

Block, F.M., Burgess, I.W., Davison, J.B.and Plank, R.J. (2006b), 'A Component-Based Approach for Modelling the Effect of Fire on Steel Joints', 19th Australasian Conference on the Mechanics of Structures and Materials, Canterbury, New Zealand.

Block, F.M., Davison, J.B., Burgess, I.W. and Plank, R.J. (2007), 'The Development of a Component-Based Connection Element for Endplate Connections in Fire', Fire Safety Journal, 42 pp 498–506.

Block, F.M., Davison, J.B., Burgess, I.W. and Plank, R.J.(2013a), 'Principles of a Component-Based Connection Element for the Analysis of Steel Frames in Fire', Engineering Structures, 49 pp 1059–1067.

Block, F.M., Davison, J.B., Burgess, I.W. and Plank, R.J.(2013b), 'The Treatment of Cooling and Deformation-Reversal in Component-Based Connection Elements for the Analysis of Steel Frames in Fire', Journal of Constructional Steel Research, 86 pp54–65.

Burgess I.W. (2007), "Connection Modelling in Fire",Proc. COST C26 Workshop *Urban Habitat Constructions under Catastrophic Events*, Prague, pp. 25-34.

Burgess I.W. (2009), "Robustness of Composite Multi-Storey Buildings in Fire", PowerPoint slides for the presentation in Tsinghua University at October 2009.

Bursi OS, and Jaspart JP. (1997). Benchmarks for finite element modelling of bolted steel connections. J Construct Steel Res;43(1):17–42.

Case J. and Chilver A.H. (1959) 'Strength of Materials'. Edward Arnold (Publishers) LTD.

CEN (2005a), "BS EN1993-1-1:2005: Eurocode 3: Design of steel structures, Part 1.1: General rules and rules for buildings", European Committee for Standardization, Brussels.

CEN (2005b), "BS EN1993-1-8:2005: Eurocode 3: Design of steel structures, Part 1.8: Design of Joints", European Committee for Standardization, Brussels.

CEN (2005c), "BS EN1993-1-2:2005: Eurocode 3: Design of steel structures, Part 1.2: Structural Fire Design", European Committee for Standardization, Brussels.

Coates R.C., Coutie M.G. and Kong F.K. (1988), "Structural Analysis" (third edition). Chapman & Hall.

Custer R.L.P., and Meacham B.J. (1997), "Introduction to Performance-based Fire Safety", Society of Fire Protection Engineers and National Fire Protection Association.

Dai X.-H., Wang Y.-C.and Bailey C. G. (2009a), "An experimental study of structural behaviour of joints in restrained steel frames in fire", Proc. Int.Conf. Applications of Structural Fire Engineering. Prague, ed.Wald, F.,Kallerova, P., Chlouba, J., pp. 350-355.

Dai X.-H., Wang Y.-C.and Bailey C. G. (2009b), "Effects of Partial Fire Protection on Temperature Development in Steel Joints Protected by Intumescent Coating", Fire Safety Journal., 44, pp. 376-386.

Dai X.-H., Wang Y.-C. and Bailey C. G. (2010a), "A Simple Method to Predict Temperatures in Steel joints With Partial Intumescent Coating Fire Protection", Journal of Fire Technology, 46, pp. 19-35.

Dai X.-H., Wang Y.-C. and Bailey C. G. (2010b), "Numerical Modelling of Structural Fire Behaviour of Restrained Steel Beam_Column Assemblies using Typical Joint Types", Engineering Structures, 32, pp. 2337-2351.

El-Rimawi J.A., Burgess I.W. and Plank R.J. (1997), "The Influence of Connection Stiffness on the Behaviour of Steel Beams in Fire". Journal of Constructional Steel Research, 43(1-3), pp. 1–15.

Faella C, Piluso V, Rizzano G. (1998). Experimental analysis of bolted connections: snug versus preloaded bolts. J Struct Eng ASCE;124(7):765–74.

Federal Emergency Management Agency (FEMA) (2002), "World Trade Centre Building Performance Study: Data Collection, Preliminary Observations and Recommendations", FEMA Technical Report 403, Federal Emergency Management Agency, Washington, DC, USA.

Gebbeken N, and Wanzek T. (1999). Benchmark experiments for numerical simulations of T-stubs. In: Virdi KS, editor. Numerical simulation of semi-rigid connections by the finite element method. COST C1,Report of working group 6—Numerical simulation, Brussels;. p. 61–70.

Gerstle, K.H., (1988), "Effect of Connections on Frames", Journal of Constructiona lSteel Research, 10, pp. 241-267.

Grantham R., Enjily V., Milner M., Bullock M.G.andPittsT.F. (2000),"Multi-Storey Timber Frame Buildings: A Design Guide", BREPress, Garston.

Horne, M.R. (1971) 'Plastic Theory of Structures'. Thomas Nelson and Sons Ltd. pp5-32.

Hu Y., Davison J.B., Burgess I.W. and Plank R.J., "Component Modelling of Flexible End-plate Connections in Fire", International Journal of Steel Structures,9, (2009) pp. 29-38.

Huang, S.S., Davison, J.B. and Burgess (2013a), I.W., 'High-Temperature Tests on Joints to Steel and Partially-Encased H-Section Columns', Journal of Constructional Steel Research, 80 pp 243-251.

Huang, S.S., Davison, J.B. and Burgess (2013b), I.W., 'Experiments on Reverse-Channel Connections at Elevated Temperatures', Engineering Structures. 49 pp 973-982.

Izzudin BA (2005), "Finite Element Analysis Hand-out for MSc structural steel".

Jaspart JP. (1991). Etude de la semi-rigidite des noeuds poutre-colonne et son influence sur la resistance et la stabilite des ossatures en acier. Ph.D. Thesis. University of Lie`ge, Lie`ge; [in French].

Jaspart J.-P. (2000), "General Report: Session on Connections" Journal of Constructional Steel Research, 55, pp.69-89.

Jaspart, J.-P., Pietrapertosa C., Weynand K., Busse E., and Klinkhammer R. (2005), "Development of a Fully Consistent Design Approach for Bolted and Welded Joints in

Building Frames and Trusses between Steel Members Made of Hollow and/or Open Sections: Application of the Component Method". CIDECT Research Project 5BP, Draft final report – Volume 1: Practical design guide.

Jones M. and Wang Y.-C. (2008), "Experimental Studies and Numerical Analysis of the Shear Behaviour of Fin Plate Connections to Tubular Columns at Ambient and Elevated Temperatures", Steel and Composite Structures: An International Journal, 8(3), pp. 179-200.

Jones M.H. (2009), "Tensile and Shear Behaviour of Fin-Plate Connections to Hollow and Concrete-Filled Steel Tubular Columns at Ambient and Elevated Temperatures", PhD thesis, University of Manchester.

Jones M.H. and Wang Y.-C. (2010a), "Shear and Bending Behaviour of Fin Plate Connection to Concrete-Filled Rectangular Steel Tubular Column – Development of a Simplified Calculation Method", Journal of Constructional Steel Research, http://dx.doi.org/10.1016/j.jcsr.2010.10.006

Jones M.H. and Wang Y.-C. (2010b), "Tying Behaviour of Fin Plate Connection to Concrete-Filled Rectangular Steel Tubular Column: Development of a Simplified Calculation Method", Journal of Constructional Steel Research, 66, pp. 1-10, doi:10.1016/j.jcsr.2009.07.011

Kruppa J. (1976), "Resistance en Feudes Assemblages par Boulons", CTICM Report, Document No. 1013-1, Centre Technique Industrial de la Construction Metallique, St. Remy les Chevreuse, France, 1976. [English translation available:"Fire Resistance of Joints with High Strength Bolts

Lawson R.M. (1990), "Behaviour of Steel Beam-to-Beam Connections in Fire", The Structural Engineer,68(14), pp. 263-71.

Leston-Jones L.C. (1997), "The Influence of Semi-Rigid Connections on the Performance of Steel Framed Structures in Fire", PhD Thesis, University of Sheffield.

Li, T.Q., Choo, B.S. and Nethercot, D.A. (1995), 'Connection Element Method for the Analysis of Semi-rigid Frames', Journal of Constructional Steel Research, 32, pp. 143-171.

Liu T.C.-H.and Morris L.J. (1994),"Theoretical Modelling of Steel Bolted Connections under Fire Exposure",Proceedings of the International Conference on Computational Mechanics, Hong Kong.

Liu T.C.-H. (1996),"Finite Element Modelling of Behaviour of Steel Beams and Connections in Fire", Journal of Constructional Steel Research,35(3), pp.181–99.

Liu T.C.-H. (1998a),"Effect of Connection Flexibility on Fire Resistance of Steel Beams", Journal of Constructional Steel Research, 45(1), pp. 99–118.

Liu T.C.-H (1998b),"Three-dimensional Modelling of Steel/Concrete Composite Connection Behaviour in Fire.' Journal of Constructional Steel Research,46(1-3), pp. 319–20.

Liu T.C.-H. (1999),"Moment–Rotation–Temperature Characteristics of Steel/Composite Connections". Journal of Structural Engineering,125(10), pp. 1188–97.

Luo M.-C., Yin Y.-Z., Lamont S., and Lane B. (2005), "Eastern Solutions Focus: Building Design", Fire Engineering Journal and Fire Protection (FEJ FP), pp.29-31.

National Institute of Standards and Technology (NIST) (2005), "Federal Building and Fire Safety Investigation of the World Trade Centre Disaster: Final Report of the National Construction Safety Team on the Collapse of the World Trade Centre Towers (Draft)", NIST Report NCSTAR 1(Draft), Gaithersburg, MD, USA.

National Institute of Standards and Technology (NIST) (2008), "Federal Building and Fire Safety Investigation of the World Trade Centre Disaster: Structural Response and Probable Collapse Sequence of World Trade Centre Building 7", NIST Report NCSTAR 1-9(2), Gaithersburg, MD, USA.

Nethercot, D.A., and Zandonini, R. (1989), "Methods of Prediction of Joint Behaviour: Beam-to-Column Connections", Structural Connections, Stability and Strength, Narayanan, R., ed., Elsevier Applied Science Publishers, pp. 23-62, London.

Newman G.M., Robinson J.T., and Bailey C.G. (2006), "Fire Safe Design: A New Approach to Multi-Storey Steel-Frame Buildings", 2nd ed., SCI Publication P288, Steel Construction Institute, Ascot, UK.

Packer JA and Morris LJ. (1977). A limit state design method for the tension region of bolted beam-to-column connections. Struct Eng;55(10):446–58.

Piluso V, Faella C, and Rizzano G. (2001). Ultimate behavior of bolted T-stubs. II: Model validation. J Struct Eng ASCE;127(6):694–704.

Purkiss J.A. (2007), "Fire Safety Engineering Design of Structures",2nd ed., Butterworth-Heinemann.

Ramberg, W., and Osgood, W.R. (1943), "Description of Stress-Strain Curves by Three Parameters", National Advisory Committee for Aeronautics, Technical Report 902.

RFCS (2009),"COMPFIRE – Design of joints to composite columns for improved fire robustness", Research Fund for Coal and Steel, Grant agreement n° RFSR-CT-2009-00021, European Commission, Brussels,2009.

RFCS (2012a) Deliverable 3 (D3) Report on simplified structural behaviour of components Research Fund for Coal and Steel, Grant agreement n° RFSR-CT-2009-00021, European Commission, Belgium.

RFCS (2012b) Deliverable 4 (D4) Report on Simplified Structural Behaviour of Components, Research Fund for Coal and Steel, Grant agreement n° RFSR-CT-2009-00021, European Commission, Belgium.

Robertson, A. (1925), "The strength of struts". Selected Engineering Paper No. 28.. Institution of Civil Engineers.

Santiago A., Simões da Silva L., Vila Real P. and Veljkovic M.(2008a), "Numerical Study of a Steel SubframeinFire", Computers and Structures, 86(15-16), pp. 1619-1632.

Santiago A., Simões da Silva L., Vaz G., Vila Real P. and Gameiro Lopes A. (2008b), "Experimental Investigation of the Behaviour of a Steel Subframeunder a Natural Fire", International Journal of Steel and Composite Structures, 8(3), pp. 243-264.

Santiago A., Simões da Silva L., Vila Real P., Gameiro Lopes A. and Vaz G. (2009), "Experimental Evaluation of the Influence of Connection Typology on the Behaviour of Steel Structures under Fire', Engineering Journal AISC, 46(2), pp. 81-98.

Santiago A., Simões da Silva L. and Vila Real P.(2010), "Numerical Modelling of the Influence of Joint Typologies on the 3D Behaviour of a Steel Subframe under a Natural Fire",Fire Technology,46, pp. 49–65.

SCI (1997). Joints in Steel Construction: Moment Connections", The Steel Construction Institute. pp 7-49.

Simões da Silva L., Santiago A. and Vila Real P. (2001), "A Component Model for the Behaviour of Steel Joints at Elevated Temperatures', Journal of Constructional Steel Research, 57, pp. 1169-1195.

Sokol Z., Wald F.,Pultar M. andBeneš M. (2003),"Numerical Simulation of Cardington Fire Test on Structural Integrity", Proceedings of the International Conference, Mathematical and Computer Modelling in Science and Engineering"CTUPrague,pp. 339-343. ISBN 80-7015-912-X.

Spyrou S. (2002), "Development of a component-based model of steel beam-to-column joints at elevated temperatures", PhD Thesis, University of Sheffield.

Sun, R.R. (2012), 'Numerical Modelling for Progressive Collapse of Steel Frame Structures in Fire', PhD Thesis, University of Sheffield.

Swanson JA, and Leon RT. (2000). Bolted steel connections: tests on T-stub components. J Struct Eng ASCE;126(1):50–6.

Taib, M.(2012), 'The Performance of Steel Framed Structures with Fin-Plate Connections in Fire', PhD thesis, University of Sheffield, July 2012.

Tschemmernegg, F., Tautschnig, A., Klein, H., Braun, Ch. and Humer, Ch. (1987), "ZurNachgiebigkeit von Rahmenknoten – Teil 1" (Semi-rigid joints of frame structures Vol. 1– in German), Stahlbau 56, Heft 10, S. 299-306.

TF(2000), Grantham R, Enjily v, Milner M, Bullock M, G Pitts. Multi-story Timber Frame Buildings: A Design Guide, BRE Press, Garston.

Wang Y.-C., Burgess I.W., Wald F. and Gillie M. (2013),"Performace-Based Fire Engineering of Structures", CRC Press.

Yee YL and Melchers RE. (1986). Moment–rotation curves for bolted connections. J Struct Eng ASCE;112(3):615–35.

Yu H.-X., Burgess I.W., Davison J.B. and Plank R.J. (2008a), "Experimental Investigation of the Behaviour of Flush End-plate Connections in Fire", Proc. Structures in Fire Conference, Singapore, pp. 150-157.

Yu H.-X., Burgess I.W., Davison J.B. and Plank R.J. (2008b), "Numerical Simulation of Bolted Steel Connections in Fire Using Explicit Dynamic Analysis", Journal of Constructional Steel Research, 64, pp. 515–525.

Yu H.-X., Burgess I.W., Davison J.B. and Plank R.J. (2009a),"Development of a Yield-Line Model for End-plate Connections in Fire", Journal of Constructional Steel Research, 65 (6), pp. 1279-1289.

Yu H.-X., Burgess I.W., Davison J.B., and Plank R.J. (2009b),"Experimental Investigation of the Behaviour of Fin Plate Connections in Fire", Journal of Constructional Steel Research, 65,pp. 723–736.

Yu H.-X., Burgess I.W., Davison J.B. and Plank R.J. (2009c), "Tying Capacity of Web Cleat Connections in Fire. Part 1: Test and Finite Element Simulation", Engineering Structures,31(3), pp. 651-663.

Yu H.-X., Burgess I.W., Davison J.B. and Plank R.J. (2009d), "Tying Capacity of Web Cleat Connections in Fire. Part 2: Development of Component-Based Model", Engineering Structures, 31(3), pp. 697-708.

Yu H.-X., Burgess I.W., Davison J.B. and Plank R.J. (2011), "Experimental and Numerical Investigations of the Behaviour of Flush End-plate Connections at Elevated Temperatures", Journal of Structural Engineering, ASCE,137 (1), pp. 80-87.

Zoetemeijer P. (1974), "A Design Method for the Tension Side of Statically Loaded, Bolted Beam-to-Column Connections", Heron, 20 (1), pp.8-34.

Appendix A Input of connection element in Vulcan

Vulcan is a finite element analysis (FEA) program, which has been developed particularly for the analysis of building structures in fire situation. This component-based connection element is currently implemented in its FORTRAN version. The following table shows the format of the part of the data input file for the connection elements. The remaining structural information input is included in the latest Input explanation for the Vulcan software.

For the connection element, there are two definitions:

> **Connection data:** informs Vulcan about the connection geometries, locations, and material properties.

> **Connection Temperature (TEMP) Pattern:** informs Vulcan about the connection temperature distribution.

The following is the general connection element input format. The variables are explained in the following two tables.

<CONNECTION DATA >

Block 1: (compulsory input for every connection type)

Numcontype

Contype iendtype inumrow

Block 2: (optional input only for flush endplate connection type)

Contype internal imajorminor iec3bolt iductile ductmul

Contype endwidth ednthick endheight colroot endweld enddist coldist

Contype washerdia washerthick boltarea bolthethick nutthick

Contype d0 d1 d2 d3 d4 d5 d6 d7

Contype endym endfy colfanym colfanfy boltym boltfy boltfu endfu colfu endet colet boltet

Contype colwebym colwebfy colflanfy

Block 3: (optional input only for reverse channel connection type)

Contype internal imajorminor iec3bolt iductile ductmul ipull-out

Contype endwidth ednthick endheight colroot endweld enddist coldist

Contype washerdia washerthick boltarea bolthethick nutthick

Contype d0 d1 d2 d3 d4 d5 d6 d7

Contype endym endfy colfanym colfanfy boltym boltfy boltfu endfu colfu endet colet boltet

Contype colwebym colwebfy colflanfy

Contype revym revfy revfu revet

Contype revwebth revlegth revweble revlegle revroot revlegweld

Block 4: (optional input only user defined connection)

Contype capacityfac   ductilityfac

Subblock1:

Contype c1f1 c1f2 c1f3 c1d1 c1d2 c1d3 1ccapfaccfy 1cducfaccfy

Contype c2f1 c2f2 c2f3 c2d1 c2d2 c2d3 2ccapfaccfy 2cducfaccfy

Contype 1t1f1 1t1f2 1t1f3   1t1f4   1t1f5 1t1d1 1t1d2 1t1d3 1t1d4 1t1d5 1t1capfaccfy 1t1ducfaccfy

Contype 1t2f1 1t2f2 1t2f3   1t2f4   1t2f5 1t2d1 1t2d2 1t2d3 1t2d4 1t2d5 1t2capfaccfy 1t2ducfaccfy

Contype 1t3f1 1t3f2 1t3f3   1t3f4   1t3f5 1t3d1 1t3d2 1t3d3 1t3d4 1t3d5 1t3capfaccfy 1t3ducfaccfy

Contype 1t4f1 1t4f2 1t4f3   1t4f4   1t4f5 1t4d1 1t4d2 1t4d3 1t4d4 1t4d5 1t4capfaccfy 1t4ducfaccfy

Contype 1t5f1 1t5f2 1t5f3   1t5f4   1t5f5 1t5d1 1t5d2 1t5d3 1t5d4 1t5d5 1t5capfaccfy 1t5ducfaccfy

…………….

Subblock5:

Contype 3t1f1 3t1f2 3t1f3 3t1f4 3t1f5 3t1d1 3t1d2 3t1d3 3t1d4 3t1d5 3t1capfaccfy 3t1ducfaccfy

Contype 3t2f1 3t2f2 3t2f3 3t2f4 3t2f5 3t2d1 3t2d2 3t2d3 3t2d4 3t2d5 3t2capfaccfy 3t2ducfaccfy

Contype 3t3f1 3t3f2 3t3f3 3t3f4 3t3f5 3t3d1 3t3d2 3t3d3 3t3d4 3t3d5 3t3capfaccfy 3t3ducfaccfy

Contype 3t4f1 3t4f2 3t4f3 3t4f4 3t4f5 3t4d1 3t4d2 3t4d3 3t4d4 3t4d5 3t4capfaccfy 3t4ducfaccfy

Contype 3t5f1 3t5f2 3t5f3 3t5f4 3t5f5 3t5d1 3t5d2 3t5d3 3t5d4 3t5d5 3t5capfaccfy 3t5ducfaccfy

<CONNECTION TEMP PATTERN>

Numtemppat

Temppat tendtemp1 tcolflantemp1 tbolttemp1

Temppat tendtemp1 tcolflantemp1 tbolttemp1

Temppat tendtemp1 tcolflantemp1 tbolttemp1

Temppat tendtemp1 tcolflantemp1 tbolttemp1

Temppat tendtemp1 tcolflantemp1 tbolttemp1

Temppat ccolwebtemp1 ccolflantemp1

Temppat ccolwebtemp2 ccolflantemp2

<CONNECTION DATA >		
Numcontype	Numcontype = number of different connection types	Block 1: (compulsory input for every connection type)
Contype iendtype inumrow	Contype = connection type number; iendtype = specifies the endplate type: 1 =flush endplate, 2 = reverse channel connection, 3=user defined connection; inumrow = number of bolt rows (min 3 for extended endplate, min2 for flush endplate);	
Contype internal imajorminor iec3bolt iductile ductmul	Contype= connection type number; internal = specifies if the compression zone is loaded from both sides (internal =1) or from one side (internal =2); imajorminor = specifies if the beam is connected to the column flange (imajorminor =0) or the column web (not considered yet); iec3bolt = specifies which temperature reduction model is used for the bolts (for Kirby iec3bolt = 0, for EC3-1.2 Annex D iec3bolt = 1); iductile = this extends the ductility of the connection components [not in use for this version, but have to put a number here] (normal failure displacement: iductile = 0, ductile failure displacement: iductile = 1); ductmul = (if ductile = 1 then ductmul is a multiplication factor for the normal failure [not in use for this version, but have to put a number here] displacement (ductmul = 0 for normal failure)	Block 2: (optional input only for flush endplate connection type)

Contype endwidth ednthick endheight colroot endweld enddist coldist	Contype = connection type number;
	
	endwidth = endplate width;
	
	ednthick =endplate thickness;
	
	endheight =endplate height;
	
	colroot = root radius of the column;
	
	endweld =throught thickness of the weld between beam and endplate (same for web and flange);	

	enddist = edge distance of the bolt holes in the endplate (measured from center holes); coldist = edge distance of the bolt holes in column flange (measured from center holes);	182
Contype washerdia washerthick boltarea bolthethick nutthick	Contype = connection type number; Washerdia = outer diameter of the washer; washerthick = washer thickness; boltarea = stress area of the bolts; bolthethick = thickness of the bolt head; nutthick = thickness of the nut;	
Contype d0 d1 d2 d3 d4 d5 d6 d7	Contype = connection type number; d0 = vertical distance from the centre of the beam to the upper edge of the endplate; d1 = vertical distance from the centre of the beam to the first bolt row ; d2 = vertical distance from the centre of the beam to the 2nd bolt row; d3 = vertical distance from the centre of the beam to the 3rd bolt row; d4 = vertical distance from the centre of the beam to the 4th bolt row; d5 = vertical distance from the centre of the beam to the 5th bolt row; d6 = vertical distance from the centre of the beam to the upper edge of the reverse channel [this version only considers the endplate and reverse channel have the same length]; d7 = vertical distance from the centre of the beam to the lower edge of the reverse channel [negative];	
Contype endym endfy colfanym colfanfy boltym boltfy boltfu endfu colfu endet colet boltet	Contype= connection type number; Endym = young's modulus of endplate; Endfy = yield stress of endplate ; colfanym = young's modulus of column flange; colfanfy =yield stress of column flange;	

	boltym = young's modulus of bolts;	
	boltfy = yield stress of bolts;	
	boltfu = ultimate stress of bolts;	
	endfu = ultimate stress of endplate;	
	colfu = ultimate stress of column flange;	
	endet = tangent modulus of endplate ;	
	colet = tangent modulus of column flange ;	
	boltet = tangent modulus of bolt;	
Contype colwebym colwebfy colflanfy	Contype= connection type number; Colwebym = Young's modulus of column web ; colwebfy = yield stress of column web; colflanfy = yield stress of column flange;	
Contype internal imajorminor iec3bolt iductile ductmul	Contype= connection type number; internal = specifies if the compression zone is loaded from both sides (internal =1) or from one side (internal =2); imajorminor = specifies if the beam is connected to the column flange (imajorminor =0) or the column web (not considered yet); iec3bolt = specifies which temperature reduction model is used for the bolts (for Kirby iec3bolt = 0, for EC3-1.2 Annex D iec3bolt = 1); iductile = this extends the ductility of the connection components [not in use for this version, but have to put a number here] (normal failure displacement: iductile = 0, ductile failure displacement: iductile = 1); ductmul = if ductile = 1 then ductmul is a multiplication factor for the normal failure [not in use for this version, but have to put a number here] displacement (ductmul = 0 for normal failure).	Block 3: (optional input only for reverse channel connection type)

Contype endwidth ednthick endheight colroot endweld enddist coldist	Contype = connection type number;
	
	endwidth = endplate width;
	
	ednthick =endplate thickness;
	
	endheight =endplate height;	

	colroot = root radius of the column;
	endweld =throught thickness of the weld between beam and endplate (same for web and flange);
	enddist = edge distance of the bolt holes in the endplate (measured from center holes);
	coldist = edge distance of the bolt holes in column flange (measured from center holes);
Contype washerdia washerthick boltarea bolthethick nutthick	Contype = connection type number;
	Washerdia = outer diameter of the washer;
	washerthick = washer thickness;
	boltarea = stress area of the bolts;
	bolthethick = thickness of the bolt head;
	nutthick = thickness of the nut;
Contype d0 d1 d2 d3 d4 d5 d6 d7	Contype = connection type number;
	d0 = vertical distance from the centre of the beam to the upper edge of the endplate;
	d1 = vertical distance from the centre of the beam to the first bolt row ;
	d2 = vertical distance from the centre of the beam to the 2nd bolt row;
	d3 = vertical distance from the centre of the beam to the 3rd bolt row;
	d4 = vertical distance from the centre of the beam to the 4th bolt row;
	d5 = vertical distance from the centre of the beam to the 5th bolt row;
	d6 = vertical distance from the centre of the beam to the upper edge of the reverse channel [this version only considers the endplate and reverse channel have the same length];
	d7 = vertical distance from the centre of the beam to the lower edge of the reverse channel [negative];
Contype endym endfy colfanym colfanfy boltym boltfy boltfu endfu colfu endet colet boltet	Contype= connection type number;
	Endym = young's modulus of endplate;

	Endfy = yield stress of endplate ; colfanym = young's modulus of column flange; colfanfy =yield stress of column flange; boltym = young's modulus of bolts; boltfy = yield stress of bolts; boltfu = ultimate stress of bolts; endfu = ultimate stress of endplate; colfu = ultimate stress of column flange; endet = tangent modulus of endplate ; colet = tangent modulus of column flange ; boltet = tangent modulus of bolt;	
Contype colwebym colwebfy colflanfy	Contype= connection type number; Colwebym = Young's modulus of column web ; colwebfy = yield stress of column web; colflanfy = yield stress of column flange;	
Contype revym revfy revfu revet	Contype = connection type number; Revym = reverse channel young's modulus; Revfy = reverse channel yield stress; Revfu = reverse channel ultimate stress; Revet = reverse channel tangent modulus;	
Contype revwebth revlegth revweble revlegle revroot revlegweld	Revwebth = reverse channel web thickness; Revlegth =reverse channel leg thickness; Revweble = reverse channel web length; Revlegle = reverse channel leg length; Revroot = reverse channel root; Revlegweld = throught thickness of welding at reverse channel leg.	
Block 4: (optional input only user	Line 1: CXfY: compression component (column flange	Block 4: (optional

defined connection)	under compression) force.	input only user defined connection) ***
Contype capacityfac ductilityfac	X = 1,2; 1 top compression row; 2 bottom compression row;	
Subblock1:	Y = 1,2,3; 3 nodes for each typical tension component;	
Contype c1f1 c1f2 c1f3 c1d1 c1d2 c1d3 1ccapfaccfy 1cducfaccfy	The first node must be zero for each compression curve	
Contype c2f1 c2f2 c2f3 c2d1 c2d2 c2d3 2ccapfaccfy 2cducfaccfy	CXdY: compression component (column flange under compression) deformation.	
Contype 1t1f1 1t1f2 1t1f3 1t1f4 1t1f5 1t1d1 1t1d2 1t1d3 1t1d4 1t1d5 1t1capfaccfy 1t1ducfaccfy	X = 1,2; 1 top compression row; 2 bottom compression row;	
	Y = 1,2,3; 3 nodes for each typical tension component;	
Contype 1t2f1 1t2f2 1t2f3 1t2f4 1t2f5 1t2d1 1t2d2 1t2d3 1t2d4 1t2d5 1t2capfaccfy 1t2ducfaccfy	The first node must be zero for each compression curve	
	Xccapfaccfy = capacity reduction factor for the compression component (column web under compression) at the top compression row	
Contype 1t3f1 1t3f2 1t3f3 1t3f4 1t3f5 1t3d1 1t3d2 1t3d3 1t3d4 1t3d5 1t3capfaccfy 1t3ducfaccfy	X = 1,2; 1 top compression row; 2 bottom compression row;	
Contype 1t4f1 1t4f2 1t4f3 1t4f4 1t4f5 1t4d1 1t4d2 1t4d3 1t4d4 1t4d5 1t4capfaccfy 1t4ducfaccfy	Xcducfaccfy = ductility factor for the compression component at the top compression row	
Contype 1t5f1 1t5f2 1t5f3 1t5f4 1t5f5 1t5d1 1t5d2 1t5d3 1t5d4 1t5d5 1t5capfaccfy 1t5ducfaccfy	X = 1,2; 1 top compression row; 2 bottom compression row;	
	XtYfZ: tension component (column flange under compression) force.	
………….	X = 1,2,3; 1: column flange under bending; 2: bolt in tension; 3: endplate in bending.	
Subblock5:	Y = 1,2,3,4,5; tension bolt row number;	
Contype 3t1f1 3t1f2 3t1f3 3t1f4 3t1f5 3t1d1 3t1d2 3t1d3 3t1d4 3t1d5 3t1capfaccfy 3t1ducfaccfy	Z = node number. Each tension component is represented by 5node. The first node is zero	
Contype 3t2f1 3t2f2 3t2f3 3t2f4 3t2f5 3t2d1 3t2d2 3t2d3 3t2d4 3t2d5 3t2capfaccfy 3t2ducfaccfy	XtYcapfaccfy = capacity reduction factor for the tension component at the Xth tension bolt row	
	X = 1,2,3; 1: column flange under bending; 2: bolt in tension; 3: endplate in bending.	
Contype 3t3f1 3t3f2 3t3f3 3t3f4 3t3f5 3t3d1 3t3d2 3t3d3 3t3d4 3t3d5 3t3capfaccfy 3t3ducfaccfy	Y = 1,2,3,4,5; tension bolt row number;	
	XtYducfaccfy = ductility factor for the tension	

Contype 3t4f1 3t4f2 3t4f3 3t4f4 3t4f5 3t4d1 3t4d2 3t4d3 3t4d4 3t4d5 3t4capfaccfy 3t4ducfaccfy Contype 3t5f1 3t5f2 3t5f3 3t5f4 3t5f5 3t5d1 3t5d2 3t5d3 3t5d4 3t5d5 3t5capfaccfy 3t5ducfaccfy	component at the Xth tension bolt row X = 1,2,3; 1: column flange under bending; 2: bolt in tension; 3: endplate in bending. Y = 1,2,3,4,5; tension bolt row number;	
{CONNECTION DATA}		

<CONNECTION TEMP PATTERN>		
Numtemppat	Numtemppat = number of different connection temperature pattern (currently only consider 1);	
Temppat tendtemp1 tcolflantemp1 tbolttemp1	Temppat = connection temperature pattern number;	
Temppat tendtemp1 tcolflantemp1 tbolttemp1	Tendtempn = temperature multiplier for endplate at height of nth bolt row;	
Temppat tendtemp1 tcolflantemp1 tbolttemp1	Tcolflantempn=temperature multiplier for column flange at height of nth bolt row;	
Temppat tendtemp1 tcolflantemp1 tbolttemp1	Tbolttempn = temperature multiplier for bolt at height of nth bolt row;	
Temppat tendtemp1 tcolflantemp1 tbolttemp1		
Temppat ccolwebtemp1 ccolflantemp1	Tempat = connection temperature pattern number;	
	Ccolwebtem1 = temperature multiplier for column web at height of upper beam flange;	
	Ccolflantemp1=temperature multiplier for column flange at height of upper beam flange;	
Temppat ccolwebtemp2 ccolflantemp2	Temppat = connection temperature pattern number;	
	Ccolwebtem1 = temperature multiplier for column web at height of lower beam flange;	
	Ccolflantemp1=temperature multiplier for column flange at height of lower beam flange;	
{**CONNECTION TEMP PATTERN**}		

Appendix B Example of Vulcan input

In order to explain how to write the Vulcan connection element input data, the input for an endplate connection (test EP_20_35_04-02-08_8mm) is taken as an example. The joint test details are included in 4.3.2 .

<HEADER>

 EP_20_35_04-02-08_8mm

{HEADER}

<VERSION>

    6

{VERSION}

<PROGRAM CONTROL>

0   0   0

1.000   1.000

1   0.000   0.000 0.0003   1.000

5000 0

{PROGRAM CONTROL}

<STRUCTURE INFORMATION>

15   9   9   4   0   0

100   0.000   1   13

3   2   1   1

{STRUCTURE INFORMATION}

<NODAL GEOMETRY>

1   0   0   0

2	61.69703308	0	28.76945836
3	242.9589738	0	113.2922886
4	424.2209146	0	197.8151189
5	475.929427	0	193.4046499
6	527.6379395	0	188.9941809
7	537.4860202	0	187.257717
8	762.5146637	0	147.5795166
9	987.5433073	0	107.9013162
10	997.391388	0	106.1648523
11	1007.367029	0	105.4672948
12	1139.998164	0	96.19291908
13	1282.60494	0	86.22098586
14	1347.100215	0	-35.13170352
15	1696.809043	0	-176.4282593

{NODAL GEOMETRY}

<NEW BEAM SECTION>

1　1　1

1

1

1

3　3　　1　　1

357　176000　0.3

357　176000　0.3

3560000 20500000　0.3

275   210000   0.3

-30   0.25   0.2

1   2   1   1   1

303.4 165   165 10.2 10.2 6.0   8   5   5

2   2   2   1   1

260.3 256.3 256.3 17.3 17.3 10.3 8   5   5

3   1   3   1   1

25   25   5   5

5   0   0   5   0   0

5   0   5   5   0   0

5   5   5   5   5   5

5   0   5   5   5   0

5   0   0   5   0   0

4   4   4   4   4

4   4   4   4   4

4   4   4   4   4

4   4   4   4   4

4   4   4   4   4

{NEW BEAM SECTION}

<MEMBER DATA>

1   1   0   0

1   1   2   9   1   1   2   1   0   180

2   7   0   0

2   2   4   3   0   1   1   1   1   0   0

3   7   0   0

3   4   6   5   0   1   1   1   1   0   0

4   1   0   0

4   6   7   3   3   3   1   1   0   180

5   7   0   0

5   7   9   8   0   3   1   1   1   0   0

6   1   0   0

6   9   10   3   3   1   1   1   0   180

7   1   0   0

7   10   11   3   3   1   1   1   0   180

8   7   0   0

8   11   13   12   0   3   1   1   1   0   0

9   7   0   0

9   10   15   14   0   3   1   1   1   0   0

{MEMBER DATA}

<CONNECTION DATA>

1

1   1   3

1 1   0   0   0   0

1   200   8   323.4   12.7   8   55   83.15

1   37   3   314.156   13   16

1   161.7   101.7   31.7   -101.7 0   0

1   149000   293   176000   357   210000   677   998   492   568

1002 1062 1629

1   176000   357   357

{CONNECTION DATA}

<CONNECTION TEMP PATTERN>

1

1   1.0   1.0   1.0

1   1.0   1.0   1.0

1   1.0   1.0   1.0

1   1.0   1.0   1.0

1   1.0   1.0   1.0

1   1.0   1.0

1   1.0   1.0

{CONNECTION TEMP PATTERN}

<BOUNDARY CONDITIONS>

    1   111111

    2   10101

```
        3    10101

        4    10101

        5    10101

        6    10101

        7    10101

        8    10101

        9    10101

       10    10101

       11    10101

       12    10101

       13    111101

       14    10101

       15    110101

        0    0
```

{BOUNDARY CONDITIONS}

<JOINT LOADS>

```
   15    0    0    -500000    0    0    0

    0    0    0    0    0    0    0
```

{JOINT LOADS}

<DISPLAY DEFLECTIONS>

```
 5

 1  2  4  6  15
```

{DISPLAY DEFLECTIONS}

<DISPLAY FORCES>

5

1 2 5 8 9

{DISPLAY FORCES}

<DISPLAY CONNECTIONS>

4

1 4 6 7

{DISPLAY CONNECTIONS}

<TEMPERATURE DATA>

    1   1   20

    1   0   20

{TEMPERATURE DATA}

{END OF FILE}

.